Molecular mechanism and enzymological studies of dye-decolorizing peroxidases (DyPs) from *Thermomonospora curvata* and *Enterobacter lignolyticus*

by

Ruben Shrestha

B.S., Tribhuvan University, 2005
M.S., Tribhuvan University, 2007

AN ABSTRACT OF A DISSERTATION

submitted in partial fulfillment of the requirements for the degree

DOCTOR OF PHILOSOPHY

Department of Chemistry
College of Arts and Sciences

KANSAS STATE UNIVERSITY
Manhattan, Kansas

2017

Abstract

Dye-decolorizing peroxidases (DyPs) comprise a new family of heme peroxidases, which have received much attention due to their potential applications in degradation of lignin and anthraquinone dyes. In this research, studies of two types of DyPs are carried out and reported in the following three sections. The first section includes the identification and characterization of class-A *Tc*DyP from *Thermomonospora curvata,* a thermophilic actinomycete found in composted manure. The *Tc*DyP was found to be highly active toward a wide range of substrates including phenolic lignin model compounds. Transient- and steady state- kinetics involving wild-type (*wt*) and mutant *Tc*DyPs revealed that Asp220 and Arg327 are essential for compound I formation and reduction of compound II to resting state is the rate-limiting step. Additionally, replacement of His312 and Arg327 shifted the redox potential ($E^{\circ\prime}$) to a more negative value. In the second section, the residues involved in the radical generation and substrate oxidation were explored. *Tc*DyP contains 7 tryptophans and 3 tyrosines, which are the likely candidates of protein radicals and substrate oxidation sites. Crystal structure of *Tc*DyP solved at 1.75Å revealed Trp263, Trp376 and Tyr332 as surface-exposed protein radical sites. Further studies using site-directed mutagenesis, steady-state and stopped-flow kinetics determined that the Trp263 is also one of the surface-exposed substrate oxidation sites. The Trp376 was characterized as the residue essential for covalent crosslinking of the enzyme units and an off-pathway electron sink. The highly conserved Tyr332 was found to be unimportant for substrate oxidation due to its extremely narrow surface exposure. The final section involves mechanistic study of a class-B DyP from *Enterobacter lignolyticus* (*El*DyP), a bacterium capable of growing on lignin anaerobically. The crystal structure of *El*DyP revealed the presence of two heme access channels measuring at ~3.0 and 8.0 Å in diameter and a water molecule as the sixth ligand to the

heme center. Bisubstrate Ping-Pong mechanism was found operational in the catalytic cycle of *El*DyP, in which conformational change of the enzyme resting state was proposed as the final step and the rate limiting step in the presence of ABTS. Microscopic events leading to Compound I formation was analyzed using D_2O_2. A kinetic isotope effect (KIE) of 2.4 at pD 3.5 suggested that Compound 0 is formed initially with protonation/deprotonation as the rate-limiting step. Compound I was directly reduced to the enzyme resting state via a 2-electron process, for which the rate increases as the pH decreases. Based on viscosity effect and solvent KIE (sKIE) with the reducing substrate, aquo release was found to be mechanistically important. Distal aspartate was proposed as the key residue that modulates the acidic pH optimum in Compound I reduction. These findings will pave the way for engineering DyPs for their applications in the degradation of lignin and synthetic dyes.

Molecular mechanism and enzymological studies of dye-decolorizing peroxidases (DyPs) from *Thermomonospora curvata* and *Enterobacter lignolyticus*

by

Ruben Shrestha

B.S., Tribhuvan University, 2005
M.S., Tribhuvan University, 2007

A DISSERTATION

submitted in partial fulfillment of the requirements for the degree

DOCTOR OF PHILOSOPHY

Department of Chemistry
College of Arts and Sciences

KANSAS STATE UNIVERSITY
Manhattan, Kansas

2017

Approved by:

Major Professor
Dr. Ping Li

Copyright

Abstract

Dye-decolorizing peroxidases (DyPs) comprise a new family of heme peroxidases, which have received much attention due to their potential applications in degradation of lignin and anthraquinone dyes. In this research, studies of two types of DyPs are carried out and reported in the following three sections. The first section includes the identification and characterization of class-A *Tc*DyP from *Thermomonospora curvata,* a thermophilic actinomycete found in composted manure. The *Tc*DyP was found to be highly active toward a wide range of substrates including phenolic lignin model compounds. Transient- and steady state- kinetics involving wild-type (*wt*) and mutant *Tc*DyPs revealed that Asp220 and Arg327 are essential for compound I formation and reduction of compound II to resting state is the rate-limiting step. Additionally, replacement of His312 and Arg327 shifted the redox potential ($E^{\circ\prime}$) to a more negative value. In the second section, the residues involved in the radical generation and substrate oxidation were explored. *Tc*DyP contains 7 tryptophans and 3 tyrosines, which are the likely candidates of protein radicals and substrate oxidation sites. Crystal structure of *Tc*DyP solved at 1.75Å revealed Trp263, Trp376 and Tyr332 as surface-exposed protein radical sites. Further studies using site-directed mutagenesis, steady-state and stopped-flow kinetics determined that the Trp263 is also one of the surface-exposed substrate oxidation sites. The Trp376 was characterized as the residue essential for covalent crosslinking of the enzyme units and an off-pathway electron sink. The highly conserved Tyr332 was found to be unimportant for substrate oxidation due to its extremely narrow surface exposure. The final section involves mechanistic study of a class-B DyP from *Enterobacter lignolyticus* (*El*DyP), a bacterium capable of growing on lignin anaerobically. The crystal structure of *El*DyP revealed the presence of two heme access channels measuring at ~3.0 and 8.0 Å in diameter and a water molecule as the sixth ligand to the

heme center. Bisubstrate Ping-Pong mechanism was found operational in the catalytic cycle of *El*DyP, in which conformational change of the enzyme resting state was proposed as the final step and the rate limiting step in the presence of ABTS. Microscopic events leading to Compound I formation was analyzed using D_2O_2. A kinetic isotope effect (KIE) of 2.4 at pD 3.5 suggested that Compound 0 is formed initially with protonation/deprotonation as the rate-limiting step. Compound I was directly reduced to the enzyme resting state via a 2-electron process, for which the rate increases as the pH decreases. Based on viscosity effect and solvent KIE (sKIE) with the reducing substrate, aquo release was found to be mechanistically important. Distal aspartate was proposed as the key residue that modulates the acidic pH optimum in Compound I reduction. These findings will pave the way for engineering DyPs for their applications in the degradation of lignin and synthetic dyes.

Table of Contents

List of Figures

List of Tables

List of Abbreviation

*Aau*DyP: DyP from *Auricularia auricular-judae*

ABTS: 2,2'-azino-bis(3-ethylbenzothiazoline-6-sulphonic acid)

Ala or A: alanine

APX: ascorbate peroxidase

AQ: anthraquinone

Arg or R: arginine

Asp or D: aspartate

BMS: benzyl methyl sulfide

BCA: bicinchoninic acid

BSA: bovine serum albumin

CAPS: N-cyclohexyl-3-aminopropanesulfonic acid

C2LP: compound II-like product

CiP: *Coprinus cinereus* peroxidase

CcP: cytochrome c peroxidase

CPO: chloroperoxidase

Cys or S: cysteine

D_2O: deuterium oxide (heavy water)

DMP: 2,6-dimethoxy phenol

DyP: dye-decolorizing peroxidase

*El*DyP: DyP from *Enterobacter lignolyticus*

EPR: electron paramagnetic resonance

EPS: ethyl phenyl sulfide

ERS: enzyme resting state

H_2O_2: hydrogen peroxide

HEPES: 4-(2-hydroxyethyl)piperazine-1-ethanesulfonic acid

His or H: histidine

HQ: hydroquinone

HS: high spin

KIE: kinetic isotope effect

Kpi: potassium phosphate, inorganic

LiP: lignin peroxidase

LPO: lactoperoxidase

LS: low spin

MMA: 4-methoxymandelic acid

MnP: manganese peroxidase

MPO: myeloperoxidase

MPS: methyl phenyl sulfide

MTS: methyl *p*-tolyl sulfide

MW: molecular weight

NHE: normal hydrogen electrode

ICP-OES: inductively coupled plasma optical emission spectrometry

IPTG: isopropyl β-D-1-thiogalactopyranoside

pD: pH measured in D_2O

PDA: photo diode array

PDB: protein data bank

PEG: polyethylene glycol

Phe or F: phenylalanine

QS: quantum mechanically mixed spin

RB: reactive blue

RBlk5: reactive black 5

RDS: rate determining step

ROS: reactive oxygen species

Rz: reinheitszahl value

SA: specific activity

SDS-PAGE: sodium dodecyl sulfate polyacrylamide gel electrophoresis

SEC: size-exclusion chromatography

SHE: standard hydrogen electrode

sKIE: solvent kinetic isotope effect

SVD: single value decomposition

TAP: hydrogen peroxide-dependent phenol oxidase from *Termitomyces albuminosus*

*Tc*DyP: DyP from *Thermomonospora curvata*

*Tc*DyP-0/*Tc*DyP-I/*Tc*DyP-II: resting state/compound I/compound II of *Tc*DyP

TPO: thyroid peroxidase

Tris: tris(hydroxymethyl)aminomethane

Trp or W: tryptophan

Tyr or Y: tyrosine

VP: versatile peroxidase

Acknowledgements

First of all, I would like to express my sincere and utmost gratitude to my advisor Professor Ping Li for his continuous support throughout my Ph.D. program. Everything I was able to accomplish and everything I became as a researcher during the program I owe it all to him. I am immensely grateful for his constant guidance and push in carrying out a meaningful research, thinking critically and writing a good paper. I feel very fortunate to have the opportunity to work in his lab and I could not have asked for a better mentor.

Next, I would like to thank my Ph.D. advisory committee chair Professor Sherry Haar and committee members Professor Phillip Klebba, Professor Stefan Bossmann and Professor Christer Aaekeröy for their advice and their valuable time.

I would also like to thank the other organic chemistry faculty members, Professor Duy Hua, Professor Mark Hollingsworth, Professor Ryan Rafferty and Professor Santos Aryal who helped expand my knowledge in chemistry.

A special thanks to our collaborator Professor Brian Geisbrecht and his co-workers who helped us to obtain and solve the valuable crystal structures of our enzymes.

I would like to acknowledge Department of Chemistry at Kansas State University for providing me with graduate teaching assistantship, and Johnson Cancer Research Center and National Institute of Health for funding my Ph.D. research.

My sincere appreciation also goes out to Dr. Louis Wojcinski, Mr. Michael Hinton, Mr. Tobe Eggers, Mr. Jim Hodgson, Mr. Ron Jackson, Ms. Mary Dooley, Ms. Kimberly Ross and Mr. Bart Bath for all of their great help throughout my journey at K-State.

I would also like to extend my deepest gratefulness to my past and present lab mates, especially Wei Zhang, Ruikai Cao, XueJie Chen, Kaimin Jia and Gaochao Huang who made my Ph.D. life more meaningful, enjoyable and encouraging.

I would also like to remember my teachers who have taught me at different stages of my life and have influenced me in pursuing my dreams. And my friends back in my home country and here in Manhattan, KS who have been my constant cheerleaders. I am also indebted to the Nepalese Students' Association at K-State, the community which never have made me feel that I am away from my home.

At last but not the least, I would like to express my heartfelt gratitutudes to my family members who always have been with me, loved me and nurtured me. I would like to first thank my mother and father, for their unconditional love and sacrifices in bringing me up to this stage. Thank you both for giving me this life! Next, I would like to thank my awesome wife Sony, who endured with me throughout the tough life of a graduate student. Her constant love, support and understanding has made my student life more pleasant and meaningful. Thank you, my love, for all the joys you brought in my life! Finally, our son Ian, who is two and half years as of now, has been a great gift of life and is the reason I go back home from work everyday and is the reason I go to work the everday. We love you son!

Dedication

To my parents

For their unconditional love and sacrifice!

&

To my beloved wife

For being my greatest cheerleader!

Preface

The major goal of my doctoral research was focused on understanding the molecular mechanism of recently discovered family of peroxidase called dye decolorizing peroxidase (DyP). DyP from two bacterial sources were studied extensively and the results obtained led to following three publications in the scientific journal which make the main core of this thesis.

1. Chen, C.; Shrestha, R.; Jia, K.; Gao, P. F.; Geisbrecht, B. V.; Bossmann, S. H.; Shi, J.; Li, P., Characterization of Dye-decolorizing Peroxidase (DyP) from Thermomonospora curvata Reveals Unique Catalytic Properties of A-type DyPs. *J Biol Chem* **2015**, 290 (38), 23447-63

2. Shrestha, R.; Chen, X. J.; Ramyar, K. X.; Hayati, Z.; Carlson, E. A.; Bossmann, S. H.; Song, L. K.; Geisbrecht, B. V.; Li, P., Identification of Surface-Exposed Protein Radicals and A Substrate Oxidation Site in A-Class Dye-Decolorizing Peroxidase from Thermomonospora curvata. *ACS Catalysis* **2016**, 6 (12), 8036-8047.

3. Shrestha, R.; Huang, G.; Meekins, D. A.; Geisbrecht, B. V.; Li, P., Mechanistic Insights into Dye-Decolorizing Peroxidase Revealed by Solvent Isotope and Viscosity Effects. *ACS Catalysis* **2017**, 6352-6364.

In addition, during the course of my Ph.D. program I was also able to co-author following papers:

1. Huang, G.; Shrestha, R.; Jia, K.; Geisbrecht, B. V.; Li, P. Enantioselective synthesis of dilignol model compounds and their stereodiscrimination study with a dye-decolorizing peroxidase. *Org. Lett.* **2017,** *19*, 1820-1823.

2. Chen, C.; Cao, R.; Shrestha, R.; Ward, C.; Katz, B. B.; Fischer, C. J.; Tomich, J. M.; Li, P., Trapping of intermediates with substrate analog HBOCoA in the polymerizations catalyzed by class III polyhydroxybutyrate (PHB) synthase from *Allochromatium vinosum*. *ACS Chem Biol* **2015,** *10* (5), 1330-1339.

3. Zhang, W.; Shrestha, R.; Buckley, R. M.; Jewell, J.; Bossmann, S. H.; Stubbe, J.; Li, P., Mechanistic insight with HBCH2CoA as a probe to polyhydroxybutyrate (PHB) synthases. *ACS Chem Biol* **2014,** *9* (8), 1773-9.

4. Shrestha, R.; Huang, G.; Jia, K.; Li, P. Molecular Aspects and Enzymology of Dye-Decolorizing Peroxidases. Invited review for *Acc. Chem. Res*.

Chapter 1 - Introduction

1.1 Peroxidases in general

Heme peroxidases are oxidoreductases having heme (Fe^{3+}-Protoporphyrin IX) as a cofactor. Ubiquitously found in animals, plants, fungi and bacteria, they use one-equivalent H_2O_2 to oxidize two-equivalents of substrate molecules, generating two-equivalents of water molecules in the process. The report of the first peroxidase reaction dates as early as two centuries back when Planche observed the development of blue color in the tincture of Guaiacum plant resin upon soaking with fresh horseradish roots in 1810[1]. But it wasn't until a century later that, the enzyme isolated from horseradish was identified and characterized as a peroxidase by Alexander Bach and Chodat in 1903[2-3]. Since its characterization at the turn of the twentieth century, horse-radish peroxidase (HRP) was the sole enzyme that ruled the realm of peroxidase study. Discovery of other peroxidases later during the 1940s like yeast cytochrome c peroxidase (CcP) and chloroperoxidase (CPO) in 1940, myeloperoxidase (MPO) in 1941 and lactoperoxidase in 1947 paved the path for much broader enzymological study of peroxidases. Theorell, who was awarded the Nobel Prize in Medicine in 1955 for his work on oxidative enzymes, discovered Compound I, the first catalytic intermediate of peroxidases, in 1941[4]. Interestingly, the second intermediate named Compound II was discovered even before that in 1937 by Keilin and Mann,[5] which was also the first intermediate ever detected for any enzyme[6].

Peroxidases, based on their origin and sequence similarity, are broadly classified into two superfamilies, animal and plant peroxidases. The animal peroxidases include members like myeloperoxidase (MPO), eosinophil peroxidase (EPO), lactoperoxidase (LPO) and thyroid peroxidase (TPO). Except for TPO, these enzymes are antimicrobial in function and are chiefly involved in innate immunity. TPO, on the other hand, is responsible for thyroid hormone

synthesis.[7] The plant peroxidase superfamily, as proposed by Welinder, is further subdivided into three classes, class I, II and III[8]. Class I peroxidases are intracellular and prokaryotic in origin and is comprised of very well studied mitochondrial yeast CcP, the very first heme peroxidase to have its crystal structure solved[9]. CcP is involved in mitochondrial electron transport chain where it oxidizes cytochrome c[10]. Other members of this class include ascorbate peroxidase (APX) which is responsible for getting rid of excess H_2O_2 in chloroplast using ascorbate as the electron donor and bifunctional catalase-peroxidase KatG that functions as a virulence factor in *Mycobacterium tuberculosis* by scavenging toxic H_2O_2 produced by macrophages[11]. Class II consists of fungal peroxidases which are secreted extracellularly and mainly involved in lignin degradation. Examples of class II peroxidases include manganese peroxidase (MnP) and lignin peroxidase (LiP) from *Phanerochaete chrysosporium,* versatile peroxidase (VP) from *Pleurotus eryngii* and *Coprinus cinereus* peroxidase (CiP) and *Arthromyces ramosus* peroxidase (ARP)[12]. The class III peroxidase comprises the plant peroxidases like 'good old' HRP, soybean peroxidase (SBP) and barley grain peroxidase (BGP) which are also extracellular and are involved in crosslinking of cell wall units, lignin polymerization, auxin metabolism and self-defense against the plant pathogens[13]. Yet there are other types of peroxidases that do not fit in any of the aforementioned categories. These include chloroperoxidase (CPO) and vanadium haloperoxidase which are the nature's recruit in generation of hypohalites (OX^-) from halide salts to halogenate biomolecules[14]. Moreover, they also act as an oxygenase and catalase[15]. Catalase is a special class of peroxidase that uses only H_2O_2 as the substrate in generating dioxygen and it functions to counteract the oxidative strees in organisms[6]. The classification of different tpes of peroxidases is summarized in Fig. 1.1.

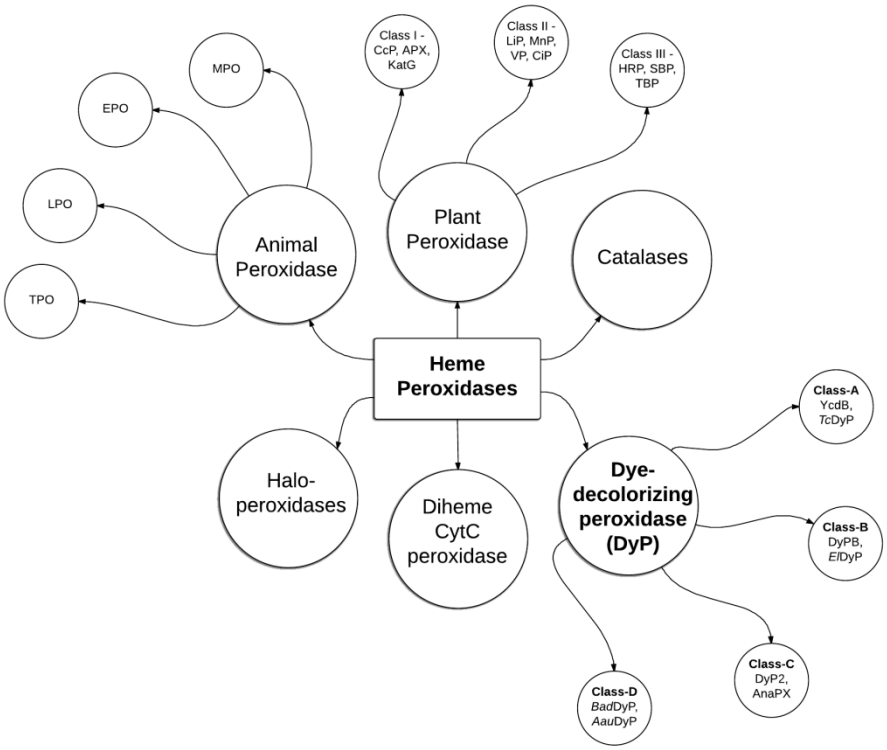

Figure 1.1 Classification of heme peroxidases.

Adapted from http://peroxibase.toulouse.inra.fr (Chart prepared by using Lucidchart.)

1.2 Dye-decolorizing peroxidase (DyP)

1.2.1 Discovery of DyP

In 1995, Kim, Shoda and colleagues discovered that *Bjerkandera adusta* Dec 1 (formerly *Geotrichum candidum* Dec 1 or *Thanatephorus cucumeris* Dec 1), a basidiomycete, is capable of decolorizing 21 different types of reactive dyes including azo and anthraquinone dyes[16]. The crude extracellular enzyme mixtures showed peroxidase activity. The same group successfully isolated and characterized the heme peroxidase responsible for the dye decolorization in 1999[17]. This peroxidase had unprecedented high activity towards anthraquinone (AQ) dyes with high redox potentials and showed the spectra for degradation of 2,6-dimethoxy-phenol (DMP), guaiacol and veratryl alcohol (VA) that was different from other peroxidases. Hence this novel

enzyme was named 'Dye Decolorizing Peroxidase' (DyP)[17]. (Note: To avoid confusions, the term 'DyP' and '*Bad*DyP' represent the DyP in general and DyP from *Bjerkandera adusta* Dec1, respectively.) In the same year, *dyp* gene from *B. adusta* was cloned and its primary sequence was determined. Since *B. adusta* is a fungus, *Bad*DyP was initially assigned as class II fungal peroxidase. However, its primary sequence beared no resemblance to any other plant peroxidases, including the class II peroxidases[18]. Since its first discovery 18 years ago and with increasing number of genomes sequenced, DyPs have been found in numerous other fungi and more importantly in far greater number in bacteria[19]. Hence, they were classified as a new type of heme peroxidases. InterPro database, a resource dedicated to protein sequence analysis and classification, has categorized these enzymes under the family 'DyP-type peroxidase' (IPR006314). A search on 9/14/17 has resulted in 11,321 putative member enzymes, of which 93% are from bacteria[20]. The first bacterial DyP, YcdB/EfeB from *Escherichia coli*, was characterized in 2006 by Sturm and co-workers[21].

1.2.2 Phylogeny and classification of DyP

There are several classification schemes that have tried to assemble DyPs methodically into families, subfamilies and classes. For example, like the InterPro database mentioned above, DyPs are listed under DyP-type peroxidase family by Pfam database (Pfam 04261)[22]. Based on the sequence and structural analysis DyPs are classified as a member of 'structural' superfamily CDE, which also includes chlorite dismutase (Cld) and EfeB. EfeB, which in fact is a DyP belonging to class A, was classified here as a separate family[23]. Later Zamocky et al. regrouped Clds and DyPs under peroxidase-chlorite dismutase superfamily and mentioned the further classification of DyPs in to four sub-families A, B, C and D (Fig. 1.7)[24]. Similarly, PeroxiBase,

the database devoted just for peroxidases, also classifies DyP-type peroxidase family into four classes A, B, C and D[25]. On the other hand, the structural classification based on SCOP database, DyPs are grouped with 24 other families which also include Clds under the dimeric α+β barrel superfamily with ferredoxin like fold[26].

Among the four classes of DyP, those belonging to class A, B and C are of bacterial in origin while the class D have fungi as their source. Phylogenetically, Class C DyPs are more closely related to fungal Class D. Class B DyPs have the shortest amino acid sequence and the most compact structure followed by Class A DyPs with TAT signal. Classes C and D are characterized by longest sequences and the largest structures of all classes. A summary of DyPs and their sources are presented in Table 1.1.

Table 1.1 Classification of DyPs into four classes, their member enzymes characterized to date and their sources.

DyP classes	DyP enzymes	Source organism	Organism type
A	EfeB/YcdB	*Escherichia coli* O157	Proteobacteria
	DyPA	*Rhodococcus jostii* RHA1	Actinobacteria
	*Tfu*DyP	*Thermobifida fusca*	Actinobacteria
	*Bs*DyP(YwbN)	*Bacillus subtilis*	Firmicutes
	*Svi*DyP	*Saccharomonospora viridis*	Actinobacteria
	*Tc*DyP	*Thermomonospora curvata*	Actinobacteria
	DyPA	*Pseudomonas fluorescens* Pf-5	Proteobacteria
	DtpA	*Streptomyces lividans*	Actinobacteria
B	YfeX	*Escherichia coli* O157	Proteobacteria
	DyPB	*Rhodococcus jostii* RHA1	Actinobacteria
	TyrA	*Sheanella oneidensis*	Proteobacteria
	*Bt*DyP	*Bacteriodes thetaiotaomicron*	Bacteroidetes

	*Pp*DyP	*Pseudomonas putida*	Proteobacteria
	DyP*Pa*	*Pseudomonas aeruginosa* PKE117	Proteobacteria
	DyP1B	*Pseudomonas fluorescens* Pf-5	Proteobacteria
	DyP2B	*Pseudomonas fluorescens* Pf-5	Proteobacteria
	*Mt*DyP	*Mycobacterium tuberculosis*	Actinobacteria
	*Vc*DyP	*Vibrio cholera*	Proteobacteria
	*El*DyP	*Enterobacter lignolyticus*	Proteobacteria
C	DyP2	*Amycolatopsis species* 75iv2	Proteobacteria
	AnaPX(*Ana*DyP)	*Anabaena species* PCC7120	Cyanobacteria
	*Sa*DyP2	*Streptomyces avermitilis*	Actinobacteria
D	DyP(*Bad*DyP)	*Bjerkandera adusta* Dec1	Basidiomycota
	*Aau*DyP I (AjP I)	*Auricularia auricular-judae*	Basidiomycota
	*Aau*DyP II (AjP II)	*Auricularia auricular-judae*	Basidiomycota
	MsP1 (*Msc*DyP1)	*Mycetinis scorodonius*	Basidiomycota
	MsP2 (*Msc*DyP2)	*Mycetinis scorodonius*	Basidiomycota
	TAP (*Tal*DyP)	*Termitomyces albuminosus*	Basidiomycota
	Pleos-DyP1	*Pleurotus ostreatus*	Basidiomycota
	Pleos-DyP2	*Pleurotus ostreatus*	Basidiomycota
	*Egl*DyP	*Exidia glandulosa*	Basidiomycota
	I. lacteus DyP	*Irpex lacteus*	Basidiomycota

1.2.3 Biochemical properties of DyP

1.2.3.1 UV-Vis spectra, heme content and Rz value

UV-Vis absorption spectroscopy is one of the most important and common techniques employed in the study of heme enzymes. Similar to other peroxidases, UV-Vis spectrum of DyPs contains several characteristic absorption peaks corresponding to the heme (Fig. 1.2) which range from near UV to visible region. This makes heme enzymes and their intermediates highly

colored and convenient to study. The porphyrin ring is a highly conjugated 18 π electron system and reveals two distinct peaks arising from π→π* transition. The orbitals of porphyrin system can be depicted in Fig. 1.3. Such system has two HOMOs (a_{1u} and a_{2u} orbitals) and two LUMOs (two degenerate e_g orbitals). One of the transition from the ground state a_{1u} to the e_g excited state ($a_{1u} \rightarrow e_g$) is of higher energy and gives rise to the Soret band or B band at 390 to 440 nm. The other transitions, a_{2u} ground state to excited state of e_g ($a_{2u} \rightarrow e_g$) forms an α band and a_{2u} ground state to vibrationally excited state e_g ($a_{2u} \rightarrow e_g$) forms a β band (Fig. 1.3)[27]. When the porphyrin is not coordinated to any metal ion, all these transitions appear as four peaks, I, II, III and IV between 500 and 700 nm. These bands are collectively called Q bands and are responsible for the red color of heme[28]. When the porphyrin is coordinated to a metal ion, higher D_{4h} symmetry is acquired and the four aforementioned peaks coalesce into two peaks called α and β bands[29]. Coordination to iron atom gives rise to one additional peak named charge transfer peak which is due to transition of electron from highest energy-filled orbitals of the porphyrin to the lowest energy-unfilled orbitals of the iron. In the resting state, a DyP thus has a soret band around 400 to 410 nm, Q bands between 500 and 600 nm and charge transfer (CT) bands around 630 to 645 nm. When the DyP is reduced by sodium dithionite another peak around 567 nm is formed accompanied by the red shift of the soret band to ~ 430 nm. Formation of compound I can be followed by ~60% decrease of the soret band intensity along with slight blue shift (Fig. 1.4-A). DyP compound II formation can be followed by increase in absorbance around 416 nm together with two characteristic peaks at ~525 and 555 nm (Fig. 1.4-B).

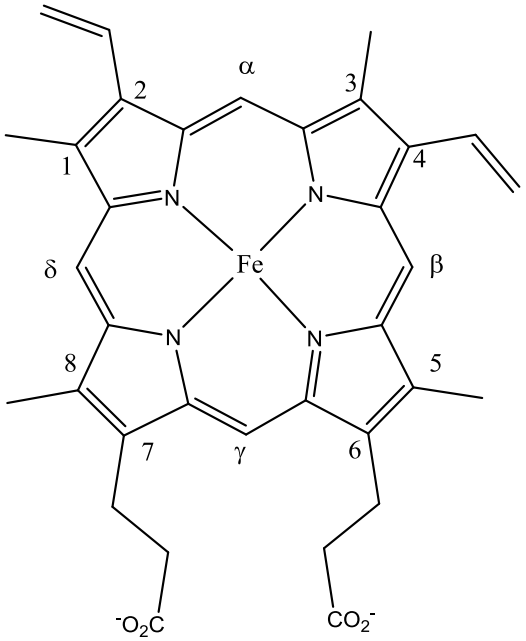

heme *b*

Figure 1.2 Heme *b* showing different edges.

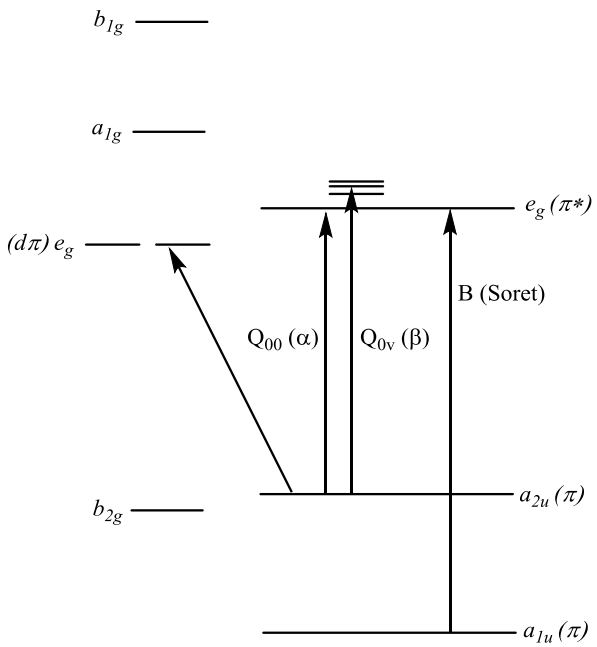

Figure 1.3 Energy levels of iron (left) and porphyrin ring (right) in heme[27].

(adapted from ref [27])

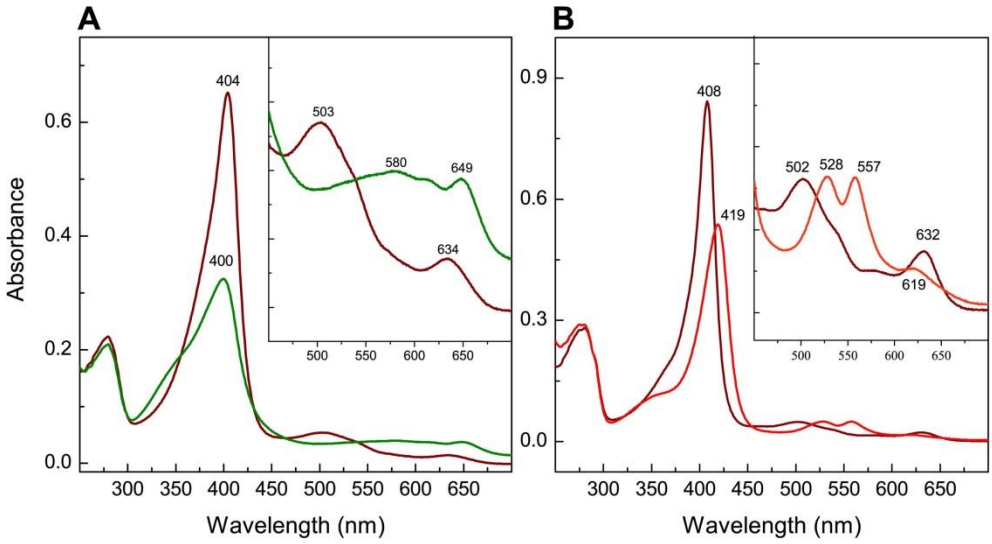

Figure 1.4 UV-vis spectra of DyPs and their intermediates from *R. jostii*.

A. The resting state DyPB (marron-404, 503, 634 nm) and its Compound I (green-400, 580, 649 nm) B. The resting state DyPA (marron-406, 502, 632 nm) and its Compound II (red-419, 528, 557 nm). The inset shows the zoomed portion from 450-700nm[30]. (Reproduced with permission from ref. 30)

Since, heme is essential for the activity of a heme peroxidase it is imperative to know the extent of its loading in these enzymes which can be determined by pyridine hemochromogen method[31]. Reinheitszahl (Rz) value is another parameter frequently used in characterization of heme peroxidases which is the ratio of the absorbance maximum of the soret band to that of 280 nm corresponding to the protein residues (A_{soret}/A_{280nm}). Given the full heme occupancy for a peroxidase, Rz value is an indicator of enzyme purity because the presence of protein impurities increases A_{280nm} and decrease the Rz value[32]. Therefore, Rz value can be used as a way to monitor the degree of heme occupancy assuming a fairly pure peroxidase is obtained.

1.2.3.2 Effect of pH and pI

DyPs are very acidic proteins with an isoelectronic point (pI) ranging from 3 to 4. For example, AnaPX, Msp1, Msp2, and *Bad*DyP have pI values at 3.7, 3.1, 3.7 and 3.8 respectively[17, 33-34], indicating that these enzymes bear net negative charges at physiological pH. Moreover, the pH optimum for DyP activity is also significantly acidic ranging between pH 3

and 4.5 which has been partially attributed to catalytic distal Asp residue (pKa 3.7)[35]. The relationship of pH and DyP stability has also been studied. For instance, AnaPX, a class-C DyP with an optimal pH at 4.0, showed maximal stability between pH 3.5 and 9.5 with the retention of 90-100% residual[33]. A fungal *Aau*DyPI was stable even at pH as low as 2.5 as incubation of this enzyme at pH 2.5 for 4 hrs at 20^{o}C did not result in any diminished activity. *Aau*DyPII from the same fungus was less stable but still retaining ~60% residual activity under the same condition. Such impressive acidic pH stability could be the result of adaptation of these types of wood rotting fungi and the secretory enzymes thereof essential for depolymerization of lignin in wood, as the wood itself has the pH between 3 and 6[36]. Another DyP well characterized for the effect of pH on enzyme stability is the fungal DyP from *Irpex lacteus* (*I. lacteus*DyP) which has demonstrated remarkable stability at a wide pH range. When *I. lacteus*DyP, which has a pH optimum at 3.0, was kept at 4^{o}C for 1 week at pH 2 to 9, only ~30% loss in activity was observed except for pH 9 where the loss was 80%. Under the same condition but at 25^{o}C more than 50% residual activity was still maintained between pH 3 and 7[37].

1.2.3.3 Effect of temperature

The optimum temperature for the reported DyPs lies between 25 to 40^{o}C and they are thermostable up to ~50^{o}C. AnaPX, which has an optimum temperature at 35^{o}C, showed 60 and 15% residual activities when equilibrated for 1 hr. at 50 and 60^{o}C respectively[33]. The *Tfu*DyP (opt. temp. 25^{o}C and opt. pH 3.5) from thermophilic bacteria *Thermobifida fusca* showed 50% decrease in activity when equilibrated at 60^{o}C for 2 hrs[38]. Fungal DyPs also offer some remarkable thermostability as observed in the cases of *Bad*DyP and *I. lacteus*DyP. *Bad*DyP has an optimum temperature at 30^{o}C and was found very thermostable, as the incubation of the enzyme at 50^{o}C for 11 hrs caused only ~30% decrease in activity. Such extra thermostability of

*Bad*DyP was attributed to heavy glycosylation or high thermal reversibility of the enzyme[17]. Likewise, *I. lacteus*DyP, displayed 50% of residual activity even after 8 hrs of incubation at 50^{o}C at pHs 4 and 5[37].

1.2.3.4 Oxidation and spin states of heme iron

The heme iron in resting state DyP is exclusively in ferric (Fe^{3+}) form which could be either in high spin (HS), low spin (LS) or quantum mechanically mixed spin (QS) states. Their relative population is highly influenced by the temperature, pH and heme microenvironment. With the increase in pH the HS ferric heme transitions into LS heme, as seen in Arg232Leu mutant of DyPB[39]. Knowledge of the spin state of heme iron is essential since it is an important factor that modulates the reactivity of the heme center and its redox potential. EPR can give some information on the spin states, for example, the rhombically distorted EPR signal of DyPB suggested the presence of high spin (HS) ferric enzyme in the resting state. While in DyPA, EPR with rhombic symmetry indicated the co-presence of low spin (LS) ferric heme in addition to HS ones[40]. RR spectroscopy is more powerful technique that can measure oxidation state and coordination number of heme iron together with its spin state. Sezer and co-workers carried out the detailed RR study of class-A *Bs*DyP and class-B *Pp*DyP which revealed the presence of multiple spin states at room temperature and pH 7.6[41].

1.2.3.5 Redox potential

Redox potential is the direct measure of substrate oxidizing power of peroxidase and whether a substrate can be oxidized or not depends on the redox potentials of both substrate and the oxidizing enzyme. Besides redox potential, however, heme core topology, substrate accessibility, and other factors also influence overall reactivity of peroxidases. The redox couples of a typical peroxidase include Fe^{3+}/Fe^{2+}, Compound I/Fe^{3+}, Compound II/Compound I and

Compound II/Fe^{3+}. The redox potential of later two modulates the oxidizing ability of the given peroxidase, however, to generate these intermediates a resting enzyme with stable Fe^{3+} heme is required which inturn is determined by the redox potential of Fe^{3+}/Fe^{2+} couple[42-43]. The measurement of redox potential of the redox couple involving Compound I and Compound II is more challenging due to their transient nature and high reactivity compared to more amenable Fe^{3+}/Fe^{2+} couple. So, whenever DyP redox potentials are reported in literature these are majorly for the Fe^{3+}/Fe^{2+} with few other reports of additional redox couples.

The redox potential of a heme enzyme is very sensitive to heme microenvironment and is dependent up on several factors such as pH, temperature, charge distribution and so on. However, one of the most obvious factors is the anionic nature of proximal heme ligand. This proximal ligand could either be histidine as in classical peroxidases or cystine as in CPO. The distal histidine ligand is hydrogen bonded to evolutionarily conserved acid residues Asp or Glu which reduces the positive charge density on imidazole side chain of His and imparts it an imidazolate character[42]. DyP is no different to this remarkably conserved Asp-His-[Fe^{3+}]Heme motif with a very rare exception of Glu replacing Asp in some of the members as in *Bad*DyP[44]. The higher the imidazolate character of distal His, higher is the preference for Fe^{3+} over Fe^{2+} and hence lower is the redox potential value of Fe^{3+}/Fe^{2+} redox couple[42]. The redox potentials among DyPs vary by as much as 250 mV, for instance from -40 mV in *Bs*DyP to -290 mV in *El*DyP[41, 45]. In comparison, other peroxidases vary from +21 mV in MPO to -266 mV of HRP[42]. Acidic pH increases the redox potential of Fe^{3+}/Fe^{2+} redox couple and correspondingly that of Compound I/Compound II and Compound II/Fe^{3+} couples. This is suggested to be due to the protonation of proximal Asp that weakens the H-bond to proximal His and reduces its the imidazolate character[46]. Hence, as will be discussed later, this phenomenon has remarkable

significance in the reactivity of peroxidases and their acidic pH optimum. Huge effect of electrostatic environment of heme pocket on redox potential was also demonstrated by mutational experiments.

As mentioned above, it is difficult to measure the redox potential of the redox couples involving Compound I and Compound II. However, there are some indirect approaches used in figuring out such values. For example, Ayala et al., developed a method for estimation of Compound II/Fe^{3+} redox potential by using catalytic approach based on Marcus theory of outer-sphere electron transfer. According to the Marcus theory, rate of electron transfer is semilogarithmatically proportional to the thermodynamic driving force[47], or in other words, the rate of oxidation (k_{cat}) of a substrate by Compound II, which being the rate limiting step, is directly proportional to the difference in redox potential of the substrate and the couple Compound II/Fe^{3+}. As a result, linear correlation can be achieved when the peroxidase activity is plotted against the redox potentials of different phenolic compounds that eventually gives the estimation of Compound II/Fe^{3+} redox potential. The redox potential of 0.89 and 0.98 V estimated in this way for HRP and LPO respectively were in close agreement with the values of 0.9 and 1.04 V respectively determined by other spectroscopic means[48]. Liers et al., determined the redox potential of Compound II/Fe^{3+} couple in some fungal DyPs using this 'phenol oxidation' method. The estimated redox potentials of reference peroxidases CiP (0.93 V) and SBP (1.06 V) were comparable to two different sets of independently reported values. The results showed that the redox potential of fungal DyPs are very high (1.09 to 1.26 V), higher than that of CiP and SBP, and only slightly less than class II LiP[49].

In a different approach, Mendes and co-workers reported the redox potential of Compound I/Fe^{3+} couple for *Pp*DyP from transient-state measurement of Compound I formation

from the native ferric state. In this method, they determined the corresponding equilibrium concentrations of Compound I and native ferric state enzyme at each increasing initial concentration of H_2O_2. The equilibrium constant (K_{eq}), calculated using Furtmüller equation finally gives the redox potential value. The redox potential determined in this way for the Compound I/Fe^{3+} redox couple of *PpD*yP was 1.10 V at pH 7.0[50] very close to the redox potential value of Compound II/Fe^{3+} couple for fungal peroxidases ranging, generally assumed as being similar in range as Compound I/Fe^{3+}, from 1.1 to 1.2 V[49] In addition, this value was closer to that of mammalian peroxidases, like EPO (1.1 V)[51] MPO (1.16 V)[51-52]and LPO (1.09 V)[53] and was ~0.2 V higher than that of APX[54] CcP[55] ARP[56]and HRP[42]. Since Compound I is directly involved in the oxidation of the substrate, the redox potential value of Compound I/Fe^{3+} reflects the oxidizing power of the enzyme.

However, the higher redox potential of the Fe^{3+}/Fe^{2+} couple does not necessarily correlate to the higher activity of the peroxidase. A very good example of this is *Bs*DyP which has the most positive redox potential value of -40 mV among all DyPs. However, the activity of *Bs*DyP with various substrates is significantly lower than the DyP of lower redox potential. Hence, several other factors, such as constricted heme access channel as seen in some A-type DyPs, might be in play when it comes to modulating the overall activity of peroxidase[41].

1.2.4 Structure of DyP

1.2.4.1 Tertiary structure

DyPs are globular to roughly cylindrical proteins with unique protein scaffold. The primary amino acid sequences and the tertiary structures of DyPs are much different from classical peroxidases. Unlike the plant and animal peroxidases which are predominantly α helical

in their framework (Fig. 1.5 & 1.6), DyPs are characterized by the presence of both α helices and β sheets (Fig. 1.6)[44]. Further, DyPs are characterized by two major domains, N- and C-terminal domains and each domain has four anti-parallel β sheets (β1 and β4, β2 and β3) sandwiched between two α helices (α3 and α8) forming ferredoxin like fold as shown in Fig. 1.6[44]. For this reason, DyPs have been classified as dimeric α + β barrel family in the SCOPE database. Although such tertiary structure is highly conserved among all DyP classes the primary sequence identity among different classes of DyPs is at most 16% (Fig. 1.7)[57].

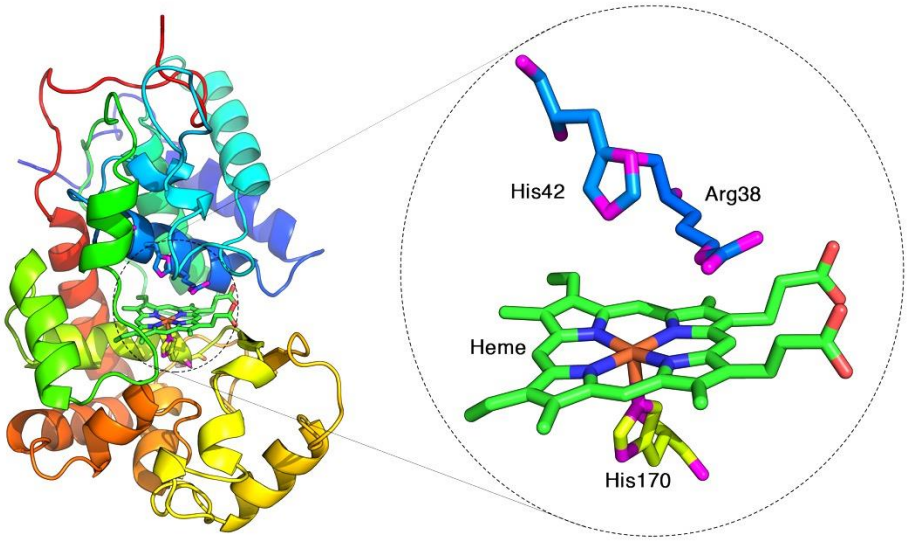

Figure 1.5 Structure of HRP showing chiefly α helices.

The zoomed in portion on the right shows the catalytic center with heme ligated by proximal His ligand and the distal catalytic His and Arg residues. [PDB accession code: 1ATJ]

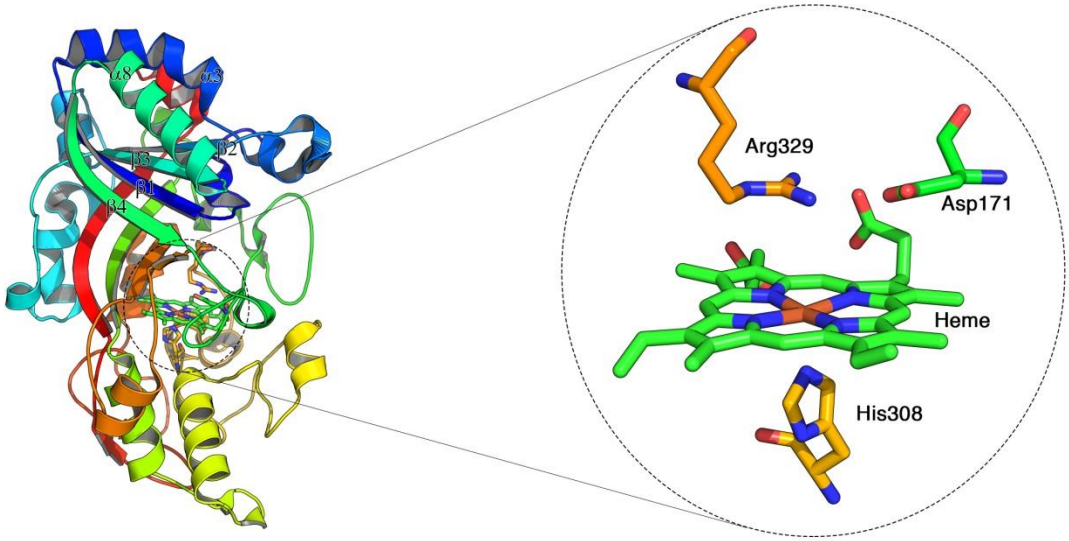

Figure 1.6 Structure of *Bad*DyP showing α helices and β sheets forming ferredoxin like fold.

The zoomed in picture on the right shows the heme catalytic center with proximal His ligand and distal catalytic Asp and Arg residues. [PDB accession code: 3AFV]

Classes-A and -D DyPs are respectively periplasmic and extracellular enzymes characterized by N-terminal pro-sequence or signal peptide sequence for their secretions outside of the cytoplasm. In class-A DyPs such signal peptide is characterized by presence of two consecutive arginines and hence called 'Twin Arginine Translocation' or TAT signal peptide. EfeB or YcdB from *E. coli* was the first heme peroxidase discovered to have 35 residues long translocation system[21]. Similarly, the pro-sequence in class-D DyP, however not a TAT system, are about 55 (as in TAP) to 63 (as in *Mep*DyP) residues long[57]. These pro-sequences or signal peptides undergo post translational modification where these are cleaved once the proteins are delivered to their final locations[21]. The remaining classes-B and -C DyPs are cytoplasmic in origin and hence are devoid of such prosequences. Interestingly however, downstream of the genes encoding *dyp* in the operon of some B-class DyPs have genes encoding C-terminal extension sequence followed by the gene encoding encapsulin. Encapsulin is a protein shell

nanocompartment that encloses the enzymes significant in certain biochemical pathways and offers protection and assistance in the transportation of the 'cargo' enzymes. DyPB complexed with such encapsulin was found in extracellular extract despite its cytoplasmic origin and absence of signal peptide sequence[58]. The icosahedral encapsulin from *B. linens* was also found to enclose an oligomeric (trimer of dimer) *Bl*DyP[59]. Similarly, such encapsulin was also reported in *M. tuberculosis* that enclosed *Mt*DyP. Hence, it is highly likely that these enzymes contribute to the virulence factor of *M. tuberculosis* by counteracting oxidative stress brought upon by the reactive oxygen species (ROS). Consequently, the 'encapsulin-cargo enzyme' systems could serve as the novel drug target in curing the diseases caused by the pathogenic bacteria that are continuously evolving in becoming drug resistant[60].

Classes-C and -D DyPs are the bulkiest enzymes comprising about 450 to 500 amino acid residues followed by class-A DyPs which have about 400 residues. Class-B DyPs are the most compact ones with only about 300 residues (Fig. 1.7). There has been no report yet of any inter or intra-subunit disulfide bridges in DyPs except for AnaPX where the 3-D structure revealed that two dimers are linked via Cys224-Cys224 disulfide bond forming a tetramer of dimer[61]. Only class-D DyPs, due to their fungal origin, are glycosylated and the glycosylations observed are majorly spread out along the lower proximal region relative to heme which are exclusively Asn-N-glycosylation with N-acetylglucosamine linkage[62-63].

Class-D type DyPs are mostly monomeric, while the classes-A, B and C DyPs shows various higher oligomeric forms. Class-A DyPs are mostly dimeric and class-B DyPs varies from dimeric as in TyrA[64] and *Vc*DyP[65] to hexameric (trimer of dimer) as in *Bt*DyP[66]. The crystal structure of class-C DyP2 showed that it is a dimer, however the dimeric association was considered an artifact induced by crystallization conditions and suggested that its native state

should be monomeric[67]. AnaPX, an another class-C DyP on the other hand, is a tetramer formed by the association of two dimeric units[33]. It has been suggested that, the lack of higher oligomerization in fungal DyPs is the result of the dimer interface being unfavorable for association due to the insertion of extra loops inherent in such bulky DyPs, which otherwise are minimal in other DyP classes[64]. Heme incorporation also seemed to have an important influence in the oligomeric state of DyP. For instance, EfeB, *Mt*DyP and DyP2 existed as monomer in their inactive apo forms but as dimer, tetramer and tetramer to hexamer in their holo forms respectively[60, 67-68].

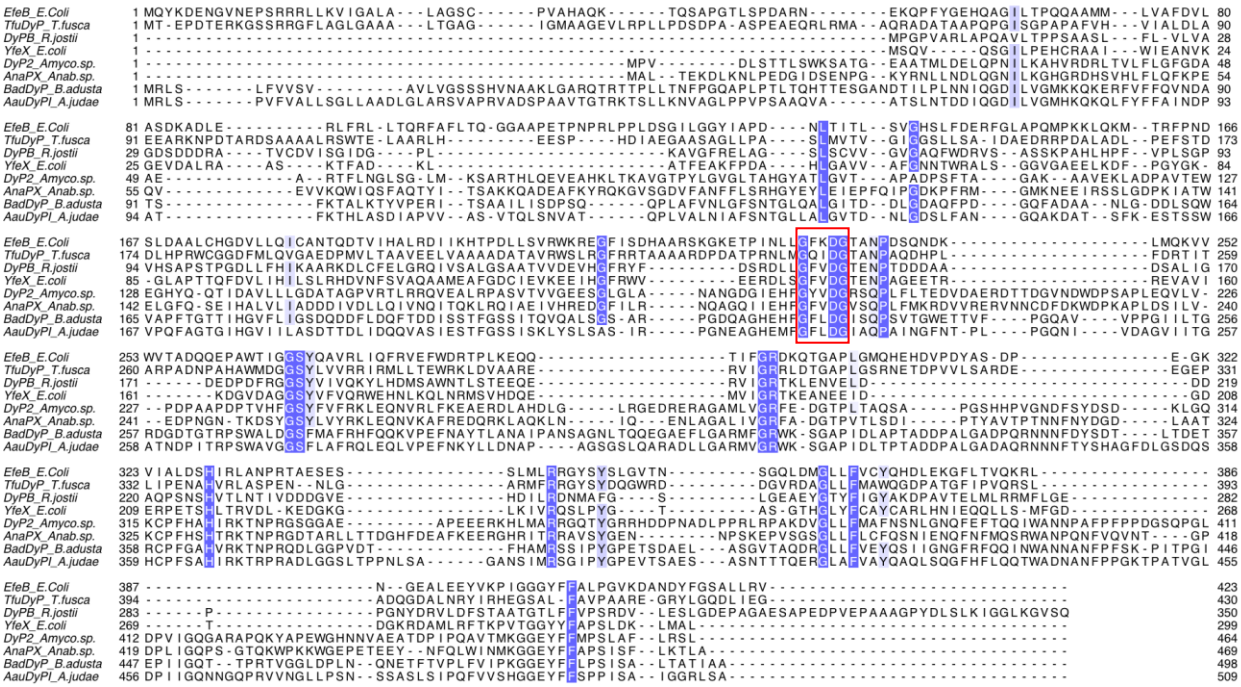

Figure 1.7 Sequence alignment of DyPs from all four classes.

Highly conserved residues are highlighted with dark blue and less conserved ones with lighter shades of blue. The finger print GXXDG motif of DyP is boxed in red.

1.2.4.2 Heme core and catalytic residues

The heme molecule in DyP is usually found buried in the hydrophobic crevice formed by the ferredoxin like fold of C-terminal domain (Fig. 1.6)[66]. The heme molecule in DyP is heme *b*

and consists of the protoporphyrin IX (PPIX) ring with ferric iron at the center, tetra coordinated to four pyrrole rings (Fig. 1.2). Comparison of different DyP structures show that the heme molecule preserve the same conformation and the residues associated in the heme binding motif are highly conserved[68]. While it is the same heme *b* that is found in all plant peroxidases, the conformation of heme in DyP is different than that of other peroxidases. In plant peroxidases, the two propionate groups at pyrrole rings C and D of heme are parallel but in DyP while the propionate on pyrrole D preserves similar conformation, the propionate on pyrrole C is twisted out of plane by ~90^{o}[64]. This unusual conformation of propionate C is due to the strong H-bonding interactions of the propionate with protein backbone[62]. A highly conserved histidine residue in the proximal side acts as the fifth ligand which is coordinated perpendicularly at a distance of ~1.9-2.2 Å from the heme iron. This proximal His ligand responsible for holding the heme in position is located in the C-terminal region of DyP, as opposed to the central location in other peroxidases[8]. The sixth co-ordination site on the distal face is either vacant or occupied by the solvent molecule (H_2O) which is replaced by H_2O_2 during the catalytic cycle[63]. In DyP2 and *Aau*DyPI, although the sixth ligand sites are occupied by a water molecule, they are at the distance of 3.8 and 3.11 Å from the heme iron which is too long for a co-ordination bond[62, 67]. While in DyPB and *Bad*DyP they are closer at the distance of ~2.1 Å in both, and in EfeB at 2.3 Å[44, 69]. Two catalytic residues on the distal surface are also highly conserved among different classes of DyPs. These two residues are aspartate and arginine. The highly conserved Asp acts as a general acid base catalyst that helps in transfer of a proton from proximal oxygen atom to the distal oxygen atom of H_2O_2 during the formation of Compound I[19]. This Asp residue is also a part of the GXXDG motif (Fig. 1.7) which is found in all class members of DyP family. One of the striking differences between the conventional peroxidases and DyP is the highly conserved distal

His acting as the general acid base catalyst in the former. Meaning, DyPs lack distal His residue which otherwise is highly conserved among other classical peroxidases and replaced by Asp instead. CPO, on the other hand, has glutamic acid as the catalytic residue and in this respect DyP resembles more closely to CPO than other peroxidases[70]. Arg is absolutely conserved in all families of peroxidases including DyP and is termed 'essential' Arg which plays the role of stabilizing the negative charge during the formation of compound I through H-bonding. In DyPs, this Arg is located in the C-terminal region while in other peroxidases it is located in the N-terminal section, for example Arg329 of *Bad*DyP vs. Arg38 or HRP[44, 71].

1.2.4.3 Heme access channels and substrate binding site

The distal side of heme in DyP comprises a space carved out by heme plane and distal residues where almost all of the redox chemistry takes place. From this distal side cavity a channel leads to the exterior of protein and most likely serves as the heme access channel for H_2O_2. This channel is ~3-4 Å wide and shaped more-or-less like a funnel (Fig. 1.8), and is mostly lined with hydrophobic residues and with hydrophilic residues at the channel entrance. H_2O_2, having O-O bond distance of 1.49 Å, most likely reaches the distal cavity through this channel, however, it is unlikely that large substrate like dye molecules can pass through this channel. A second heme access channel also has been reported for several DyPs which leads to the heme propionate group and with the diameter of ~ 6.0 and 7.5 Å in DyPB and *Vc*DyP respectively. This channel has been proposed as the most likely binding site for reducing substrates where the most direct electron transfer can take place between porphyrin radical and substrate via the heme propionate group. This hypothesis was supported by co-crystallization of *Bad*DyP with ascorbic acid and 2,6-dimethoxy phenol (DMP) where substrate molecules were

located very close, at a distance of 5.4 Å, to the heme 6-propionate group and H-bonded with each other via intermediary residue Asn313[72].

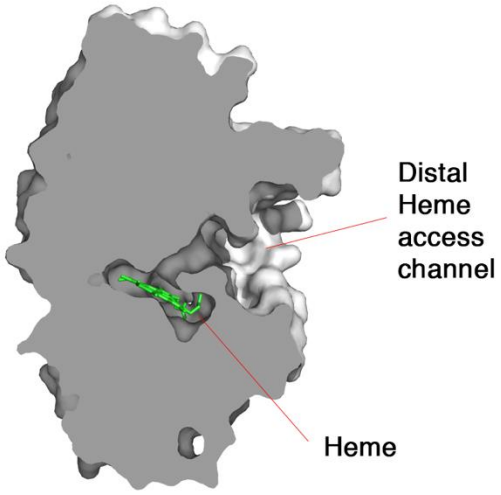

Figure 1.8 Structure of *Bad*DyP showing distal heme access channel
[PDB accession code : 3AFV]

Another substrate binding site reported for DyP is for Mn^{2+} binding, as in DyPB and DyP2. The potential Mn^{2+} binding site in DyPB comprised of Glu156, Glu239 and heme propionate-D besides nearby Asp241 and Glu215[40]. Co-crystallization of Mn^{2+} with Asn246Ala variant of DyPB showed the acid residues formed the second co-ordination sphere with the first co-ordination shell occupied by water molecules at a distance between 1.8 and 2.4 Å[73]. In DyP2, the Mn^{2+} binding site was unusual and was bound at ~15Å from the heme center. Mn^{2+} was held in place by coordination to the acid residues like Glu258, Glu273 and Glu284 and a water molecule where Tyr188 was proposed as the intermediary residue assisting in electron transfer between heme and Mn^{2+}[67].

1.2.5 Functions of DyP

DyP was first discovered as the peroxidase capable of decolorizing anthraquinone based dyes, however, such dyes are xenobiotic and are not the real natural substrates of DyP. Although, it has been proposed that DyP might play a protective role, especially in fungi where it is secreted as an extracellular enzyme, by decomposing toxic xenobiotic compounds, the physiological substrate of DyP has not been identified yet and its biological function is still unclear[35]. Nonetheless, there have been some attempts aimed at unraveling the physiological role of DyP. The most commonly cited example of this is the deferrochelatase activity of two DyP paralogs EfeB and YcdB from *E. coli*[74]. The novel deferrochelatase activity corresponds to the retrieval of the heme iron without causing the disruption of the porphyrin ring[74]. However, this notion has been challenged and porphyrinogen oxidase function has been proposed instead[75]. Thus, the function of YfeX or EfeB has not been defined with certainty.

The close association of genes encoding DyP with the genes encoding enzymes of known function could provide some clues to other possible physiological functions of DyP. For example, the *auk2* gene encoding an class-A DyP, but yet uncharacterized, from *Actinoplanes sp.* ATCC 53533 has been found as a part of a biosynthetic cluster involved in the sulfated glycopeptide synthesis[76]. TyrA, a class-B DyP from *Shewanella oneidensis* has been annotated as the putative enzyme involved in melanin biosynthesis, although the physiological substrate is again unconfirmed[64]. DyPB has been described, in addition to having Mn^{2+} oxidation activity, as bacterial equivalent of fungal lignin peroxidase capable of degrading lignin, however, such function might not be physiologically relevant since the activity towards such substrates are very low compared to fungal peroxidases[77]. C type DyPs, the most potent bacterial DyPs, have shown some remarkable activities on par with fungal peroxidases and it is highly likely that such

functions might be physiologically pertinent[33,67]. Moreover, genes encoding the class-C DyPs have been reported in number of different biological functions[19]. For example, *dyp* gene is found in association with the genes encoding halo-acid dehalogenase and methyl-accepting chemoreceptor in *Rhizobium leguminosarum*[78], the gene encoding a DeoR transcriptional regulator in *Amycolatopsis orientalis*[79], and doxorubicin resistant gene cluster in *Saccharothrix espanaensis*[80]. Thus, based on above observations, depending upon their type or class, DyPs are most likely involved in more than one type of functions in the biological system.

1.3 Catalytic cycle of DyP

Though peroxidases take part in a strikingly diverse array of biological redox chemistry and vary remarkably in their functions, they all have uniting features regarding the reactive intermediates in a highly conserved catalytic cycle. A general peroxidase cycle can be summarized as shown in scheme 1.1:

Scheme 1.1 Catalytic cycle of DyP

Resting enzyme + H_2O_2→ Compound 0 → Compound I + H_2O

Compound I + AH_2 → Compound II + AH ·

Compound II + AH_2 → Resting enzyme + AH ·+ H_2O

Overall:

$2AH_2 + H_2O_2 \rightarrow 2AH\cdot + 2H_2O$

Where, AH_2 represents a reducing substrate.

1.3.1 Mechanism of compound I formation

The mechanism of Compound I formation proposed first by Poulos and Kraut based on CcP[81] has proved useful for long period of time and has been used to describe the phenomenon of Compound I formation in other classes of peroxidases as well[6]. The first step of Compound I formation involves abstraction of the proton from H_2O_2 by the ionizable group in the resting

enzyme, distal His in classical peroxidase or Asp in DyP, acting as a general base. The α oxygen (or the proximal oxygen atom of H_2O_2 closest to Fe^{3+}) then binds to the Fe^{3+} forming a complex termed 'Compound 0'. This step of formation of Compound 0 is reversible and the rate of its formation decreases at pH below the pKa of the ionizable residue since at such pH the ionizable residue is protonated and hence would have lesser tendency to act as a general base. The next step involves the flow of electrons from the porphyrin ring and Fe^{3+} toward the α oxygen and the double bond is formed between Fe and α oxygen. During the process, Fe^{3+} is oxidized to Fe^{4+} forming oxo-ferryl species Fe^{4+}=O and porphyrin π-cation radical, and the heterolytic fission of O_α–O_β bond takes place. In the transient state OH^- starts leaving and the transient negative charge is stabilized by nearby catalytic Arg residue. Finally, the OH^- accepts the proton from the distal ionizable group, now serving as a general acid, and leaves as H_2O forming Compound I[6]. This whole process is summarized in Fig. 1.9. Compound I thus formed is a cation radical which is two reducing equivalents more oxidized than the resting ferric enzyme. One of the reducing equivalents resides in the Fe^{4+} and the other in the tetrapyrrole ring or protein residue. Compound I upon gaining an electron from a substrate forms compound II which still is an oxo-ferryl species but differs in lacking the cation radical. Compound II can further gain another electron from the second substrate eventually restoring the resting ferric enzyme and thus completing the catalytic cycle. However, the formation of both compound I and compound II has not always been observed in all types of DyPs[30].

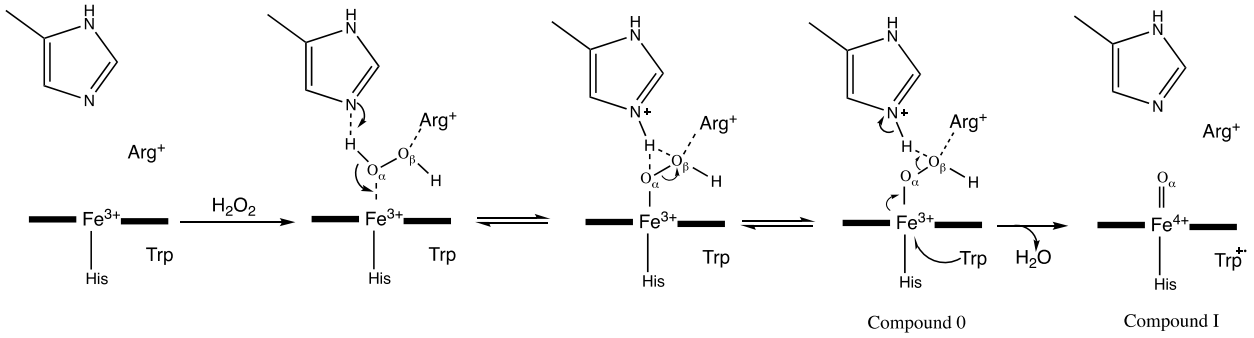

Figure 1.9 Mechanism of compound 0 and compound I formation in CcP[15].
(Adapted from ref. 15)

1.3.2 Protein radicals

Compound I thus formed can have the radical located either at the porphyrin ring or at one of the protein residue side chains. While most of the plant peroxidases have the radical located in the porphyrin ring, some like CcP has radical located at Trp191[82] including Class II peroxidases with the second oxidizing equivalent residing in nearby Trp or Tyr residue[83]. UV-Vis spectrum of Compound I with porphyrin π cation radical has hypochromic soret band and most of the time slightly blue shifted compared to resting state enzyme. On the other hand, the spectrum of Compound I protein radical is very similar to that of Compound II characterized by hyperchromic red shifted soret band. This is because the radical located on protein side chain has little to no interference on the heme chromophore and would essentially yield the spectrum similar to the oxo ferryl species without radical cation or Compound II[6]. Aromatic side chains in Tyr (phenol) and Trp (Indole) are easy to oxidize and are an attractive destination for cation radical. DyPs are rich in such residues, for example, Class-D type DyPs on average have 8.8 Tyr and 5.7 Trp per enzyme molecule[84]. Thus, it comes as no surprise that Compound I in DyPs are protein radical, at least more common than porphyrin radical if not entirely. For example, *Bs*DyP shows the H_2O_2 independent formation of Compound II like species[85-86]. Another direct evidence

of protein radical in Compound I can be gained from EPR spectroscopy as EPR spectrum of Compound I with porphyrin radical is different from that of Compound I with the protein radical. Protein radicals are important since they can bring about the oxidation of bulkier substrates that cannot access heme. In *Aau*DyP, Tyr337 was identified as surface exposed radical and substrate oxidation site[62]. However, later studies revealed that Trp377 might be involved as the radical site instead[87]. In *Vc*DyP, Tyr129 and Tyr235 were identified as the surface radical site essential for RB19 activity at acidic pH[65].

1.4 DyP kinetics with reducing substrates

1.4.1 Dyes

1.4.1.1 Anthraquinone (AQ) dyes

Majority of synthetic dyes used in textile and other industries worldwide include azo dyes and anthraquinone (AQ) dyes. About 10 to 15 % of such dyes are discharged in to the industrial effluent and pose a serious environmental threat[88]. Even such that, some dyes and their degradation products are potentially carcinogenic[89]. The physico-chemical methods used to treat the dye waste water use hazardous chemical additives and produce massive bulk of sludge, managing which becomes another problem[90]. In lieu of such crisis, an environment friendly approach using enzyme catalyzed dye degradation has gained much attention. Lignolytic enzymes like LiP[91-93], MnP[94-95] and VP[96] have been reported to decolorize azo dyes, however, these enzymes are unreactive towards AQ dyes. DyPs, as stated earlier, get their name because of their ability to degrade these xenobiotic AQ based dyes in the absence of mediators. Reactive Blue 4 (RB4), Reactive Blue 5 (RB5) and Reactive Blue 19 (RB19) being the most commonly studied dye substrates among the long list of AQ dyes. And since these dyes are resistant to

chemical oxidation due to high resonance stabilization offered by aromatic anthracene-9,10-dione motif and were previously not known to be decolorized by classical peroxidases, the discovery of the novel enzyme capable of degrading such dyes was certainly intriguing. But on the contrary, DyPs perform poorly towards azo dyes like Reactive Black 5 (RBlk5), which otherwise makes a good substrate for other peroxidases like versatile peroxidase (VP). The reactivity towards such dyes varies among different classes of DyPs (Table 1.2) with classes-C and -D being the most active with the catalytic efficiency as high as 10^5 to 10^7 $M^{-1}s^{-1}$ followed by class-A in the range 10^4 to 10^6 $M^{-1}s^{-1}$. Class-B DyPs seems to be the least reactive towards AQ dyes which spans from 10^2 to 10^5 $M^{-1}s^{-1}$. Table 1.2 summarizes the activity of different DyPs towards various AQ dyes. The structures of some of the most commonly used dye substrates are shown in Fig. 1.10.

Table 1.2 Activity of various DyPs against common AQ dyes.

Enzyme	Variant	Dye	pH	k_{cat} s^{-1}	K_m µM	k_{cat}/K_m $M^{-1}s^{-1}$	Vmax U/mg	Ref
*Tfu*DyP	wt	RB19	3.5	10	29	3.5×10^5	4.3	38
DyPA	wt	RB4	4.5	13	1000	1.3×10^4		40
*Bs*DyP	wt	RB5	4.0	7.9	157	5.0×10^4	11	97
		RB19	3.0				11.55	98
		RB4	3.0	110	170	6.5×10^5		
		RB5	3.0	29	43	6.6×10^5		
DyPA	wt	RB4	5.5	1.90	210	9.0×10^3		99
TyrA	wt	RB5	3.2	5.9	84	7.0×10^4		64
DyPPa	wt	RB5	3.5	0.02	107	2.2×10^2		100
*Pp*DyP	wt	RB5	5.0	8.0	40	2.0×10^5	15	97
DyPB	wt	RB4	4.5	0.05	350	1.4×10^2		40
*Vc*DyP	wt	RB19	4.0	1.3	50	2.6×10^4		65
DyP1B	wt	RB4	5.5	1.04	120	9.0×10^3		99
DyP2B	wt			N.D.	N.D.	N.D.		
DyP2	wt	RB5	4.5	34	48	7.1×10^5		67
AnaPX	wt	RB4	4.0				167	33, 101
		RB5		384 (384)	3.6 (5.8)	1.2×10^7 (6.6×10^6)	282	
	D204H	RB5					17	
	wt	RB19					401	
		RB114					491	
*Sa*DyP2	wt	RB19	4.0				0.15	101
		AB324*	4.5	0.8	61	1.2×10^4	0.9	
*Bad*DyP	wt	RB5	3.2	260	54	4.8×10^6		17, 61

				(260)	(26)	(1.0×10^7)		
		RB19		980	80	1.2×10^7		
*Aau*DyPI	wt	RB5	3.0	114	23	5.0×10^6	134	36
		RB19	3.5	224	90	2.5×10^6		
		RBlk5	3.0	4.8	15.6	3.1×10^5	3	
*Aau*DyPII	wt	RB5	3.0	256.0	15	1.7×10^7	375	
*I.lacteus*DyP	wt	RB19	4.0	79.9	13.5	5.9×10^6		37
Pleos-DyP1	wt	RB19	4.0	5.0	45	1.1×10^5		102
Pleos-DyP4			3.5	152	82	1.7×10^6		
HRP	wt	RB5	4.0	140 (140)	58 (36)	2.4×10^6 (3.8×10^6)	28	17

*AB324: Acid Blue 324, an AQ based dye

1.4.1.2 Azo dyes

Azo dye is the major dye used worldwide and is also recalcitrant to degradation due to the presence of its defining 'azo' functional group (R-N=NR′). Although DyPs have low activity towards azo dyes, *Aau*DyPI was found to degrade RBlk5 (Fig. 1.10), with a remarkable efficiency of 5 orders of magnitude, very close to that of Class II plant peroxidases[87]. *Pp*DyP and *Bs*DyP have been tested against another azo dye called mordant black 9 (MB9) in which significant activity was measured with k_{cat} values of 32 and 5 s^{-1} and k_{cat}/K_m values of 5.0×10^4 and 1.0×10^5 $M^{-1}s^{-1}$. The k_{cat} values for *Pp*DyP against MB9 was remarkably higher compared to k_{cat} values of fungal DyPs and VPs for RBlk5 degradation, while that of *Bs*DyP were still similar in the similar range[97]. AnaPX also decolorized azo dyes at rates of 8, 13, 91, and 21 $U.mg^{-1}$ for Reactive Yellow 86, Reactive Red 120, Reactive Green 19, and Reactive Black 5, respectively. Such activity was remarkably increased by 15, 2 and 50 folds in the presence of 40µM syringaldehyde as a mediator for Reactive Red 120, Reactive Green 19, and Reactive Black 5, respectively. Syringaldehyde is phenolic lignin unit and most probably mediates via generation of phenoxy radical[33].

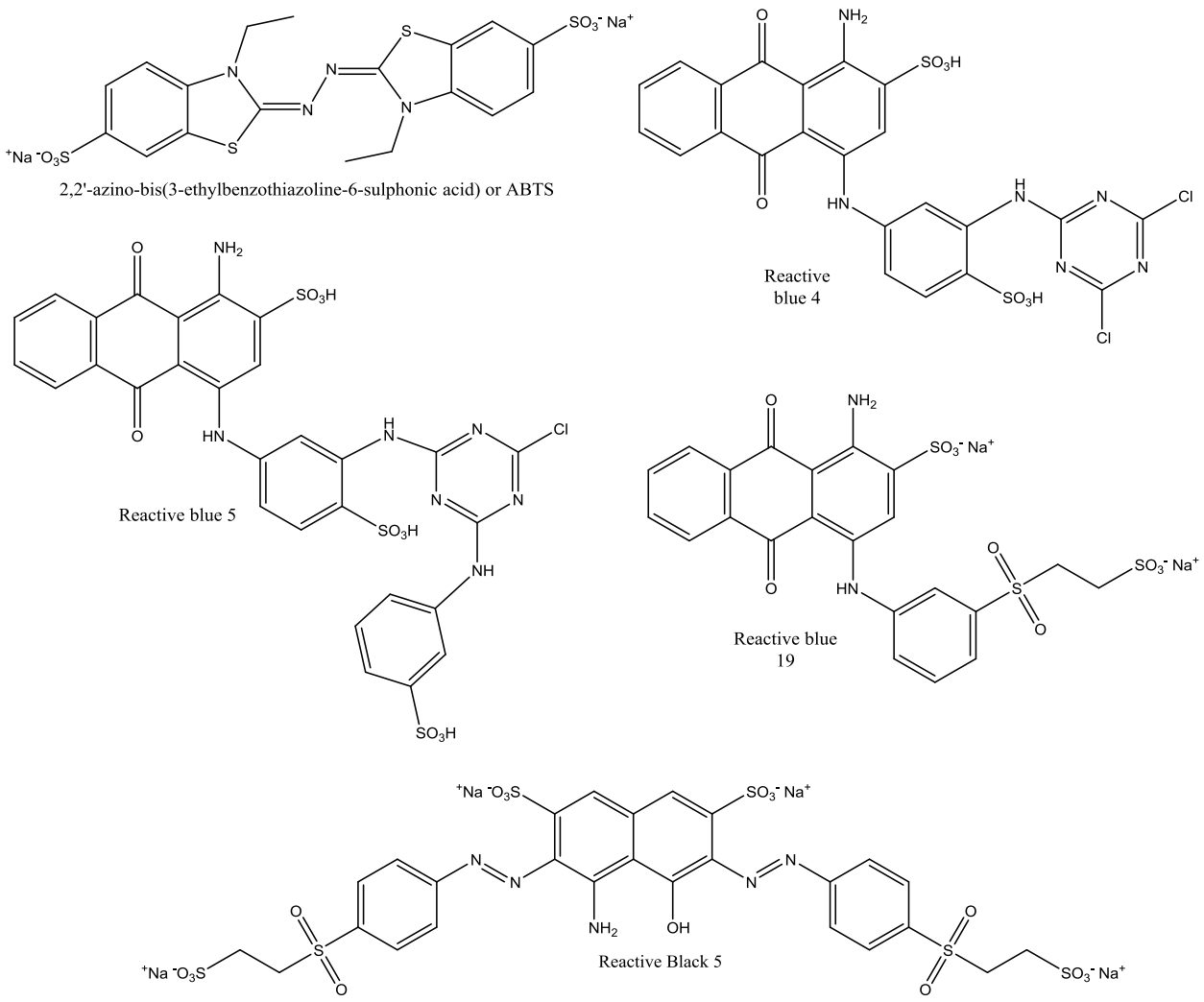

Figure 1.10 Structures of ABTS and some common AQ and azo dyes used in DyP assays

1.4.2 ABTS

2,2'-Azino-di-(3-ethyl-benzthiazoline-6-sulphonic acid) or ABTS (Fig. 1.10) is the generic peroxidase substrate being used most commonly, for more than four decades, to study the catalytic properties of peroxidases. Its use in peroxidase study has proven indispensable and indeed many crucial aspects of peroxidase catalytic mechanism have been elucidated using this substrate. Historically, this heterocyclic azine compound was used in assessing the blood glucose level by quantitatively measuring H_2O_2 produced by the action of glucose oxidase on blood

glucose[103]. ABTS is the favorite choice as a chromogenic substrate in many peroxidase related studies or similar fields involving redox chemistry due to the convenience in its handling and ease of its colorimetric detection supplemented by its very low toxicity. It finds its application mainly due to the generation of brilliant green color corresponding to its radical cation ($ABTS^{+\cdot}$) which is formed by peroxidase catalyzed one electron oxidation of ABTS, measured usually at 420nm with extinction coefficient value of 36 $mM^{-1}cm^{-1}$. But this same property makes this substrate unusable in stopped-flow kinetic studies because of the intense absorption of $ABTS^{+\cdot}$ at 420nm interferes with the absorption of soret band occurring at the similar region (400-420 nm). However, ascorbate can be used as radical scavenger since it can reduce the $ABTS^{+\cdot}$ back to colorless ABTS at the rates faster than the formation of compound I and II or their reduction to resting state[104]. ABTS is an acidic substrate with pKa of 2.2[105-106]. Above pH2.2, where almost all activity assays are carried out, ABTS exists in deprotonated form and since the oxidation of ABTS to $ABTS^{+\cdot}$ does not involve protons its standard redox potential is virtually independent of pH[107]. ABTS is a one electron donating reducing substrate with the formal redox potentials of ABTS/$ABTS^{+\cdot}$ couple of 0.68 V vs NHE. $ABTS^{+\cdot}$ can still lose a second electron but with more difficulty since the second redox potential for the $ABTS^{+\cdot}/ABTS^{2+}$ couple is 1.09 V vs NHE[106, 108]. The dicationic ABTS can be formed by the disproportion of $ABTS^{+\cdot}$ where one of the cation radical forms ABTS upon electron abstraction from another radical which form dicationic $ABTS^{++}$. Almost all of the peroxidase activity reported with ABTS is for the removal of the first electron generating brilliantly green colored radical while the dicationic ABTS has a reddish tint. The characterization of most of the DyPs also has employed ABTS as the most common substrate. Whether it is in measuring the pH and temperature rate profiles or measuring the pH and thermal stabilities or measuring the effect of mutagenesis, ABTS is the substrate of choice in

many DyP experiments. The compilation of steady-state kinetic parameters for DyP/ABTS system or DyP/H_2O_2 system in the presence of ABTS is presented in Table 1.3.

Table 1.3 Activity of DyPs and other peroxidases with ABTS.

The values in parentheses are the activity the H_2O_2 in the presence of ABTS.

ABTS	Variants	pH	k_{cat} s^{-1}	K_m μM	k_{cat}/K_m $M^{-1}s^{-1}$	*Ref*
*Bs*DyP	wt	3.8	11 (12)	166 (7)	7.0×10^4 (2.6×10^6)	86
	D240N	4.4	13 (11)	362 (48)	3.0×10^5 (3.0×10^4)	
	R339L	3.8	40 (46)	14 (1082)	3.0×10^6 (4.0×10^4)	
	D240N/R339L	4.4	3.0 (2.3)	11 (2736)	3.0×10^5 (1.0×10^3)	
	N244L	3.8	98 (138)	48 (545)	2.0×10^6 (3.0×10^5)	
	D383N	3.8	15 (17)	321 (56)	5.0×10^4 (3.0×10^5)	
DyPA †	wt	5.5	23.1 (35)	820 (70)	2.8×10^4 (4.8×10^5)	99
DyPA ††	wt	4.5	16.8 (68)	8200 (4100)	2.0×10^3 (1.68×10^4)	40
DtpA	wt	5.0	1.12	730	1.53×10^3	109
		7.0	0.50	10400	48	
DyPB	wt	4.5	55 (14.1)	23000 (67)	2.4×10^3 (2.1×10^5)	40
*Vc*DyP	wt	4.0	500	180	2.8×10^6	65
DyP1B	wt	5.5	13.5 (23.3)	1130 (48)	1.2×10^4 (4.8×10^5)	99
DyP2B	wt		10.2 (9.2)	1700 (61)	5.8×10^3 (1.5×10^5)	110
*Pp*DyP	wt	4.3	21 (13.7)	2500 (79)	8.0×10^3 (1.8×10^5)	111
	D132N	7.4	23 (25)	126 (1998)	2.0×10^5 1.0×10^4	
	R214L	3.6	0.07 (0.065)	566 (615)	2.0×10^2 (1.0×10^2)	
	N136L	5.6	34 (26)	347 (314)	1.0×10^5 (1.0×10^5)	
	9F6-E188K	4.3	128 (128)	220 (200)	6.0×10^5 (6.4×10^5)	

	17F11-E188K/A142V	5.5	15 (15)	1000 (160)	1.5×10^4 (9.0×10^4)	
	6E10-E188K/A142V/H125Y	5.5	15 (15)	1100 (44)	1.4×10^4 (3.4×10^5)	
	A142V	5.5	4.4 (4.4)	260 (47)	1.7×10^4 (9.0×10^4)	
	31F3-H125R	4.3	26 (26)	500 (200)	(5.2×10^4) (1.2×10^5)	
	21G11-E188K/H125R	4.3	6.9 (6.9)	280 (200)	2.5×10^5 (3.5×10^5)	
*Mt*DyP	wt	5.5	0.035			60
DyP2	wt	4.5	87s	13	6.6×10^6	67
AnaPX	wt	4.0			204‡	33
*Sa*DyP2	wt	4.5	1.2	790	1.7×10^3	101
TAP	wt		698	28.4	2.5×10^7	112
*Aau*DyPI	wt	4.5	368 (268)	20 (10)	1.8×10^7 (2.7×10^7)	36
*Aau*DyPII		4.5	322 (238)	20 (5)	1.6×10^7 (4.8×10^7)	
*rMsc*DyP	wt	4.5	(55)	(5)	(1.1×10^7)	113
*Mep*DyP	wt	4.5	(1047)	(11)	(9.5×10^7)	
*Egl*DyP	wt	4.5	(272)	(14)	(2.0×10^7)	
*I. lacteus*DyP	wt	3.0	224 (419)	28 (79.5)	8.0×10^6 (5.3×10^6)	37
Pleos-DyP1	wt	3.5	208	779	2.7×10^5	102
Pleos-DyP4	wt		277	787	3.5×10^5	
*Pch*LiP	Wt	3.0	(1)	(89)	(1.1×10^4)	114
*Tc*LiP*	wt	3.5	210	868	2.4×10^5	115
VP	wt	3.5	(28)	(3)	(9.3×10^6)	
*Bad*VP	wt	3.0	(57)	(17)	(3.4×10^6)	113
CiP	Wt	6.8	(2495)	(152)	(1.6×10^7)	116
SBP	wt	5.5	(1)	(6)	(1.7×10^5)	
HRP	wt	7.0	52.5 (52.5)	5100 (11.5)	1.0×10^4 (4.6×10^6)	117
*Gs*CcPA**	wt	5.5	(15.5)	(6.2)	(2.5×10^6)	118

†DyPA from *P. fluorescens* Pf-5, ††DyPA from *R. jostii* RHA1, ‡ activity in terms of $U.mg^{-1}$.

**Tc*LiP: (recombinant) lignolytic peroxidase from *Trametes cervina*

***Gs*CcPA: diheme cytochrome c peroxidase from a proteobacteria *Geobacter sulfurreducens*

1.4.3 Phenolic substrates

DyPs also show some moderate activity towards phenolic aromatic substrates like catechol, guaiacol, pyrogallol etc., however with rates still slower compared to that of classical

peroxidases. The common theme among phenolic substrate oxidation by peroxidases is the generation of phenolic radical by one electron abstraction that can undergo either quinoid product formation or polymerization to form higher molecular weight products[119]. Much of the interest towards peroxidase activity against these mono-aromatic substrate stems from their occurrence in nature as lignin sub-structure. These phenolic compounds are the product of thermal decomposition of lignin precursors or monolignols during pyrolysis of biomass. Hence, these make important components of bio-oil or pyrolysis oil which is prepared by rapid and simultaneous depolymerization and fragmentation of wood biomass with a rapid elevation in temperature[120]. These common phenolic substrates are single aromatic ring derivative and are smaller in size compared to the dye molecules, ABTS or even lignin model compounds. Hence, they are hypothesized to be oxidized at the heme active center and indeed some structural evidences have emerged and shown that it might very well be the case. For example, *Bad*DyP was co-crystalized with ascorbic acid (native substrate of APX) and 2,6-DMP where the substrates were very close to the heme center, even such that the location of ascorbic acid compared to heme in the DyP was very similar to that observed in APX[121].

2,6-Dimethoxy phenol or syringol is the dimethyl ether of pyrogallol and together with guaiacol it is one of the products of pyrolysis of lignin. It is formed by thermal decomposition of sinapyl alcohol, one of the monolignols[122]. Hence, it is one of the major components of bio-oil and wood smoke and imparts the smoky aroma, while guaiacol providing the smoky taste, to the food cooked with fire wood[123]. Peroxidases oxidize DMP into phenoxy radical that exclusively dimerizes to form 2,2',6,6'-tetramethoxydibenzo-1,l'-diquinone which is detected at 469 nm[124-125]. Guaiacol, on the other hand, is the synringol with one methoxy group removed and as mentioned above it is also one of the products of lignin pyrolysis. Guaiacol is formed by

dissociation of coniferyl alcohol, another precursor of lignin polymer, at high temperature. The peroxidase catalyzed oxidation product of guaiacol is yellow colored tetraguaiacol formed by polymerization of guaiacol radical[126]. Binding simulation of guaiacol with *Aau*DyPI Compound I model shows that it fits narrowly at the heme access channel[62]. Catechol or 1,2-dihydroxy benzene or also called pyrocatechol is also the product of destructive distillation of plant extract, mainly catechin, a flavan-3-ol secondary metabolite. Catechol units are found spread throughout plant and animal kingdom. A small amount of catechol in fruits and vegetables by the action of co-found catechol oxidase in the presence of oxygen turns it into reddish-brown benzoquinone as seen with apple cut and left out. Benzoquinone being antimicrobial prevents its fast rotting. Catechol moieties are found in vascular plants and also as chitin in the cuticles of arthropods[127]. While catechol finds its application in many fields, its extensive usage also generates pollutants with catechol and its derivatives. It is used in making pesticides and also found as major phenolic water pollutant from various industries like paper factories. Oxidoreductase enzyme like LiP treatment has been tried in detoxification of catechol contaminated water with some promising results[128]. DyPs as well are known to degrade this compound with some moderate activity[85]. Pyrogallol or 1,2,3-trihyroxybenzene is a common substrate that forms red colored purpurogallin upon the action of peroxidase and measured conveniently at 420nm. Pyrogallol has a very old history, and its preparation from gallic acid (3,4,5-trihydroxybenzoic acid) found in number of terrestrial plants was reported as early as 1786[129]. It is also the oldest photographic developer due to its silver precipitating behavior from silver salts first reported in 1832. Interestingly the polyphenolic compounds tested for cytotoxicity towards cancerous cells showed that the pyrogallol motif in those compounds was essential for induction of apoptosis[130]. The structures of the most commonly used phenolic substrated are listed in Fig. 1.11.

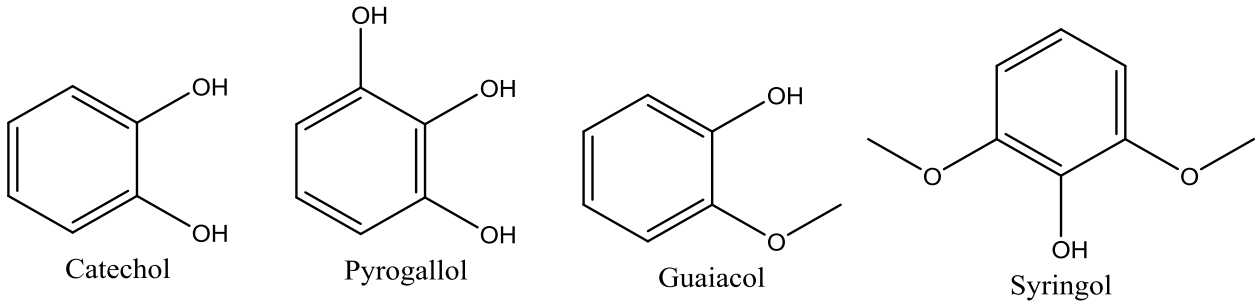

Figure 1.11 Some common lignin based phenolic peroxidase substrates.

1.4.4 Mn^{2+}

Mn^{2+} is the native substrate of MnP and it oxidizes Mn^{2+} to Mn^{3+} which has high redox potential and is highly unstable but is stabilized by chelation to some dicarboxylic acid molecules. This Mn^{3+}-acid complex diffuses out of the enzyme and brings about the oxidation of high redox potential substrates like lignin, hence acting as a mediator[125]. The required Mn^{2+} for lignin degradation is found in the wood itself and catalytic efficiency of MnP for Mn^{2+} oxidation is in the range of 10^7 $M^{-1}s^{-1}$ and that of VP is 10^{6} [131]. Such remarkable ability of Mn^{2+} utilization by MnP and VP stems from their high affinity Mn^{2+} binding site comprising chiefly of acid residues[132]. In DyPs, instances of Mn^{2+} usage are very rare; nonetheless, some interesting activities have been reported. No Mn^{2+} oxidizing phenomenon was observed for class-A DyP but DyPB from *R. jostii* was found to have Mn^{2+} oxidizing capability albeit with largely diminished efficiency compared to MnP or VP[77]. DyP2 on the other hand, a class-C DyP from *Amycolatopsis sp.* 75vi2 was found to oxidize Mn^{2+} with the efficiency of 5 orders of magnitude only slightly lower than that of MnP or VP[67]. Recently, two fungal DyPs *Pleos*-DyP1 and *Pleos*-DyP4 were isolated from *Pleurotus ostreatus* that were able to oxidize Mn^{2+}. These were the first

Mn^{2+} oxidizing DyP reported from a fungal source, of which *Pleos*-DyP4 was as efficient as DyP2 in Mn^{2+} oxidation, *Pleos*-DyP1 was slower by 2 orders of magnitude[102].

1.4.5 Non-phenolic substrates

In addition, depending on which class they belong to, DyPs are also capable of oxidizing, although very poorly, some of the non-phenolic aromatic compounds like veratryl alcohol (VA) (Fig. 1.12) which is the native substrate for LiP. VA is a secondary metabolite of white rot fungus *Phanerochaete chrysosporium*[133] where LiP oxidizes VA in to radical cation ($VA^{+\cdot}$) which eventually forms veratradehyde (VAD)[134]. VA acts as a mediator in bringing about the oxidation of substrates (lignin) located at distance from the enzyme catalytic center via one electron oxidant $VA^{+\cdot}$. VA also protects LiP from H_2O_2 induced inactivation by converting LiP Compound III to the resting state enzyme[135]. Capability of VA oxidation is benchmark of high redox potential heme enzyme such as LiP and VP. *Aau*DyPs and *I. lacteus*DyP show the highest activities with VA among all the DyPs and interestingly some bacterial DyPs are also capable of acting against this high redox potential substrate[36-37, 98].

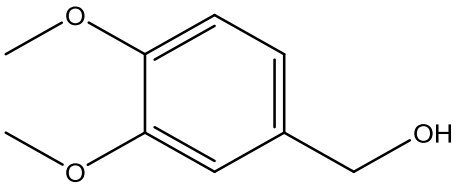

veratryl alcohol

Figure 1.12 Structure of veratryl alcohol (VA)

1.4.6 Lignin

1.4.6.1 Introduction

Ranking only second to cellulose, lignin is one of the most abundant sources of carbon in nature and comprises about 25% of total terrestrial biomass dry weight. Lignin is a three-dimensional

heterogeneous aromatic polymer formed by oxidative cross-coupling of 4-hydroxyphenylpropanoid monomer units or monolignols. There are three types of monolignols, namely *p*-coumaryl alcohol, coniferyl alcohol and sinapyl alcohol and when these are associated with lignin polymer they respectively form *p*-hydroxyphenyl (H), guaiacyl (G) and syringyl (S) units (Fig.1.13). The cross-linking of monolignols is prompted by the generation of phenolic radicals that dimerize and subsequently polymerize after one electron oxidation. The oxidative phenolic radical generation is brought about by peroxidases and laccase. The cross-linking can take place via different types of carbon-carbon and ether bonds like β-O-4, β-5, β-β, 5-5, 4-O-5, and β-1 of which the β-O-4 linkage is the most predominant[136] (Fig.1.14). Lignin provides structural support and strength to plants along with protection against microbial degradation of the cellulose and hemicellulose and since it is hydrophobic at physiological pH it makes the plants water resistant[137].

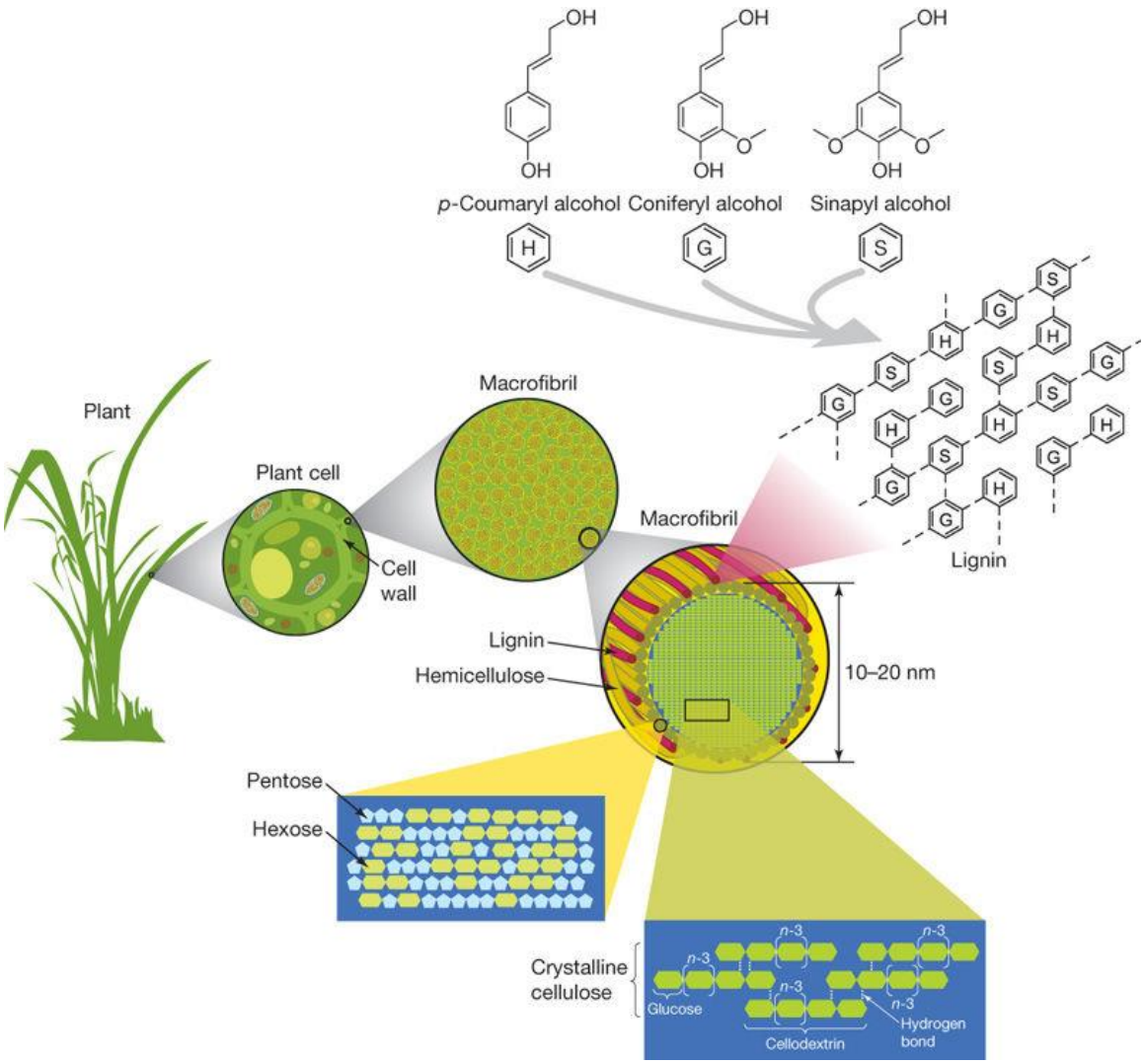

Figure 1.13 Occurrence of lignin in biomass together with cellulose and hemicellulose.

The main component of lignocellulose is cellulose, a beta(1–4)-linked chain of glucose molecules. Hydrogen bonds between different layers of the polysaccharides contribute to the resistance of crystalline cellulose to degradation. Hemicellulose, the second most abundant component of lignocellulose, is composed of various 5- and 6-carbon sugars such as arabinose, galactose, glucose, mannose and xylose. Lignin is composed of three major phenolic components, namely p-coumaryl alcohol (H), coniferyl alcohol (G) and sinapyl alcohol (S). Lignin is synthesized by polymerization of these components and their ratio within the polymer varies between different plants, wood tissues and cell wall layers. Cellulose, hemicellulose and lignin form structures called microfibrils, which are organized into macrofibrils that mediate structural stability in the plant cell wall[138]. (Reproduced with permission from ref 138.)

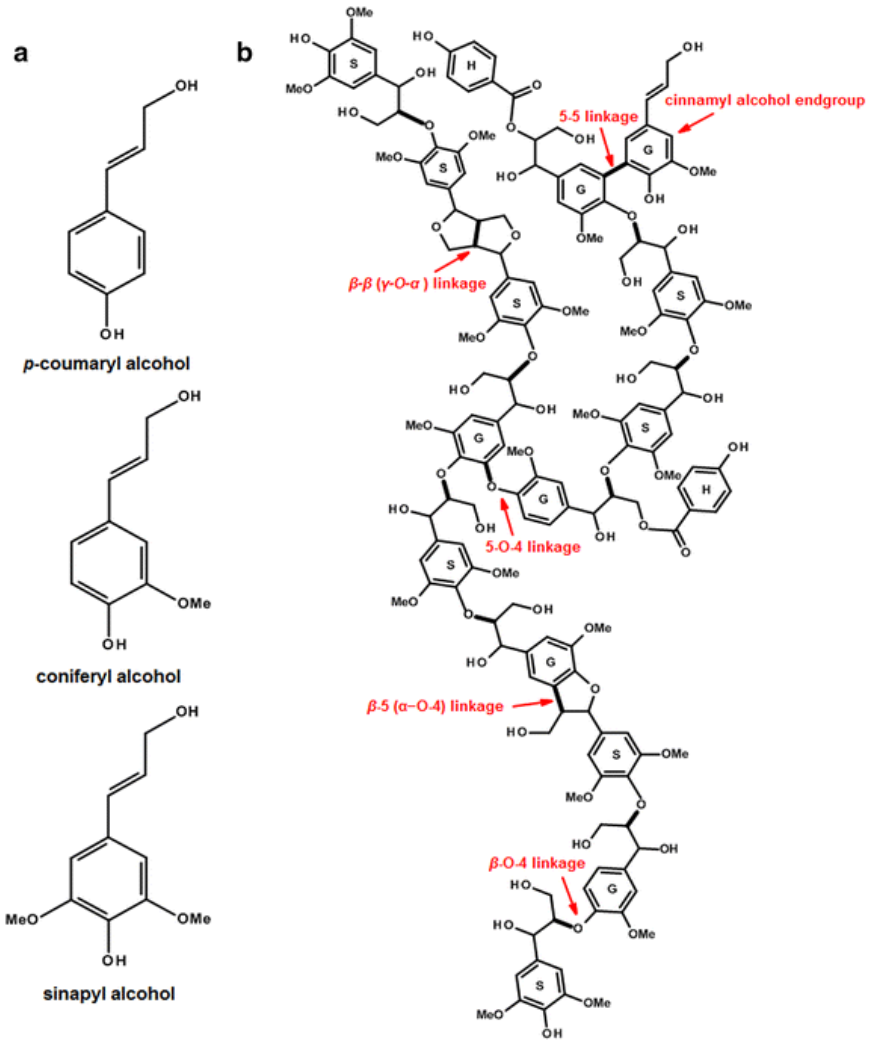

Figure 1.14 Monolignols and a lignin polymer model.

a. Primary lignin monomers: p-coumaryl alcohol, coniferyl alcohol and sinapyl alcohol. The three monolignols differ in the degree of methoxylation, and are catalyzed by peroxidase and/or laccases to form the corresponding p-hydroxyphenyl (H), guaiacyl (G), and syringyl (S) lignin unit, respectively. b. A polymer model depicting the general feature of lignin. The model is constructed by Accelrys Draw 4.2 with two H units, six G units and eight S units, showing the main linkage types. The bolded bonds are formed in the radical coupling reactions. This is only a model, and do not imply any primary structure or composition of plant lignin[139]. (Reproduced with permission from ref. 139)

Production of biofuel from lignocellulosic biomass is deemed more carbon neutral than other sources of energy and hence recent decade has seen ever-growing interest in obtaining such fuel which could both replace the fossil-based non-renewable energy sources and also reverse the

damage caused by fossil fuels to the earth's greenhouse machinery[138]. Due to close networking between lignin, hemicellulose, and cellulose, some sort of delignifying pretreatment process of the biomass is required before the polysaccharides could be processed to give biofuels. Paper production industries also require the delignification process of wood pulp before the paper can be made from cellulose[140]. However, the deconstruction of this nature's heavy-duty polymer is no trivial task. The very sturdy nature of lignin that makes the plant resistant to mechanical and microbial forces of nature is also the stumbling stone in progress towards biomass to biofuel conversion. Many physicochemical approaches have been implemented towards overcoming such hindrances, most common of them being the steam explosion and acid treatment[141]. However, these pretreatment procedures cause unwanted degradation of useful hemicellulose as well as the toxicity in the downstream process brought upon by the byproducts[142]. Hence, needless to say, our noble goal of harnessing much greener and more stable source of fuel from the plants has not been fully realized yet. Moreover, after the biofuel has been 'squeezed out' of the biomass the remaining solid masses are treated as waste. The ambitious project aimed at producing 79 billion liters of biofuels annually by 2022 as mandated by U.S. Energy Security and Independence Act of 2007, is estimated to accrue 62 million tons of lignin[142]. While 40% of the lignin by-products are burnt to supply the energy demand in biorefineries, the significant 60% still waits for proper utilization. Since lignin is the only most abundant and renewable natural source of aromatics, it can decrease our dependency on the petroleum based carbon source and provide a cheap alternative in generation of carbon derived chemicals and materials[142]. There is an ever growing list of the value-added chemicals and materials, carbon fiber being one the most highly sought after[143], that can be obtained from valorization of lignin

which otherwise is discarded as waste. But in the absence of an efficient machinery to depolymerize it, the promising benefits of lignin are sure to elude mankind.

In nature, white rot fungi belonging to class II type of peroxidase have evolved in recycling this otherwise recalcitrant lignin polymer by secretion of heme peroxidases like LiP, MnP, VP and laccases. It is interesting to note that the heme peroxidase enzymes used by nature to construct lignin in plants is also used by nature to mineralize this polymer. Hence, inspired by the tools used by nature, enzymatic digestion could be an appealing alternative means that can be employed to circumvent the problems inherent in physico chemical approaches used in lignin digestion[144]. Such biological approach is less demanding in energy or cost and the process is totally environment friendly. In a sense, the enzymatic approach is the 'greener' approach in the production of 'greener' source of carbon based fuels, chemicals and materials. Nonetheless, there are challenges to this and there are limits set by the inherent nature of those enzymes.

In last four decades, a lot of work has been done on fungal lignolytic enzymes and we now know more than ever about how these enzymes work. However, no commercial biocatalyst designed for lignin degradation is yet unavailable due to the limits, as mentioned earlier, set by difficulties in fungal gene manipulation and protein expression. Comparatively, the field of bacterial lignin degrading enzyme is far too underexplored while much evidence is being accumulated that bacterial lignolytic enzymes could be as powerful as the fungal counterparts[145]. While there have been no homologs of fungal LiPs, MnPs or VPs found yet in bacteria, DyP is reported to be present in a very large number of bacteria. Much of the interest in DyP has risen because some DyPs of bacterial origin, besides fungal DyPs of class-D, have shown the ability of to degrade lignin model compounds in addition to Kraft lignin and wheat straw lignin. Hence, these peroxidases have been proposed as the bacterial counterpart of fungal lignin peroxidase,

the decomposer of wood lignin in nature[77]. Bacterial peroxidases capable of performing such function are certainly more attractive than fungal sources since the maneuvering of a bacterial gene and their heterologous expression is much easier to handle than in fungi. This means such enzyme can potentially be produced at industrial scale in order to carry out lignin digestion of biomass[146]. Below are discussed the activities of DyP with some common type of lignin related compounds.

1.4.6.2 Lignin model compounds or arylglycerol-*β*-guaiacol ether (AGE)

The occurrence of the most predominant *β*-*O*-4 linkage in lignin varies from ~ 50% in softwood to 80% in hardwood plants[147]. Hence, the dimer model compound with *β*-*O*-4 linkage, arylglycerol-*β*-guaiacol ether (AGE) (Fig. 1.15), has served as an iconic substrate in the measurement of lignin degradation abilities of many lignin degrading enzymes. The phenolic model compound has lower redox potential and is easier to oxidize via formation of phenolic radical. On the other hand, non-phenolic lignin model compound is more difficult to oxidize since it has higher redox potential (> 1.4 V) and requires formation of aromatic radical cation, reminiscent of non-phenolic substrate VA. In nature, the free phenolic hydroxyl group is found in a small percentage as they are used mostly to form oxidative linkages via phenolic radical[148]. The fungal lignolytic enzymes have been reported to degrade both phenolic and non-phenolic lignin model compounds. While most of the fungal and bacterial DyPs are reported to degrade phenolic lignin model compounds, none of other bacterial DyPs, with the exception of *Bs*DyP, have been shown to be active towards non-phenolic lignin model compound.

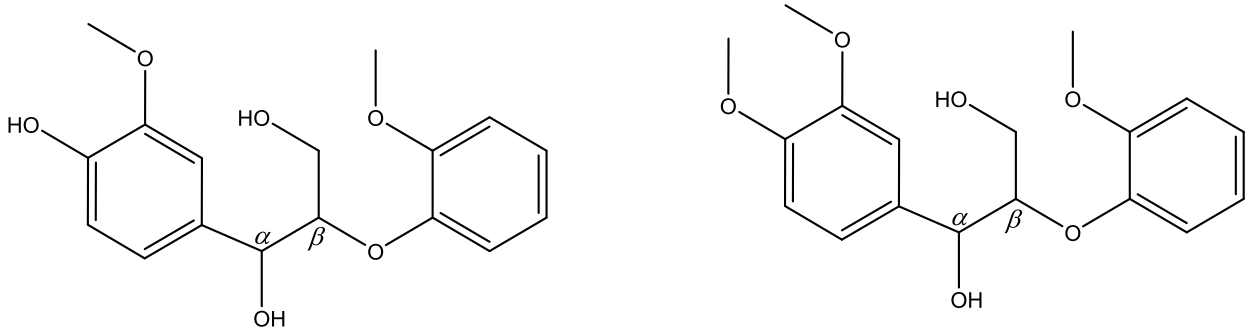

Guaiacyl-*β*-guaiacol ether (GGE)

Veratrylglycerol-*β*-guaiacol ether (VGE)

Figure 1.15 Structures of phenolic (GGE) and non-phenolic (VGE) lignin model compounds

LiP catalyzes the C_α-C_β bond cleavage of non-phenolic *β-O*-4 dimer or veratrylglycerol-*β*-guaiacol ether (VGE) with a second-order rate constant of 6.5×10^3 $M^{-1}s^{-1}$ at pH 6.0. [149]. The reaction initiates with the formation of aryl cation radical that undergoes bond cleavage followed by demethylation, intramolecular addition, and rearrangements to give final products, veratraldehyde being one of them[147]. *Bs*DyP was found to degrade the non-phenolic LMC in fashion similar to LiP by breaking C_α-C_β bond forming veratraldehyde as one of the major products[98]. Similarly, the fungal DyPs *Egl*DyP, and *Mep*DyP, *Aau*DyPI and *Aau*DyPII also oxidized the VGE by similar mechanism with specific activity of 0.03–0.1 $U.mg^{-1}$ forming veratryldehyde as the end product[150]. The VGE oxidizing capacity of DyP is lesser than that of LiP such that the fungal DyP at best is at 10% and *Bs*DyP, the only bacterial DyP known to be active against VGE, is at ~9% compared to that of LiP[98, 150].

By now it is clear that bacterial DyPs have lower redox potential than that of fungal DyPs and this is reflected in their ability to act against just the phenolic lignin model compound or guaiacyl-β-guaiacol (GGE). The redox potential of GGE ranges from 0.6 to 0.8 V vs. SHE[151]. In the reaction against GGE of DyP, there seems to be two different pathways. For example, DyPB

(pH 5.5) catalyzed the cleavage of C_α-C_β bond that was followed by coupling of the radical products. The end products from DyPB were guaiacol trimer, oxidized product of vanillin and trace amount of vanillin and the rate was 23-fold higher in the presence of 1mM Mn^{2+} [77, 85]. However, on the contrary, no such cleavage was observed in *Tfu*DyP catalyzed the oxidation of GGE where only dimers and trimers of GGE were identified as the end products[152]. DyP2 was also found to react only with phenolic GGE but the products were not analyzed[67].

1.4.6.3 Kraft lignin

Alkali kraft lignin is the byproduct of Kraft process used in paper industries to convert wood into wood pulp by alkaline sulfide treatment. The molecular weight of Kraft lignin is lower than that of natural lignin since it is the partial dissociation product of natural wood lignin. Hence, it has been used as the equivalent of natural lignin in the study of lignolytic properties of microbes and enzymes[153]. Some DyPs have been found active against Kraft lignin. DyPB was first shown to have activity against Kraft lignin with Michaelis-Menten kinetics, which was 6.2 times more efficient in the presence of 1.5mM Mn^{2+}[77]. A later study of N246A variant of DyPB, which had higher MnP activity, showed improved ligninase activity towards hard wood Kraft lignin in the presence of 20mM Mn^{2+} at pH 5.5. The end products were also analyzed and identified as 2,6-dimethoxybenzoquinone (2,6-DMBQ) and trimethylsilyl derivative of 4-hydroxy-3,5-dimethoxybenzaldehyde (syringaldehyde)[73]. These products were also reported in MnP and laccase catalyzed the degradation of lignin model compound and were the result of C_α-C_β and C_1-C_α bond cleavages respectively[73]. Similarly, *Tfu*DyP and DyPA and DyP1B were also reported to have activity against kraft lignin showing saturation kinetics with K_M of 10, 11 and 6 μM respectively[99, 154].

1.4.7 Sulfides

Enantioselective sulfoxidation of sulfides is well-known phenomenon reported for various peroxidases like CcP, LiP, CiP, HRP, CPO and many animal peroxidases[6]. Such enzymatic enantioselective reaction is useful in the organic synthesis of chiral sulfoxides which is the integral motif of many pharmaceutical drugs[155]. Some DyPs are also reported to carry out the sulfoxidation of different sulfides to yield the sulfoxides rich in one of the enantiomers. *Tfu*DyP was the first DyP to have tested for its asymmetric sulfoxidation ability against some aromatic sulfides like methyl phenyl sulfide (MPS), benzyl methyl sulfide (BMS), methyl *p*-tolyl sulfide (MTS) and ethyl phenyl sulfide (EPS). The reaction yielded (*R*)-sulfoxide in predominance, however with poor conversion rate and low enantioselectivity ranging from 31% *ee* with BMS to the best of 61% *ee* with MPS. Nonetheless, it showed that the sulfides and possibly other substrates could enantioselectively bind to DyP[38]. Another experiment involving *Aau*DyP showed highly improved enantioselective sulfoxidation towards MPS and MTS. Strangely, the wt of *Aau*DyP did not have any sulfoxidation ability but only the F359G mutant was highly stereoselective, and L357G yielded both *R* and *S* sulfoxides. With the F359G variant, 99% *ee* of (*S*)-sulfoxide was achieved at a much higher rate with total conversion of 95-99%. The rationale for sulfoxidation ability of F359G, but not the wt, was suggested as the heme pocket in the variant being better at housing the substrate molecule closer to the ferryl oxygen. The better accommodation of the substrate by the mutant was due to the enlarged heme space compared to that of wt as revealed by their crystal structures and computational modeling. The study performed in the presence of $H_2{}^{18}O_2$ revealed that the oxygen that gets incorporated in sulfoxides comes from the ferryl oxygen and hence the close association between Fe^{4+}=O species of DyP and the substrate molecule is of utmost importance in carrying out such peroxygenase

function. Further, the QM/MM calculations provided the explanation for stereoselectivity and the preference for the *S* enantiomer formation was suggested to be due to higher reactivity of pro-*S* sulfides as a result of interaction with the Arg residue in the catalytic center[155].

Table 1.4 Kinetic data-Sulfides

Enzymes	Substrate	pH	Temp (^oC)	Rxn time (hr)	k_{cat} s^{-1}	K_m µM	k_{cat}/K_m $M^{-1}s^{-1}$	*ee* (%)	Conversion (%)	Config	Ref
*Tfu*DyP	MPS	3.5	30	36				61		*R*	38
	BMS							31		*R*	
	MTS							49		*R*	
	EPS							50		*R*	
*Aau*DyP	MPS	5.0	25	0.5	17.2	370	4.59×10^4	92	95	*S*	155
	MTS				3.6	130	2.65×10^4	99	99	*S*	

1.4.8 Hydrogen peroxide (H_2O_2): Compound III and suicide inactivation

In biological system, H_2O_2 is one of the reactive oxygen species (ROS) among other species like superoxide radical ($O_2^{\cdot -}$) and hydroxyl radical ($OH^{\cdot -}$). It is produced as toxic by-product of the cellular respiration or from other oxidative reactions and can act as the source of another ROS like highly reactive hydroxyl radical, as generated by fenton reaction. However, it has also been recognized recently as the signaling molecule in signal transduction pathway[156-157]. To counteract the deleterious effects of H_2O_2 the cells of organisms have developed several types of enzymatic machinery. For instance, catalase, the heme-containing enzyme found in almost all aerobic organisms, offers protection against the oxidative stress caused by H_2O_2 by converting it into O_2 and H_2O[158] and APX located in chloroplasts and cytosol of plants and eukaryotic algae has the major function of scavenging H_2O_2 generated by dismutation of superoxide using ascorbate as the reducing substrate[159]. The physiological concentration of H_2O_2 is at sub-micromolar level, for example *E. coli* has an intracellular H_2O_2 concentration of ~0.2 µM and becomes toxic at ≥ 0.5 µM. And even in plants the level of H_2O_2 is within in similar range[157]. In

vitro study of the activity of peroxidases towards non-native substrates, however, quite often uses non-physiological concentration of H_2O_2 which could be several folds higher lying at millimolar range. Such high concentration of H_2O_2 is required for detecting the activities using common techniques such as UV-Vis spectrophotometry[160]. Ironically, high concentration of H_2O_2 is toxic not just for the cells but also for the enzyme machinery that is built to carry out its detoxification. In *I. lacteus*DyP, which showed maximum activity with ABTS at H_2O_2 concentrations ranging between 0.4 and 0.8 mM, was found to have 70% decrease in activity at 12.5 mM H_2O_2 concentration and at 50 mM the enzyme was completely inactivated[37]. Hence, at higher H_2O_2 concentrations the peroxidases are rendered inactive and such suicide inactivation of peroxidases by their essential native co-substrate H_2O_2 is one of the very serious and daunting problems in realizing these enzymes as the biocatalyst for their large-scale industrial application[161]. Higher H_2O_2 concentrations are desirable in industries to increase the product yield as well as shorten the time required to generate those products. Hence, there have been rising interests in make these enzymes more tolerant against H_2O_2 caused loss in activity. Sound understanding of such inactivation pathway is necessary before the peroxidases can be engineered to more H_2O_2 resistant variants.

Deactivation of peroxidases by H_2O_2 can take place in two possible ways. First of these possible ways is via formation of Compound III in the presence of high H_2O_2 concentration. Compound III is the peroxidase intermediate, not a part of the catalytic cycle, comprising either the dioxygen attached to the ferrous heme center (Fe^{2+}-O_2) or the superoxide radical attached to the ferric heme center (Fe^{3+}-$O_2^{\cdot-}$). Compound III is formed by the decay of Compound I or Compound II when using an excess of H_2O_2 and is considered as the catalytic dead-end of peroxidase catalytic cycle, unless a substrate capable of reverting it to the resting state

rejuvenates it. Compound III can also be prepared directly by treating O_2 with ferrous enzyme or $O_2^{\cdot-}$ with ferric enzyme[161]. In DyPB, Compound III was observed as the decay product of Compound I, in the absence of reducing substrate, over the period of 50 to 200 s when more than 100-fold excess H_2O_2 was used. The intermediate was characterized with red shifted soret band at 410 nm and α and β bands at 581 and 543 nm. By comparison, the resting state DyPB and its Compound I have their soret bands at 404 nm and 397 nm respectively and the corresponding visible region bands at 503 nm and 634 nm in resting state enzyme and 580 nm, 613 nm and 648 nm in Compound I[40]. The Compound III in heme peroxidase can follow the irreversible enzyme deactivation pathway due to the destruction of heme[161]. H_2O_2 at a higher concentration can also decrease the activity of peroxidase by causing the oxidation of residues such as Arg, Asn, Met, Lys, Thr and Trp which more oxidation labile than other residues. In *Pp*DyP, the single mutants of solvent exposed residues which were prone to peroxide oxidation were generated and these mutants, namely Thr134Val, Thr138Val and Met212Leu, showed higher resistance towards H_2O_2 induced inhibition[111].

1.5 Purpose of this study

Since its discovery at the turn of the twenty-first century, many other DyPs from different sources have been characterized. With a few exceptions, these characterizations have focused on revealing the biochemical properties and exploring their substrate scope. However, only a handful of studies have attempted the exploration of their mechanistic aspects at the molecular level and thus the knowledge gap regarding their peroxidatic machinery has persisted. This not only has limited the research progress in DyP but also has hindered the development of this enzyme into an industrial biocatalyst. In this study, we attempt to close this knowledge gap by studying two different types of DyPs namely, *Tc*DyP a class-A DyP from *Thermomonospora*

curvata and *El*DyP a class-B DyP from *Enterobacter lignolyticus* at molecular level. From the study of these two DyPs as the representative members of each two classes we try to elucidate the molecular enzymology and mechanism of their respective classes. Some interesting results and valuable information obtained from this study, we believe, will propel the DyP research field ahead and will accelerate the progress towards the goal of realizing this enzyme as a biocatalyst.

1.6 References

1. Planche, L. A., Note sur la sophistication de la résine de jalap et sur les moyens de la reconnaître. *Bull Pharm* **1810,** *2*, 578-580.

2. Nicholls, P., The oxygenase-peroxidase theory of Bach and Chodat and its modern equivalents: change and permanence in scientific thinking as shown by our understanding of the roles of water, peroxide, and oxygen in the functioning of redox enzymes. *Biochemistry (Mosc)* **2007,** *72* (10), 1039-46.

3. Bach, A. N. C., R., *Ber. Deut. Chem. Ges* **1902,** *35*, 2466-2470.

4. Theorell, H., Crystalline Peroxidase. *Enzymologia* **1941,** *10*, 250-252.

5. Keilin, D.; Mann, T., On the Haematin Compound of Peroxidase. *Proceedings of the Royal Society of London. Series B - Biological Sciences* **1937,** *122* (827), 119.

6. Dunford, H. B., *Peroxidases and Catalases: Biochemistry, Biophysics, Biotechnology and Physiology*. John Wiley & Sons: 2010.

7. Zederbauer, M.; Furtmuller, P. G.; Brogioni, S.; Jakopitsch, C.; Smulevich, G.; Obinger, C., Heme to protein linkages in mammalian peroxidases: impact on spectroscopic, redox and catalytic properties. *Nat Prod Rep* **2007,** *24* (3), 571-84.

8. Welinder, K. G., Superfamily of plant, fungal and bacterial peroxidases. *Current Opinion in Structural Biology* **1992,** *2* (3), 388-393.

9. Poulos, T. L., Thirty years of heme peroxidase structural biology. *Arch Biochem Biophys* **2010,** *500* (1), 3-12.

10. Van de Water, K.; Sterckx, Y. G.; Volkov, A. N., The low-affinity complex of cytochrome c and its peroxidase. *Nat Commun* **2015,** *6*, 7073.

11. Zamocky, M.; Furtmuller, P. G.; Obinger, C., Evolution of structure and function of Class I peroxidases. *Arch Biochem Biophys* **2010,** *500* (1), 45-57.

12. Hiner, A. N.; Hernandez-Ruiz, J.; Rodriguez-Lopez, J. N.; Garcia-Canovas, F.; Brisset, N. C.; Smith, A. T.; Arnao, M. B.; Acosta, M., Reactions of the class II peroxidases, lignin peroxidase and Arthromyces ramosus peroxidase, with hydrogen peroxide. Catalase-like activity, compound III formation, and enzyme inactivation. *J Biol Chem* **2002,** *277* (30), 26879-85.

13. Hiraga, S.; Sasaki, K.; Ito, H.; Ohashi, Y.; Matsui, H., A large family of class III plant peroxidases. *Plant Cell Physiol* **2001,** *42* (5), 462-8.

14. Winter, J. M.; Moore, B. S., Exploring the Chemistry and Biology of Vanadium-dependent Haloperoxidases. *Journal of Biological Chemistry* **2009,** *284* (28), 18577-18581.

15. Poulos, T. L., Heme enzyme structure and function. *Chem Rev* **2014,** *114* (7), 3919-62.

16. Kim, S. J.; Ishikawa, K.; Hirai, M.; Shoda, M., Characteristics of a newly isolated fungus, Geotrichum candidum Dec 1, which decolorizes various dyes. *Journal of Fermentation and Bioengineering* **1995,** *79* (6), 601-607.

17. Kim, S. J.; Shoda, M., Purification and Characterization of a Novel Peroxidase from Geotrichum candidum Dec 1 Involved in Decolorization of Dyes. *Applied and Environmental Microbiology* **1999,** *65* (3), 1029-1035.

18. Sugano, Y.; Sasaki, K.; Shoda, M., cDNA cloning and genetic analysis of a novel decolorizing enzyme, peroxidase gene dyp from Geotrichum candidum Dec 1. *Journal of Bioscience and Bioengineering* **1999,** *87* (4), 411-417.

19. Colpa, D. I.; Fraaije, M. W.; van Bloois, E., DyP-type peroxidases: a promising and versatile class of enzymes. *J Ind Microbiol Biotechnol* **2014,** *41* (1), 1-7.

20. Finn, R. D.; Attwood, T. K.; Babbitt, P. C.; Bateman, A.; Bork, P.; Bridge, A. J.; Chang, H.-Y.; Dosztányi, Z.; El-Gebali, S.; Fraser, M.; Gough, J.; Haft, D.; Holliday, G. L.; Huang, H.; Huang, X.; Letunic, I.; Lopez, R.; Lu, S.; Marchler-Bauer, A.; Mi, H.; Mistry, J.; Natale, D. A.; Necci, M.; Nuka, G.; Orengo, C. A.; Park, Y.; Pesseat, S.; Piovesan, D.; Potter, S. C.; Rawlings, N. D.; Redaschi, N.; Richardson, L.; Rivoire, C.; Sangrador-Vegas, A.; Sigrist, C.; Sillitoe, I.; Smithers, B.; Squizzato, S.; Sutton, G.; Thanki, N.; Thomas, P. D.; Tosatto, Silvio C. E.; Wu, C. H.; Xenarios, I.; Yeh, L.-S.; Young, S.-Y.; Mitchell, A. L., InterPro in 2017—beyond protein family and domain annotations. *Nucleic Acids Research* **2017,** *45* (D1), D190-D199.

21. Sturm, A.; Schierhorn, A.; Lindenstrauss, U.; Lilie, H.; Bruser, T., YcdB from Escherichia coli reveals a novel class of Tat-dependently translocated hemoproteins. *J Biol Chem* **2006,** *281* (20), 13972-8.

22. Finn, R. D.; Coggill, P.; Eberhardt, R. Y.; Eddy, S. R.; Mistry, J.; Mitchell, A. L.; Potter, S. C.; Punta, M.; Qureshi, M.; Sangrador-Vegas, A.; Salazar, G. A.; Tate, J.; Bateman, A., The Pfam protein families database: towards a more sustainable future. *Nucleic Acids Research* **2016,** *44* (D1), D279-D285.

23. Goblirsch, B.; Kurker, R. C.; Streit, B. R.; Wilmot, C. M.; DuBois, J. L., Chlorite dismutases, DyPs, and EfeB: 3 microbial heme enzyme families comprise the CDE structural superfamily. *J Mol Biol* **2011,** *408* (3), 379-98.

24. Zamocky, M.; Hofbauer, S.; Schaffner, I.; Gasselhuber, B.; Nicolussi, A.; Soudi, M.; Pirker, K. F.; Furtmuller, P. G.; Obinger, C., Independent evolution of four heme peroxidase superfamilies. *Arch Biochem Biophys* **2015,** *574*, 108-19.

25. Fawal, N.; Li, Q.; Savelli, B.; Brette, M.; Passaia, G.; Fabre, M.; Mathé, C.; Dunand, C., PeroxiBase: a database for large-scale evolutionary analysis of peroxidases. *Nucleic Acids Research* **2013,** *41* (D1), D441-D444.

26. Andreeva, A.; Howorth, D.; Chandonia, J.-M.; Brenner, S. E.; Hubbard, T. J. P.; Chothia, C.; Murzin, A. G., Data growth and its impact on the SCOP database: new developments. *Nucleic Acids Research* **2008,** *36* (suppl_1), D419-D425.

27. Dunford, H. B., *Heme peroxidases*. John Wiley: 1999.

28. Giovannetti, R., The Use of Spectrophotometry UV-Vis for the Study of Porphyrins. In *Macro To Nano Spectroscopy*, Uddin, J., Ed. InTech: 2012; pp P001-366.

29. Huang, X. F.; Nakanishi, K.; Berova, N., Porphyrins and metalloporphyrins: Versatile circular dichroic reporter groups for structural studies. *Chirality* **2000,** *12* (4), 237-255.

30. Singh, R.; Eltis, L. D., The multihued palette of dye-decolorizing peroxidases. *Arch Biochem Biophys* **2015,** *574*, 56-65.

31. Berry, E. A.; Trumpower, B. L., Simultaneous Determination of Hemes-a, Hemes-B, and Hemes-C from Pyridine Hemochrome Spectra. *Analytical Biochemistry* **1987,** *161* (1), 1-15.

32. Everse, J.; Grisham, M. B., *Peroxidases in Chemistry and Biology*. CRC Press: 1990.

33. Ogola, H. J. O.; Kamiike, T.; Hashimoto, N.; Ashida, H.; Ishikawa, T.; Shibata, H.; Sawa, Y., Molecular Characterization of a Novel Peroxidase from the Cyanobacterium Anabaena sp Strain PCC 7120. *Applied and Environmental Microbiology* **2009,** *75* (23), 7509-7518.

34. Scheibner, M.; Hulsdau, B.; Zelena, K.; Nimtz, M.; de Boer, L.; Berger, R. G.; Zorn, H., Novel peroxidases of Marasmius scorodonius degrade beta-carotene. *Appl Microbiol Biotechnol* **2008,** *77* (6), 1241-50.

35. Sugano, Y., DyP-type peroxidases comprise a novel heme peroxidase family. *Cell Mol Life Sci* **2009,** *66* (8), 1387-403.

36. Liers, C.; Bobeth, C.; Pecyna, M.; Ullrich, R.; Hofrichter, M., DyP-like peroxidases of the jelly fungus Auricularia auricula-judae oxidize nonphenolic lignin model compounds and high-redox potential dyes. *Appl Microbiol Biotechnol* **2010,** *85* (6), 1869-79.

37. Salvachua, D.; Prieto, A.; Martinez, A. T.; Martinez, M. J., Characterization of a novel dye-decolorizing peroxidase (DyP)-type enzyme from Irpex lacteus and its application in enzymatic hydrolysis of wheat straw. *Appl Environ Microbiol* **2013,** *79* (14), 4316-24.

38. van Bloois, E.; Torres Pazmino, D. E.; Winter, R. T.; Fraaije, M. W., A robust and extracellular heme-containing peroxidase from Thermobifida fusca as prototype of a bacterial peroxidase superfamily. *Appl Microbiol Biotechnol* **2010,** *86* (5), 1419-30.

39. Singh, R.; Grigg, J. C.; Armstrong, Z.; Murphy, M. E. P.; Eltis, L. D., Distal Heme Pocket Residues of B-type Dye-decolorizing Peroxidase ARGININE BUT NOT ASPARTATE IS ESSENTIAL FOR PEROXIDASE ACTIVITY. *Journal of Biological Chemistry* **2012,** *287* (13), 10623-10630.

40. Roberts, J. N.; Singh, R.; Grigg, J. C.; Murphy, M. E.; Bugg, T. D.; Eltis, L. D., Characterization of dye-decolorizing peroxidases from Rhodococcus jostii RHA1. *Biochemistry* **2011,** *50* (23), 5108-19.

41. Sezer, M.; Santos, A.; Kielb, P.; Pinto, T.; Martins, L. O.; Todorovic, S., Distinct structural and redox properties of the heme active site in bacterial dye decolorizing peroxidase-type peroxidases from two subfamilies: resonance Raman and electrochemical study. *Biochemistry* **2013,** *52* (18), 3074-84.

42. Battistuzzi, G.; Bellei, M.; Bortolotti, C. A.; Sola, M., Redox properties of heme peroxidases. *Arch Biochem Biophys* **2010,** *500* (1), 21-36.

43. Torres, E.; Ayala, M., *Biocatalysis Based on Heme Peroxidases: Peroxidases as Potential Industrial Biocatalysts*. Springer Science & Business Media: 2010.

44. Sugano, Y.; Muramatsu, R.; Ichiyanagi, A.; Sato, T.; Shoda, M., DyP, a unique dye-decolorizing peroxidase, represents a novel heme peroxidase family: ASP171 replaces the distal histidine of classical peroxidases. *J Biol Chem* **2007,** *282* (50), 36652-8.

45. Shrestha, R.; Huang, G.; Meekins, D. A.; Geisbrecht, B. V.; Li, P., Mechanistic Insights into Dye-Decolorizing Peroxidase Revealed by Solvent Isotope and Viscosity Effects. *ACS Catalysis* **2017**, 6352-6364.

46. DiCarlo, C. M.; Vitello, L. B.; Erman, J. E., Reduction potential of yeast cytochrome c peroxidase and three distal histidine mutants: dependence on pH. *J Inorg Biochem* **2011,** *105* (4), 532-7.

47. Marcus, R. A.; Sutin, N., Electron Transfers in Chemistry and Biology. *Biochimica Et Biophysica Acta* **1985,** *811* (3), 265-322.

48. Ayala, M.; Roman, R.; Vazquez-Duhalt, R., A catalytic approach to estimate the redox potential of heme-peroxidases. *Biochem Biophys Res Commun* **2007,** *357* (3), 804-8.

49. Liers, C.; Aranda, E.; Strittmatter, E.; Piontek, K.; Plattner, D. A.; Zorn, H.; Ullrich, R.; Hofrichter, M., Phenol oxidation by DyP-type peroxidases in comparison to fungal and plant peroxidases. *J Mol Catal B-Enzym* **2014,** *103*, 41-46.

50. Mendes, S.; Brissos, V.; Gabriel, A.; Catarino, T.; Turner, D. L.; Todorovic, S.; Martins, L. O., An integrated view of redox and catalytic properties of B-type PpDyP from Pseudomonas putida MET94 and its distal variants. *Arch Biochem Biophys* **2015,** *574*, 99-107.

51. Arnhold, J.; Furtmuller, P. G.; Regelsberger, G.; Obinger, C., Redox properties of the couple compound I/native enzyme of myeloperoxidase and eosinophil peroxidase. *Eur J Biochem* **2001,** *268* (19), 5142-8.

52. Furtmuller, P. G.; Arnhold, J.; Jantschko, W.; Pichler, H.; Obinger, C., Redox properties of the couples compound I/compound II and compound II/native enzyme of human myeloperoxidase. *Biochem Biophys Res Commun* **2003,** *301* (2), 551-7.

53. Furtmuller, P. G.; Arnhold, J.; Jantschko, W.; Zederbauer, M.; Jakopitsch, C.; Obinger, C., Standard reduction potentials of all couples of the peroxidase cycle of lactoperoxidase. *J Inorg Biochem* **2005,** *99* (5), 1220-9.

54. Efimov, I.; Papadopoulou, N. D.; McLean, K. J.; Badyal, S. K.; Macdonald, I. K.; Munro, A. W.; Moody, P. C.; Raven, E. L., The redox properties of ascorbate peroxidase. *Biochemistry* **2007,** *46* (27), 8017-23.

55. Mondal, M. S.; Fuller, H. A.; Armstrong, F. A., Direct measurement of the reduction potential of catalytically active cytochrome c peroxidase compound I: Voltammetric detection of a reversible, cooperative two-electron transfer reaction. *Journal of the American Chemical Society* **1996,** *118* (1), 263-264.

56. Farhangrazi, Z. S.; Copeland, B. R.; Nakayama, T.; Amachi, T.; Yamazaki, I.; Powers, L. S., Oxidation-Reduction Properties of Compound-I and Compound-Ii of Arthromyces-Ramosus Peroxidase. *Biochemistry* **1994,** *33* (18), 5647-5652.

57. Yoshida, T.; Sugano, Y., A structural and functional perspective of DyP-type peroxidase family. *Arch Biochem Biophys* **2015,** *574*, 49-55.

58. Rahmanpour, R.; Bugg, T. D., Assembly in vitro of Rhodococcus jostii RHA1 encapsulin and peroxidase DypB to form a nanocompartment. *FEBS J* **2013,** *280* (9), 2097-104.

59. Sutter, M.; Boehringer, D.; Gutmann, S.; Gunther, S.; Prangishvili, D.; Loessner, M. J.; Stetter, K. O.; Weber-Ban, E.; Ban, N., Structural basis of enzyme encapsulation into a bacterial nanocompartment. *Nat Struct Mol Biol* **2008,** *15* (9), 939-47.

60. Contreras, H.; Joens, M. S.; McMath, L. M.; Le, V. P.; Tullius, M. V.; Kimmey, J. M.; Bionghi, N.; Horwitz, M. A.; Fitzpatrick, J. A.; Goulding, C. W., Characterization of a Mycobacterium tuberculosis nanocompartment and its potential cargo proteins. *J Biol Chem* **2014,** *289* (26), 18279-89.

61. Yoshida, T.; Ogola, H. J. O.; Amano, Y.; Hisabori, T.; Ashida, H.; Sawa, Y.; Tsuge, H.; Sugano, Y., Anabaena sp DyP-type peroxidase is a tetramer consisting of two asymmetric dimers. *Proteins-Structure Function and Bioinformatics* **2016,** *84* (1), 31-42.

62. Strittmatter, E.; Liers, C.; Ullrich, R.; Wachter, S.; Hofrichter, M.; Plattner, D. A.; Piontek, K., First crystal structure of a fungal high-redox potential dye-decolorizing peroxidase: substrate interaction sites and long-range electron transfer. *J Biol Chem* **2013,** *288* (6), 4095-102.

63. Strittmatter, E.; Plattner, D. A.; Piontek, K., Dye-Decolorizing Peroxidase (DyP). In *Encyclopedia of Inorganic and Bioinorganic Chemistry*, John Wiley & Sons, Ltd: 2011.

64. Zubieta, C.; Joseph, R.; Krishna, S. S.; McMullan, D.; Kapoor, M.; Axelrod, H. L.; Miller, M. D.; Abdubek, P.; Acosta, C.; Astakhova, T.; Carlton, D.; Chiu, H. J.; Clayton, T.; Deller, M. C.; Duan, L.; Elias, Y.; Elsliger, M. A.; Feuerhelm, J.; Grzechnik, S. K.; Hale, J.; Han, G. W.; Jaroszewski, L.; Jin, K. K.; Klock, H. E.; Knuth, M. W.; Kozbial, P.; Kumar, A.; Marciano, D.; Morse, A. T.; Murphy, K. D.; Nigoghossian, E.; Okach, L.; Oommachen, S.; Reyes, R.; Rife, C. L.; Schimmel, P.; Trout, C. V.; van den Bedem, H.; Weekes, D.; White, A.; Xu, Q.; Hodgson, K. O.; Wooley, J.; Deacon, A. M.; Godzik, A.; Lesley, S. A.; Wilson, I. A., Identification and structural characterization of heme binding in a novel dye-decolorizing peroxidase, TyrA. *Proteins* **2007,** *69* (2), 234-43.

65. Uchida, T.; Sasaki, M.; Tanaka, Y.; Ishimori, K., A Dye-Decolorizing Peroxidase from Vibrio cholerae. *Biochemistry* **2015,** *54* (43), 6610-21.

66. Zubieta, C.; Krishna, S. S.; Kapoor, M.; Kozbial, P.; McMullan, D.; Axelrod, H. L.; Miller, M. D.; Abdubek, P.; Ambing, E.; Astakhova, T.; Carlton, D.; Chiu, H. J.; Clayton, T.; Deller, M. C.; Duan, L.; Elsliger, M. A.; Feuerhelm, J.; Grzechnik, S. K.; Hale, J.; Hampton, E.; Han, G. W.; Jaroszewski, L.; Jin, K. K.; Klock, H. E.; Knuth, M. W.; Kumar, A.; Marciano, D.; Morse, A. T.; Nigoghossian, E.; Okach, L.; Oommachen, S.; Reyes, R.; Rife, C. L.; Schimmel, P.; van den Bedem, H.; Weekes, D.; White, A.; Xu, Q.; Hodgson, K. O.; Wooley, J.; Deacon, A. M.; Godzik, A.; Lesley, S. A.; Wilson, I. A., Crystal structures of two novel dye-decolorizing peroxidases reveal a beta-barrel fold with a conserved heme-binding motif. *Proteins* **2007,** *69* (2), 223-33.

67. Brown, M. E.; Barros, T.; Chang, M. C., Identification and characterization of a multifunctional dye peroxidase from a lignin-reactive bacterium. *ACS Chem Biol* **2012,** *7* (12), 2074-81.

68. Liu, X.; Du, Q.; Wang, Z.; Zhu, D.; Huang, Y.; Li, N.; Wei, T.; Xu, S.; Gu, L., Crystal structure and biochemical features of EfeB/YcdB from Escherichia coli O157: ASP235 plays divergent roles in different enzyme-catalyzed processes. *J Biol Chem* **2011,** *286* (17), 14922-31.

69. Singh, R.; Grigg, J. C.; Armstrong, Z.; Murphy, M. E.; Eltis, L. D., Distal heme pocket residues of B-type dye-decolorizing peroxidase: arginine but not aspartate is essential for peroxidase activity. *J Biol Chem* **2012,** *287* (13), 10623-30.

70. Sundaramoorthy, M.; Terner, J.; Poulos, T. L., The crystal structure of chloroperoxidase: a heme peroxidase--cytochrome P450 functional hybrid. *Structure* **1995,** *3* (12), 1367-77.

71. Rodriguez-Lopez, J. N.; Smith, A. T.; Thorneley, R. N. F., Recombinant horseradish peroxidase isoenzyme C: the effect of distal haem cavity mutations (His42→Leu and Arg38→Leu) on compound I formation and substrate binding. *JBIC Journal of Biological Inorganic Chemistry* **1996,** *1* (2), 136-142.

72. Yoshida, T.; Tsuge, H.; Hisabori, T.; Sugano, Y., Crystal structures of dye-decolorizing peroxidase with ascorbic acid and 2,6-dimethoxyphenol. *Febs Letters* **2012,** *586* (24), 4351-4356.

73. Singh, R.; Grigg, J. C.; Qin, W.; Kadla, J. F.; Murphy, M. E.; Eltis, L. D., Improved manganese-oxidizing activity of DypB, a peroxidase from a lignolytic bacterium. *ACS Chem Biol* **2013,** *8* (4), 700-6.

74. Letoffe, S.; Heuck, G.; Delepelaire, P.; Lange, N.; Wandersman, C., Bacteria capture iron from heme by keeping tetrapyrrol skeleton intact. *Proc. Natl. Acad. Sci. U. S. A.* **2009,** *106* (28), 11719-24.

75. Dailey, H. A.; Septer, A. N.; Daugherty, L.; Thames, D.; Gerdes, S.; Stabb, E. V.; Dunn, A. K.; Dailey, T. A.; Phillips, J. D., The Escherichia coli protein YfeX functions as a porphyrinogen oxidase, not a heme dechelatase. *MBio* **2011,** *2* (6), e00248-11.

76. Yim, G.; Kalan, L.; Koteva, K.; Thaker, M. N.; Waglechner, N.; Tang, I.; Wright, G. D., Harnessing the synthetic capabilities of glycopeptide antibiotic tailoring enzymes: characterization of the UK-68,597 biosynthetic cluster. *Chembiochem* **2014,** *15* (17), 2613-23.

77. Ahmad, M.; Roberts, J. N.; Hardiman, E. M.; Singh, R.; Eltis, L. D.; Bugg, T. D., Identification of DypB from Rhodococcus jostii RHA1 as a lignin peroxidase. *Biochemistry* **2011,** *50* (23), 5096-107.

78. Wadhams, G. H.; Armitage, J. P., Making sense of it all: bacterial chemotaxis. *Nat Rev Mol Cell Biol* **2004,** *5* (12), 1024-37.

79. Gaigalat, L.; Schluter, J. P.; Hartmann, M.; Mormann, S.; Tauch, A.; Puhler, A.; Kalinowski, J., The DeoR-type transcriptional regulator SugR acts as a repressor for

genes encoding the phosphoenolpyruvate:sugar phosphotransferase system (PTS) in Corynebacterium glutamicum. *BMC Mol Biol* **2007,** *8*, 104.

80. Kaur, P., Expression and characterization of DrrA and DrrB proteins of Streptomyces peucetius in Escherichia coli: DrrA is an ATP binding protein. *J Bacteriol* **1997,** *179* (3), 569-75.

81. Poulos, T. L.; Kraut, J., The stereochemistry of peroxidase catalysis. *J Biol Chem* **1980,** *255* (17), 8199-205.

82. Sivaraja, M.; Goodin, D. B.; Smith, M.; Hoffman, B. M., Identification by ENDOR of Trp191 as the free-radical site in cytochrome c peroxidase compound ES. *Science* **1989,** *245* (4919), 738-40.

83. Choinowski, T.; Blodig, W.; Winterhalter, K. H.; Piontek, K., The crystal structure of lignin peroxidase at 1.70 A resolution reveals a hydroxy group on the cbeta of tryptophan 171: a novel radical site formed during the redox cycle. *J Mol Biol* **1999,** *286* (3), 809-27.

84. Linde, D.; Ruiz-Duenas, F. J.; Fernandez-Fueyo, E.; Guallar, V.; Hammel, K. E.; Pogni, R.; Martinez, A. T., Basidiomycete DyPs: Genomic diversity, structural-functional aspects, reaction mechanism and environmental significance. *Arch Biochem Biophys* **2015,** *574*, 66-74.

85. Chen, C.; Shrestha, R.; Jia, K.; Gao, P. F.; Geisbrecht, B. V.; Bossmann, S. H.; Shi, J.; Li, P., Characterization of Dye-decolorizing Peroxidase (DyP) from Thermomonospora curvata Reveals Unique Catalytic Properties of A-type DyPs. *J Biol Chem* **2015,** *290* (38), 23447-63.

86. Mendes, S.; Catarino, T.; Silveira, C.; Todorovic, S.; Martins, L. O., The catalytic mechanism of A-type dye-decolourising peroxidase BsDyP: neither aspartate nor arginine is individually essential for peroxidase activity. *Catalysis Science & Technology* **2015,** *5* (12), 5196-5207.

87. Linde, D.; Pogni, R.; Canellas, M.; Lucas, F.; Guallar, V.; Baratto, M. C.; Sinicropi, A.; Saez-Jimenez, V.; Coscolin, C.; Romero, A.; Medrano, F. J.; Ruiz-Duenas, F. J.; Martinez, A. T., Catalytic surface radical in dye-decolorizing peroxidase: a computational, spectroscopic and site-directed mutagenesis study. *Biochem J* **2015,** *466* (2), 253-62.

88. Stolz, A., Basic and applied aspects in the microbial degradation of azo dyes. *Appl Microbiol Biot* **2001,** *56* (1-2), 69-80.

89. Brown, M. A.; Devito, S. C., Predicting Azo-Dye Toxicity. *Crit Rev Env Sci Tec* **1993,** *23* (3), 249-324.

90. Robinson, T.; McMullan, G.; Marchant, R.; Nigam, P., Remediation of dyes in textile effluent: a critical review on current treatment technologies with a proposed alternative. *Bioresource Technol* **2001,** *77* (3), 247-255.

91. Ollikka, P.; Alhonmaki, K.; Leppanen, V. M.; Glumoff, T.; Raijola, T.; Suominen, I., Decolorization of Azo, Triphenyl Methane, Heterocyclic, and Polymeric Dyes by Lignin Peroxidase Isoenzymes from Phanerochaete chrysosporium. *Appl Environ Microbiol* **1993,** *59* (12), 4010-6.

92. Chivukula, M.; Spadaro, J. T.; Renganathan, V., Lignin Peroxidase-Catalyzed Oxidation of Sulfonated Azo Dyes Generates Novel Sulfophenyl Hydroperoxides. *Biochemistry* **1995,** *34* (23), 7765-7772.

93. Ferreira-Leitao, V. S.; Carvalho, M. E. A.; Bon, E. P. S., Lignin peroxidase efficiency for methylene blue decolouration: Comparison to reported methods. *Dyes Pigments* **2007,** *74* (1), 230-236.

94. Young, L.; Yu, J., Ligninase-catalysed decolorization of synthetic dyes. *Water Res* **1997,** *31* (5), 1187-1193.

95. Heinfling, A.; Martinez, M. J.; Martinez, A. T.; Bergbauer, M.; Szewzyk, U., Purification and characterization of peroxidases from the dye-decolorizing fungus Bjerkandera adusta. *FEMS Microbiol Lett* **1998,** *165* (1), 43-50.

96. Camarero, S.; Sarkar, S.; Ruiz-Duenas, F. J.; Martinez, M. J.; Martinez, A. T., Description of a versatile peroxidase involved in the natural degradation of lignin that has both manganese peroxidase and lignin peroxidase substrate interaction sites. *Journal of Biological Chemistry* **1999,** *274* (15), 10324-10330.

97. Santos, A.; Mendes, S.; Brissos, V.; Martins, L. O., New dye-decolorizing peroxidases from Bacillus subtilis and Pseudomonas putida MET94: towards biotechnological applications. *Appl Microbiol Biotechnol* **2014,** *98* (5), 2053-65.

98. Min, K.; Gong, G.; Woo, H. M.; Kim, Y.; Um, Y., A dye-decolorizing peroxidase from Bacillus subtilis exhibiting substrate-dependent optimum temperature for dyes and beta-ether lignin dimer. *Sci Rep* **2015,** *5*, 8245.

99. Rahmanpour, R.; Bugg, T. D., Characterisation of Dyp-type peroxidases from Pseudomonas fluorescens Pf-5: Oxidation of Mn(II) and polymeric lignin by Dyp1B. *Arch Biochem Biophys* **2015,** *574*, 93-8.

100. Li, J.; Liu, C.; Li, B.; Yuan, H.; Yang, J.; Zheng, B., Identification and molecular characterization of a novel DyP-type peroxidase from Pseudomonas aeruginosa PKE117. *Appl Biochem Biotechnol* **2012,** *166* (3), 774-85.

101. Sugawara, K.; Nishihashi, Y.; Narioka, T.; Yoshida, T.; Morita, M.; Sugano, Y., Characterization of a novel DyP-type peroxidase from Streptomyces avermitilis. *J Biosci Bioeng* **2017,** *123* (4), 425-430.

102. Fernandez-Fueyo, E.; Linde, D.; Almendral, D.; Lopez-Lucendo, M. F.; Ruiz-Duenas, F. J.; Martinez, A. T., Description of the first fungal dye-decolorizing peroxidase oxidizing manganese(II). *Appl Microbiol Biotechnol* **2015,** *99* (21), 8927-42.

103. Gawehn, K.; Wielinger, H.; Werner, W., Screening of Chromogens for Determination of Glucose in Blood According to God/Pod-Method. *Z Anal Chem Freseniu* **1970,** *252* (2-3), 222-+.

104. Goodwin, D. C.; Yamazaki, I.; Aust, S. D.; Grover, T. A., Determination of Rate Constants for Rapid Peroxidase Reactions. *Analytical Biochemistry* **1995,** *231* (2), 333-338.

105. Xu, F.; Shin, W. S.; Brown, S. H.; Wahleithner, J. A.; Sundaram, U. M.; Solomon, E. I., A study of a series of recombinant fungal laccases and bilirubin oxidase that exhibit significant differences in redox potential, substrate specificity, and stability. *Bba-Protein Struct M* **1996,** *1292* (2), 303-311.

106. Scott, S. L.; Chen, W. J.; Bakac, A.; Espenson, J. H., Spectroscopic Parameters, Electrode-Potentials, Acid Ionization-Constants, and Electron-Exchange Rates of the 2,2'-Azinobis(3-Ethylbenzothiazoline-6-Sulfonate) Radicals and Ions. *J Phys Chem-Us* **1993,** *97* (25), 6710-6714.

107. Xu, F., Effects of redox potential and hydroxide inhibition on the pH activity profile of fungal laccases. *Journal of Biological Chemistry* **1997,** *272* (2), 924-928.

108. Bourbonnais, R.; Leech, D.; Paice, M. G., Electrochemical analysis of the interactions of laccase mediators with lignin model compounds. *Bba-Gen Subjects* **1998,** *1379* (3), 381-390.

109. Chaplin, A. K.; Wilson, M. T.; Worrall, J. A. R., Kinetic characterisation of a dye decolourising peroxidase from Streptomyces lividans: new insight into the mechanism of anthraquinone dye decolourisation. *Dalton Trans* **2017,** *46* (29), 9420-9429.

110. Wasak, A.; Drozd, R.; Struk, L.; Grygorcewicz, B., Entrapment of DyP-type peroxidase from Pseudomonas fluorescens Pf-5 into Ca-alginate magnetic beads. *Biotechnol Appl Biochem* **2017**.

111. Brissos, V.; Tavares, D.; Sousa, A. C.; Robalo, M. P.; Martins, L. O., Engineering a Bacterial DyP-Type Peroxidase for Enhanced Oxidation of Lignin-Related Phenolics at Alkaline pH. *Acs Catalysis* **2017,** *7* (5), 3454-3465.

112. Johjima, T.; Ohkuma, M.; Kudo, T., Isolation and cDNA cloning of novel hydrogen peroxide-dependent phenol oxidase from the basidiomycete Termitomyces albuminosus. *Appl Microbiol Biotechnol* **2003,** *61* (3), 220-5.

113. Liers, C.; Pecyna, M. J.; Kellner, H.; Worrich, A.; Zorn, H.; Steffen, K. T.; Hofrichter, M.; Ullrich, R., Substrate oxidation by dye-decolorizing peroxidases (DyPs) from wood- and litter-degrading agaricomycetes compared to other fungal and plant heme-peroxidases. *Appl Microbiol Biot* **2013,** *97* (13), 5839-5849.

114. Tien, M.; Kirk, T. K., Lignin Peroxidase of Phanerochaete-Chrysosporium. *Method Enzymol* **1988,** *161*, 238-249.

115. Miki, Y.; Calvino, F. R.; Pogni, R.; Giansanti, S.; Ruiz-Duenas, F. J.; Martinez, M. J.; Basosi, R.; Romero, A.; Martinez, A. T., Crystallographic, Kinetic, and Spectroscopic Study of the First Ligninolytic Peroxidase Presenting a Catalytic Tyrosine. *Journal of Biological Chemistry* **2011,** *286* (17), 15525-15534.

116. Mceldoon, J. P.; Pokora, A. R.; Dordick, J. S., Lignin Peroxidase-Type Activity of Soybean Peroxidase. *Enzyme Microb Tech* **1995,** *17* (4), 359-365.

117. Rodriguez-Lopez, J. N.; Smith, A. T.; Thorneley, R. N., Role of arginine 38 in horseradish peroxidase. A critical residue for substrate binding and catalysis. *J Biol Chem* **1996,** *271* (8), 4023-30.

118. Hoffmann, M.; Seidel, J.; Einsle, O., CcpA from Geobacter sulfurreducens Is a Basic Di-Heme Cytochrome c Peroxidase. *Journal of Molecular Biology* **2009,** *393* (4), 951-965.

119. Yadav, M.; Rai, N.; Yadav, H. S., The role of peroxidase in the enzymatic oxidation of phenolic compounds to quinones from Luffa aegyptiaca (gourd) fruit juice. *Green Chemistry Letters and Reviews* **2017,** *10* (3), 154-161.

120. Mohan, D.; Pittman, C. U.; Steele, P. H., Pyrolysis of wood/biomass for bio-oil: A critical review. *Energ Fuel* **2006,** *20* (3), 848-889.

121. Yoshida, T.; Tsuge, H.; Hisabori, T.; Sugano, Y., Crystal structures of dye-decolorizing peroxidase with ascorbic acid and 2,6-dimethoxyphenol. *FEBS Lett* **2012,** *586* (24), 4351-6.

122. Hepbasli, A., A key review on exergetic analysis and assessment of renewable energy resources for a sustainable future. *Renew Sust Energ Rev* **2008,** *12* (3), 593-661.

123. Gilbert, J.; Knowles, M. E., The chemistry of smoked foods: a review. *International Journal of Food Science & Technology* **1975,** *10* (3), 245-261.

124. Gierer, J.; Opara, A. E., Studies on Enzymatic Degradation of Lignin - Action of Peroxidase and Laccase on Monomeric and Dimeric Model Compounds. *Acta Chem Scand* **1973,** *27* (8), 2909-2922.

125. Wariishi, H.; Valli, K.; Gold, M. H., Manganese(II) oxidation by manganese peroxidase from the basidiomycete Phanerochaete chrysosporium. Kinetic mechanism and role of chelators. *J Biol Chem* **1992,** *267* (33), 23688-95.

126. Koduri, R. S.; Tien, M., Oxidation of Guaiacol by Lignin Peroxidase - Role of Veratryl Alcohol. *Journal of Biological Chemistry* **1995,** *270* (38), 22254-22258.

127. Hopkins, T. L.; Starkey, S. R.; Xu, R.; Merritt, M. E.; Schaefer, J.; Kramer, K. J., Catechols involved in sclerotization of cuticle and egg pods of the grasshopper, Melanoplus sanguinipes, and their interactions with cuticular proteins. *Archives of Insect Biochemistry and Physiology* **1999,** *40* (3), 119-128.

128. Cohen, S.; Belinky, P. A.; Hadar, Y.; Dosoretz, C. G., Characterization of catechol derivative removal by lignin peroxidase in aqueous mixture. *Bioresource Technol* **2009,** *100* (7), 2247-2253.

129. Fernandes, F. H. A.; Salgado, H. R. N., Gallic Acid: Review of the Methods of Determination and Quantification. *Critical Reviews in Analytical Chemistry* **2016,** *46* (3), 257-265.

130. Mitsuhashi, S.; Saito, A.; Nakajima, N.; Shima, H.; Ubukata, M., Pyrogallol Structure in Polyphenols is Involved in Apoptosis-induction on HEK293T and K562 Cells. *Molecules* **2008,** *13* (12), 2998-3006.

131. Salame, T. M.; Yarden, O.; Hadar, Y., Pleurotus ostreatus manganese-dependent peroxidase silencing impairs decolourization of Orange II. *Microb Biotechnol* **2010,** *3* (1), 93-106.

132. Sundaramoorthy, M.; Kishi, K.; Gold, M. H.; Poulos, T. L., Crystal structures of substrate binding site mutants of manganese peroxidase. *J Biol Chem* **1997,** *272* (28), 17574-80.

133. Shimada, M.; Nakatsubo, F.; Kirk, T. K.; Higuchi, T., Biosynthesis of the Secondary Metabolite Veratryl Alcohol in Relation to Lignin Degradation in Phanerochaete-Chrysosporium. *Arch Microbiol* **1981,** *129* (4), 321-324.

134. Harvey, P. J.; Schoemaker, H. E.; Palmer, J. M., Veratryl Alcohol as a Mediator and the Role of Radical Cations in Lignin Biodegradation by Phanerochaete-Chrysosporium. *Febs Letters* **1986,** *195* (1-2), 242-246.

135. Valli, K.; Wariishi, H.; Gold, M. H., Oxidation of Monomethoxylated Aromatic-Compounds by Lignin Peroxidase - Role of Veratryl Alcohol in Lignin Biodegradation. *Biochemistry* **1990,** *29* (37), 8535-8539.

136. Vanholme, R.; Demedts, B.; Morreel, K.; Ralph, J.; Boerjan, W., Lignin Biosynthesis and Structure. *Plant Physiol* **2010,** *153* (3), 895-905.

137. Boerjan, W.; Ralph, J.; Baucher, M., Lignin biosynthesis. *Annu Rev Plant Biol* **2003,** *54*, 519-546.

138. Rubin, E. M., Genomics of cellulosic biofuels. *Nature* **2008,** *454* (7206), 841-845.

139. Wang, J.; Feng, J.; Jia, W.; Chang, S.; Li, S.; Li, Y., Lignin engineering through laccase modification: a promising field for energy plant improvement. *Biotechnology for Biofuels* **2015,** *8* (1), 145.

140. Camarero, S.; Ibarra, D.; Martinez, A. T.; Romero, J.; Gutierrez, A.; del Rio, J. C., Paper pulp delignification using laccase and natural mediators. *Enzyme Microb Tech* **2007,** *40* (5), 1264-1271.

141. Jacquet, N.; Maniet, G.; Vanderghem, C.; Delvigne, F.; Richel, A., Application of Steam Explosion as Pretreatment on Lignocellulosic Material: A Review. *Ind Eng Chem Res* **2015,** *54* (10), 2593-2598.

142. Sannigrahi, P.; Ragauskas, A. J., Characterization of Fermentation Residues from the Production of Bio-Ethanol from Lignocellulosic Feedstocks. *J Biobased Mater Bio* **2011,** *5* (4), 514-519.

143. Langholtz, M.; Downing, M.; Graham, R.; Baker, F.; Compere, A.; Griffith, W.; Boeman, R.; Keller, M., Lignin-Derived Carbon Fiber as a Co-Product of Refining Cellulosic Biomass. *SAE Int. J. Mater. Manf.* **2014,** *7* (1), 115-121.

144. Pollegioni, L.; Tonin, F.; Rosini, E., Lignin-degrading enzymes. *Febs Journal* **2015,** *282* (7), 1190-1213.

145. Bugg, T. D. H.; Ahmad, M.; Hardiman, E. M.; Singh, R., The emerging role for bacteria in lignin degradation and bio-product formation. *Curr Opin Biotech* **2011,** *22* (3), 394-400.

146. Lambertz, C.; Ece, S.; Fischer, R.; Commandeur, U., Progress and obstacles in the production and application of recombinant lignin-degrading peroxidases. *Bioengineered* **2016,** *7* (3), 145-154.

147. Wong, D. W. S., Structure and Action Mechanism of Ligninolytic Enzymes. *Appl Biochem Biotech* **2009,** *157* (2), 174-209.

148. Santos, R. B.; Hart, P. W.; Jameel, H.; Chang, H. M., Wood Based Lignin Reactions Important to the Biorefinery and Pulp and Paper Industries. *Bioresources* **2013,** *8* (1), 1456-1477.

149. Lundell, T.; Wever, R.; Floris, R.; Harvey, P.; Hatakka, A.; Brunow, G.; Schoemaker, H., Lignin Peroxidase L3 from Phlebia-Radiata - Pre-Steady-State and Steady-State Studies with Veratryl Alcohol and a Nonphenolic Lignin Model-Compound 1-(3,4-Dimethoxyphenyl)-2-(2-Methoxyphenoxy)Propane-1,3-Diol. *European Journal of Biochemistry* **1993,** *211* (3), 391-402.

150. Liers, C.; Pecyna, M. J.; Kellner, H.; Worrich, A.; Zorn, H.; Steffen, K. T.; Hofrichter, M.; Ullrich, R., Substrate oxidation by dye-decolorizing peroxidases (DyPs) from wood- and litter-degrading agaricomycetes compared to other fungal and plant heme-peroxidases. *Appl Microbiol Biotechnol* **2013,** *97* (13), 5839-49.

151. Wei, K.; Luo, S. W.; Fu, Y.; Liu, L.; Guo, Q. X., A theoretical study on bond dissociation energies and oxidation potentials of monolignols. *J Mol Struc-Theochem* **2004,** *712* (1-3), 197-205.

152. Loncar, N.; Colpa, D. I.; Fraaije, M. W., Exploring the biocatalytic potential of a DyP-type peroxidase by profiling the substrate acceptance of Thermobifida fusca DyP peroxidase. *Tetrahedron* **2016,** *72* (46), 7276-7281.

153. Chen, Y. H.; Chai, L. Y.; Zhu, Y. H.; Yang, Z. H.; Zheng, Y.; Zhang, H., Biodegradation of kraft lignin by a bacterial strain Comamonas sp B-9 isolated from eroded bamboo slips. *J Appl Microbiol* **2012,** *112* (5), 900-906.

154. Rahmanpour, R.; Rea, D.; Jamshidi, S.; Fulop, V.; Bugg, T. D., Structure of Thermobifida fusca DyP-type peroxidase and activity towards Kraft lignin and lignin model compounds. *Arch Biochem Biophys* **2016,** *594*, 54-60.

155. Linde, D.; Canellas, M.; Coscolin, C.; Davo-Siguero, I.; Romero, A.; Lucas, F.; Ruiz-Duenas, F. J.; Guallar, V.; Martinez, A. T., Asymmetric sulfoxidation by engineering the heme pocket of a dye-decolorizing peroxidase. *Catalysis Science & Technology* **2016,** *6* (16), 6277-6285.

156. Mueller, S., Sensitive and nonenzymatic measurement of hydrogen peroxide in biological systems. *Free Radical Bio Med* **2000,** *29* (5), 410-415.

157. Giorgio, M.; Trinei, M.; Migliaccio, E.; Pelicci, P. G., Hydrogen peroxide: a metabolic by-product or a common mediator of ageing signals? *Nat Rev Mol Cell Bio* **2007,** *8* (9), 722a-728.

158. Song, X.; Mosby, N.; Yang, J.; Xu, A.; Abdel-Malek, Z.; Kadekaro, A. L., alpha-MSH activates immediate defense responses to UV-induced oxidative stress in human melanocytes. *Pigment Cell Melanoma Res* **2009,** *22* (6), 809-18.

159. Hiner, A. N.; Hernandez-Ruiz, J.; Williams, G. A.; Arnao, M. B.; Garcia-Canovas, F.; Acosta, M., Catalase-like oxygen production by horseradish peroxidase must predominantly be an enzyme-catalyzed reaction. *Arch Biochem Biophys* **2001,** *392* (2), 295-302.

160. Muller, M.; Sorrell, T. C., Modulation of neutrophil superoxide response and intracellular diacylglyceride levels by the bacterial pigment pyocyanin. *Infect Immun* **1997,** *65* (6), 2483-7.

161. Valderrama, B.; Ayala, M.; Vazquez-Duhalt, R., Suicide inactivation of peroxidases and the challenge of engineering more robust enzymes. *Chem Biol* **2002,** *9* (5), 555-65.

Chapter 2 - Characterization of dye-decolorizing peroxidase (DyP) from *Thermomonospora curvata* reveals unique catalytic properties of A-type DyPs[1,2]

2.1 Abstract

Dye-decolorizing peroxidases (DyPs) comprise a new family of heme peroxidases, which has received much attention due to their potential applications in lignin degradation. A new DyP from *Thermomonospora curvata* (*Tc*DyP) was identified and characterized. Unlike other A-type enzymes, *Tc*DyP is highly active towards a wide range of substrates including model lignin compounds, in which the catalytic efficiency with ABTS [k_{cat}^{app}/K_M^{app} = (1.7 × 10^7) $M^{-1}s^{-1}$] is close to that of fungal DyPs. Stopped-flow spectroscopy was employed to elucidate the transient intermediates as well as the catalytic cycle involving wild-type (*wt*) and mutant *Tc*DyPs. While residues D220 and R327 are found necessary for compound I formation, the H312 is proposed to play roles in compound II reduction. Transient kinetics of hydroquinone (HQ) oxidation by *wt*-*Tc*DyP showed that conversion of the compound II to resting state is a rate-limiting step, which will explain the contradictory observation made with the aspartate mutants of A-type DyPs. Moreover, replacement of H312 and R327 shifted the redox potential $E^{\circ\prime}$ to a more negative values. Not only do these results reveal the unique catalytic property of the A-type DyPs, but they will also facilitate the development of these enzymes as lignin degraders.

---

[1] Reprinted with permission from Chen, C.; Shrestha, R.; Jia, K.; Gao, P. F.; Geisbrecht, B. V.; Bossmann, S. H.; Shi, J.; Li, P., Characterization of Dye-decolorizing Peroxidase (DyP) from *Thermomonospora curvata* Reveals Unique Catalytic Properties of A-type DyPs. *J Biol Chem* **2015,** *290* (38), 23447-63. Copyright 2015, The American Society for Biochemistry and Molecular Biology, Inc.

[2] As a second co-author, my contributions to this project are cloning, expression and purification of *Tc*DyP wt and mutant enzymes, measurements of heme contents and spectroelectrochemical determination of redox potential.

2.2 Introduction

Continuing interest in utilization of renewable biomass for generation of biofuels and fine chemicals has brought enormous attention to lignin that is the most abundant aromatic polymer on earth [1-2]. However, due to its extreme recalcitrance, the lignin degradation has to be performed under harsh conditions such as strong acids and bases and high temperature, which will produce toxics to inhibit downstream treatment of the biomass[3]. Thus, methods of mild lignin degradation are being actively sought. A variety of microorganisms have been known to react with and depolymerize lignin. Among them, the fungal system has the highest efficiency using multiple heme- and copper-containing oxidative enzymes[4]. Yet no fungal-based biocatalysts have been developed so far due to difficulties in genetic manipulation and protein expression of fungi. Therefore, there is a growing interest in identifying lignin-degrading enzymes from bacterial sources[5]. *Thermomonospora curvata* is a thermophilic actinomycete isolated from composted stable manure[6]. It is used for breaking down plant materials for biomass conversion at high temperatures[7-8]. Its genome has recently been sequenced[9].

Dye-decolorizing peroxidases (DyPs) are a new family of heme peroxidases that catalyze H_2O_2-dependent oxidation of various molecules[10]. Although their physiological substrates are unknown, they have been demonstrated to carry out lignin degradation, albeit with a low activity[11-13]. Analysis of genome sequence has revealed that DyPs are mostly present in bacteria, whereas only a limited number exists in fungi and higher eukaryotes[14]. They can be subdivided into four types, A, B, C, and D, based on their primary sequences[15]. Identities between different types are at most 15%, each having a unique characteristic sequence. For example, the A-type DyPs contain a *Tat*-dependent signal sequence. However, tertiary structures of all DyPs are surprisingly similar and adopt a ferredoxin-like fold [14]. Among the four classes of DyPs, A-type is studied the least due to low activity. However, increasing evidence [13, 16], including the present report, suggests that A-type DyPs may have potentials in lignin depolymerization.

The mechanism of DyPs has been proposed to be similar to that of plant peroxidases[17-18]. Generally, the catalytic cycle of a plant peroxidase includes the resting state and transient intermediates that consist of compound I and compound II. The resting ferric enzyme [Fe^{3+}] is oxidized by H_2O_2 to produce a high-valence compound I that is designated as $[Fe^{4+}=O]^{+\cdot}$. Reaction of compound I with one equivalent electrons from a reducing substrate generates a $[Fe^{4+}=O]^{+}$ intermediate named compound II. Reduction of compound II by a second substrate molecule regenerates the resting state. While kinetics of these intermediates has been studied with B-type DypB from *Rhodococcus jostii*, it is still unclear which intermediate is involved in the rate-limiting step of the catalytic cycle[11]. Moreover, the catalytic mechanism is yet to be established with A-type DyPs although detection of intermediates was briefly mentioned recently[19].

Sequence analysis of four types of DyPs (Fig. 2.1A) has revealed that three residues surrounding the heme region, histidine, aspartate, and arginine, may play important roles in catalysis. Moreover, a homology model (Fig. 2.1B) was generated for DyP from *T. curvata* (*Tc*DyP) complexed with heme (less of iron) using an online COACH server[20-21]. Compared with the structures of classical plant peroxidases that primarily contain α-helices (*e.g.* horseradish peroxidase, HRP, Fig. 2.1C)[22], DyP enzymes are rich in both α-helices and β-sheets and adopt ferrodoxin-like folds. Similar to the proximal histidine in plant peroxidases (H170 in HRP), the histidine in DyPs (H312 in *Tc*DyP) binds noncovalently with the heme and acts as the 5th ligand to the iron. The distal histidine essential for the plant peroxidases (H42 in HRP) is absent from the DyPs, in which it has been replaced with a conserved aspartate (D220 in *Tc*DyP). This aspartate also forms the so-called GXXDG motif (boxed in Fig. 2.1A) that has been assigned as the fingerprint of all DyPs[18, 23]. In plant peroxidases, the arginine within the heme distal area (R38 in HRP) is necessary for peroxidase activity. However, the role of arginine in DyPs (R327 in *Tc*DyP) is still debatable. While the arginine residue is indispensible for the activity of DypB[24], its substitution with lysine in DyP from *Thanatephorus cucumeris* Dec 1 retains partial

peroxidase activity[23]. Nevertheless, the effects of these three residues on formation of the catalytic intermediates, redox potentials, and oligomeric states of DyPs have yet to be addressed.

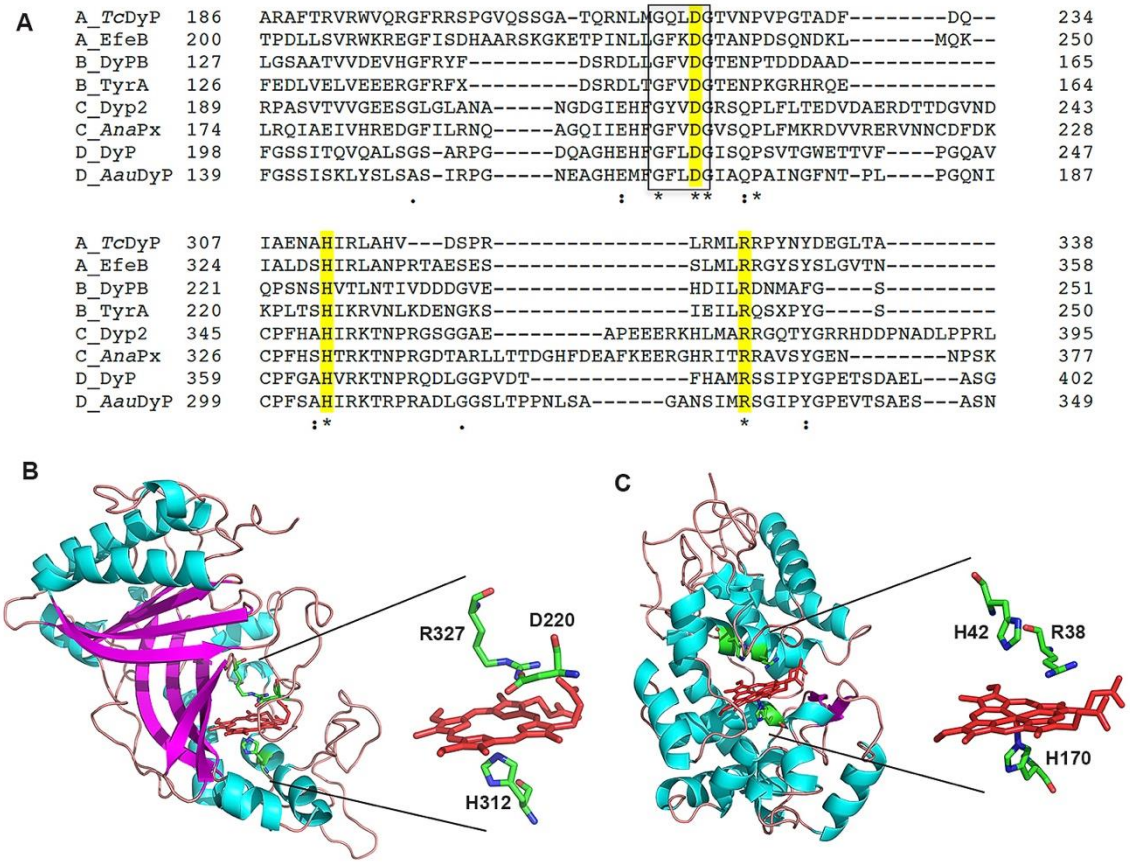

Figure 2.1 Comparison of sequences and structures.

A. Sequence alignment of four types of DyPs. Putative catalytic residues surrounding the heme center are highlighted. The fingerprint motif of DyPs is boxed. *B.* Predicted structure and active site of *Tc*DyP using COACH based on a DyP-type peroxidase from *Stretomyces coelicolor* (PDB 4GRC). The sequence identity between the two proteins and C-score of the homology model are 42% and 0.98, respectively. *C,* Structure and active site of HRP (PDB 1ATJ).

Here we report identification and biochemical characterization of *Tc*DyP (UniProt accession number D1A807). The matured protein was expressed and purified from *Escherichia coli*. The catalytic cycle of the wild-type (*wt*) and mutant *Tc*DyPs were studied by steady-state and transient-state kinetics. Roles of D220, H312, and R327 were identified using a combination of approaches including stopped-flow spectroscopy, spectroelectrochemical titration, and size-exclusion chromatography (SEC). Moreover, degradation of model lignin compounds by *wt-Tc*DyP was investigated using HPLC and

mass spectroscopy (MS). The results are discussed to reveal the unique catalytic property of A-type DyPs.

2.3 Experimental procedures

2.3.1 Instruments, biochemicals, and chemicals

All activity assays and steady-state kinetics were performed in a 96-well format on a SpectraMax Plus 384 microplate reader manufactured by Molecular Devices. Transient-state kinetics was performed using an SX20 stopped-flow spectrometer (Applied PhotoPhysics Ltd, UK) equipped with a sequential mixing, PDA detector, and monochromator. Spectroelectrochemical titrations were carried out on a Cary 100 Bio UV-Vis spectrometer (Agilent) equipped with a temperature controller and magnetic stirring. The redox potentials were measured by a potentiostat (model 650B, CH Instrument). High-pressure liquid chromatography (HPLC) and SEC were performed with a Waters Breeze 2 system equipped with a PDA detector. The electrospray ionization mass spectroscopy (ESI-MS) was performed with Waters Acquity TQD. The inductively coupled plasma optical emission spectrometry (ICP-OES) was carried out on a Varian 720 series system. All chemical and biochemical reagents were of the highest grade commercially available and were used without further purification. Stocks of H_2O_2 were prepared freshly before the experiments and the concentrations were determined at 240 nm (ε_{240} = 43.6 $M^{-1}cm^{-1}$).

2.3.2 Cloning, expression, and purification of matured *Tc*DyP and its mutants

The gene fragments of *Tc*DyP were synthesized by IDT using a gBlocks method. They were amplified and assembled together by PCR following standard protocols [25]. After the PCR products were purified by gel extraction, they were inserted into the SspI site of *p*TBSG [26] to generate *p*PL2014L01, which contains a His_6 tag and TEV cleavage site at the *N*-terminus. Mutants of *Tc*DyP were generated using the QuikChange from Agilent Technologies according to the instructions from manufacturer.

The *wt*-*Tc*DyP were overexpressed in *E. coli* BL21(DE3) cells (Lucigen). A 160 mL starter culture was grown overnight from a single colony in LB media in the presence of 100 μg/mL ampicillin

at 37°C with shaking at 225 rpm and then used to inoculate 8 L of LB medium. When OD_{600} reached 0.6, IPTG and hemin chloride were added to a final concentration of 0.2 mM and 30 μg/mL. The cells were grown at 30°C for additional 14 h and then harvested by centrifugation at 5,000*g* for 30 min at 4 °C. The cell pellets were collected and stored at −80 °C.

All of the following steps were carried out at 4 °C. Purification buffers consisted of buffer A (400 mM NaCl and 50 mM KPi, pH 7.8) and increasing concentrations of imidazole. Buffers B (lysis), C (wash), and D (elution) contained 10, 30, and 250 mM imidazole, respectively. The cell pellets were re-suspended in buffer B and lysed by sonication (25 × 30 s pulsed cycle). The cell debris was removed by centrifugation at 30,000*g* for 45 min and the supernatant was incubated with 30 mL Ni-NTA resin that had been pre-equilibrated with buffer B. The resin was washed with five column volume buffer C and then eluted with buffer D. The fractions containing *Tc*DyP were collected, concentrated, and exchanged into buffer E (100 mM NaCl and 50 mM KPi, pH 7.8) using an Amicon Ultra-15 (10K, EMD Millipore). The purified protein was stored in aliquots at −80 °C until further use. Protein purity was assessed by 12% acrylamide SDS-PAGE. Protein concentration was determined by the BCA assay using a BSA calibration curve [27].

Expression and purification of the mutants were carried out in the same way as described above for the *wt* enzyme except that the H312 mutants were reconstituted before further analysis. Two-fold molar excess of hemin chloride was incubated with the H312 mutants at 4 °C for 4 hrs. The unbound hemin was removed by passing the mixture through DEAE sephacel resin eluted with 30−500 mM NaCl in 20 mM KPi (pH 8.0). Additionally, the excess heme bound with R327A was removed in the same manner as the H312 mutants.

2.3.3 Determination of heme contents

The heme contents of the *wt* and mutants were determined by following a protocol described previously [28]. The amount was calculated using the absorbance difference between the peak at 557 nm and the trough at 541 nm from the subtraction spectrum using $\varepsilon = 20.7\ mM^{-1}cm^{-1}$.

Furthermore, the heme contents were confirmed with ICP-OES. A standard curve of $Fe(NO_3)_3$ with concentrations between 100 and 1,000 μg/L was generated. The protein samples were dialyzed for 12 h against buffer E supplemented with 1 mM EDTA to chelate excess metals and then diluted to a concentration ~ 500 μg Fe^{3+}/L (assuming 100% heme occupancy) before analysis.

2.3.4 Enzyme assay and steady-state kinetics

The peroxidase activity of *wt*-*Tc*DyP against various substrates was determined using a continuous assay by monitoring the absorbance change at a certain wavelength at 22 °C. Briefly, in a 160 μL solution consisting of 50 mM sodium citrate (pH 3.0), 0.5 mM H_2O_2, 0.5 mM substrate, and 0.2 mg/mL bovine serum albumin (BSA), the purified *wt*-*Tc*DyP was added to initiate the reaction. Controls were performed in absence of the enzyme, H_2O_2, or both. The measurements were performed in triplicates. The tested substrates, wavelengths (nm) and corresponding extinction coefficients (ε, $cm^{-1}mM^{-1}$), and the enzyme concentrations (μM) used were: 2,2'-azino-bis(3-ethylbenzothiazoline-6-sulphonic acid) (ABTS): 420, 36, 0.006; catechol: 392, 1.456, 2; 2,4-dichlorophenol: 510, 18.5, 2; 2,6-dimethoxyphenol: 470, 49.6, 2; veratryl alcohol: 340, 93, 2; guaiacol: 465, 26.6, 2; hydroquinone (HQ): 247, 21, 0.2; reactive black 5: 598, 30, 2; reactive blue 4 (RB4): 610, 4.2, 0.3; reactive blue 5 (RB5): 600, 8, 0.1; RB19: 595, 10, 0.05.

To determine steady-state kinetic parameters of the *wt*-*Tc*DyP, the reactions were performed in the same way as described above except that concentration of one substrate was varied in the presence of the other substrate at saturation. The rates were determined by the slopes of the initial reactions. The obtained data were fitted either to Michaelis-Menten Eq. 1 or Hill Eq. 2 using OriginPro 2015. All measurements were done in triplicates.

$$v = \frac{v_{max}[S]}{K_M + [S]} \qquad \text{(Eq. 1)}$$

$$v = \frac{v_{max}[S]^h}{K_M + [S]^h} \qquad \text{(Eq. 2)}$$

Specific activities (SAs) of mutants were measured with 0.5 mM ABTS, 5 mM HQ, or 5 mM guaiacol in the presence of 0.5 mM H_2O_2 following the same protocol as described above. The concentrations of enzyme were: *wt*: 6 nM; D220H, D220N, H312A, H312C: 0.2 μM; D220A, D220F, D220G, D220K, R327A: 2 μM. Additionally, steady-state kinetic parameters of D220A and H312C with guaiacol were also determined in the same way as described above for the *wt*-*Tc*DyP.

2.3.5 Influence of pH on enzyme activity

The pH optimum of *wt*-*Tc*DyP was determined using ABTS in Mcilvaine buffers covering pH 2.5−8.0 [29]. The assay conditions were the same as described above.

2.3.6 Influence of temperature on enzyme activity

The optimal temperature of *wt*-*Tc*DyP was determined by measuring ABTS oxidation as described above at temperatures ranging from 15 to 60 °C.

The thermostability of *wt*-*Tc*DyP was carried out by incubating 12 μM enzyme in buffer E for 1 h in a water bath set to a temperature ranging from 22 to 80 °C. The samples were withdrawn, cooled to 22 °C for 15 min, and immediately analyzed for the residual activity with ABTS as described above.

2.3.7 Reactions with model lignin compounds and mass analysis

The model lignin dimers, guaiacylglycerol-β-guaiacol ether **1** and veratrylglycerol-β-guaiacol ether **2**, were prepared as previously reported [30]. Twenty μM *wt*-*Tc*DyP was incubated with 5.0 mM **1** or **2** and 5.0 mM H_2O_2 in 50 mM sodium citrate (pH 3.0) at 22 °C for 16 h. The mixture was heated at 95 °C for 5 min and the enzyme precipitates were removed by centrifugation. The supernatant was loaded onto an HPLC column (Luna C18-2, 5 μm, 4.6 mm × 250 mm) that was eluted at 1.00 mL/min using a linear gradient from 30 to 90% methanol in *dd*H_2O over 30 min. Each HPLC peak was collected, lyophilized, and analyzed by ESI-MS.

Reactions and analyses with 4-methoxymandelic acid (MMA) were performed in the same way as described above except that 2.5 mM MMA was used in the presence and absence of 5.0 mM $MnCl_2$.

2.3.8 Stopped-flow kinetics

Transient-state kinetics of *wt-Tc*DyP were performed at 22°C at pH 3.0 and 7.8. All reactions were investigated both at defined (monochromator) and multiple (PDA) wavelengths. The PDA data were analyzed using singular value decomposition with the Pro-KIV Global Analysis program provided by Applied PhotoPhysics to obtain the number of reaction intermediates and their corresponding spectra. Reactions were then monitored at selected single wavelengths to follow the formation and decay of intermediates, and single exponential equations were fitted to the data to obtain pseudo-first-order rate constants (k_{obs}). Second-order rate constants were calculated from plots of k_{obs} *vs.* substrate concentrations. All experiments were performed in triplicate.

All concentrations mentioned here were concentrations before mixing. Formation of *wt-Tc*DyP-I was carried out in a conventional mixing mode with 5 μM enzyme and equal volume of H_2O_2 at various concentrations and monitored at 406 nm. Formation of *wt-Tc*DyP-II was performed in a sequential mixing mode, in which 5 μM *wt-Tc*DyP was premixed with equal volume of 5 μM H_2O_2. After maximum formation of *Tc*DyP-I was reached in 100 ms, HQ at various concentrations were mixed with *Tc*DyP-I and the reaction was followed at 416 nm. Reduction of *wt-Tc*DyP-II was performed in a sequential mixing mode, in which 5 μM *wt-Tc*DyP and 5 μM ferrocyanide were premixed with equal volume of 5 μM H_2O_2. The mixture was incubated in the delay line for 5 s and regeneration of *wt-Tc*DyP-0 was monitored at 406 nm after mixing with HQ at various concentrations. Stopped-flow experiments of mutants were carried out in the same way as described above for the *wt-Tc*DyP.

2.3.9 Spectroelectrochemical determination of redox potentials

In a 3.5 mL cuvette, a 3.0 mL solution consisting of 50 mM KPi (pH 7), 100 mM NaCl and a mixture of redox mediators (10 μM each, methyl viologen, anthraquinone-2,6-disulfonic acid, 2-hydroxy-1,4-naphthoquinone, 2,5-dihydroxy-1,4-benzoquinone, duroquinone, 1,2-naphthoquinone, and ferricyanide) was purged with water-saturated argon for 1 h. The electrodes (Ag/AgCl, 012167; Pt gauze, 011498; ALS Co, Japan) were connected to a potentiostat. The *wt*- or mutant *Tc*DyP was added

to a final concentration of 10 μM. The entire mixture was completely reduced to ferrous state with ~5 μL of 100 mM freshly prepared sodium dithionite stock solution. This was then oxidized by stepwise addition of 2−5 μL aliquots of argon-purged 2.5 mM $K_3Fe(CN)_6$. The reaction mixture was kept under water-saturated argon protection during the whole experiment. After each addition, the reaction was allowed to equilibrate with stirring until the difference in potential readings was less than 1 mV/min. Once the equilibrium was established, the UV-Vis spectrum was recorded. The fraction of oxidized *Tc*DyP was calculated by the $\Delta A_{433\ nm}$ and the mid-point reduction potential ($E^{\circ\prime}$) was determined by fitting the data into the Nernst Eq. 3 using OriginPro 2015.

$$f = \frac{1}{1+exp\frac{n\times(E^{\circ}-E^{\circ\prime})}{25.6}} \qquad \text{(Eq. 3)}$$

where *f* is the reduced fraction, *n* is the number of electrons, E° is the potential at each point in mV, and $E^{\circ\prime}$ is the midpoint reduction potential in mV.

The $E^{\circ\prime}$ of *wt*-*Tc*DyP was also determined under pH 6 and 8. All measurements were done in duplicates.

2.4 Results

2.4.1 Protein purification and basic biochemical properties

The gene encoding a DyP-type peroxidase is predicted from the genome sequence of *T. curvata*. Since the efforts to clone it were unsuccessful, the gene (Tcur_2987) corresponding to the predicted matured *Tc*DyP, in which the signal sequence was removed, was synthesized and inserted into the vector *p*TBSG [26] to construct a new plasmid *p*PL2014L01.

The *N*-terminal His-tagged *wt* or mutant *Tc*DyP was purified to homogeneity by Ni-NTA affinity chromatography and migrated as a single band at the predicted size of 42.2 KDa on SDS-PAGE (Fig. 2.2A). The purified *Tc*DyPs exhibited an absorbance maximum at 406−412 nm in its UV-Vis spectrum (Fig. 2.2B), which was consistent with the prediction that *Tc*DyP is a hemoprotein. While the *Reinheitszahl* values ($R_z = A_{406}/A_{280}$) of *wt* and D220 mutants were at ~1.8, H312 and R327 mutants

were determined to be at ~0.9 (due to loss of proximal histidine) and 2.5 (due to nonspecific heme binding), respectively. Thus, the histidine mutants were reconstituted with hemin chloride before further analysis. The excess heme bound with R327A was removed by DEAE ion-exchange chromatography. Heme quantitation by pyridine hemochrome assay (Fig. 2.2C) and ICP-OES revealed that one molecule of *wt*-*Tc*DyP binds one molecule of heme cofactor. The enzyme is most active at pH 3 (Fig. 2.2D), which is slightly more acidic than the other reported DyPs [12, 31]. While the enzyme could retain ~70% maximal activity after incubation at 60 °C for 1 h, the optimal enzyme assay temperature was determined to be 30 °C (Fig. 2.2E). Since the His-tag did not interfere with enzyme activity, future experiments were performed with its presence.

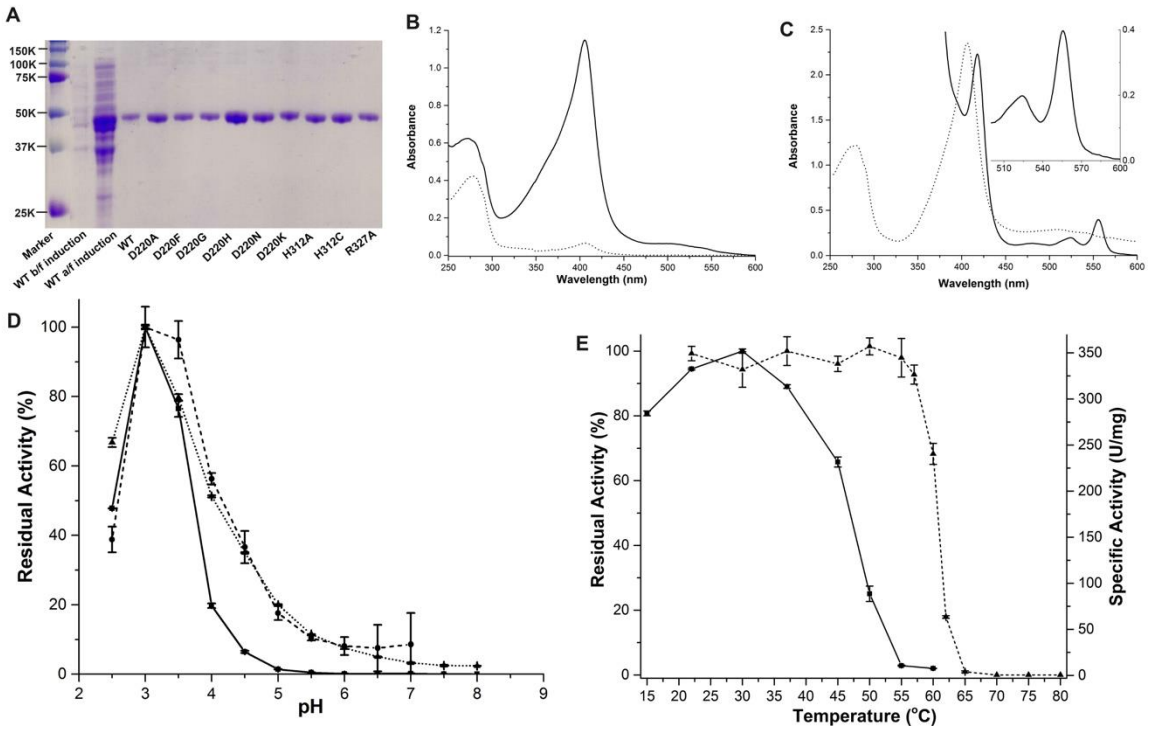

Figure 2.2 Biochemical characterization of *Tc*DyP.

A, SDS-PAGE of *wt*- and mutant *Tc*DyP. *B*, UV-Vis spectra of *wt*-*Tc*DyP in *apo* (dotted line) and *holo* (solid line) forms. *C*, Pyridine hemochrome assay of *Tc*DyP calculated by the absorbance difference between the reduced (solid line) and oxidized (dotted line) spectra using $\Delta\varepsilon = 20.7\ mM^{-1}cm^{-1}$. *D*. Rate-pH profiles of *wt*-*Tc*DyP with ABTS (solid line), HQ (dash line), and guaiacol (dotted line). E. Profiles of optimal assay temperature (solid line) and enzyme stability (dotted line).

2.4.2 Peroxidase activity and steady-state kinetics of *Tc*DyP

In order to explore its substrate scopes, *wt*-*Tc*DyP was tested against a panel of well-known peroxidase substrates including ABTS, aromatics, azo, and anthraquinone dyes. It was found that the peroxidase is inactive toward 2,6-dimethoxyphenol, 2,4-dichlorophenol, veratryl alcohol, and reactive black 5. As shown in Fig. 2.3A, the *wt*-*Tc*DyP displayed low activities towards phenolic compounds such as guaiacol, catechol and HQ. However, unlike other A-type enzymes, the *wt*-*Tc*DyP exhibits extremely high activity towards reactive blue (RB) 4, 5, and 19 (anthraquinone dyes) and ABTS. No catalase activity was detected when the enzyme was incubated with H_2O_2 (data not shown), suggesting that it does not function as a peroxidase-catalase.

It is worth noting that reactions catalyzed by peroxidases generally do not involve Michaelis-Menten intermediates because the catalytic cycle is considered irreversible[32]. However, there is no doubt that adsorption complexes between the enzyme and its substrates exist physically[33]. The microscopic constants governing the equilibrium between reducing substrates and peroxidase have been estimated[34]. Even though the cosubstrates (reducing donor or H_2O_2) modulate each other's affinity to the enzyme, it is possible for the mechanism to proceed via random binding. This observation, together with some special kinetic features[35], supports the notion that there is no need for the peroxide to bind to the enzyme prior to donor adsorption[36]. Since the oxidations of the compounds shown in Fig. 2.3A exhibited classical steady-state kinetics with respect to both substrates, the system was analyzed using Michaelis-Menten equation. The resulting apparent Michaelis constant (K_M^{app}) and turnover number (k_{cat}^{app}) are summarized in Table 2.1. It has to be pointed out that oxidation of ABTS and anthraquinone dyes (RB series) displayed sigmoidal rate curves (not shown). This "apparent cooperative phenomenon" suggests that *Tc*DyP may have multiple oxidation sites like the fungal DyP from *Auricularia auricular-judae*[37-39].

To characterize importance of the proposed catalytic residues, they were mutated and the mutants were tested for their activity against ABTS, HQ, and guaiacol. As shown in Fig. 2.3B, all

mutants lose activity towards ABTS, indicating that these residues are important for ABTS oxidation. In contrast, oxidation of phenolic compounds showed a different profile. While substitution of H312 and R327 resulted in marginal enzyme activities, mutants of D220 displayed up to 83% (patterned bars in Fig. 2.3B). Similar phenomenon was also observed with EfeB from *E. coli O157* [16]. Thus, questions were raised about the catalytic importance of the aspartate in A-type DyPs [14]. The present study of catalytic cycle has resolved the contradiction, which will be described in DISSCUSSION section. It has to be pointed out that the residual activity of H312C with phenolic compounds may result from partial ligand compensation by cysteine.

To determine kinetic parameters of mutants, D220A and H312C were selected because they exhibited relatively high residual peroxidase activities towards guaiacol and would be used for study of catalytic intermediates. As summarized in Table 2.1, while both mutants display similar catalytic efficiency towards guaiacol as the *wt* enzyme, their catalytic efficiency towards H_2O_2 drop by 22- and 88-fold for D220A and H312C, respectively. The decrease is caused by the fact that the mutants have a much higher K_M for H_2O_2 than the *wt*.

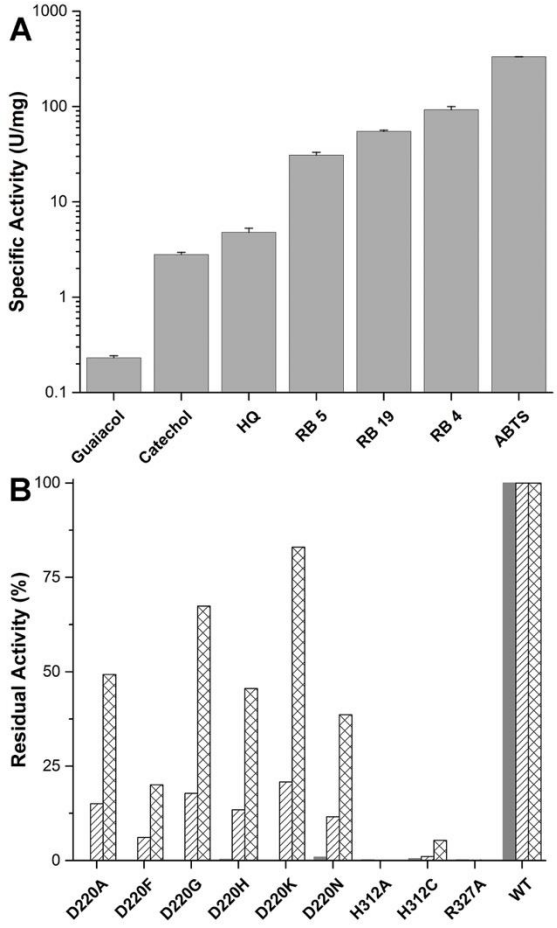

Figure 2.3 Profiles of enzyme activities.

A. The *wt*-*Tc*DyP with various substrates. *B.* Activities of *wt* and mutant enzymes with ABTS (solid bar), HQ (line patterned bar), and guaiacol (cross patterned bar).

Table 2.1 Kinetic parameters of *wt* and mutant *Tc*DyPs[a,b,c]

Enzyme	Substrate		K_M^{app} (μM)	k_{cat}^{app} (s^{-1})	k_{cat}^{app}/K_M^{app} (M^{-1} s^{-1})
wt	ABTS		15 ± 6	260 ± 7	1.7×10^7
	RB4		170 ± 80	110 ± 9	6.5×10^5
	RB19		5.2 ± 0.5	41 ± 1	7.8×10^6
	RB5		43 ± 4	29 ± 1	6.6×10^5
	HQ		6300 ± 880	31 ± 2	4.8×10^3
	Catechol		19000 ± 3500	24 ± 3	1.5×10^3
	Guaiacol		370 ± 90	0.33 ± 0.03	8.8×10^2
	H_2O_2	(ABTS)	84 ± 6	280 ± 6	3.4×10^6
		(HQ)	33 ± 4	27 ± 1	8.2×10^5
		(Guaiacol)	77 ± 20	0.36 ± 0.03	4.7×10^3
D220A	Guaiacol		280 ± 6	0.58 ± 0.03	2.1×10^3
	H_2O_2		2000 ± 160	0.59 ± 0.02	2.1×10^2
H312C	Guaiacol		660 ± 7	0.52 ± 0.02	7.9×10^2
	H_2O_2		11000 ± 1000	0.58 ± 0.01	5.3×10

[a] Assays were performed in 50 mM sodium citrate pH 3.0 at 22 °C. [b] Kinetics of ABTS, RB4, RB19, and RB5 were fitted to the Hill equation. [c] No activity was detected for H312A and R327A mutants.

2.4.3 Oxidation of model lignin compounds by wt-*Tc*DyP

Due to the high catalytic efficiency found with *wt-Tc*DyP, we decided to test its ability to degrade lignin model dimers containing the β-O-4 linkage with (**1**) and without (**2**) a phenolic site. Their structures and HPLC profiles of the reactions are shown in Fig. 2.4A. The results indicate that only the phenolic compound **1** could be depolymerized in the absence of redox mediators, which suggests that the low potential phenolic site ($\Delta E^{\circ\prime} = 0.6-0.8$ V) [40] is required for enzyme activity as no degradation of **2** was observed under the same condition. Similar results have also been obtained with B- and C-type DyPs [12-13]. The incomplete degradation of **1** (retention time at 13.8 min) was due to enzyme instability at pH 3.0 for prolonged time.

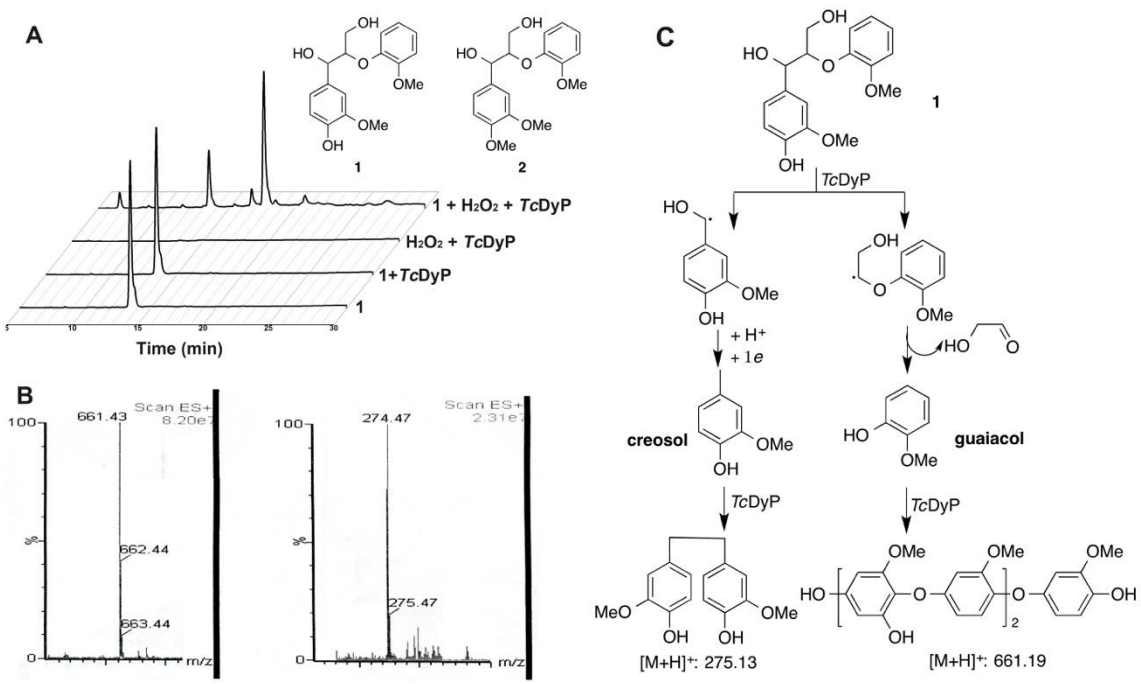

Figure 2.4 Degradation of lignin dimers by *wt-Tc*DyP.

A. Structures of lignin model compounds and degradation HPLC profiles of **1** monitored at 254 nm. *B.* ESI-MS of the HPLC peak at 17.5 (left) and 20.8 (right) min. *C.* Proposed pathway for formation of the degradation products.

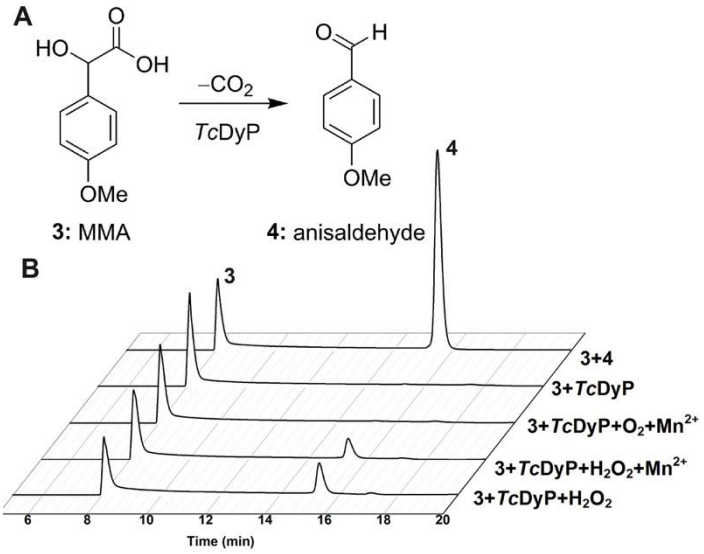

Figure 2.5 Degradation of MMA by *wt*-*Tc*DyP.

A. Oxidative decarboxylation of MMA **3** to anisaldehyde **4**. *B*. HPLC profiles monitored at 254 nm.

To characterize the degradation products of **1**, peaks at 6.5, 16.6, 17.5, and 20.8 min were collected and analyzed by ESI-MS. Only the latter two peaks were identified and their mass spectra are shown in Fig. 2.4B. The peak at 17.5 min had an *m/z* of 661.43, indicating that the radical recombination was taking place to give a high molecular species that is likely the hydroxylated guaiacol pentamer (MH^+ 661.19). The peak at 20.8 min was assigned as a creosol dimer (MH^+ 275.13) that corresponds to the observed *m/z* of 274.47. The pathway for the formation of these products is proposed in Fig. 2.4C, indicating that C_α–C_β cleavage occurred upon incubation with *wt*-*Tc*DyP.

Since no activity was observed with nonphenolic lignin dimer **2**, we decide to test another nonphenolic lignin peroxidase substrate, MMA **3** (Fig. 2.5A) that has been used to detect high potential oxidative events ($\Delta E^{o\prime} > 1.4$ V) occurred in lignin breakdown by fungi [41-42]. MMA has also been reported to undergo decarboxylation to form anisaldehyde **4** through Mn^{2+}-dependent oxidase activity of C-type DyP2 [12]. In our case, when *wt*-*Tc*DyP was incubated with MMA, it was found that only H_2O_2 was required for MMA oxidative decarboxylation (Fig. 2.5B). Because *wt*-*Tc*DyP could not oxidize MMA in the presence of Mn^{2+} and O_2, it suggested that the enzyme did not contain oxidase activity like the DyP2 [12].

2.4.4 Detection of catalytic intermediates using stopped-flow spectroscopy

Since the *wt*-*Tc*DyP displayed high activities towards various substrates and could depolymerize model lignin compound **1** and MMA, we decided to investigate the intermediates involving heme center to better understand catalytic cycle of DyPs.

2.4.4.1 Compound I (*Tc*DyP-I) formation.

The left panel in Fig. 2.6A shows the spectral changes upon conventional mixing of *wt*-*Tc*DyP and H_2O_2 at 7.8. When it was analyzed by Pro-KIV, a two-step reaction of A→B→C was given as the best fit. Since the resting state, compound I, and compound II have been reported with many heme peroxidases including their spectral characters [43], A and B were assigned as the resting state (*Tc*DyP-0, blue line) and compound I (*Tc*DyP-I, green line), respectively. As summarized in Table 2.2, when *Tc*DyP-0 was converted into *Tc*DyP-I, the Soret band shifted slightly to a longer wavelength (406 to 407 nm) along with a new Q-band at 512 nm. To calculate the rate of compound I formation, *wt*-*Tc*DyP was rapidly mixed with H_2O_2 and the reaction was monitored at 406 nm for the decay of *Tc*DyP-0 (left panel in Fig. 2.6B). The results were fitted into a single-exponential equation to obtain the pseudo-first-order rate constant $k_{obs\ (406\ nm)}$. By plotting $k_{obs\ (406\ nm)}$ *vs* H_2O_2 concentrations, the second-order rate constant was determined to be $(5.92 \pm 0.31) \times 10^6\ M^{-1}\ s^{-1}$ at pH 7.8 (right panel in Fig. 2.6B).

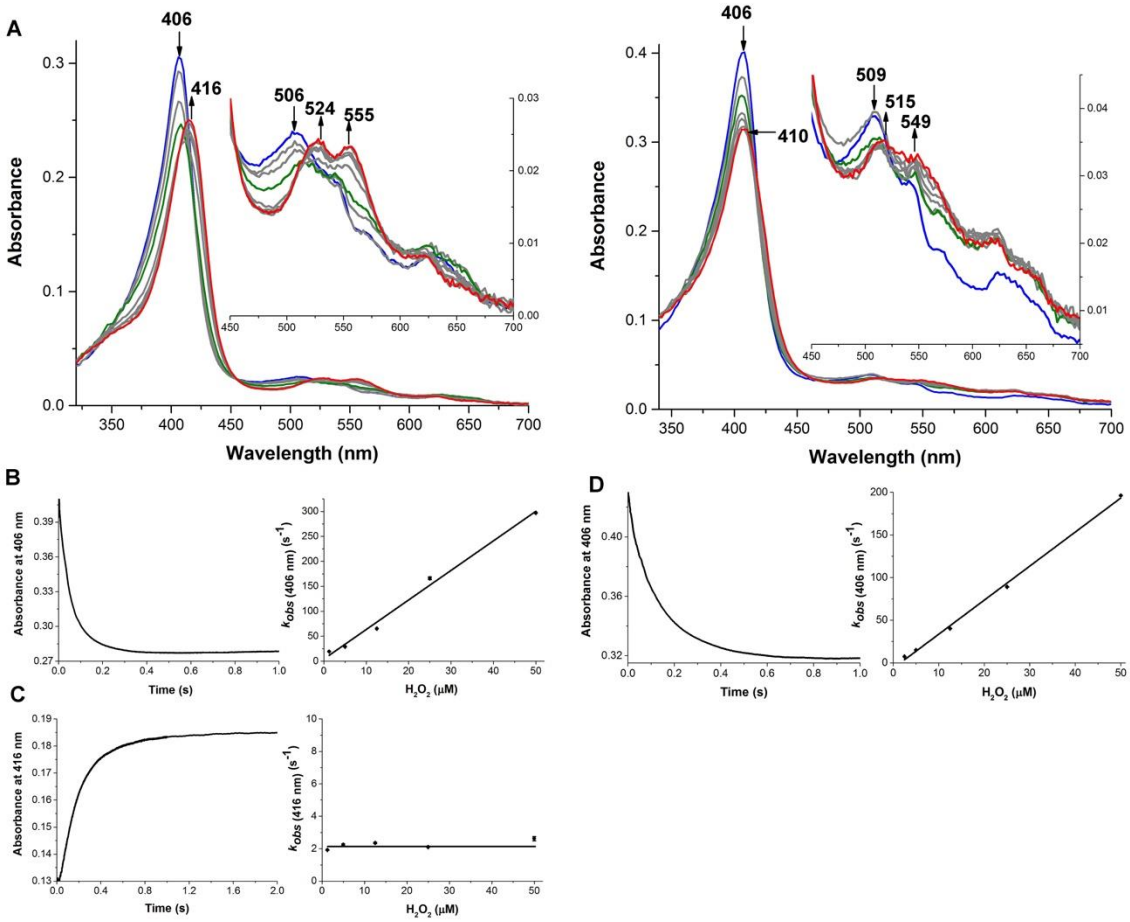

Figure 2.6 Reactions of *wt-Tc*DyP with H_2O_2.

A. Spectral transition of 5 μM enzyme and 5 μM H_2O_2 at pH 7.8 (left) and 3.0 (right) recorded in 2.0 s. The blue, green, and red lines represent *Tc*DyP-0, *Tc*DyP-I, and decay product, respectively. Arrows indicate changes of absorbance over time. *B.* Typical time trace at 406 nm (left) and dependence of $k_{obs\ (406\ nm)}$ *vs* [H_2O_2] (right) for *Tc*DyP-I formation at pH 7.8. *C.* Typical time trace at 416 nm (left) and dependence of $k_{obs\ (416\ nm)}$ *vs* [H_2O_2] (right) for decay of *Tc*DyP-I at pH 7.8. *D.* Same as *B* except that the pH was 3.0.

The spectrum corresponding to intermediate C (red line) has a Soret band at 416 nm and two Q-bands at 524 and 555 nm, which is consistent with features of compound II identified in DyPs and plant peroxidases [18-19, 44]. Thus, it was initially assigned as a compound II species and was expected to have a relationship with H_2O_2. To define the relationship, formation of C was monitored at 416 nm (left panel in Fig. 2.6C). It was found that the $k_{obs\ (416\ nm)}$ was independent of H_2O_2 concentration (right panel, Fig. 2.6C), which indicated that C was not a compound II species. Due to its spectral resemblance to the

reported compound II-type species [43], it was reassigned as a compound II-like decay product of *Tc*DyP-I.

To facilitate comparison with the steady-state results, the transient kinetics was repeated at pH 3.0. The second-order rate constant of *Tc*DyP-I formation was determined to be $(4.06 \pm 0.02) \times 10^6$ M^{-1} s^{-1} (right panel in Fig. 2.6D), which is comparable to the rate constant at pH 7.8.

2.4.4.2 Compound II (*Tc*DyP-II) formation.

Since *Tc*DyP-II was not found with H_2O_2, we decided to determine whether it would form in a reaction in the presence of a substrate. HQ was selected because its oxidation does not interfere with absorbance of the enzyme at 380−450 nm range [45]. The reaction was performed in a sequential mixing mode and the delay time was set at 100 ms, during which maximal *Tc*DyP-I had been reached but the decay had not occurred yet. As shown in Fig. 2.7A, the initial spectrum (green lines) corresponds to *Tc*DyP-I. When the reaction was carried out under neutral conditions (top panel in Fig. 2.7A), a Soret band at 416 nm and two Q-bands at 524 and 555 nm appeared and their intensities increased over the time. In contrast with the experiments where only H_2O_2 was present, the pseudo-first-order rate constants monitored at 416 nm displayed a linear relationship with the HQ concentrations (right panel in Fig. 2.7B), giving a second-order rate constant of $(2.24 \pm 0.09) \times 10^4$ M^{-1} s^{-1}. Thus, this new species was assigned as the *Tc*DyP-II. Since the spectral change at pH 3 (bottom panel in Fig. 2.7A) was small, the second-order rate constant was not determined because an appropriate wavelength for monitoring *Tc*DyP-II could not be identified.

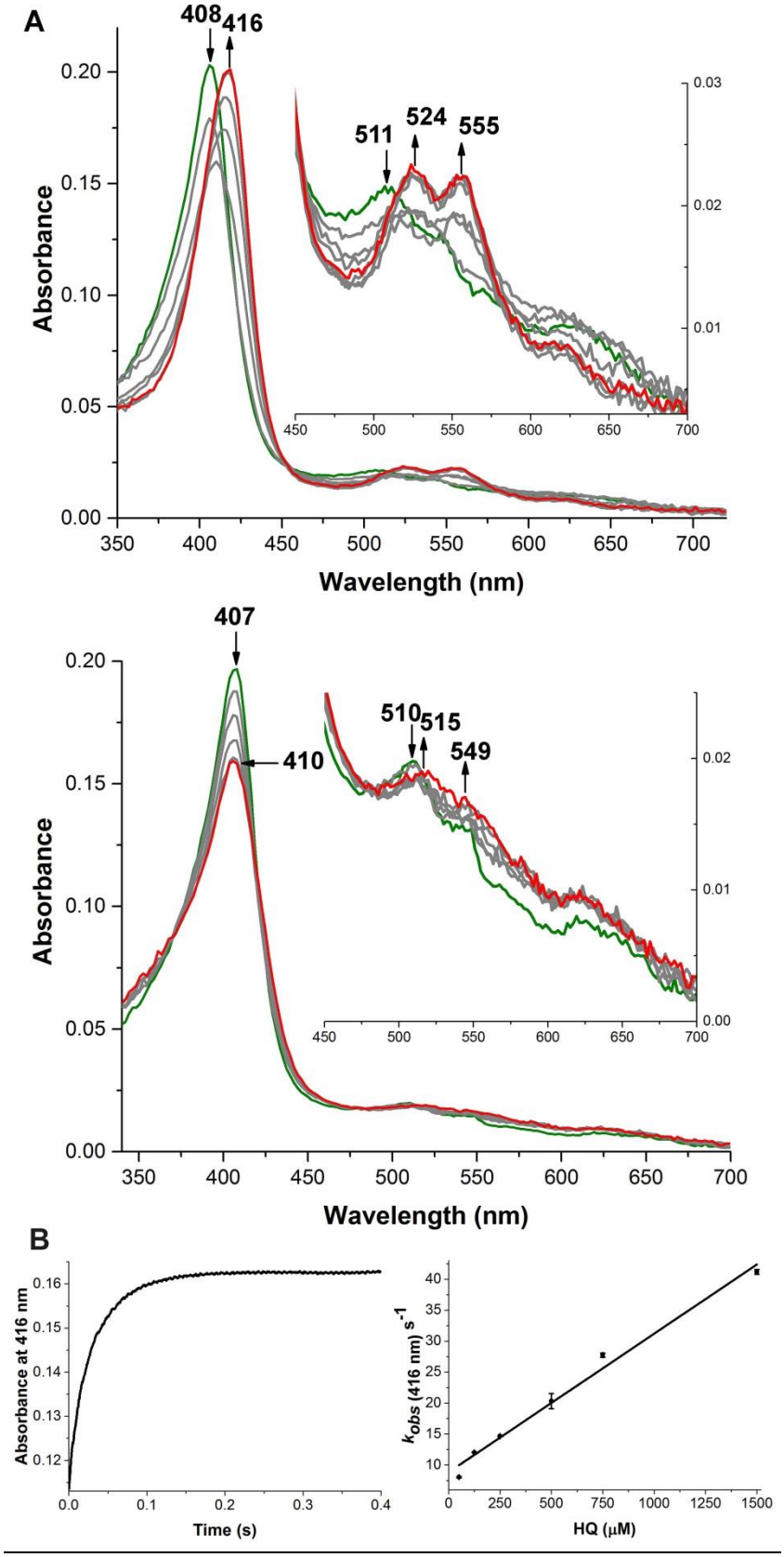

Figure 2.7 Reactions of *Tc*DyP-I with HQ in a sequential mixing mode.

A. Spectral transition of 3 mM HQ and *Tc*DyP-I at pH 7.8 (top) and 3.0 (bottom) recorded in 1.0 s. The green and red lines represent *Tc*DyP-I and *Tc*DyP-II, respectively. Arrows indicate changes of absorbance over time. *B.* Typical time trace at 416 nm (left) and dependence of $k_{obs\ (416\ nm)}$ *vs* [HQ] (right) for *Tc*DyP-II formation at pH 7.8.

2.4.4.3 Reduction of *Tc*DyP-II.

Finally, the reduction of compound II was investigated using HQ as the substrate in a sequential mixing mode. The compound II was produced by premixing solution of 5 μM *wt*-*Tc*DyP and 5 μM ferrocyanide with 1 equiv. H_2O_2. Reduction of *Tc*DyP-II was not observed at pH 7.8, which agrees with our steady-state results that the enzyme displayed marginal activity under neutral conditions. In contrast, *Tc*DyP-II was reduced at pH 3.0 and the intensity of the Soret band at 406 nm that corresponded to the resting state *Tc*DyP-0 increased as depicted in Fig. 2.8A. Plot of the pseudo-first-order rate constants monitored at 406 nm with the HQ concentrations exhibited a saturation kinetics (right panel in Fig. 2.8B), which suggested that binding between HQ and *Tc*DyP-II prior to the reduction was required as described by Eq. 4. The observed k_{obs} was represented by Eq. 5 and the second-order rate constant, k/K_D was calculated by nonlinear fit of the data to Eq. 6, giving a value of $(6.36 \pm 0.52) \times 10^3\ M^{-1}\ s^{-1}$. The corresponding K_D and k are 6.7 mM and 42 s^{-1}, which is in excellent agreement with the results of steady-state kinetics summarized in Table 2.1.

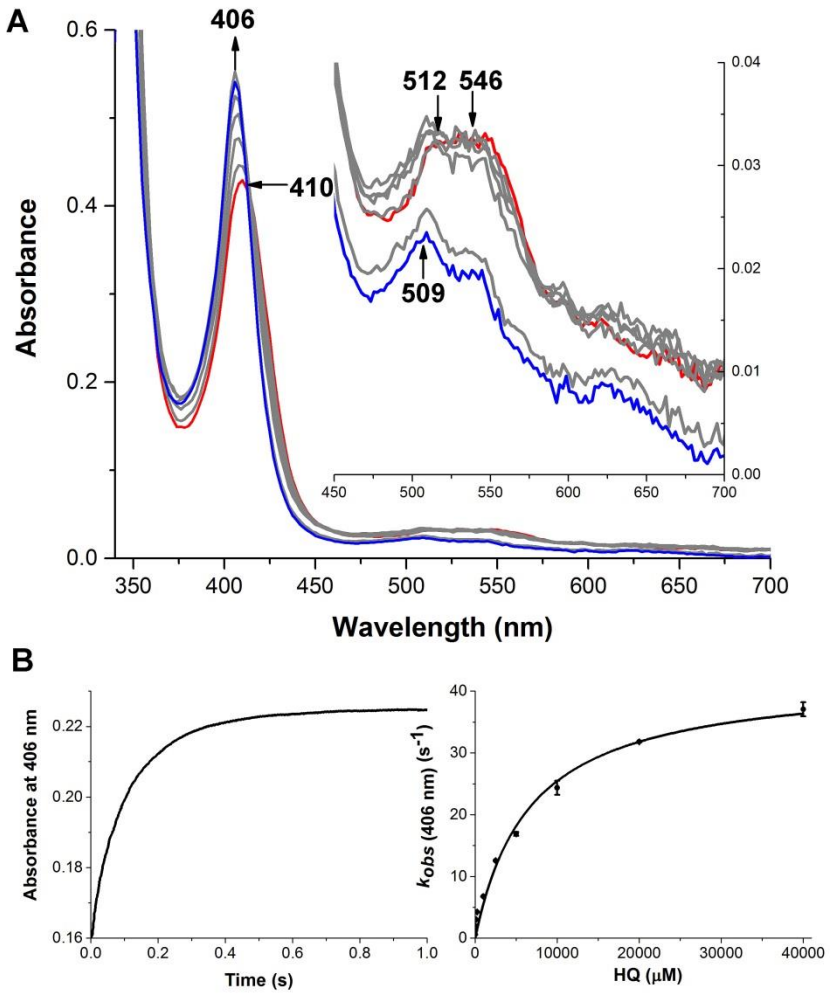

Figure 2.8 Reductions of *Tc*DyP-II with HQ in a sequential mixing mode.

A. Spectral transition of 5 mM HQ and *Tc*DyP-II at pH 3.0 recorded in 1.0 s. The blue and red lines represent *Tc*DyP-0 and *Tc*DyP-II, respectively. Arrows indicate changes of absorbance over time. *B.* Typical time trace at 406 nm (left panel) and dependence of $k_{obs\ (406\ nm)}$ *vs* [HQ] (right panel) for *Tc*DyP-II reduction.

$$\textit{Tc}\text{DyP–II} + \text{HQ} \underset{}{\overset{K_D}{\rightleftharpoons}} \textit{Tc}\text{DyP–II–HQ} \xrightarrow{k} \textit{Tc}\text{DyP–0} + \text{HQ}^{\cdot} \quad \text{(Eq.4)}$$

$$k_{obs} = \frac{k}{1+\frac{K_D}{[HQ]}} \qquad \text{(Eq. 5)}$$

$$k_{obs} = \frac{\frac{k}{K_D}[HQ]}{1+\frac{[HQ]}{K_D}} \qquad \text{(Eq. 6)}$$

2.4.4.4 Formation of *Tc*DyP-I with mutants

To understand how the catalytic residues surrounding the heme influence the formation of *Tc*DyP-I, the UV-Vis spectra of the reactions between mutants and H_2O_2 were recorded and are shown in Fig. 2.9A-D. Normalized spectra of the resting state and compound I of the *wt* and mutant *Tc*DyPs are shown in Fig. 2.9E-F. Their spectral characters are summarized in Table 2.2.

Table 2.2 Absorption maxima of resting state and catalytic intermediates of *Tc*DyPs and other heme peroxidases[a]

Enzyme		pH	Resting State	Compound I	Compound II	Ref.
*Tc*DyP	*wt*	7.8	406, 506, 544(*sh*), 567(*sh*), 624	407, 512, 546, 623, 648(*sh*)	416, 524, 555, 623	this study
		3.0	406, 509, 542(*sh*), 573, 630	406, 510, 547, 569, 621, 646(*sh*)	410, 515, 549, 621, 662 (*sh*)	
	D220A	7.8	412, 542, 572	416, 532, 549	ND	
	H312A		408, 488, 520	408, 524, 598(*sh*)	412, 526, 551	
	H312C		408, 515, 640	410, 515, 557 (*sh*)	412, 515, 557 (*sh*)[b]	
	R327A		406, 503, 630	ND	ND	
wt-DypA		7.5	408, 502, 632		419, 528, 557, 619	19
wt-DypB			404, 503, 634	400, 580, 613, 648		19
DyP_{Dec1}		3.2	406, 506, 636	401, 530, 556, 615, 644(*sh*)	399, 529, 555, 615, 644(*sh*)	18
HRP		6.6	403, 498, 640	400, 525(*sh*), 577, 622(*sh*), 651	420, 527, 555	44
LiP		6.0	408, 496, 630	408, 550, 608, 650	420, 525, 556	46
MnP		4.5	406, 502, 632	407, 558, 617, 650	420, 528, 555	47-48

[a]The *sh* and ND stand for a shoulder peak and not detectable, respectively. [b]Decay product of *Tc*DyP-I.

Substitution of D220 with the alanine did not prevent formation of *Tc*DyP-I. The second-order rate constant of its formation was determined to be $(1.24 \pm 0.04) \times 10^2$ M^{-1} s^{-1} at pH 7.8, which is 4 orders of magnitude slower than the *wt*. Significant red shift was observed for the Soret bands of *Tc*DyP-0 and *Tc*DyP-I, suggesting that the aspartate plays important roles in heme microenvironment. Moreover, two Q-bands at 542 and 572 nm appeared in the resting state of D220A (red line in Fig. 2.9E), which is reminiscent of 6-coordinated low spin heme and indicates potential reactivity difference between the *wt* and mutant.

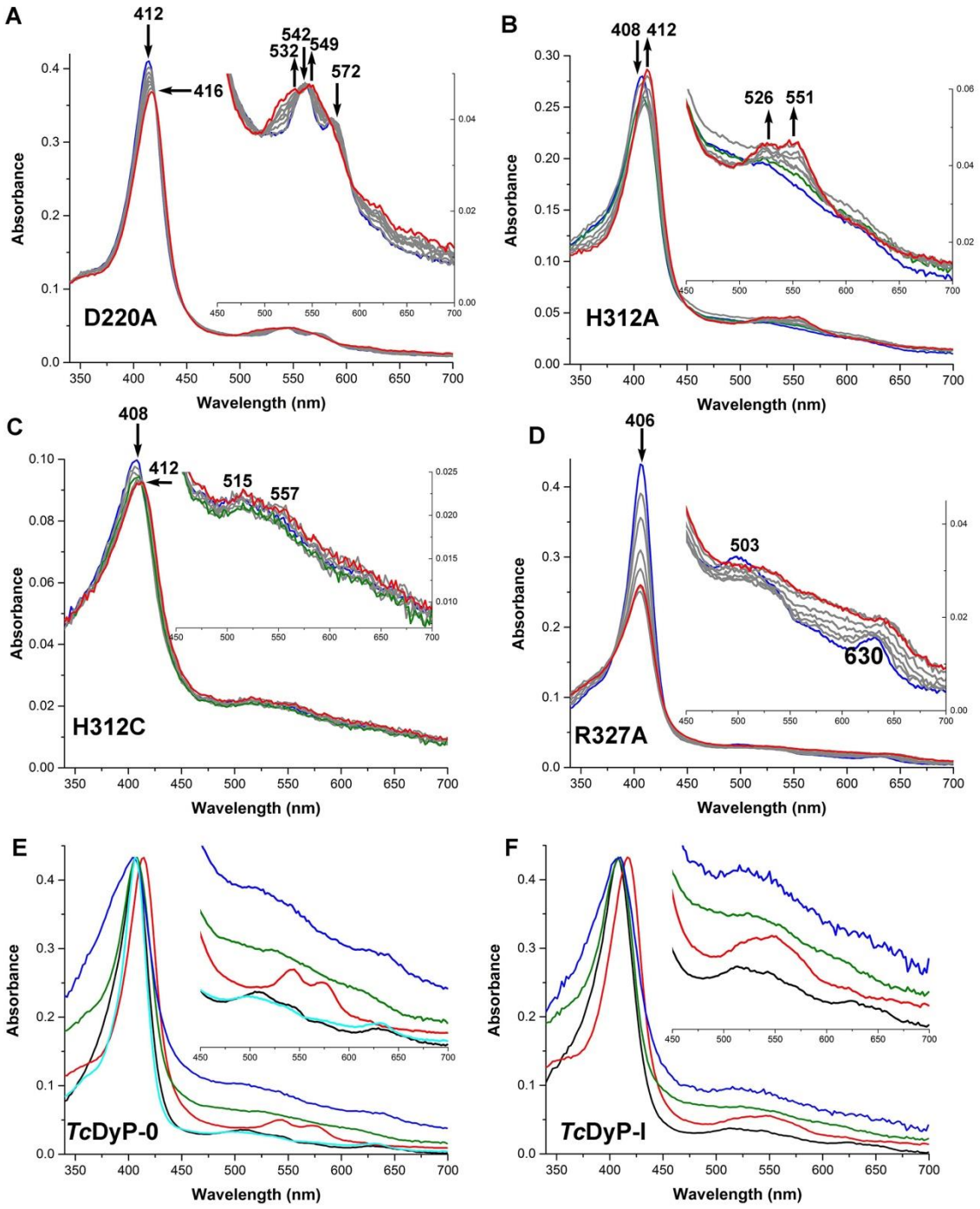

Figure 2.9 Reactions of mutants with H_2O_2 (*A*−*D*) and spectral overlay (*E*−*F*).

The blue, green, and red lines in *A*−*D* represent initial, intermediate, and final states of the mutants, respectively. Reactions were performed with 5 μM mutants and different concentrations of H_2O_2 at pH 7.8 and monitored for 5 s. Arrows indicate changes of absorbance over time. The black, red, green, blue, and cyan lines in *E*−*F* represent overlay of normalized spectra of *wt*, D220A, H312A, H312C, and R327A, respectively. *A.* D220A with 5 mM H_2O_2. *B.* H312A with 5 μM H_2O_2. *C.* H312C with 5 μM H_2O_2. *D.* R327A with 500 μM H_2O_2. *E.* Enzyme resting state. *F.* Compound I.

The most interesting observation was made with the H312 mutants. The proximal histidine is considered as a fifth ligand to the heme iron. A Fe−His−Glu triad has been identified in EfeB, which is thought to play important roles in maintaining heme center for high peroxidase activity[16]. Thus, substitution of histidine was expected to result in significant change of heme microenvironment as well as the catalytic intermediates due to loss of the ligand. However, in contrast to our prediction, both the H312A and H312C mutants reacted rapidly with H_2O_2 (pH 7.8) to form *Tc*DyP-I at the second-order rate constants of $(2.04 \pm 0.03) \times 10^6$ M^{-1} s^{-1} and $(3.28 \pm 0.03) \times 10^6$ M^{-1} s^{-1}, respectively, which are close to the rate of the *wt* enzyme. This suggests that histidine is not absolutely necessary in the formation of *Tc*DyP-I. The loss of interaction in Fe−His−Glu triad must have been compensated by reorganization of local residues and/or other factors such as hydrophobicity, electrostatic interaction, and hydrogen bonding. The observed faster rate of the cysteine mutant than the alanine one may result from partial ligation of the thiolate. Additionally, the *Tc*DyP-0 of H312A loses charge transfer band at 624 nm that exists in the *wt* enzyme. The H312C has a much broader Soret band than the other mutants for both *Tc*DyP-0 and *Tc*DyP-I. These spectral changes indicate that the histidine mutation has altered the heme microenvironment. Moreover, the broadening effect of H312C may also reflect formation of multiple species (thio-ligated and non-ligated species).

Consistent with the steady-state kinetics, *Tc*DyP-I was not found for R327A mutant. The decrease of intensity at 406 nm (Fig. 2.9D) was attributed to the enzyme instability at high concentration of H_2O_2, which also occurred in R244L-DypB[24]. The R327A mutant and *wt* enzyme have nearly identical spectra for their resting states, which suggests that the distal arginine does not have direct interaction with the heme.

2.4.4.5 Formation and reduction of *Tc*DyP-II with mutants

Since *Tc*DyP-I was observed only with D220 and H312 mutants, they were selected for further study of formation and reduction of *Tc*DyP-II. However, the efforts were only successful with H312A.

Due to slow rate of formation of *Tc*DyP-I, high concentration of more than 20 mM H_2O_2 was needed in order for D220A to rapidly produce the precursor to *Tc*DyP-II in a sequential mixing mode. However, such a high concentration of H_2O_2 was found to be detrimental to the enzyme, which is not uncommon in heme peroxidases[49]. For the H312C mutant, broad peak and small shift of the Soret band prevented us from monitoring *Tc*DyP-II (data not shown). Thus, the second-order rate constants of formation and reduction of *Tc*DyP-II with D220A and H312C were not determined although their residual activities with HQ were observed in steady-state kinetics.

Reactions of H312A, H_2O_2, and HQ in a sequential mixing mode generated a *Tc*DyP-II intermediate. The corresponding spectral change from *Tc*DyP-I to *Tc*DyP-II is shown in Fig. 2.10A. Formation of *Tc*DyP-II was monitored at 412 nm, giving a second-order rate constant of $(1.62 \pm 0.03) \times 10^4\ M^{-1}\ s^{-1}$, which is close to that of the *wt* [$(2.24 \pm 0.09) \times 10^4\ M^{-1}\ s^{-1}$].

Reduction of *Tc*DyP-II was performed in the same way as the *wt* enzyme by premixing and incubating equal amounts of H312A, ferrocyanide, and H_2O_2 for 5s. Addition of HQ produced a new species that has a Soret band at 392 nm, Q-band at 505 nm, and charge transfer band at 638 nm as depicted in Fig.10B. This indicates that the H312A mutant did not return to the resting state to complete a catalytic cycle, which explains the observed loss of enzyme activity in steady-state kinetics. It has to be noted that the new species was formed extremely fast and then decayed slowly. When the HQ was added at 1 equiv. to *Tc*DyP-II (final concentration of 2.5 μM), formation of the new species was complete in less than 100 ms. It then underwent decomposition over the next 10 s as the intensity of 392 nm decreased without further spectral shift (Fig. 2.10B). Attempts to slow down the rate of formation resulted in difficulty to monitor the species. Thus, the second-order rate constant for its formation was not determined.

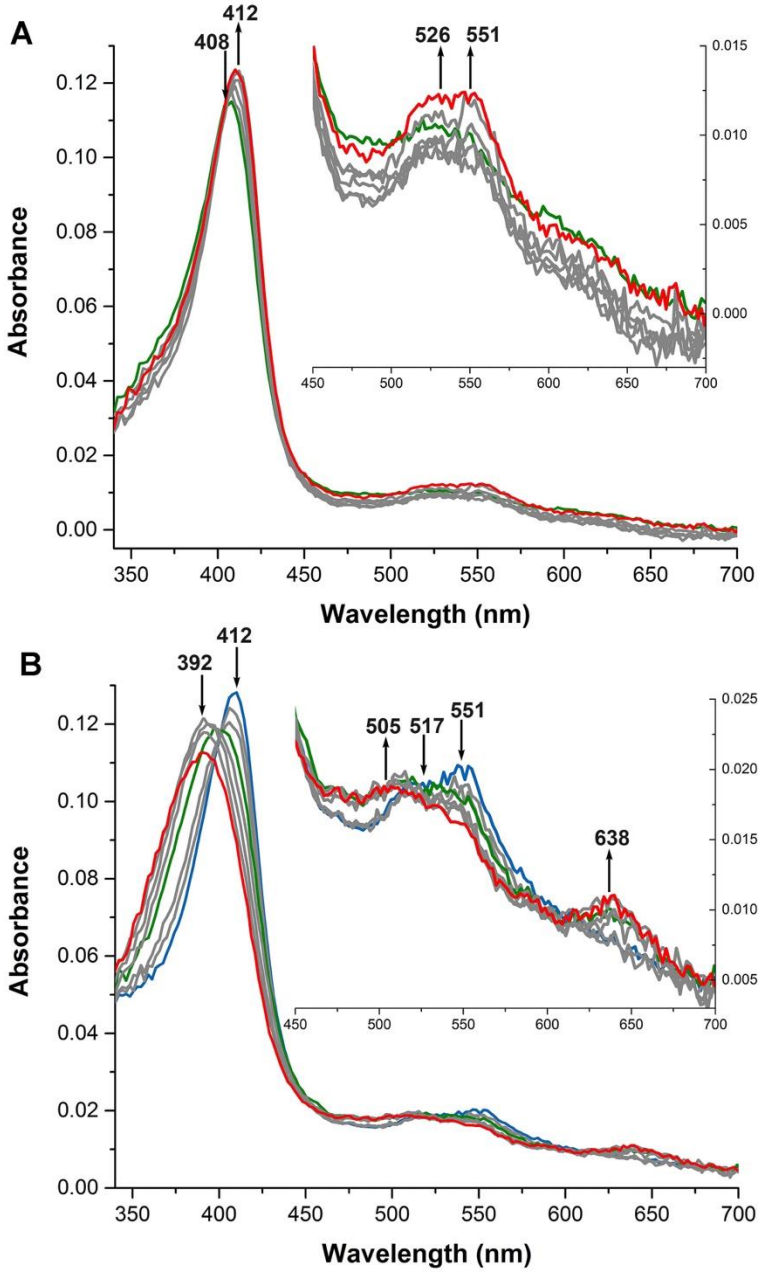

Figure 2.10 Formation and reduction of *Tc*DyP-II with H312A.

The reactions were performed in a sequential mixing mode. Arrows indicate changes of absorbance over time. *A.* Spectral transition of 5 mM HQ and 5 μM *Tc*DyP-I at pH 7.8 recorded in 1.0 s (formation of *Tc*DyP-II). The green and red lines represent *Tc*DyP-I and *Tc*DyP-II, respectively. *B.* Spectral transition of 5 mM HQ and 5 μM *Tc*DyP-II at pH 3.0 recorded in 10 s (reduction of *Tc*DyP-II). The blue, green, and red lines represent *Tc*DyP-II, an intermediate state at 30 ms, and formed new species, respectively.

2.4.5 Spectroelectrochemical titration and redox potentials

The redox behavior of heme iron is an indicator of peroxidase functionality though it is not directly involved in the catalytic cycle [50]. In fact, a stable Fe^{3+} is required for the peroxidases to carry out

H_2O_2-mediated oxidation to form compound I, which depends on the redox potential ($E^{\circ\prime}$) of the Fe^{3+}/Fe^{2+} couple. To date, the $E^{\circ\prime}$ have only been reported for three DyPs: *Bs*DyP (−40 mV, A-type), *Pp*DyP from *Pseudomonas putida* MET94 (−260 mV, B-type), and DyP2 (−85 mV, C-type) [12, 31]. Moreover, it is unknown how the catalytic residues surrounding the heme affect the $E^{\circ\prime}$ of DyPs. Thus, we decided to determine the $E^{\circ\prime}$ of *wt* and mutant *Tc*DyPs.

The experiments were carried out under argon using a spectroelectrochemical titration method. A typical UV-Vis spectrum for the stepwise oxidation of Fe^{2+}−*Tc*DyP is shown in Fig. 2.11A and the titration curves of the *wt* and mutants are depicted in Fig. 2.11B and Fig. 2.11C, respectively. The data were fitted to Nernst Eq. 3 and the results are summarized in Table 2.3.

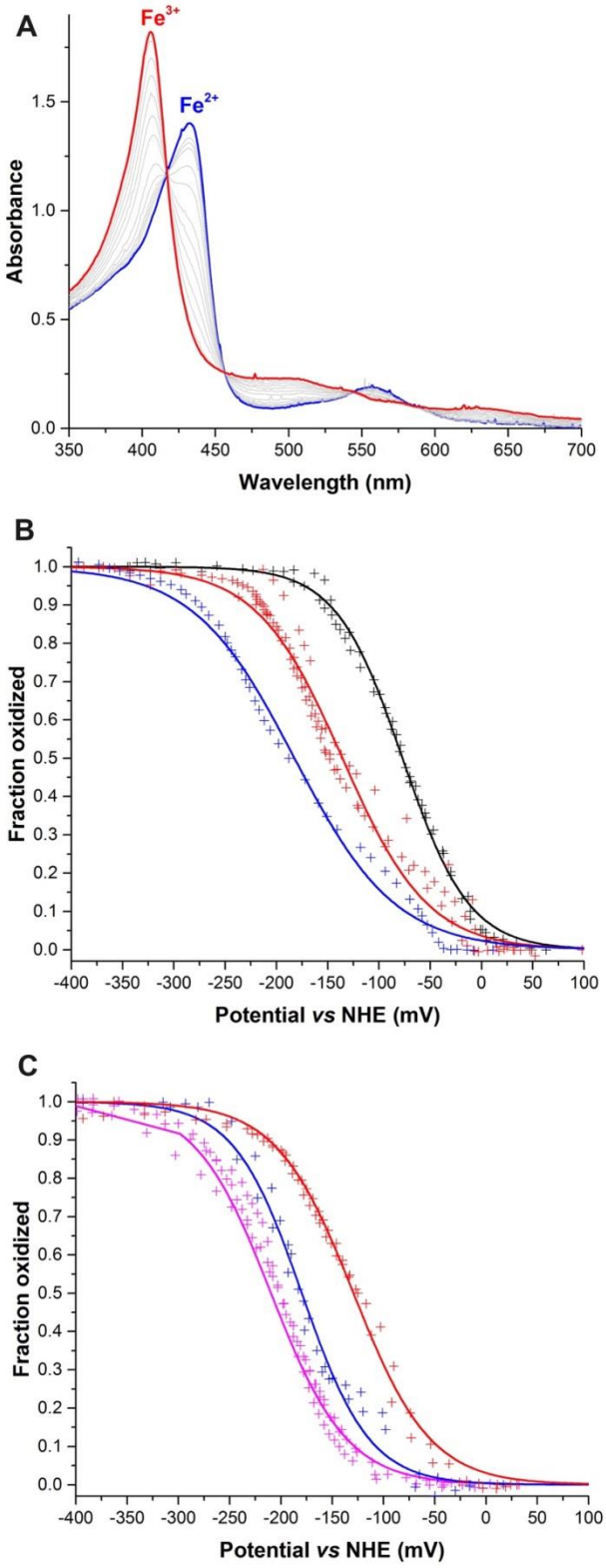

Figure 2.11 Spectroelectrochemical titration of *Tc*DyP monitored by ΔA_{433nm}.

A. Spectral transition of oxidizing Fe^{2+}–*wt*-*Tc*DyP (blue) to Fe^{3+}–*wt*-*Tc*DyP (red). *B.* Two individual titrations of *wt*-*Tc*DyP at pH 6.0 (black), 7.0 (red), and 8.0 (blue). *C.* Two individual titrations of D220A (red), H312A (blue), and R327A (pink, monitored by ΔA_{428nm}) at pH 7.0.

Table 2.3 Redox potentials ($E^{o\prime}$) of *Tc*DyP

Enzyme	pH	$E^{o\prime}$(mV)	n_{app}
	6	−77 ± 0.8	0.79 ± 0.02
wt	7	−136 ± 1.4	0.61 ± 0.02
	8	−182 ± 1.7	0.52 ± 0.02
D220A		−129 ± 0.9	0.68 ± 0.02
H312A	7	−180 ± 1.4	0.77 ± 0.04
R327A		−210 ± 1.0	0.69 ± 0.02

The titration of the *wt* enzyme under neutral conditions revealed an $E^{o\prime}$ of −136 mV and apparent number of transferred electrons (n_{app}) of 0.61. Similar to *BsDyP* [31], the transition was broad (Fig. 2.11B), which was thought to result from multiple 5- and 6-coordinated iron species consisting of low- and high-spin states [51]. Thus, the n_{app} was off from theoretical number of 1.00 ($Fe^{3+}+e\rightarrow Fe^{2+}$) due to difficulty to fit multiple species into the Nernst equation. Since the enzyme displayed highest activity at pH 3, it was predicted that the heme species would become homogeneous under an acidic condition and exist as a reactive high-spin state. A narrow transition, more positive $E^{o\prime}$, and higher n_{app} were expected. Indeed, when the titration was performed at pH 6, the observed n_{app} (0.79) was much closer to the theoretical value. Moreover, the $E^{o\prime}$ of *Tc*DyP was strongly influenced by pH, which is consistent with other peroxidases [52-54]. One pH unit corresponded to a $\Delta E^{o\prime}$ of ~60 mV for *wt*-*Tc*DyP.

To understand contribution of catalytic residues to redox potentials of the Fe^{3+}/Fe^{2+} couple, the $E^{o\prime}$ of the alanine mutants were determined. It was found that the aspartate mutation had a small effect, with the $E^{o\prime}$ becoming more positive by 7 mV relative to the *wt*. Both H312A and R327A mutants had more negative $E^{o\prime}$ than the *wt*-*Tc*DyP, suggesting that the Fe^{3+} state is stabilized in these two substitutions. The observed changes were relatively large, −44 mV for H312A and −74 mV for R327A. The implications of these changes will be discussed in the next section.

2.5 Discussion

2.5.1 Biochemical property of wt-*Tc*DyP

It was found that *wt*-*Tc*DyP was highly active towards a variety of substrates. As summarized in Table 2.4, bacterial A- and B-type DyPs generally show much lower catalytic efficiency (k_{cat}^{app}/K_M^{app}) than the C- and D-type DyPs. However, the *wt*-*Tc*DyP was found to have as high catalytic efficiency with ABTS as the most active D-type fungal enzymes. Furthermore, its activity with anthraquinone dyes is much higher than the other A- and B-type DyPs and comparable to C- and D-type enzymes. In addition, the *wt*-*Tc*DyP also showed peroxidase activity towards model lignin compounds **1** and **3**. Analysis of the degradation products indicated that the C_α–C_β bonds in both compounds were cleaved, which represents the first example of such activity with the type-A DyPs. Combined with the recent report on *Bs*DyP [13], our results suggest that type-A DyPs could be potentially useful for lignin degradation.

2.5.2 Catalytic cycle and transient kinetics of wt-*Tc*DyP

The proposed catalytic cycle and obtained second-order rate constants for each step are summarized in Fig. 2.13. To date, DypA is the only A-type DyP that has been briefly studied for its reaction with H_2O_2, in which formation of compound II was claimed based on the UV-Vis spectra [19]. Similar spectral transition was also observed with *wt*-*Tc*DyP. However, fitting the multiwavelength data revealed that a two-step reaction involving *Tc*DyP-0, *Tc*DyP-I, and compound-II like decay product of *Tc*DyP-I occurred. Thus, for the first time, compound I was observed in A-type DyPs. Its second-order rate constant was found to be independent of pH. Since the rate of compound I formation is only reported for DypB (~1.80×10^5 M^{-1} s^{-1} at pH 7.5) in all DyPs [19], a comparison reveals that the catalytic efficiency of *Tc*DyP (5.92×10^6 M^{-1} s^{-1}) is nearly 30-fold higher than that of DypB.

The decay product of *Tc*DyP-I could be a protein radical that has been observed with many heme peroxidases[55-56]. Analysis of residues within 8Å of the heme center using our homology model reveals that Y332, which is highly conserved among all DyP enzymes (Fig. 2.1), is a candidate residue for

radical localization. However, mutation of this residue did not affect *Tc*DyP's peroxidase activity. Identification of the radical residue is being actively pursued.

Table 2.4 Comparison of peroxidase activities*

Subclass	Protein	$k_{cat}^{app} / K_M^{app}$ ($M^{-1} s^{-1}$)						Ref.
		ABTS	H_2O_2(ABTS)	RB4	RB 5	RB19	Guaiacol	
A	*Tc*DyP	**1.7×10^7**	**3.4×10^6**	**6.5×10^5**	**6.6×10^5**	**7.8×10^6**	**8.8×10^2**	this study
	*Tfu*DyP		3.3×10^5			3.5×10^5		57
	DyPA	2.0×10^3	1.7×10^4	1.3×10^4				19
	*Bs*DyP	7.0×10^4	2.0×10^6		5.0×10^4		3.0×10^2	31
B	DyPB	2.4×10^3	2.1×10^5	1.0×10^2				19
	$DyPP_a$				2.2×10^2			58
	TyrA				7.0×10^4			59
	*Pp*DyP	8.0×10^3	1.8×10^5		2.0×10^5		3.4×10^3	31
C	DyP2	6.6×10^6			7.1×10^5			12
	AnaPX				1.2×10^7			60
D	DyP				4.8×10^6			61
	AjP I	1.8×10^7	2.7×10^7		5.0×10^6			62
	AjP II	1.6×10^7	4.8×10^7		1.7×10^7			62
	TAP	2.5×10^7						63
Other	LiP	5.6×10^5						64
	MnP	ND						65-66
	VP	9.4×10^6						67

*ND: not detected. Blank: not reported.

Formation and reduction of the *Tc*DyP-II were elucidated with HQ in a sequential mixing mode. It was determined that the rate of *Tc*DyP-II formation was ~2.5-fold slower than that of the *Tc*DyP-I formation. Reduction of *Tc*DyP-II was found to be the slowest in the catalytic cycle, suggesting that regeneration of *Tc*DyP-0 from *Tc*DyP-II is a rate-limiting step in HQ oxidation. Thus, the catalytic cycle involving an A-type DyP was fully characterized for the first time. It has to be pointed out that the rate-limiting step may be substrate-dependent. For example, the k_{cat}^{app}/K_M^{app} of ABTS (1.7×10^7 M^{-1} s^{-1}) is higher than the second-order rate constant of *Tc*DyP-I formation (4.06×10^6 M^{-1} s^{-1} at pH 3). Thus, it is reasonable to assume that the formation of *Tc*DyP-I in ABTS oxidation is the rate-limiting step.

2.5.3 Roles of catalytic residues surrounding the heme center

To probe the roles of catalytic residues, steady-state and transient kinetics, spectro-electrochemical titrations, and SEC chromatography were performed.

2.5.3.1 Aspartate

It is proposed that the catalytic importance of aspartate is dependent on the enzyme types [14]. It has also been demonstrated that aspartate is essential for D-type DyPs, but not required for B-type enzymes [14]. Its role in A-type DyPs is still in question [16]. In the present study, while mutation of D220 resulted in the loss of enzyme activity towards ABTS, the mutants retained up to 85% *wt* activity with guaiacol.

The seemingly contradictory observations can be explained as follows. Based on the structural similarity between HQ and guaiacol, it is proposed that the reduction of *Tc*DyP-II to *Tc*DyP-0 is a rate-limiting step for guaiacol oxidation, in which the rate is estimated at 0.33 s^{-1} according to its steady-state kinetics. This is close to the rate of *Tc*DyP-I formation in D220A at 0.07 s^{-1}. Thus, the aspartate mutation will not have significant impacts on guaiacol oxidation because it does not cause the change of rate-limiting step in the catalytic cycle. However, *Tc*DyP-I formation is proposed as the rate-limiting step for ABTS oxidation. A decrease of rate by 4 orders of magnitude caused by the aspartate mutation will result in the loss of activity towards ABTS. Thus, our results have shown that aspartate is crucial for the formation of compound I as well as the peroxidase activity of A-type DyPs.

As shown in Fig. 2.9E-F and summarized in Table 2.2, substitution of D220 has the most significant impact on the heme microenvironment among all active site mutants. It causes red shift in UV-Vis spectra of *Tc*DyP-0 and *Tc*DyP-I as well as the appearance of two Q-bands in *Tc*DyP-0, all of which are indicative of generation of a six-coordinated iron species, a disfavored species for peroxidases. However, the aspartate mutation has minimal effects on oligomeric state of the protein, which may imply that the aspartate is not involved in the networks extended to the protein surface.

Finally, a predicted increase (more positive) of $E^{o\prime}$ was observed due to loss of the electrostatic interaction between the Fe^{3+} in heme and carboxylate anion of the aspartate side chain.

2.5.3.2 Histidine

It has been reported that mutation of the proximal histidine in DyPs prevents formation of *holo*enzymes [16, 57] Furthermore, this mutation was found to decrease the stability of plant peroxidases [68]. However, these deleterious effects were not observed in our histidine mutants. Substitution of H312 with a non-ligating (A312) or ligating (C312) residue has significant impacts on the enzyme activity. While H312A showed no peroxidase activity, H312C displayed 0.5%, 1.1% and 5.4% *wt* activity towards ABTS, HQ and guaiacol, respectively (Fig. 2.3B). This suggests that H312 is catalytically important. Loss of the proximal ligation (H312A) inactivated the enzyme. Ligation compensation from cysteine (H312C) partially recovered the enzyme activity although the recovery was marginal.

Several striking features were observed with histidine mutants. Replacement of the proximal histidine is expected to result in the change of Fe^{3+} coordination and thus, affect the formation of *Tc*DyP-I and *Tc*DyP-II. Yet, it was discovered that both mutants were able to form compound I as efficiently as the *wt*-*Tc*DyP. Our results also demonstrated that the rate of formation of *Tc*DyP-II was not retarded by histidine mutation. The spectral features of histidine mutants and *wt* enzyme were nearly identical for all intermediates (*Tc*DyP-0, *Tc*DyP-I, and *Tc*DyP-II), which led us to propose that the H312 may not be the only residue that can serve as the axial ligand. In fact, the H312 is located on a short α-helix in between two large loops (G276−A311 and H317−P329) according to our homology model (Fig. 2.1B). The high structural flexibility in this region may allow other residues to fill the role of proximal histidine when it is mutated. Yet, the mutation to alanine prevents the enzyme from returning to resting state. A new species with the Soret band at 392 nm was rapidly formed during reduction of *Tc*DyP-II. Its identity is still need to be characterized.

Additionally, the H312A mutant had a more negative $E^{o\prime}$ than the *wt*-*Tc*DyP by −44 mV, suggesting that Fe^{3+} was stabilized by the alanine substitution. Combining with the results of catalytic

intermediates discussed above, our study indicates that introduction of alanine may reorganize local structure, resulting in a net stabilization of Fe^{3+} to facilitate the formation of compound I and compound II. The reorganization is also amplified in the shift of oligomeric state from a mixture of dimer, tetramer, and octamer for the *wt* to a dimer for the H312A in solution.

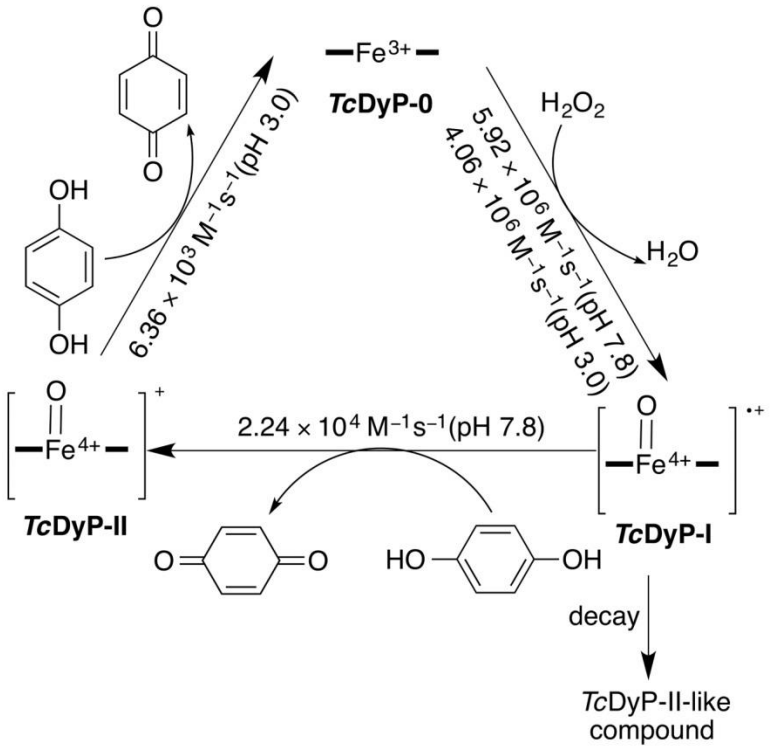

Figure 2.12 Catalytic cycle of *wt*-*Tc*DyP.

Second-order rate constants are shown for each step.

2.5.3.3 Arginine

Our results have shown that arginine is essential for compound I formation in A-type DyPs, which is similar to B-type DypB [24] yet quite different from HRP and cytochrome *c* peroxidase [69-70]. For the latter two peroxidases, replacement of this distal arginine does not inhibit the formation of compound I, but lowers the rate by 2-3 orders of magnitude [69-70]. It has been proposed that the arginine is involved in the general acid-base catalysis in DypB [24], which may also be the case for R327 in *Tc*DyP. An X-ray crystal structure is needed in order to identify the residues involved in the acid-base catalysis.

Electrostatic repulsions may exist between the Fe^{3+} and positively charged guanidinium group of the arginine in *wt*-*Tc*DyP. Thus, replacement of R327 with A327 is predicted to reduce interaction and stabilize the Fe^{3+}, which will shift the $E^{o\prime}$ to a more negative value. Indeed, large change of redox potential was observed with R327A that has a more negative potential than the *wt* enzyme by −74 mV. Furthermore, the crystal structure of DypB has shown that the arginine participates in a network that consists of hydrogen bonds extending to the protein surface [24]. The network is thought to be important for peroxidase activity by mediating proton transfer as has been suggested in ascorbate peroxidase and other enzymes [71-72]. This same network may be also present in A-type DyPs because oligomeric state of R327A mutant is different from the *wt* enzyme and exists as a dimer in solution. The observed loss of peroxidase activity in R327A could also be attributed to disruption of this network that has been considered important for compound I formation [24].

2.6 Summary

A new DyP-type peroxidase, *Tc*DyP has been purified and characterized. Unlike other A-type DyPs, the *Tc*DyP is highly active towards a wide range of substrates including model lignin compounds. Transient kinetics was employed to reveal the catalytic cycle involving *Tc*DyP, which is used to resolve the contradiction regarding the catalytic importance of aspartate in A-type DyPs. It is concluded that D220 and R327 are crucial for compound I formation while H312 is involved in reduction of compound II to resting state. Moreover, H312 and R327 also play important roles in *Tc*DyP's oligomeric state and regulating redox potential. Substitution of each residue with alanine resulted in the formation of dimeric state and shift of $E^{o\prime}$ to a more negative potential. The latter observation suggests that the Fe^{3+} in *Tc*DyP appears to be stabilized in a nonpolar environment, which is different from plant peroxidases [50]. This may explain the difference in substrate specificity and catalytic efficiency between DyPs and plant peroxidases. Thus, fine-tuning heme microenvironment may allow *Tc*DyP to efficiently oxidize

substrates with high redox potentials. The present study offers insights into the unique catalytic property of the A-type DyPs and facilitates to develop them into a biocatalyst for lignin degradation.

2.7 References

1. Paliwal, R.; Rawat, A. P.; Rawat, M.; Rai, J. P. N., Bioligninolysis: Recent Updates for Biotechnological Solution. *Appl Biochem Biotech* **2012,** *167* (7), 1865-1889.

2. FitzPatrick, M.; Champagne, P.; Cunningham, M. F.; Whitney, R. A., A biorefinery processing perspective: Treatment of lignocellulosic materials for the production of value-added products. *Bioresource technology* **2010,** *101* (23), 8915-8922.

3. Banerjee, S.; Mudliar, S.; Sen, R.; Giri, B.; Satpute, D.; Chakrabarti, T.; Pandey, R. A., Commercializing lignocellulosic bioethanol: technology bottlenecks and possible remedies. *Biofuel Bioprod Bior* **2010,** *4* (1), 77-93.

4. ten Have, R.; Teunissen, P. J., Oxidative mechanisms involved in lignin degradation by white-rot fungi. *Chem Rev* **2001,** *101* (11), 3397-413.

5. Brown, M. E.; Chang, M. C. Y., Exploring bacterial lignin degradation. *Curr Opin Chem Biol* **2014,** *19*, 1-7.

6. Kroppenstedt, R. M.; Goodfellow, M., The Family Thermomonosporaceae: Actinocorallia, Actinomadura, Spirillospora and Thermomonospora. In *The Prokaryotes: Volume 3: Archaea. Bacteria: Firmicutes, Actinomycetes*, Dworkin, M.; Falkow, S.; Rosenberg, E.; Schleifer, K.-H.; Stackebrandt, E., Eds. Springer New York: New York, NY, 2006; pp 682-724.

7. Fennington, G.; Neubauer, D.; Stutzenberger, F., Cellulase biosynthesis in a catabolite repression-resistant mutant of Thermomonospora curvata. *Appl Environ Microbiol* **1984,** *47* (1), 201-4.

8. Stutzenberger, F. J., Degradation of Cellulosic Substances by Thermomonospora-Curvata. *Biotechnology and Bioengineering* **1979,** *21* (5), 909-913.

9. Chertkov, O.; Sikorski, J.; Nolan, M.; Lapidus, A.; Lucas, S.; Del Rio, T. G.; Tice, H.; Cheng, J. F.; Goodwin, L.; Pitluck, S.; Liolios, K.; Ivanova, N.; Mavromatis, K.; Mikhailova, N.; Ovchinnikova, G.; Pati, A.; Chen, A.; Palaniappan, K.; Djao, O. D. N.; Land, M.; Hauser, L.; Chang, Y. J.; Jeffries, C. D.; Brettin, T.; Han, C.; Detter, J. C.; Rohde, M.; Goker, M.; Woyke, T.; Bristow, J.; Eisen, J. A.; Markowitz, V.; Hugenholtz, P.; Klenk, H. P.; Kyrpides, N. C., Complete genome sequence of Thermomonospora curvata type strain (B9(T)). *Stand Genomic Sci* **2011,** *4* (1), 13-22.

10. Strittmatter, E.; Plattner, D. A.; Piontek, K., Dye-Decolorizing Peroxidase (DyP). In *Encyclopedia of Inorganic and Bioinorganic Chemistry*, John Wiley & Sons, Ltd: 2011.

11. Ahmad, M.; Roberts, J. N.; Hardiman, E. M.; Singh, R.; Eltis, L. D.; Bugg, T. D. H., Identification of DypB from Rhodococcus jostii RHA1 as a Lignin Peroxidase. *Biochemistry* **2011,** *50* (23), 5096-5107.

12. Brown, M. E.; Barros, T.; Chang, M. C. Y., Identification and Characterization of a Multifunctional Dye Peroxidase from a Lignin-Reactive Bacterium. *Acs Chem Biol* **2012,** *7* (12), 2074-2081.

13. Min, K.; Gong, G.; Woo, H. M.; Kim, Y.; Um, Y., A dye-decolorizing peroxidase from Bacillus subtilis exhibiting substrate-dependent optimum temperature for dyes and beta-ether lignin dimer. *Sci Rep-Uk* **2015,** *5*.

14. Colpa, D. I.; Fraaije, M. W.; van Bloois, E., DyP-type peroxidases: a promising and versatile class of enzymes. *Journal of industrial microbiology & biotechnology* **2014,** *41* (1), 1-7.

15. Koua, D.; Cerutti, L.; Falquet, L.; Sigrist, C. J. A.; Theiler, G.; Hulo, N.; Dunand, C., PeroxiBase: a database with new tools for peroxidase family classification. *Nucleic acids research* **2009,** *37*, D261-D266.

16. Liu, X. H.; Du, Q.; Wang, Z.; Zhu, D. Y.; Huang, Y.; Li, N.; Wei, T. D.; Xu, S. J.; Gu, L. C., Crystal Structure and Biochemical Features of EfeB/YcdB from Escherichia coli O157 ASP(235) PLAYS DIVERGENT ROLES IN DIFFERENT ENZYME-CATALYZED PROCESSES. *J Biol Chem* **2011,** *286* (17), 14922-14931.

17. Sugano, Y.; Matsushima, Y.; Tsuchiya, K.; Aoki, H.; Hirai, M.; Shoda, M., Degradation pathway of an anthraquinone dye catalyzed by a unique peroxidase DyP from Thanatephorus cucumeris Dec 1. *Biodegradation* **2009,** *20* (3), 433-40.

18. Sugano, Y.; Muramatsu, R.; Ichiyanagi, A.; Sato, T.; Shoda, M., DyP, a unique dye-decolorizing peroxidase, represents a novel heme peroxidase family. *J Biol Chem* **2007,** *282* (50), 36652-36658.

19. Roberts, J. N.; Singh, R.; Grigg, J. C.; Murphy, M. E. P.; Bugg, T. D. H.; Eltis, L. D., Characterization of Dye-Decolorizing Peroxidases from Rhodococcus jostii RHA1. *Biochemistry* **2011,** *50* (23), 5108-5119.

20. Yang, J. Y.; Roy, A.; Zhang, Y., Protein-ligand binding site recognition using complementary binding-specific substructure comparison and sequence profile alignment. *Bioinformatics* **2013,** *29* (20), 2588-2595.

21. Yang, J.; Roy, A.; Zhang, Y., BioLiP: a semi-manually curated database for biologically relevant ligand-protein interactions. *Nucleic Acids Res* **2013,** *41* (Database issue), D1096-103.

22. Gajhede, M.; Schuller, D. J.; Henriksen, A.; Smith, A. T.; Poulos, T. L., Crystal structure of horseradish peroxidase C at 2.15 A resolution. *Nat Struct Biol* **1997,** *4* (12), 1032-8.

23. Sugano, Y., DyP-type peroxidases comprise a novel heme peroxidase family. *Cell Mol Life Sci* **2009,** *66* (8), 1387-1403.

24. Singh, R.; Grigg, J. C.; Armstrong, Z.; Murphy, M. E. P.; Eltis, L. D., Distal Heme Pocket Residues of B-type Dye-decolorizing Peroxidase ARGININE BUT NOT ASPARTATE IS ESSENTIAL FOR PEROXIDASE ACTIVITY. *Journal of Biological Chemistry* **2012,** *287* (13), 10623-10630.

25. Sambrook, J.; Russell, D. W.; Sambrook, J., *The condensed protocols from Molecular cloning : a laboratory manual*. Cold Spring Harbor Laboratory Press: Cold Spring Harbor, N.Y., 2006; p v, 800 p.

26. Qin, H. J.; Hu, J.; Hua, Y. Z.; Challa, S. V.; Cross, T. A.; Gao, F. P., Construction of a series of vectors for high throughput cloning and expression screening of membrane proteins from Mycobacterium tuberculosis. *Bmc Biotechnol* **2008,** *8*.

27. Smith, P. K.; Krohn, R. I.; Hermanson, G. T.; Mallia, A. K.; Gartner, F. H.; Provenzano, M. D.; Fujimoto, E. K.; Goeke, N. M.; Olson, B. J.; Klenk, D. C., Measurement of Protein Using Bicinchoninic Acid. *Anal Biochem* **1985,** *150* (1), 76-85.

28. Berry, E. A.; Trumpower, B. L., Simultaneous Determination of Hemes-a, Hemes-B, and Hemes-C from Pyridine Hemochrome Spectra. *Analytical Biochemistry* **1987,** *161* (1), 1-15.

29. Mcllvaine, T. C., A buffer solution for colorimetric comparaison. *J Biol Chem* **1921,** *49* (1), 183-186.

30. Brown, M. E.; Walker, M. C.; Nakashige, T. G.; Iavarone, A. T.; Chang, M. C., Discovery and characterization of heme enzymes from unsequenced bacteria: application to microbial lignin degradation. *Journal of the American Chemical Society* **2011,** *133* (45), 18006-9.

31. Santos, A.; Mendes, S.; Brissos, V.; Martins, L. O., New dye-decolorizing peroxidases from Bacillus subtilis and Pseudomonas putida MET94: towards biotechnological applications. *Appl Microbiol Biot* **2014,** *98* (5), 2053-2065.

32. Dunford, H. B., *Peroxidases and Catalases: Biochemistry, Biophysics, Biotechnology and Physiology*. John Wiley & Sons: 2010.

33. Adak, S.; Mazumder, A.; Banerjee, R. K., Probing the active site residues in aromatic donor oxidation in horseradish peroxidase: Involvement of an arginine and a tyrosine residue in aromatic donor binding. *Biochemical Journal* **1996,** *314*, 985-991.

34. La Mar, G. N.; Hernandez, G.; de Ropp, J. S., H NMR investigation of the influence of interacting sites on the dynamics and thermodynamics of substrate and ligand binding to horseradish peroxidase. *Biochemistry* **1992,** *31* (38), 9158-68.

35. Childs, R. E.; Bardsley, W. G., Steady-State Kinetics of Peroxidase with 2,2'-Azino-Di-(3-Ethylbenzthiazoline-6-Sulphonic Acid) as Chromogen. *Biochemical Journal* **1975,** *145* (1), 93-103.

36. Wang, W. C.; Noel, S.; Desmadril, M.; Gueguen, J.; Michon, T., Kinetic evidence for the formation of a Michaelis-Menten-like complex between horseradish peroxidase compound II and di-(N-acetyl-L-tyrosine). *Biochem. J.* **1999,** *340*, 329.

37. Strittmatter, E.; Serrer, K.; Liers, C.; Ullrich, R.; Hofrichter, M.; Piontek, K.; Schleicher, E.; Plattner, D. A., The toolbox of Auricularia auricula-judae dye-decolorizing peroxidase - Identification of three new potential substrate-interaction sites. *Arch Biochem Biophys* **2015,** *574*, 75-85.

38. Linde, D.; Pogni, R.; Canellas, M.; Lucas, F.; Guallar, V.; Baratto, M. C.; Sinicropi, A.; Saez-Jimenez, V.; Coscolin, C.; Romero, A.; Medrano, F. J.; Ruiz-Duenas, F. J.; Martinez, A. T.,

Catalytic surface radical in dye-decolorizing peroxidase: a computational, spectroscopic and site-directed mutagenesis study. *Biochem J* **2015,** *466* (2), 253-62.

39. Strittmatter, E.; Liers, C.; Ullrich, R.; Wachter, S.; Hofrichter, M.; Plattner, D. A.; Piontek, K., First crystal structure of a fungal high-redox potential dye-decolorizing peroxidase: substrate interaction sites and long-range electron transfer. *J Biol Chem* **2013,** *288* (6), 4095-102.

40. Wei, K.; Luo, S. W.; Fu, Y.; Liu, L.; Guo, Q. X., A theoretical study on bond dissociation energies and oxidation potentials of monolignols. *J Mol Struc-Theochem* **2004,** *712* (1-3), 197-205.

41. Baciocchi, E.; Gerini, M. F.; Lanzalunga, O.; Mancinelli, S., Lignin peroxidase catalysed oxidation of 4-methoxymandelic acid. The role of mediator structure. *Tetrahedron* **2002,** *58* (40), 8087-8093.

42. Tien, M.; Ma, D., Oxidation of 4-methoxymandelic acid by lignin peroxidase - Mediation by veratryl alcohol. *Journal of Biological Chemistry* **1997,** *272* (14), 8912-8917.

43. Díaz Torres, E.; Ayala, M., *Biocatalysis based on heme peroxidases : peroxidases as potential industrial biocatalysts*. Springer-Verlag: New York, 2010; p xi, 358 p.

44. Schonbau.Gr; Lo, S., Interaction of Peroxidases with Aromatic Peracids and Alkyl Peroxides - Product Analysis. *J Biol Chem* **1972,** *247* (10), 3353-&.

45. Morales, M.; Mate, M. J.; Romero, A.; Martinez, M. J.; Martinez, A. T.; Ruiz-Duenas, F. J., Two Oxidation Sites for Low Redox Potential Substrates A DIRECTED MUTAGENESIS, KINETIC, AND CRYSTALLOGRAPHIC STUDY ON PLEUROTUS ERYNGII VERSATILE PEROXIDASE. *J Biol Chem* **2012,** *287* (49), 41053-41067.

46. Renganathan, V.; Gold, M. H., Spectral Characterization of the Oxidized States of Lignin Peroxidase, an Extracellular Heme Enzyme from the White Rot Basidiomycete Phanerochaete-Chrysosporium. *Biochemistry* **1986,** *25* (7), 1626-1631.

47. Mino, Y.; Wariishi, H.; Blackburn, N. J.; Loehr, T. M.; Gold, M. H., Spectral Characterization of Manganese Peroxidase, an Extracellular Heme Enzyme from the Lignin-Degrading Basidiomycete, Phanerochaete-Chrysosporium. *J Biol Chem* **1988,** *263* (15), 7029-7036.

48. Wariishi, H.; Akileswaran, L.; Gold, M. H., Manganese Peroxidase from the Basidiomycete Phanerochaete-Chrysosporium - Spectral Characterization of the Oxidized States and the Catalytic Cycle. *Biochemistry* **1988,** *27* (14), 5365-5370.

49. Torres, E.; Ayala, M., *Biocatalysis Based on Heme Peroxidases: Peroxidases as Potential Industrial Biocatalysts*. Springer Science & Business Media: 2010.

50. Battistuzzi, G.; Bellei, M.; Bortolotti, C. A.; Sola, M., Redox properties of heme peroxidases. *Arch Biochem Biophys* **2010,** *500* (1), 21-36.

51. Sezer, M.; Santos, A.; Kielb, P.; Pinto, T.; Martins, L. O.; Todorovic, S., Distinct structural and redox properties of the heme active site in bacterial dye decolorizing peroxidase-type peroxidases from two subfamilies: resonance Raman and electrochemical study. *Biochemistry* **2013,** *52* (18), 3074-84.

52. Petruccioli, M.; Frasconi, M.; Quaratino, D.; Covino, S.; Favero, G.; Mazzei, F.; Federici, F.; D'Annibale, A., Kinetic and redox properties of MnP II, a major manganese peroxidase isoenzyme from Panus tigrinus CBS 577.79. *J Biol Inorg Chem* **2009,** *14* (8), 1153-1163.

53. Santucci, R.; Bongiovanni, C.; Marini, S.; Del Conte, R.; Tien, M.; Banci, L.; Coletta, M., Redox equilibria of manganese peroxidase from Phanerochaetes chrysosporium: functional role of residues on the proximal side of the haem pocket. *Biochem J* **2000,** *349*, 85-90.

54. Zhang, Z.; Chouchane, S.; Magliozzo, R. S.; Rusling, J. F., Direct voltammetry and catalysis with Mycobacterium tuberculosis catalase-peroxidase, peroxidases, and catalase in lipid films. *Anal Chem* **2002,** *74* (1), 163-170.

55. Hiner, A. N.; Martinez, J. I.; Arnao, M. B.; Acosta, M.; Turner, D. D.; Lloyd Raven, E.; Rodriguez-Lopez, J. N., Detection of a tryptophan radical in the reaction of ascorbate peroxidase with hydrogen peroxide. *Eur J Biochem* **2001,** *268* (10), 3091-8.

56. Sivaraja, M.; Goodin, D. B.; Smith, M.; Hoffman, B. M., Identification by ENDOR of Trp191 as the free-radical site in cytochrome c peroxidase compound ES. *Science* **1989,** *245* (4919), 738-40.

57. van Bloois, E.; Pazmino, D. E. T.; Winter, R. T.; Fraaije, M. W., A robust and extracellular heme-containing peroxidase from Thermobifida fusca as prototype of a bacterial peroxidase superfamily. *Appl Microbiol Biot* **2010,** *86* (5), 1419-1430.

58. Li, J.; Liu, C.; Li, B. Z.; Yuan, H. L.; Yang, J. S.; Zheng, B. W., Identification and Molecular Characterization of a Novel DyP-Type Peroxidase from Pseudomonas aeruginosa PKE117. *Appl Biochem Biotech* **2012,** *166* (3), 774-785.

59. Zubieta, C.; Joseph, R.; Krishna, S. S.; McMullan, D.; Kapoor, M.; Axelrod, H. L.; Miller, M. D.; Abdubek, P.; Acosta, C.; Astakhova, T.; Carlton, D.; Chiu, H. J.; Clayton, T.; Deller, M. C.; Duan, L.; Elias, Y.; Elsliger, M. A.; Feuerhelm, J.; Grzechnik, S. K.; Hale, J.; Han, G. W.; Jaroszewski, L.; Jin, K. K.; Klock, H. E.; Knuth, M. W.; Kozbial, P.; Kumar, A.; Marciano, D.; Morse, A. T.; Murphy, K. D.; Nigoghossian, E.; Okach, L.; Oommachen, S.; Reyes, R.; Rife, C. L.; Schimmel, P.; Trout, C. V.; van den Bedem, H.; Weekes, D.; White, A.; Xu, Q. P.; Hodgson, K. O.; Wooley, J.; Deacon, A. M.; Godzik, A.; Lesley, S. A.; Wilson, I. A., Identification and structural characterization of heme binding in a novel dye-decolorizing peroxidase, TyrA. *Proteins* **2007,** *69* (2), 234-243.

60. Ogola, H. J. O.; Kamiike, T.; Hashimoto, N.; Ashida, H.; Ishikawa, T.; Shibata, H.; Sawa, Y., Molecular Characterization of a Novel Peroxidase from the Cyanobacterium Anabaena sp Strain PCC 7120. *Applied and Environmental Microbiology* **2009,** *75* (23), 7509-7518.

61. Kim, S. J.; Shoda, M., Purification and characterization of a novel peroxidase from Geotrichum candidum Dec 1 involved in decolorization of dyes. *Applied and environmental microbiology* **1999,** *65* (3), 1029-1035.

62. Liers, C.; Bobeth, C.; Pecyna, M.; Ullrich, R.; Hofrichter, M., DyP-like peroxidases of the jelly fungus Auricularia auricula-judae oxidize nonphenolic lignin model compounds and high-redox potential dyes. *Appl Microbiol Biot* **2010,** *85* (6), 1869-1879.

63. Johjima, T.; Ohkuma, M.; Kudo, T., Isolation and cDNA cloning of novel hydrogen peroxide-dependent phenol oxidase from the basidiomycete Termitomyces albuminosus. *Appl Microbiol Biot* **2003,** *61* (3), 220-225.

64. Fernandez-Fueyo, E.; Ruiz-Duenas, F. J.; Miki, Y.; Martinez, M. J.; Hammel, K. E.; Martinez, A. T., Lignin-degrading Peroxidases from Genome of Selective Ligninolytic Fungus Ceriporiopsis subvermispora. *J Biol Chem* **2012,** *287* (20), 16903-16916.

65. Heinfling, A.; Ruiz-Duenas, F. J.; Martinez, M. J.; Bergbauer, M.; Szewzyk, U.; Martinez, A. T., A study on reducing substrates of manganese-oxidizing peroxidases from Pleurotus eryngii and Bjerkandera adusta. *Febs Letters* **1998,** *428* (3), 141-146.

66. Kuan, I. C.; Johnson, K. A.; Tien, M., Kinetic-Analysis of Manganese Peroxidase - the Reaction with Manganese Complexes. *J Biol Chem* **1993,** *268* (27), 20064-20070.

67. Banci, L.; Camarero, S.; Martinez, A. T.; Martinez, M. J.; Perez-Boada, M.; Pierattelli, R.; Ruiz-Duenas, F. J., NMR study of manganese(II) binding by a new versatile peroxidase from the white-rot fungus Pleurotus eryngii. *J Biol Inorg Chem* **2003,** *8* (7), 751-760.

68. Choudhury, K.; Sundaramoorthy, M.; Hickman, A.; Yonetani, T.; Woehl, E.; Dunn, M. F.; Poulos, T. L., Role of the Proximal Ligand in Peroxidase Catalysis - Crystallographic, Kinetic, and Spectral Studies of Cytochrome-C Peroxidase Proximal Ligand Mutants. *J Biol Chem* **1994,** *269* (32), 20239-20249.

69. RodriguezLopez, J. N.; Smith, A. T.; Thorneley, R. N. F., Role of Arginine 38 in horseradish peroxidase a critical, residue for substrate binding and catalysis. *J Biol Chem* **1996,** *271* (8), 4023-4030.

70. Vitello, L. B.; Erman, J. E.; Miller, M. A.; Wang, J.; Kraut, J., Effect of Arginine-48 Replacement on the Reaction between Cytochrome-C Peroxidase and Hydrogen-Peroxide. *Biochemistry* **1993,** *32* (37), 9807-9818.

71. Efimov, I.; Badyal, S. K.; Metcalfe, C. L.; Macdonald, I.; Gumiero, A.; Raven, E. L.; Moody, P. C. E., Proton Delivery to Ferryl Heme in a Heme Peroxidase: Enzymatic Use of the Grotthuss Mechanism. *Journal of the American Chemical Society* **2011,** *133* (39), 15376-15383.

72. Sharp, K. H.; Mewies, M.; Moody, P. C. E.; Raven, E. L., Crystal structure of the ascorbate peroxidase-ascorbate complex. *Nat Struct Biol* **2003,** *10* (4), 303-307.

Chapter 3 - Identification of surface-exposed protein radicals and substrate oxidation sites in A-class dye-decolorizing peroxidase from *Thermomonospora curvata*[3]

3.1 Abstract

Dye-decolorizing peroxidases (DyPs) are a new family of heme peroxidases, in which a catalytic proximal aspartate is utilized to catalyze oxidation in acidic conditions. They have received much attention due to their potential applications in lignin degradation and biofuel production from biomass. However, the mode of oxidation in bacterial DyPs remains unknown. We have recently reported that the bacterial *Tc*DyP from *Thermomonospora curvata* is among the most active DyPs and shows activity toward lignin model compounds (*J. Biol. Chem.* **2015**, *290*, 23447). Based on the X-ray crystal structure solved at 1.75 Å, sigmoidal steady-state kinetics with reactive blue 19 (RB19), and formation of compound II-like product in the absence of reducing substrates observed with stopped-flow spectroscopy, we hypothesized that the *Tc*DyP catalyzes oxidation of large-size substrates *via* multiple surface-exposed protein radicals. Among 7 tryptophans and 3 tyrosines in *Tc*DyP consisting of 376 residues for the matured protein, W263, W376, and Y332 were identified as surface-exposed protein radicals. Only the W263 was also characterized as one of surface-exposed oxidation sites. SDS-PAGE and size-exclusion chromatography demonstrated that W376 represents an off-pathway destination for electron transfer, resulting in the crosslinking of proteins in the absence of substrates. Mutation of W376 improved compound I stability and overall catalytic efficiency toward RB19. While Y332 is highly conserved across all four classes of DyPs, its catalytic function in A-class *Tc*DyP is minimal possibly

[3] Reprinted with permission from Shrestha, R.; Chen, X. J.; Ramyar, K. X.; Hayati, Z.; Carlson, E. A.; Bossmann, S. H.; Song, L. K.; Geisbrecht, B. V.; Li, P., Identification of Surface-Exposed Protein Radicals and A Substrate Oxidation Site in A-Class Dye-Decolorizing Peroxidase from *Thermomonospora curvata*. *ACS Catalysis* **2016,** *6* (12), 8036-8047. Copyright 2016, American Chemical Society.

due to its extremely small solvent accessible areas. Identification of surface-exposed protein radicals and substrate oxidation sites is important for understanding DyP mechanism and modulating its catalytic functions for improved ligninolytic activity.

3.2 Introduction

Dye-decolorizing peroxidases (DyPs) are a newly discovered family of heme peroxidases, which are widely present in bacterial genomes.[1] While the biological function of DyPs remains unknown, they can use H_2O_2 to oxidize various industrial dyes, particularly anthraquinone derivatives that have high redox potentials and are poor substrates for classical peroxidases.[2] DyPs have recently received much attention due to their potential application in lignin degradation.[2-3] Lignin is the most abundant renewable source of aromatic polymers on earth,[4] which represents a promising feedstock for biofuel production.[5] However, degradation of lignin presents challenges, requiring strong acids and bases at high temperature to break it down.[6] Thus, there is a growing interest in lignin degradation using enzymatic approaches.[7] Studies including ours have demonstrated that DyPs can depolymerize lignin model compounds and wheat straw lignocellulose, though the efficiency is low.[8-11] Thus, more structural and mechanistic works are needed for DyP in order to develop its applications in biofuel production from lignin feedstock.

DyPs are subdivided into four classes, A through D, based on their primary sequences.[12] Except for class D that is fungal origin, the rest are mainly from bacteria.[12] It has to be noted that sequence identity between classes is very low (< 15%), especially between fungal and bacterial DyPs.[13] Several fungal lignin-degrading enzymes such as lignin peroxidase (LiP) and versatile peroxidase (VP) have been found to oxidize substrates *via* surface-exposed tryptophanyl and tyrosinyl radicals.[14-16] Similar mode of action was also suggested for the fungal *Aau*DyP from *Auricularia auricula-judae*.[17-20] While such information is critical for understanding DyP mechanism and modulating its catalytic functions through protein engineering, it remains unknown for bacterial A-, B-, and C-class DyPs.

We have recently reported an A-class DyP from *Thermomonospora curvata* (*Tc*DyP), which shows high peroxidase and dye-decolorizing activities.[11] It is also among few DyPs that have reactivity with large-size lignin model compounds,[8-11] indicating its potential application in lignin degradation. The catalytic cycle of *Tc*DyP has been demonstrated to be similar to that of plant peroxidase, which includes an enzyme resting state, compound I and compound II.[11, 21-22] Compound I ($[Fe^{4+}=O]^{+\cdot}$) is formed by oxidation of the enzyme resting state ($[Fe^{3+}]$) with a two-electron-equivalent oxidant like H_2O_2. Reduction of Compound I with a one-electron-equivalent reducing substrate generates compound II ($[Fe^{4+}=O]^{+}$), which returns to the enzyme resting state by a second one-electron-equivalent reducing substrate. It is of note that the *Tc*DyP compound I is unstable and quickly decays into compound II-like product (C2LP) in the absence of a reducing substrate.[11] While A-class DyPs have a promising future in biotechnological applications,[10-11, 23] study on this class lags far behind the others, especially on the mode of oxidation of large-size substrates. Here we report our results to identify surface-exposed protein radicals and substrate oxidation sites involving aromatic redox-active amino acids in *Tc*DyP.

3.3 Materials and methods

3.3.1 Instruments, biochemicals, and chemicals

All activity assays and steady-state kinetics were performed on a Cary 100 Bio UV-Vis spectrometer equipped with temperature controller and magnetic stirring. Transient-state kinetics was carried out on an Applied Photophysics SX20 stopped-flow spectrometer equipped with sequential mixing, a PDA detector, and a monochromator. Analytical SEC was performed on a Waters Breeze 2 system equipped with a PDA detector. EPR spectra were recorded on a Bruker E680 spectrometer equipped with a high sensitivity cavity and an ESR900 helium flow cryostat from Oxford Instruments. All chemical and biochemical reagents were purchased at the highest grade and used without further purification. Protein concentrations were determined by BCA assays.[24] Stocks of H_2O_2 were prepared

fresh before experiments and their concentrations were determined at 240 nm using ε_{240} = 43.6 $M^{-1}cm^{-1}$.

3.3.2 Protein mutation, expression and purification

Mutations were generated using QuickChange (Agilent Technologies) according to manufacturer's instructions. Fifteen mutants were generated, which included thirteen single mutants (W158F, W194F, W237F, W244F, W263F/S/A, W376F, W396F, Y330F, Y332F/L, and Y351F), one double mutant (W263F/W376F), and one triple mutant (W158F/W237F/W396F). Oligonucleotide primers used in the construction of these mutants are summarized in Table A3 (Apppendix A). Protein expression and purification were performed as described previously except that the cells were grown for an additional 4 h after IPTG induction.[11] The mutant W263S was grown at 18 °C overnight after IPTG addition in order to reach full heme occupancy. The Reinheitszahl values (R_z) of purified proteins were measured to be 1.8−2.0. Their heme contents were determined to be 0.97−1.20 using pyridine hemochromogen assays and $\Delta\varepsilon_{557-541}$ = 20.7 $mM^{-1}cm^{-1}$.[25] All mutants were analyzed by circular dichrosim to ensure that they were properly folded.

Proteins for crystallization were purified in the following way. Ten mg *wt*-*Tc*DyP were treated with 100 μg subtilisin A at 37 °C for 1 h before diisopropyl fluorophosphate was added to a final concentration of 100 μM to stop proteolysis. Following dialysis against 20 mM ethanolamine-HCl (pH 9.0), the protein was subjected to ion-exchange chromatography using a HiTrap Q column (GE Healthcare) and a linear gradient of 0−1.0 M NaCl in 20 mM ethanolamine-HCl (pH 9.0). The eluted protein was applied to a HiPrep 26/60 Sephacryl S-200 HR column (GE Healthcare) equilibrated in 20 mM ethanolamine-HCl (pH9.0) and 200 mM NaCl. Fractions corresponding to dimeric *Tc*DyP were pooled, buffer exchanged into 5 mM ethanolamine-HCl (pH 9.0), and concentrated to10 mg/ml using Amicon 10 KDa centrifugal filters.

3.3.3 Crystallization and structure determination

Crystals were grown by the sitting drop vapor diffusion method in a solution consisting of 100 mM sodium succinate (pH 7.0) and 15% (w/v) PEG3350. Crystals appeared within 24 h and matured by 48 h. Individual crystals were transferred to 100 mM sodium succinate (pH 7.0) containing 35% (w/v) PEG3350, and allowed to equilibrate for 5 minutes prior to flash freezing in liquid nitrogen. Diffraction data were collected at 100 K using beamline 22-BM of the Advanced Photon Source, Argonne National Laboratory at a wavelength of 1.0 Å and processed with the HKL2000 package. The structure was solved by molecular replacement using a PHENIX software suite with coordinates of PDB entry 4GT2 as a starting model.[26] The final structure was obtained by iterative automated model building and refinement using PHENIX and interactive model modification in *Coot*.[27] Figures were prepared using PyMol (Schrödinger, LLC). The final coordinates have been deposited in the RCSB under accession ID 5JXU.

3.3.4 EPR samples and data collection

EPR quartz tubes with an external diameter of 4 mm were used for measurements. Samples consisting of 1.0 mM *wt*-*Tc*DyP in 100 mM NaCl and 50 mM KPi (pH 7.8) and 0.1 mM *wt*-*Tc*DyP in 100 mM NaCl and 50 mM sodium citrate (pH 3.0) were used for analysis of the enzyme resting state. Compound I samples were prepared by manually mixing the enzyme and 10-fold excess H_2O_2 in EPR tubes. The mixing was conducted on ice for 8 s and then the EPR tube was flash-frozen in liquid nitrogen.

Spectra were collected at the National High Magnetic Field Laboratory (NHMFL, Tallahassee, FL). The spectra at 5 K with a 4000 G scan width were recorded using a 100 kHz modulation frequency, 5 G modulation amplitude, and a 1 mW microwave power. The spectra centered at $g = 2$ at 5−30 K were recorded using a 2 G modulation amplitude, and a 0.2 mW microwave power.

3.3.5 Analysis of reactions between *Tc*DyPs and H_2O_2 by SDS-PAGE and SEC

In a 50 µL solution of 50 mM salt at different pH values (sodium citrate, KPi, and Tris-HCl for pH 3.0−6.0, 7.0−8.0, and 9.0, respectively), 23 µM *wt*-*Tc*DyP was incubated with 23 µM H_2O_2 at room temperature for 1 min. An aliquot of 10 µL reaction mixture was withdrawn and the reaction was stopped by addition of equal volume of 2X Laemmli buffer followed by heating at 95 ^oC for 4 min, which was subsequently used for SDS-PAGE. For the reaction run at pH 8.0, 30 µL reaction mixture was withdrawn and analyzed by SEC using a BioSep SEC-S2000 HPLC column. The column was eluted with 150 mM NaCl in 50 mM KPi (pH 7.5) at a flow rate of 0.5 mL/min. The retention volumes of molecular mass standards were as follows: aprotinin (6.5 kDa, 9.75 ml), horse cytochrome *c* (12.4 kDa, 9.05 ml), chicken albumin (44.3 kDa, 7.70 ml), bovine albumin (66 kDa, 7.20 ml), yeast alcohol dehydrogenase (150 kDa, 6.85 ml), and horse apoferritin (443 kDa, 6.00 ml).

The same experiment was also carried out with *wt*-*Tc*DyP at pH 7.8 in the presence of RB19, in which 23 µM enzyme was incubated with 23 µM RB19 for 1 min prior to H_2O_2 addition. Controls were prepared, in which only RB19, or H_2O_2, or none of them was added.

Experiments of mutants and H_2O_2 were performed at pH 7.8 and analyzed by SDS-PAGE and SEC in the same way as described above.

3.3.6 Enzyme assays and steady-state kinetics

The activities of *wt* and mutant *Tc*DyPs were determined using RB19 as the substrate. Briefly, in a 480 µL solution consisting of 50 mM sodium citrate (pH 3.0), 0.02 mg /mL bovine serum albumin (BSA), 1 mM H_2O_2, and 100 µM RB19, the purified enzyme was added to a final concentration of 50 nM to initiate the decolorization reaction. Assays were done in triplicates. Enzyme activity was determined by measuring the initial rate of absorbance decrease at 595 nm using ε_{595nm} = 10 $mM^{-1}cm^{-1}$.

To determine steady-state kinetic parameters, the reactions were performed in the same way as described above except that concentrations of RB19 were varied between 5 to 100 µM in the presence of 1 mM H_2O_2, and concentrations of H_2O_2 were varied between 10 µM to 1 mM in the presence of 100

μM RB19. Rates were determined by the slopes of the initial reactions. The data obtained were fitted either to Michaelis-Menten Equation 1 or Hill Equation 2 using SigmaPlot 11. All measurements were done in triplicates.

$$v = \frac{v_{max}[S]}{K_M + [S]} \qquad (Eq. 1)$$

$$v = \frac{v_{max}[S]^h}{K_M + [S]^h} \qquad (Eq. 2)$$

3.3.7 Transient-state kinetics of compound I formation

All concentrations listed here were concentrations before mixing. Stopped-flow kinetics was performed in a single mixing mode at 22 °C in KPi (pH 7.8) using 5 μM enzyme and equal volume of H_2O_2 at various concentrations. All reactions were first investigated using a multiple-wavelength detector (PDA). The PDA data were analyzed using singular value decomposition with the Pro-KIV Global Analysis program provided by Applied PhotoPhysics to obtain the number of reaction intermediates and their corresponding spectra. Reactions were then monitored at a defined wavelength (the Soret band of enzyme resting state) using a monochromator to follow the formation of compound I. The monochromator data were fitted to a single exponential equation to obtain pseudo-first order rate constants (k_{obs}). Second-order rate constants of compound I formation were calculated from plots of k_{obs} *vs.* H_2O_2 concentrations. All experiments were performed in triplicate.

Rates of compound I decay (k_d) were extracted from PDA data of reactions between 5 μM enzyme and 5 μM H_2O_2. Spectra extracted at a defined wavelength corresponding to the Soret band of C2LP were fitted to a single exponential equation to obtain the decay rates.

3.4 Results and discussion

3.4.1 Overall structure of *Tc*DyP and heme access channels

The *Tc*DyP crystal structure was solved by molecular replacement using the DyP model from *Streptomyces coelicolor* (PDB entry 4GT2) as a search probe and refined to 1.75 Å limiting resolution. Data collection and refinement statistics are listed in Table A.4 (Appendix A). The structure shows that *Tc*DyP exists as a homodimer, which is consistent with the molecular mass of ~80 KDa estimated from SEC. The structure of a monomer unit is depicted in Fig. 3.1A, for which the dimensions are roughly 49 Å × 46 Å × 39 Å. *Tc*DyP adopts a ferredoxin-like fold consisting of antiparallel β-sheets and peripheral α-helices, which is characteristic of the DyP-type family but distinct from the classical heme peroxidases primarily made of helical proteins.[1, 13, 28] Similar to other heme peroxidases,[29] *Tc*DyP has a histidine coordinating to the heme iron as the fifth ligand at a distance of 2.1 Å. However, unlike classical heme peroxidases such as horseradish peroxidase (HRP),[28-30] which use the distal histidine to catalyze oxidation, DyPs employ an aspartate in place of the distal histidine to perform the same function.[22] Such change is thought to contribute to shifting the optimal pH of enzyme activity from neutral conditions for HRP to acidic conditions for DyPs.[22] The distal aspartate is also a part of *GXXDG* motif, which is recognized as the fingerprint of DyPs involved in heme binding.[31]

As shown in Figs. 3.1B−1D, three heme access channels are present in *Tc*DyP. Channel 1 has a diameter of ~3.3 Å and leads to the heme distal cavity where H_2O_2 binds to the heme iron. Thus, channel 1 is proposed as the channel for H_2O_2 to access the heme. Channel 2 has the largest diameter of ~5.0 Å among all three channels, which points to the propionate group on pyrrole ring C. The heme propionate has been demonstrated to provide a direct electron transfer path from the porphyrin radical to a binding substrate.[30] Channel 3 leads to the methyl group on pyrrole ring C, which is much smaller than the channel 2 with a diameter of ~3.5 Å. Both channels 2 and 3 are thought to serve as the tunnels for small-size substrates to access the heme prior to oxidation.

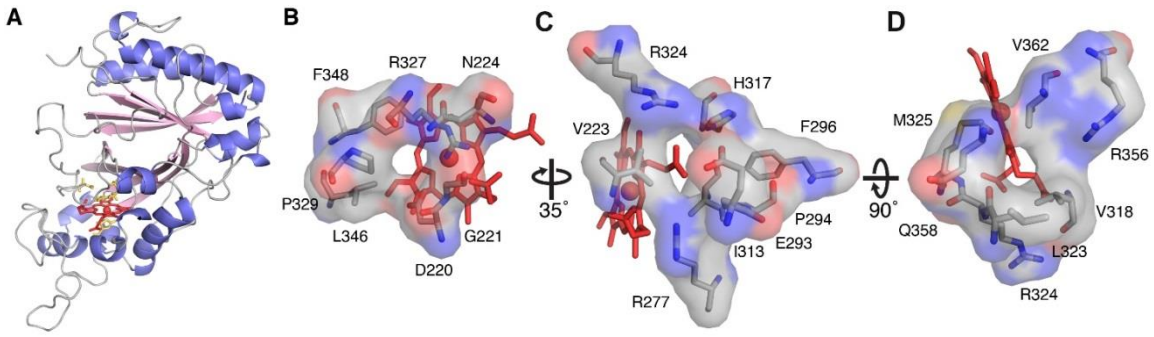

Figure 3.1 Structures of *Tc*DyP (PDB: 5JXU).

(A) α-Helices, β-strands, and loops are colored blue, pink, and grey, respectively. The heme porphyrin and catalytic residues are represented as red and yellow sticks, respectively. The heme iron is shown as a red ball; (B) Access channel 1 leading to the heme distal cavity; (C) Access channel 2 pointing to the propionate group on pyrrole ring C; (D) Access channel 3 pointing to the methyl group on pyrrole ring C.

3.4.2 Structural evidence for surface-exposed oxidation sites

Fig. 3.2 shows a superimposition of *Tc*DyP and *Aau*DyP, which reveals that their overall structures are aligned well except for a few flexible loops. Specifically, the heme center and surrounding areas are almost identical. Previous modeling work with fungal *Aau*DyP has predicted that even the small-sized guaiacol molecule narrowly fits into the distal cavity where the catalytic Asp and Arg residues lie.[18] In addition, the widest heme access channel 2 in *Tc*DyP is partially blocked by E293 (Fig. 3.1C). Thus, it cannot accommodate large-size anthraquinone-based dyes such as RB19 as the substrate in the active site. Yet *Tc*DyP has shown high activity toward RB19. We therefore hypothesized that *Tc*DyP catalyzes decolorization reactions *via* surface-exposed oxidation sites, which requires a long-range electron transfer (LRET) from the porphyrin to redox-active amino acids located at the protein surface to form protein-based radicals.

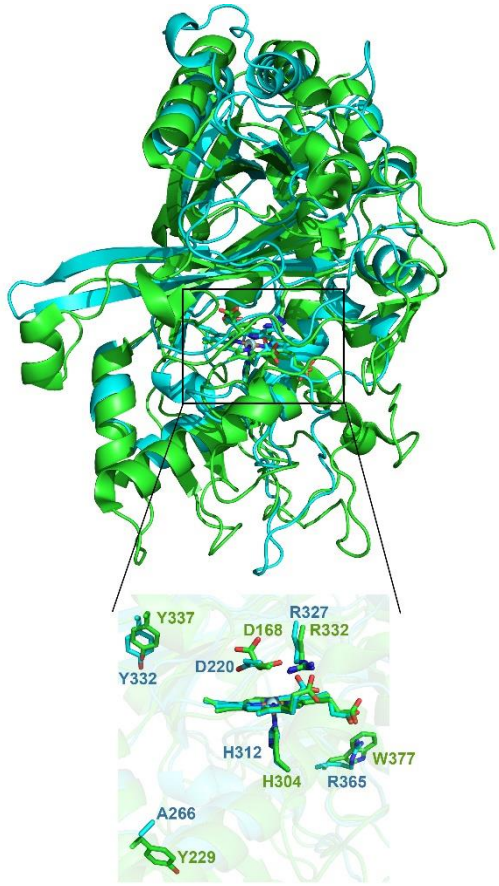

Figure 3.2 Structural superimposition of *Tc*DyP (cyan) and *Aau*DyP (green, PDB: 4AU9).

Catalytic residues of both enzymes are represented as sticks and labeled. Surface-exposed oxidation sites of *Aau*DyP and the corresponding residues in *Tc*DyP are also labeled.

Tyrosines and tryptophans are common redox-active amino acids, which can form radicals under oxidative conditions and have been shown to play important roles in catalysis.[32] Understanding the exact location and nature of protein radicals and their effect on the structure and function of proteins has been the subject of intense study.[33] Such examples include elucidation of roles of tyrosine and tryptophan radicals in myoglobins, cytochrome *c* peroxidase (CcP), LiP, VP, and more recently fungal DyP.[14-20, 34-35]

DyPs are rich in tryptophans and tyrosines,[36] for which their percentage can reach up to 5% of the total residues. On the basis of sequence study of the four classes of DyPs, we have concluded that, while tyrosines predominates in D-class as redox-active amino acids, tryptophans are in the majority for A-class DyPs. For example, while the D-class DyP from *Coprinopsis cinerea* contains 23 tyrosines and

8 tryptophans out of 648 residues for the matured protein, A-class *Tc*DyP has 7 tryptophans and 3 tyrosines in a total of 376 amino acid residues. Recent study on D-class *Aau*DyP has shown that, out of 7 tyrosines and 4 trytophans in 448 amino acids, surface-exposed residues including Y229, Y337, and W377 are identified as potential radical sites for dye decolorization.[17-19] These results suggest that DyPs may employ multiple protein radicals on the protein surface as a general strategy for oxidizing large-size substrates.

3.4.3 Formation of protein radicals in wt-*Tc*DyP as observed by EPR

The spectrum in top panel of Fig. 3.3A indicates that the *wt-Tc*DyP at pH 7.8 predominantly existed as a rhombically distorted axial resonance at $g_{\perp} \approx 6$ (g_y = 6.20, g_x = 5.50, and $g_{\parallel}$ = 2.00), corresponding to a high-spin Fe^{3+}. The absolute difference in g values ($\Delta g = g_y - g_x$) at g = 6 was used to determine the percentage of rhombicity, R (= $\Delta g/16 \times 100\%$), which was calculated to be 4.4% at pH 7.8. The resonance between g = 3 and g = 2 suggests the presence of a small proportion of low-spin Fe^{3+}. The signal pattern changed significantly when the EPR was recorded in pH 3.0 (center panel in Fig. 3.3A). A symmetrical signal was observed for high-spin Fe^{3+} at $g_{\perp}$= 6.00. The less reactive low-spin Fe^{3+} species disappeared, which is consistent with the fact that DyPs are most active under acidic conditions.

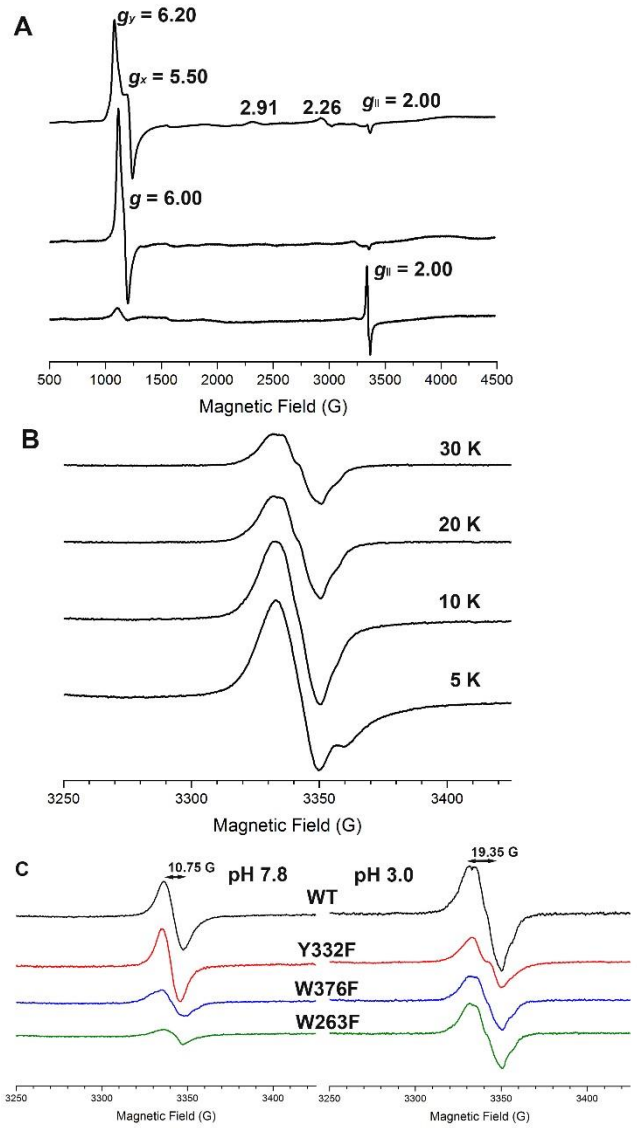

Figure 3.3 EPR spectra recorded on a 9 GHz spectrometer.

(A) Spectra of 1.0 mM *wt*-*Tc*DyP at pH 7.8 (top), 0.1 mM *wt*-*Tc*DyP at pH 3.0 (center), and 0.1 mM *wt*-*Tc*DyP plus 1.0 mM H_2O_2 at pH 3.0 (bottom) recorded at 5 K; (B) Temperature-dependent spectra of 0.1 mM *wt*-*Tc*DyP reacted with 1.0 mM H_2O_2 at pH 3.0; (C) Spectra of 1.0 mM *wt* and mutant *Tc*DyPs reacted with 10 mM H_2O_2 at pH 7.8 (left) and 0.1 mM *wt* and mutant *Tc*DyPs reacted with 1.0 mM H_2O_2 at pH 3.0 (right). The spectra were recorded at 20 K.

To explore whether a protein-based radical was generated, the EPR spectrum was recorded for 0.1 mM *Tc*DyP in the presence of 1.0 mM H_2O_2 at pH 3.0. As shown in the bottom panel of Fig. 3.3A, a radical signal with unresolved hyperfine couplings was observed at $g_\perp$ = 2.00, which had an overall width and peak-to-trough width of 90 G and 19 G, respectively. The presence of a small ferric signal was attributed to either nonreactive enzyme or most probably to native enzyme that cycled back. It has

been reported that protein-based radicals usually have a signal at $g = 2$ with a width of ~100 G.[37-40] On the other hand, oxoferryl-porphyrin radicals were shown to contain an extremely broad signal starting from $g_{\perp} = 3.45$ or 3.27 to $g_{\perp} = 2$,[41-42] which was not observed in *Tc*DyP. A temperature-dependence study at pH 3.0 (Fig. 3.3B) and pH 7.8 (not shown) revealed little or no contribution from the ferry-ion center, which is consistent with the formation of protein radicals.[39, 43] Furthermore, the shape and line width of *Tc*DyP signals obtained at 20 and 30 K (Fig. 3.3B) are similar to the protein radicals of *Synechocystis* PCC6803 peroxidase-catalase recorded at 60 K and of turnip peroxidase isozymes recorded at 30 K.[39-40] Thus, the observed radical signal in the reaction between *wt-Tc*DyP and H_2O_2 (Fig. 3.3A) is assigned as a protein-based radical, which was further confirmed with the EPR study of mutant *Tc*DyPs (Fig. 3.3C) described later. Since it has been demonstrated in our recent study that the *wt-Tc*DyP compound I is unstable and quickly decays into C2LP in the absence of reducing substrates,[11] we proposed that the C2LP corresponds to the observed protein-based radicals.

3.4.4 Crosslinking of wt-*Tc*DyP

Since many hemoproteins have been reported to undergo protein crosslinking in the presence of H_2O_2 due to formation of surface-exposed protein radicals,[35, 44-45] we decided to determine whether the crosslinking also occurred with *wt-Tc*DyP. Thus, reactions of *wt-Tc*DyP with H_2O_2 were analyzed with SDS-PAGE and SEC.

Fig. 3.4A shows the SDS-PAGE of *wt-Tc*DyP incubated with one equivalent H_2O_2 under various pH conditions. Except for the 43 KDa band that corresponded to a *Tc*DyP monomer, additional bands at 100 and 250 KDa were also observed, which were assigned as a covalent dimer and oligomer, respectively. While the formation of covalent dimer and oligomer was pH dependent, their trends were different. The covalent dimer and oligomer contents reached their maximum at pH ~8 and ~3, respectively. This indicated that, under an acidic condition and in the absence of a reducing substrate, the rate of formation of covalent oligomers from covalent dimers was much faster than that of covalent dimer formation from monomers. Additionally, when the experiment was carried out in the presence of

RB 19, the bands corresponding to covalent dimer and oligomer disappeared (lane 4 in Fig. 3.4B), which suggested that substrate binding may prevent the protein crosslinking.

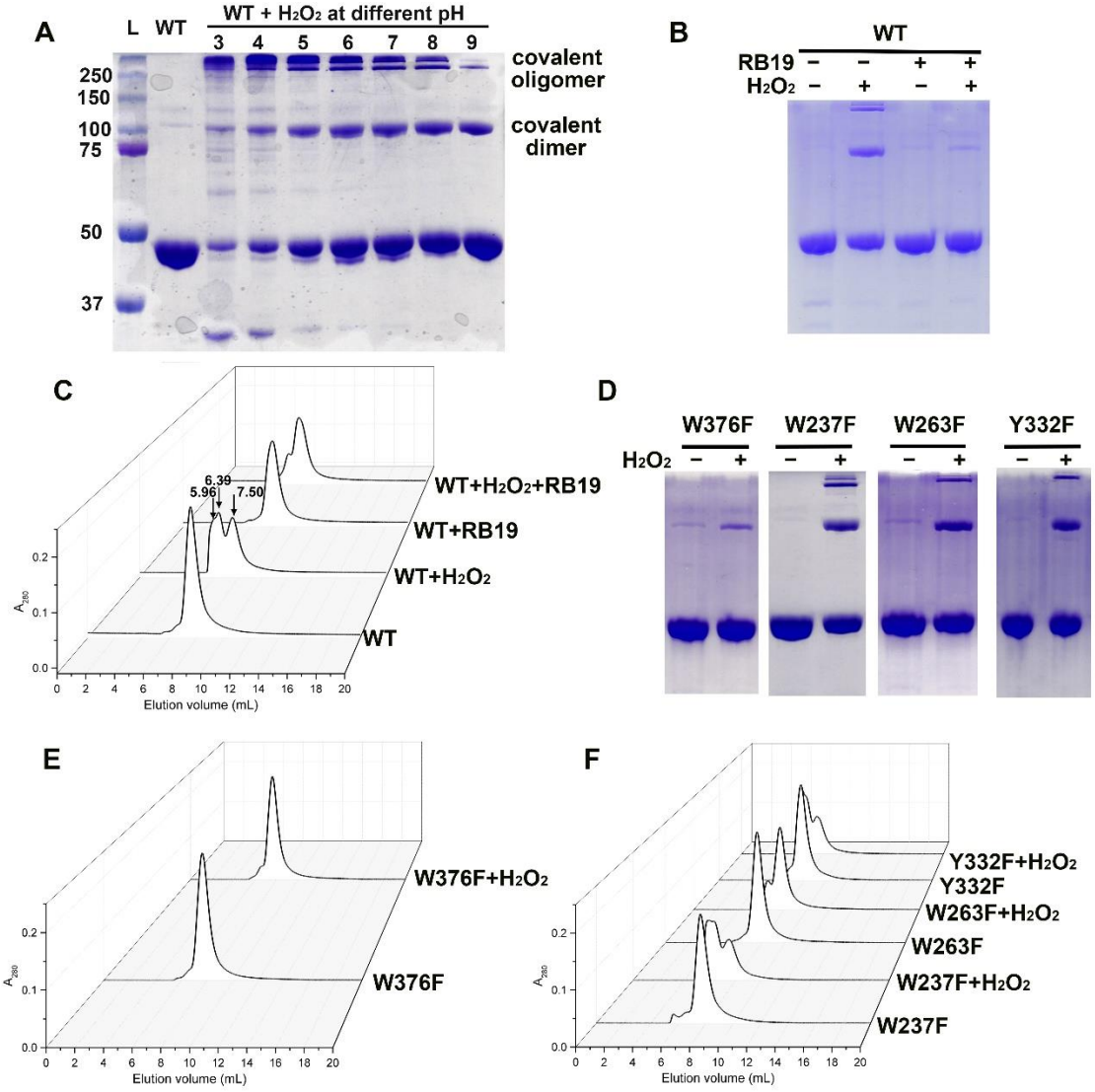

Figure 3.4 Analysis of reactions by SDS-PAGE and SEC.

(A) SDS-PAGE of reactions between *wt*-*Tc*DyP and H_2O_2 under various pH conditions; (B) SDS-PAGE of reactions between *wt*-*Tc*DyP and H_2O_2 in the presence and absence of RB19 at pH 7.8; (C) SEC of reactions shown in (B); (D) SDS-PAGE of reactions between mutants and H_2O_2; (E) SEC of reactions between W376F and H_2O_2; (F) SEC of reactions between mutants and H_2O_2.

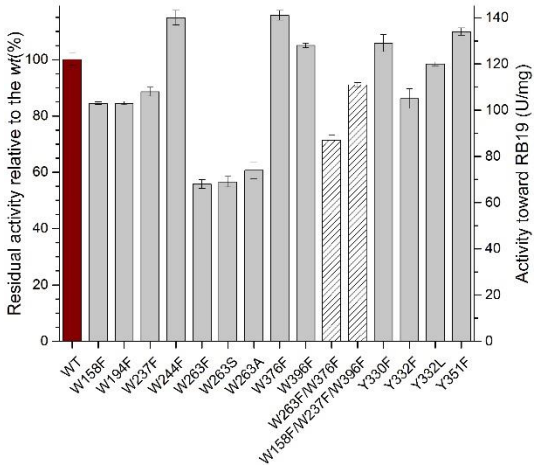

Figure 3.5 Residual activities of mutant *Tc*DyPs toward RB19.

Red, grey, and patterned bars represent *wt*, single and multiple mutants, respectively.

To test whether the crosslinking would affect enzyme activity, the reactions were also analyzed by SEC in the presence and absence of RB19. The native enzyme displayed a peak at 7.50 mL in Fig. 3.4C, corresponding to a *Tc*DyP dimer. When H_2O_2 was present, two additional peaks, accounting for 54% of the total peak areas, appeared at 6.39 and 5.96 mL, corresponding to a *Tc*DyP tetramer and oligomer, respectively. Peaks were isolated and subject to enzyme activity assay using RB19. It was found that the peak consisting of tetramer and oligomer lost ~30% activity compared with the dimer peak. The results agree with the gel image shown in Fig. 3.4A, in which ~30% protein exist as covalent dimer and oligomer at pH 8.0. When the H_2O_2 and RB19 were simultaneously present in the reaction, the tetramer and oligomer peaks only accounted for 6% of total peak areas (Fig. 3.4C), consistent with the results from SDS-PAGE (lane 4 in Fig. 3.4B).

3.4.5 Involvement of W376 in protein crosslinking

Since tryptophan and tyrosine are the most common candidates of radical sites, each of them was mutated to a less oxidizable phenylalanine in *Tc*DyP. It was discovered that, while the other mutants (*e.g.* W237F, W263F, and Y332F) displayed similar phenomena as the *wt* when incubated with H_2O_2 (Figs. 3.4D−F), only the W376F mutant significantly lost its ability to form the protein crosslinks. The bands at 100 and 250 KDa in SDS-PAGE almost disappeared when W376F was oxidized by H_2O_2 at pH

7.8 (Fig. 3.4D). Accordingly, when the reaction was analyzed by SEC, no peak corresponding to the tetramer and oligomer was observed (Fig. 3.4E).

Since W376 is located on the protein surface with a large solvent accessible area (30.2 Å), it was initially predicted to be a radical site for substrate oxidation. Unexpectedly, activity assay showed that W376F displayed a higher reactivity than the *wt* with RB19 (116%, Fig. 3.5). Thus, our data are consistent with the idea that W376 was likely to serve as a radical sink and represent an off-pathway destination for electron transfer from the heme center to the protein surface when a dye substrate is absent.

3.4.6 Surface-exposed protein-based radicals and substrate oxidation sites involving W263 and Y332

To identify surface-exposed substrate oxidation sites involving tryptophanyl and tyrosinyl radicals, the activities of all phenylalanine mutants were determined with RB19 in the presence of 1 mM H_2O_2. The results are depicted in Fig. 3.5. While all single mutants except W263F retained the *wt* activity, the W263F mutant lost ~50% its activity. Examination of *Tc*DyP crystal structure reveals that W263 is located on the proximal side of the heme at the dimer interface, and is the closest residue to the heme among all tryptophans and tyrosines at a distance of 7.4 Å (Fig. 3.6). Sequence alignment depicted in Fig. C.1 (Appendix C) shows that W263 is absolutely conserved in A-class DyPs, which suggests that it is functionally important and may serve as one of protein radicals for surface-exposed substrate oxidation.

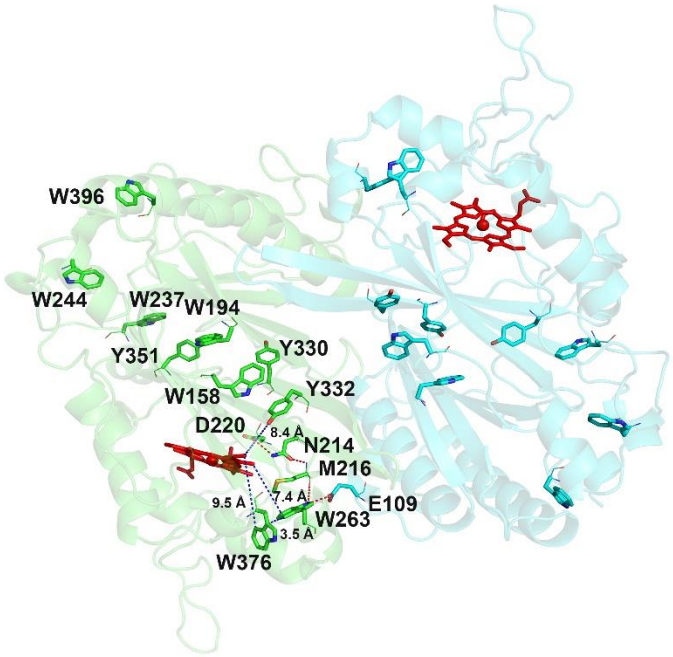

Figure 3.6 Location of Trp and Tyr residues in *wt-Tc*DyP and the hydrogen bonding network involving W263.

Main and side chains of residues are represented as lines and sticks, respectively. Red and blue dots represent hydrogen bonding and distance, respectively. The two monomeric units are colored in green and cyan.

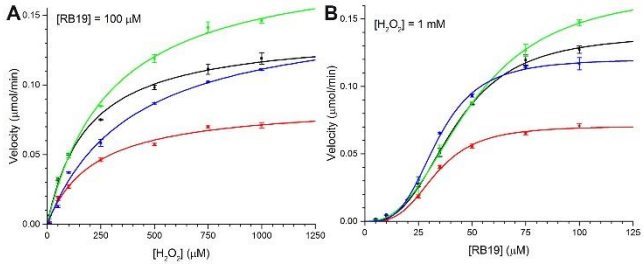

Figure 3.7 Steady-state kinetics

*wt-Tc*DyP (black), W263F (red), W376F (green), and Y332F (blue). (A) With H_2O_2; (B) With RB 19.

To further examine the importance of W263, activities of W263F mutant were tested against a series of substrates commonly used for DyPs, which included ABTS, catechol, guaiacol, hydroquinone, and reactive blue 4 and 5. The W263F mutant retained 40−60% of the *wt* activity (data not shown), consistent with the result obtained with RB19. Additionally, residues W158, W237, and W396 have large solvent exposed areas as summarized in Table B.6 (Appendix B). We therefore hypothesized that a triple mutant of these positions would magnify the activity loss if they were involved in substrate oxidation *via* surface-exposed protein radicals. Activity assays on the W158F/W237F/W396F showed

that the triple mutant retained more than 90% *wt* activity (Fig. 3.5), implying that these positions are not functionally important. Thus, of all the tryptophans in *Tc*DyP, only W263 was identified as the one that participates directly in surface-exposed substrate oxidation. It has to be noted that *Tc*DyP must have multiple substrate oxidation sites on the protein surface because (1) W263 mutation only resulted in 50% loss of the *wt* activity; (2) W263 mutation resulted in fewer radicals than the *wt* (Fig. 3.3C), which will be described in the next section; and (3) steady-state kinetics of *Tc*DyPs with RB19 displayed a sigmoidal curve, which will be discussed in the section after next.

Table 3.1 Summary of enzyme steady-state and transient-state kinetics

	RB 19 (H_2O_2 at 1 mM)				H_2O_2 (RB19 at 100 μM)			Compound I	
*Tc*DyPs	k_{cat} (s^{-1})	K_M (μM)	k_{cat}/K_M (M^{-1} s^{-1})	h	k_{cat} (s^{-1})	K_M (μM)	k_{cat}/K_M (M^{-1} s^{-1})	k_{obs}[a] (M^{-1} s^{-1})	k_d[b] (s^{-1})
wt	96 ± 2	42 ± 1	2.3×10^6	2.9	96 ± 2	188 ± 13	5.1×10^5	4.2×10^6	2.10
W263F	49 ± 1	33 ± 1	1.5×10^6	3.4	60 ± 1	219 ± 17	2.7×10^5	3.5×10^6	0.71
W263S	51 ± 1	32 ± 1	1.6×10^6	2.9	47 ± 1	178 ± 13	2.4×10^5	3.1×10^6	0.62
W263A	52 ± 1	28 ± 1	1.9×10^6	3.5	63 ± 2	303 ± 25	2.0×10^5	2.6×10^6	0.82
W376F	119 ± 5	49 ± 2	2.4×10^6	2.5	133 ± 3	295 ± 18	4.5×10^5	2.9×10^6	0.19
W376F/W263F	69 ± 1	26 ± 1	2.7×10^6	2.7	90 ± 3	283 ± 23	3.2×10^5	2.9×10^6	0.17
Y332F	83 ± 1	34 ± 1	2.5×10^6	3.4	108 ± 4	393 ± 32	2.7×10^5	3.4×10^6	1.90
Y332L	97 ± 1	37 ± 1	2.5×10^6	3.4	118 ± 2	279 ± 13	4.2×10^5	3.2×10^6	1.80

[a] Second-order rate constants (k_{obs}) of compound I formation in the presence of H_2O_2; [b] Rate constants (k_d) of compound I decaying to compound II-like product when the reaction was performed with 5 μM enzyme and 5 μM H_2O_2 at pH 7.8.

Sequence alignment in Fig. C.1 (Appendix C) has shown that Y332 is highly conserved across all four classes of DyPs. It is located at the *Tc*DyP dimer interface on the distal side of the heme with a distance of 8.4 Å (Fig. 3.6). Additionally, this tyrosine has been proposed as a potential surface-exposed protein radical site in B- and D-class DyPs.[17-18, 46] As depicted in Fig. 3.2, structural alignment of *Tc*DyP (A-class) and *Aau*DyP (D-class) based on the heme cofactor reveals that the conserved tyrosines in two proteins are overlapped. The same result was obtained when structures of *Tc*DyP and *Vc*DyP from *Vibrio cholerae* (B-class) were aligned (data not shown). Thus, Y332 was proposed to be one of the

surface-exposed protein radical sites in *Tc*DyP, which was supported by the EPR study described in the next section. To test whether Y332 could also serve as a surface-exposed oxidation site, its mutations were performed. Enzyme assays with RB19 showed that the mutants retained more than 90% *wt* activity (Fig. 3.5). While it is in contrast with *Vc*DyP, in which the tyrosine to leucine mutant abolishes enzyme activity, [46] it agrees with *Aau*DyP, in which the mutation also minimallyaffects enzyme activity.[17] The observed weak effects of Y332 are mainly attributed to its small solvent accessible surface area (2.76 $Å^2$) relative to the tyrosine at the same position in *Vc*DyP (12.47 $Å^2$). In addition, the solvent accessible surface areas for Y330 and Y351 are extremely small at 0 and 0.67 $Å^2$, respectively. Their mutations resulted in increased activities toward RB19 as shown in Fig. 3.5, which suggests that Y330 and Y351 do not participate in the formation of protein radicals for surface-exposed substrate oxidation.

3.4.7 EPR study of mutant *Tc*DyPs

Since W263, W376, and Y332 were proposed to form protein-based radicals, we studied their reactions with H_2O_2 by EPR. As described above, *Tc*DyP compound I is unstable and quickly decays into C2LP, which is hypothesized as a protein-based radical. If the hypothesis is true, the mutants are expected to show radical signals with decreased intensity as well as changes in their hyperfine coupling. Thus, the W263F, W376F, and Y332F mutants were incubated with H_2O_2 at pH 7.8 and 3.0 for 8 s prior to being flash-frozen in liquid nitrogen. The EPR spectra are shown in Fig. 3.3C. Similar to the *wt*-*Tc*DyP (Fig. 3.3A), the mutants generated fewer radicals at pH 7.8 (left panel, [*Tc*DyP] = 1.0 mM) than at pH 3.0 (right panel, [*Tc*DyP] = 0.1 mM). Since the EPR samples had the same volume, were prepared in the same manner, and were measured by the same spectrometer using the same settings, the radical intensity should be directly related to the radical yield. To our expectations, all mutants except Y332F at pH 7.8 had lower radical yields than the *wt*. Compared with the *wt* signal, small, yet significant changes of hyperfine coupling were also observed for all mutants except Y332F at pH 7.8. The change was clearer at pH 3.0, which represents an optimal pH condition for *Tc*DyP activity. At pH 7.8, Y332F had the same radical yield and shape as the *wt*, suggesting that Y332 does not participate in radical

formation. This agrees well with the observation that the Y332 mutants and *wt* had similar compound I decay rates (k_d) at pH 7.8 (Table 3.1), which will be discussed later. Moreover, the broader EPR line shape observed at pH 3.0 than at pH 7.8 implies that additional radical species exist at pH3.0, most likely contributed from Y332 and possibly other residues. Overall, the EPR study of mutants supports the hypothesis that surface-exposed W263, W376, and Y332 generate protein radicals in the presence of H_2O_2 under acidic conditions.

3.4.8 Steady-state kinetics of W263, W376, and Y332 mutants

To further understand the importance of W263, W376, and Y332, we conducted steady-state kinetic evaluations of a panel of site-directed mutants in the presence of RB19 and H_2O_2. The results are summarized in Table 3.1. We have recently reported that small- and large-size substrates display different kinetics with *wt*-*Tc*DyP,[11] which could be attributed to distinct oxidation sites for small- and large-size substrates. The small-size substrates like guaiacol could be oxidized at the heme center *via* heme access channels 2 and 3 shown in Fig. 3.1. The large-size dye substrates such as RB19 and lignin model compounds are likely to be oxidized on the protein surface *via* LRET processes as described above. As depicted in Fig. 3.8, unlike the H_2O_2 that shows the classical Michaelis-Menten kinetics, oxidation of RB19 by the *wt* and mutant *Tc*DyPs displays a sigmoidal kinetics, suggesting that cooperativity exists between the enzyme and dye substrate. The estimated Hill constant (h) is around three, implying that the *Tc*DyP has multiple substrate binding sites for RB19. Such phenomena were also observed for other hemoproteins. For example, hemoglobin binds four oxygen molecules at four separate sites, displaying a Hill constant of three.[47] Thus, single mutations are unlikely to abolish *Tc*DyP activity.

As shown in Fig. 3.6, not only is W263 the closest residue to the heme among all tryptophans and tyrosines, but also it forms a hydrogen bond network to D220 *via* M216 and N214. The D220 is a catalytic residue located in the heme distal cavity, which is characteristic of DyP enzymes and plays critical roles in compound I formation when the heme Fe^{3+} is oxidized by H_2O_2.[11] Additionally, W263

forms a hydrogen bond with E109 from another monomer unit, suggesting that W263 could also be involved in dimer formation of the native enzyme. To characterize the role of W263, we mutated this residue to phenylalanine, alanine, and serine. Phenylalanine was selected because it is a conservative substitution of tryptophan, but lacks of the ability to produce a stable radical and form hydrogen bonds. Alanine was chosen because it is a non-polar (hydrophobic) amino acid without aromacity, which could help reveal the importance of indole ring in W263. Serine was selected because it is a preferred substitution for tryptophans in many peroxidases,[14, 16-17] which may help to address polar interactions involving the indole ring.

While all W263 mutants had lower catalytic efficiency than the *wt* toward both RB19 and H_2O_2, the mutations we examined showed a much more pronounced effect on H_2O_2 consumption than on RB19 oxidation as summarized in Table 3.1. All W263 mutants displayed similar and increased binding affinities toward RB19 relative to the *wt* (~30% increase), which suggests that π−π interaction is unlikely important for the binding of dye substrates, as side chains of W263S and W263A lack of aromatic rings. Moreover, their turnover numbers toward RB19 dropped half to ~50 s^{-1}, which is consistent with our expectation as the mutants will not be able to generate a stable radical. While the *wt* and W263S had almost the same H_2O_2 affinities, W263F and W263A displayed much lower H_2O_2 affinities than the *wt*. In addition, the turnover number of W263S toward H_2O_2 decreased the most among three W263 mutants. This implies that the hydrogen bond network connecting W263 and D220 is likely to be more involved in H_2O_2 binding than electron transfer.

While mutation of W376 to F376 had no effect on the binding of RB19, it affected H_2O_2 binding significantly (~60% decrease in binding affinity). This is not surprising as it is only 9.5 and 3.5 Å away from the heme center and W263, respectively. The close proximity of W376 and W263 within Van der Waals distance (3−6 Å) suggests that an electron transfer could occur between them. The turnover numers of W376F with RB19 and H_2O_2 were determined to be 1.3- and 1.4-fold faster than those of the *wt*. Combined with the fact that W376 is responsible for crosslinking in the absence of dye substrates,

we concluded that W376 is likely to be involved in off-pathway electron transfer processes. If so, mutation of W376 would be expected to suppress this undesired pathway and thereby increase catalytic efficiency of the enzyme. To test this possibility, a double mutant, W376F/W263F, was constructed and purified. Indeed, the double mutant displayed increased catalytic efficiency toward RB19 and H_2O_2 by 80% and 20% relative to the W263F, respectively. The 80% improvement of the double mutant with RB19 over the single mutant is significant and demonstrates the importance of W376 mutation in biotechnological development of *Tc*DyP applications.

The Y332 is located at the distal side of the heme with a distance of 8.4 Å. Because it has a small solvent accessible surface area and is close to the distal cavity where Fe^{3+} in heme is oxidized by H_2O_2, its mutations are predicted to have minimal effects on RB19 oxidation, but significant impacts on reactions with H_2O_2. Indeed, the mutants displayed slightly increased binding affinities with RB19, resulting in improved catalytic efficiency relative to the *wt*. However, the mutations drastically decreased binding affinities with H_2O_2 while the turnover numbers increased. In fact, the Y332F enzyme had the lowest H_2O_2 binding affinity among all mutants shown in Table 3.1.

3.4.9 Transient-state kinetics of W263, W376, and Y332 mutants in compound I formation and decay

Since C2LP was assigned as a protein-based radical involving W263, W376, Y332, and others, the corresponding mutants were studied for their transient-state kinetics of compound I formation and decay using a stopped-flow spectrometer. Our recent study has shown that the stopped-flow experiments with the *wt*-*Tc*DyP performed at pH 3.0 are much more challenging than the ones performed at pH 7.8 due to minimal spectral shift and low enzyme stability at pH 3.0.[11] Therefore, the mutant enzymes were mixed with H_2O_2 in 1:1 ratio at pH 7.8. Their spectral changes are shown in Fig. 3.8A−D. Analysis of these spectra by Pro-KIV gave a two-step reaction A→B→C as the best fit. Based on our recent study,[11] A, B, and C were assigned as the enzyme resting state (blue lines), compound I (red lines), and C2LP (green lines), respectively. Their spectral character is summarized in Table 3.2.

To determine the effect of site-directed mutation on compound I formation, the second-order rate constants (k_{obs}) of compound I formation were measured with various mutants. The results are summarized in Table 3.1. While all mutations resulted in the decrease of k_{obs}, the W263A, W376F, and W376F/W263F mutants were diminished the most. This is not surprising because (1) W263 is spatially close to the heme and its mutation to A263 represented a significant change in terms of amino acid structure and property; (2) spectra of the resting states of W376 mutants indicated significant perturbation of the heme microenvironment relative to the other mutants (Fig. 3.8E−F). In addition, the second-order rate constant of compound I formation and overall catalytic efficiency toward RB19 for *wt*-*Tc*DyP were determined to be 4.2 $\times 10^6$ and 2.3 $\times 10^6$ M^{-1} s^{-1}, respectively, which implied that the formation of compound I was not rate-limiting in the catalytic cycle. This is further supported by the steady-state and transient-state kinetics of W376F. While the rate of compound I formation was slower for this mutant than that of the *wt*, its turnover number toward RB19 was 1.2-fold faster.

The rates of compound I decaying into C2LP (k_d) were also determined for reactions between 5 μM enzyme and 5 μM H_2O_2. As described above, C2LP was assigned as protein-based radicals. Since W263, W376, and Y332 were demonstrated to be the radical sites in the presence of H_2O_2, mutation of these residues was expected to result in the increase of compound I stability and reduction of decay rates. Indeed, the W263, W376, and Y332 mutants had slower decay rates than the *wt*. As summarized in Table 3.1, the decay rates of W263 mutants were 40−50% of the *wt*, which agrees well with their steady-state kinetics (~50% decrease of k_{cat} from the *wt* to mutants).

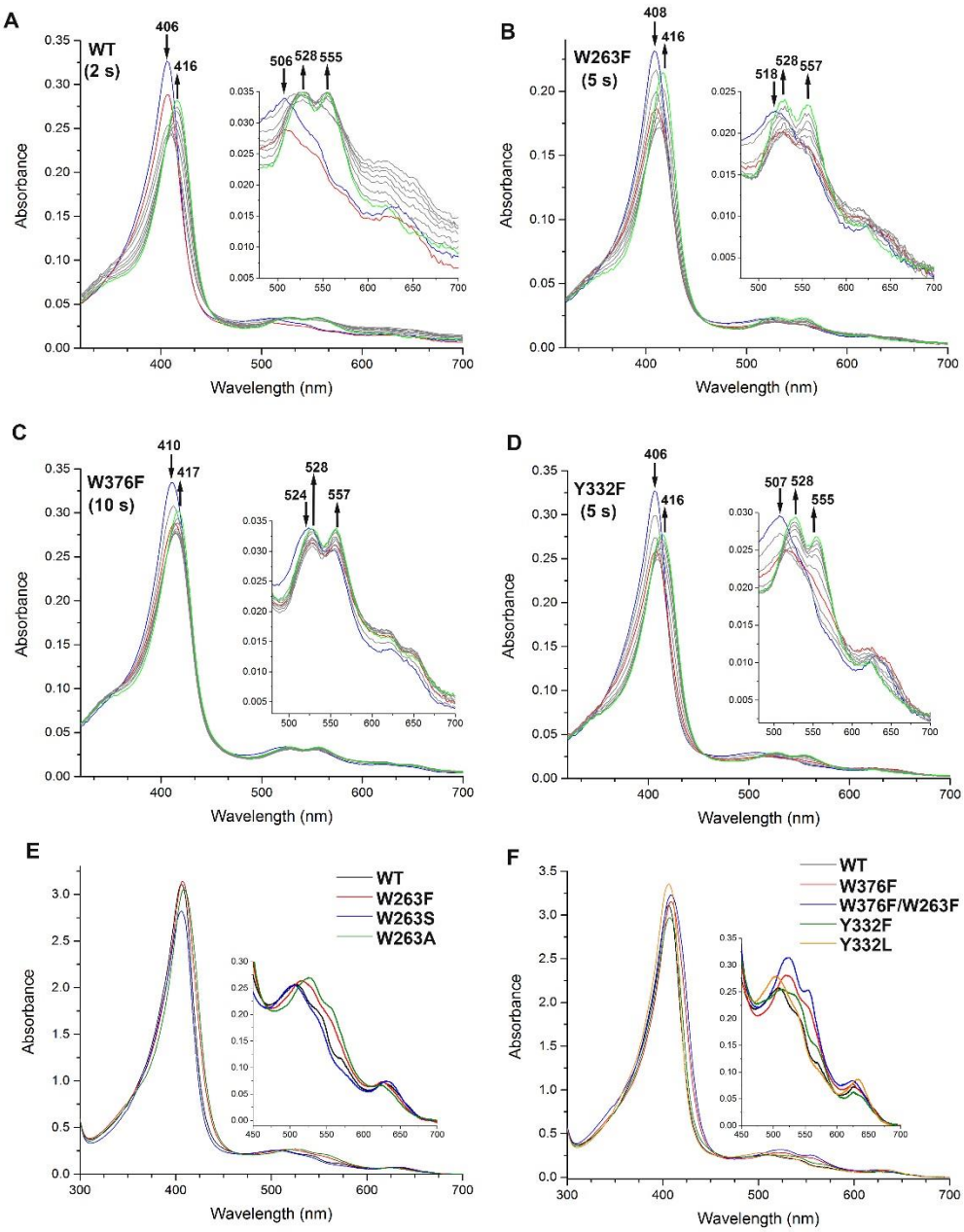

Figure 3.8 Stopped-flow & UV-Vis spectra

Stopped-flow spectra of reactions between *Tc*DyPs and H_2O_2 at 1:1 ratio (A−D) and spectral overlay of enzyme resting states (E−F). The blue, red, and green lines in A−D represent initial, intermediate, and final states of the enzymes, respectively. Reactions were performed with 5 μM enzymes at pH 7.8. Arrows indicate changes of absorbance over time.

Table 3.2 Absorption maxima of resting state and intermediates of *Tc*DyPs

*Tc*DyPs	Resting State	Compound I	Compound II-like product (C2LP)
wt	406, 506, 545, 569 (*sh*), 626	408, 524, 549, 620, 650 (*sh*)	416, 528, 555, 619
W263F	408, 518, 553, 627	412, 530, 555, 619, 648 (*sh*)	416, 528, 557, 621 (*sh*)
W263S	407, 505, 543, 632	406, 528, 614, 644	416, 528, 557, 622
W263A	408, 518, 554, 628	410, 530, 555, 617, 646	418, 528, 557, 621

W376F	410, 524, 553, 623 (*sh*)	414, 528, 555, 620, 650 (*sh*)	417, 528, 557, 623, 649 (*sh*)
W376F/W263F	410, 524, 553, 621 (*sh*)	416, 528, 557, 620, 652 (*sh*)	418, 528, 557, 619
Y332F	406, 507, 540, 628	408, 523, 620, 646	416, 528, 555, 622
Y332L	406, 505, 538, 629	406, 525, 616, 644	412, 526, 555, 618

While multiple residues are involved in the formation of protein-based radicals, W376 should act as the destination of off-pathway electron transfer because it promotes the formation of crosslinking in the absence of dye substrates (Fig. 3.4A). Thus, W376 mutation is predicted to have the largest impact on decay rates among all single mutants. Accordingly, the decay rates of W376 mutants were found to be only 8% of the *wt*. We found that the k_d of Y332 mutants was smaller than expected (from 2.10 s^{-1} for the *wt* to 1.80−1.90 s^{-1} for the Y332 mutants), which is attributed to the neutral pH of the reaction condition. As discussed above, Y332 only formed radicals when it was oxidized by H_2O_2 under acidic conditions (Fig. 3.3C). Thus, mutation of Y332 would minimally affect the compound I stability and its decay rate at pH 7.8.

3.5 Conclusions

The *Tc*DyP structure solved at 1.75 Å contains two ferredoxin-like folds, which is characteristic of proteins from the DyP family. Catalytic residues D220 and R327 are located at the heme distal side and H312 acts as a proximal ligand to the heme. Although bacterial DyPs display activities toward large-size anthraquinone-based dyes and lignin model compounds, their modes of oxidation remain unknown. Based on the *Tc*DyP structure, we predicted that *Tc*DyP uses surface-exposed protein-based radicals for oxidation of large-size substrates. Thus, efforts were focused on aromatic redox-active amino acids that are rich in DyP enzymes. Among 7 tryptophans and 3 tyrosines that are present in the *Tc*DyP, W263, W376, and Y332 are the closest residues to the heme and were identified as the sites of surface-exposed protein radicals, which correspond to a compound II-like product (C2LP) generated from the decay of compound I. In addition, the absolutely conserved W263 in A-class DyPs was also characterized as a surface-exposed substrate oxidation site, which was supported by ~50% loss of enzyme activity for the mutants and sigmoidal kinetics of *Tc*DyPs toward RB19. W376 was

characterized as a major radical sink for the off-pathway electron transfer in the absence of dye substrates, resulting in the formation of protein crosslinks demonstrated by SDS-PAGE, SEC, and significantly slowed decay rates of compound I. Mutation of W376 is beneficial and improves enzyme catalytic efficiency. Sequence alignment revealed that Y332 is highly conserved across all four classes of DyPs. While Y332 was found to function as a surface-exposed protein radical site in *Tc*DyP under acidic conditions, it could not serve as a substrate oxidation site due to its extremely small solvent accessible area. Identification of surface-exposed protein radicals and substrate oxidation sites is important for modulating *Tc*DyP functions and efficiency for improved ligninolytic activity.

3.6 References

1. Singh, R.; Eltis, L. D., The multihued palette of dye-decolorizing peroxidases. *Arch Biochem Biophys* **2015,** *574*, 56-65.

2. Colpa, D. I.; Fraaije, M. W.; van Bloois, E., DyP-type peroxidases: a promising and versatile class of enzymes. *Journal of industrial microbiology & biotechnology* **2014,** *41* (1), 1-7.

3. Abdel-Hamid, A. M.; Solbiati, J. O.; Cann, I. K. O., Insights into Lignin Degradation and its Potential Industrial Applications. *Advances in Applied Microbiology, Vol 82* **2013,** *82*, 1-28.

4. Pollegioni, L.; Tonin, F.; Rosini, E., Lignin-degrading enzymes. *Febs Journal* **2015,** *282* (7), 1190-1213.

5. Mukherjee, A.; Mandal, T.; Ganguly, A.; Chatterjee, P. K., Lignin Degradation in the Production of Bioethanol - A Review. *Chembioeng Rev* **2016,** *3* (2), 86-96.

6. Rabemanolontsoa, H.; Saka, S., Various pretreatments of lignocellulosics. *Bioresource technology* **2016,** *199*, 83-91.

7. Bugg, T. D. H.; Rahmanpour, R., Enzymatic conversion of lignin into renewable chemicals. *Curr Opin Chem Biol* **2015,** *29*, 10-17.

8. Ahmad, M.; Roberts, J. N.; Hardiman, E. M.; Singh, R.; Eltis, L. D.; Bugg, T. D. H., Identification of DypB from Rhodococcus jostii RHA1 as a Lignin Peroxidase. *Biochemistry* **2011,** *50* (23), 5096-5107.

9. Brown, M. E.; Barros, T.; Chang, M. C. Y., Identification and Characterization of a Multifunctional Dye Peroxidase from a Lignin-Reactive Bacterium. *Acs Chem Biol* **2012,** *7* (12), 2074-2081.

10. Min, K.; Gong, G.; Woo, H. M.; Kim, Y.; Um, Y., A dye-decolorizing peroxidase from Bacillus subtilis exhibiting substrate-dependent optimum temperature for dyes and beta-ether lignin dimer. *Sci Rep-Uk* **2015,** *5*.

11. Chen, C.; Shrestha, R.; Jia, K.; Gao, P. F.; Geisbrecht, B. V.; Bossmann, S. H.; Shi, J. S.; Li, P., Characterization of Dye-decolorizing Peroxidase (DyP) from Thermomonospora curvata Reveals Unique Catalytic Properties of A-type DyPs. *J Biol Chem* **2015,** *290* (38), 23447-23463.

12. Koua, D.; Cerutti, L.; Falquet, L.; Sigrist, C. J. A.; Theiler, G.; Hulo, N.; Dunand, C., PeroxiBase: a database with new tools for peroxidase family classification. *Nucleic acids research* **2009,** *37*, D261-D266.

13. Yoshida, T.; Sugano, Y., A structural and functional perspective of DyP-type peroxidase family. *Arch Biochem Biophys* **2015,** *574*, 49-55.

14. Doyle, W. A.; Blodig, W.; Veitch, N. C.; Piontek, K.; Smith, A. T., Two substrate interaction sites in lignin peroxidase revealed by site-directed mutagenesis. *Biochemistry* **1998,** *37* (43), 15097-105.

15. Floudas, D.; Binder, M.; Riley, R.; Barry, K.; Blanchette, R. A.; Henrissat, B.; Martinez, A. T.; Otillar, R.; Spatafora, J. W.; Yadav, J. S.; Aerts, A.; Benoit, I.; Boyd, A.; Carlson, A.; Copeland, A.; Coutinho, P. M.; de Vries, R. P.; Ferreira, P.; Findley, K.; Foster, B.; Gaskell, J.; Glotzer, D.; Gorecki, P.; Heitman, J.; Hesse, C.; Hori, C.; Igarashi, K.; Jurgens, J. A.; Kallen, N.; Kersten, P.; Kohler, A.; Kues, U.; Kumar, T. K. A.; Kuo, A.; LaButti, K.; Larrondo, L. F.; Lindquist, E.; Ling, A.; Lombard, V.; Lucas, S.; Lundell, T.; Martin, R.; McLaughlin, D. J.; Morgenstern, I.; Morin, E.; Murat, C.; Nagy, L. G.; Nolan, M.; Ohm, R. A.; Patyshakuliyeva, A.; Rokas, A.; Ruiz-Duenas, F. J.; Sabat, G.; Salamov, A.; Samejima, M.; Schmutz, J.; Slot, J. C.; John, F. S.; Stenlid, J.; Sun, H.; Sun, S.; Syed, K.; Tsang, A.; Wiebenga, A.; Young, D.; Pisabarro, A.; Eastwood, D. C.; Martin, F.; Cullen, D.; Grigoriev, I. V.; Hibbett, D. S., The Paleozoic Origin of Enzymatic Lignin Decomposition Reconstructed from 31 Fungal Genomes. *Science* **2012,** *336* (6089), 1715-1719.

16. Perez-Boada, M.; Ruiz-Duenas, F. J.; Pogni, R.; Basosi, R.; Choinowski, T.; Martinez, M. J.; Piontek, K.; Martinez, A. T., Versatile peroxidase oxidation of high redox potential aromatic compounds: Site-directed mutagenesis, spectroscopic and crystallographic investigation of three long-range electron transfer pathways. *J Mol Biol* **2005,** *354* (2), 385-402.

17. Linde, D.; Pogni, R.; Canellas, M.; Lucas, F.; Guallar, V.; Baratto, M. C.; Sinicropi, A.; Saez-Jimenez, V.; Coscolin, C.; Romero, A.; Medrano, F. J.; Ruiz-Duenas, F. J.; Martinez, A. T., Catalytic surface radical in dye-decolorizing peroxidase: a computational, spectroscopic and site-directed mutagenesis study. *Biochem J* **2015,** *466*, 253-262.

18. Strittmatter, E.; Liers, C.; Ullrich, R.; Wachter, S.; Hofrichter, M.; Plattner, D. A.; Piontek, K., First Crystal Structure of a Fungal High-redox Potential Dye-decolorizing Peroxidase SUBSTRATE INTERACTION SITES AND LONG-RANGE ELECTRON TRANSFER. *J Biol Chem* **2013,** *288* (6), 4095-4102.

19. Strittmatter, E.; Serrer, K.; Liers, C.; Ullrich, R.; Hofrichter, M.; Piontek, K.; Schleicher, E.; Plattner, D. A., The toolbox of Auricularia auricula-judae dye-decolorizing peroxidase - Identification of three new potential substrate-interaction sites. *Arch Biochem Biophys* **2015,** *574*, 75-85.

20. Strittmatter, E.; Wachter, S.; Liers, C.; Ullrich, R.; Hofrichter, M.; Plattner, D. A.; Piontek, K., Radical formation on a conserved tyrosine residue is crucial for DyP activity. *Arch Biochem Biophys* **2013,** *537* (2), 161-167.

21. Sugano, Y.; Matsushima, Y.; Tsuchiya, K.; Aoki, H.; Hirai, M.; Shoda, M., Degradation pathway of an anthraquinone dye catalyzed by a unique peroxidase DyP from Thanatephorus cucumeris Dec 1. *Biodegradation* **2009,** *20* (3), 433-40.

22. Sugano, Y.; Muramatsu, R.; Ichiyanagi, A.; Sato, T.; Shoda, M., DyP, a unique dye-decolorizing peroxidase, represents a novel heme peroxidase family. *J Biol Chem* **2007,** *282* (50), 36652-36658.

23. van Bloois, E.; Pazmino, D. E. T.; Winter, R. T.; Fraaije, M. W., A robust and extracellular heme-containing peroxidase from Thermobifida fusca as prototype of a bacterial peroxidase superfamily. *Appl Microbiol Biot* **2010,** *86* (5), 1419-1430.

24. Smith, P. K.; Krohn, R. I.; Hermanson, G. T.; Mallia, A. K.; Gartner, F. H.; Provenzano, M. D.; Fujimoto, E. K.; Goeke, N. M.; Olson, B. J.; Klenk, D. C., Measurement of Protein Using Bicinchoninic Acid. *Anal Biochem* **1985,** *150* (1), 76-85.

25. Berry, E. A.; Trumpower, B. L., Simultaneous Determination of Hemes-a, Hemes-B, and Hemes-C from Pyridine Hemochrome Spectra. *Analytical Biochemistry* **1987,** *161* (1), 1-15.

26. Adams, P. D.; Afonine, P. V.; Bunkoczi, G.; Chen, V. B.; Davis, I. W.; Echols, N.; Headd, J. J.; Hung, L. W.; Kapral, G. J.; Grosse-Kunstleve, R. W.; McCoy, A. J.; Moriarty, N. W.; Oeffner, R.; Read, R. J.; Richardson, D. C.; Richardson, J. S.; Terwilliger, T. C.; Zwart, P. H., PHENIX: a comprehensive Python-based system for macromolecular structure solution. *Acta Crystallogr D* **2010,** *66*, 213-221.

27. Emsley, P.; Lohkamp, B.; Scott, W. G.; Cowtan, K., Features and development of Coot. *Acta Crystallogr D* **2010,** *66*, 486-501.

28. Poulos, T. L., Thirty years of heme peroxidase structural biology. *Arch Biochem Biophys* **2010,** *500* (1), 3-12.

29. Veitch, N. C., Horseradish peroxidase: a modern view of a classic enzyme. *Phytochemistry* **2004,** *65* (3), 249-259.

30. Poulos, T. L., Heme Enzyme Structure and Function. *Chemical reviews* **2014,** *114* (7), 3919-3962.

31. Sugano, Y., DyP-type peroxidases comprise a novel heme peroxidase family. *Cell Mol Life Sci* **2009,** *66* (8), 1387-1403.

32. Bonini, M. G.; Consolaro, M. E. L.; Hart, P. C.; Mao, M.; de Abreu, A. L. P.; Master, A. M., Redox control of enzymatic functions: The electronics of life's circuitry. *Iubmb Life* **2014,** *66* (3), 167-181.

33. Warren, J. J.; Ener, M. E.; Vlcek, A.; Winkler, J. R.; Gray, H. B., Electron hopping through proteins. *Coordin Chem Rev* **2012,** *256* (21-22), 2478-2487.

34. Raven, E. L.; Mauk, A. G., Chemical reactivity of the active site of myoglobin. *Adv Inorg Chem* **2001,** *51*, 1-49.

35. Pfister, T. D.; Gengenbach, A. J.; Syn, S.; Lu, Y., The role of redox-active amino acids on compound I stability, substrate oxidation, and protein cross-linking in yeast cytochrome c peroxidase. *Biochemistry* **2001,** *40* (49), 14942-14951.

36. Linde, D.; Ruiz-Duenas, F. J.; Fernandez-Fueyo, E.; Guallar, V.; Hammel, K. E.; Pogni, R.; Martinez, A. T., Basidiomycete DyPs: Genomic diversity, structural-functional aspects, reaction mechanism and environmental significance. *Arch Biochem Biophys* **2015,** *574*, 66-74.

37. Houseman, A. L. P.; Doan, P. E.; Goodin, D. B.; Hoffman, B. M., Comprehensive Explanation of the Anomalous Epr-Spectra of Wild-Type and Mutant Cytochrome-C Peroxidase Compound-Es. *Biochemistry* **1993,** *32* (16), 4430-4443.

38. Huyett, J. E.; Doan, P. E.; Gurbiel, R.; Houseman, A. L. P.; Sivaraja, M.; Goodin, D. B.; Hoffman, B. M., Compound Es of Cytochrome-C Peroxidase Contains a Trp Pi-Cation Radical - Characterization by Cw and Pulsed Q-Band Endor Spectroscopy. *Journal of the American Chemical Society* **1995,** *117* (35), 9033-9041.

39. Ivancich, A.; Jakopitsch, C.; Auer, M.; Un, S.; Obinger, C., Protein-based radicals in the catalase-peroxidase of Synechocystis PCC6803: A multifrequency EPR investigation of wild-type and variants on the environment of the heme active site. *Journal of the American Chemical Society* **2003,** *125* (46), 14093-14102.

40. Ivancich, A.; Mazza, G.; Desbois, A., Comparative electron paramagnetic resonance study of radical intermediates in turnip peroxidase isozymes. *Biochemistry* **2001,** *40* (23), 6860-6866.

41. Patterson, W. R.; Poulos, T. L.; Goodin, D. B., Identification of a Porphyrin Pi-Cation-Radical in Ascorbate Peroxidase Compound-I. *Biochemistry* **1995,** *34* (13), 4342-4345.

42. Benecky, M. J.; Frew, J. E.; Scowen, N.; Jones, P.; Hoffman, B. M., Epr and Endor Detection of Compound-I from Micrococcus-Lysodeikticus Catalase. *Biochemistry* **1993,** *32* (44), 11929-11933.

43. Singh, R.; Switala, J.; Loewen, P. C.; Ivancich, A., Two [Fe(IV)=O Trp(center dot)] intermediates in M-tuberculosis catalase-peroxidase discriminated by multifrequency (9-285 GHz) EPR spectroscopy: Reactivity toward isoniazid. *Journal of the American Chemical Society* **2007,** *129* (51), 15954-15963.

44. Rice, R. H.; Lee, Y. M.; Brown, W. D., Interactions of Heme-Proteins with Hydrogen-Peroxide - Protein Crosslinking and Covalent Binding of Benzo[a]Pyrene and 17-Beta-Estradiol. *Arch Biochem Biophys* **1983,** *221* (2), 417-427.

45. Tew, D.; Demontellano, P. R. O., The Myoglobin Protein Radical - Coupling of Tyr-103 to Tyr-151 in the H2o2-Mediated Cross-Linking of Sperm Whale Myoglobin. *J Biol Chem* **1988,** *263* (33), 17880-17886.

46. Uchida, T.; Sasaki, M.; Tanaka, Y.; Ishimorit, K., A Dye-Decolorizing Peroxidase from Vibrio cholerae. *Biochemistry* **2015,** *54* (43), 6610-6621.

47. Ilgenfri.G; Schuster, T. M., Kinetics of Oxygen Binding to Human Hemoglobin - Temperature Jump Relaxation Studies. *J Biol Chem* **1974,** *249* (9), 2959-2973.

Chapter 4 - Mechanistic insights into dye-decolorizing peroxidase revealed by solvent isotope and viscosity effects[4]

4.1 Abstract

Dye-decolorizing peroxidases (DyPs) are a family of H_2O_2-dependent heme peroxidases, which have shown potential applications in lignin degradation and valorization. However, the DyP kinetic mechanism remains underexplored. Using structural biology and solvent isotope (sKIE) and viscosity effects, many mechanistic characteristics have been uncovered for the B-class *El*DyP from *Enterobacter lignolyticus*. Its structure revealed that a water molecule acts as the sixth axial ligand with two channels at diameters of ~3.0 and 8.0 Å leading to the heme center. A conformational change of ERS* to ERS, which have identical spectral characteristics, was proposed as the final step in DyPs' bisubstrate Ping-Pong mechanism. This step is also the rate-determining step in ABTS oxidation. The normal KIE of wild-type *El*DyP with D_2O_2 at pH 3.5 suggested that cmpd 0 deprotonation by the distal aspartate is rate-limiting in the formation of cmpd I, which is more reactive under acidic pH than under neutral or alkaline pH. The viscosity effects and other biochemical methods implied that the reducing substrate binds with cmpd I instead of the free enzyme. The significant inverse sKIEs of k_{cat}/K_M and k_{ERS*} suggested that the aquo release in DyPs is mechanistically important and may explain the enzyme's adoption of two-electron reduction for cmpd I. The distal aspartate is catalytically more important than the distal arginine and plays key roles in determining DyPs' acidic pH optimum.

[4] Reprinted with permission from Shrestha, R.; Huang, G.; Meekins, D. A.; Geisbrecht, B. V.; Li, P., Mechanistic Insights into Dye-Decolorizing Peroxidase Revealed by Solvent Isotope and Viscosity Effects. *ACS Catalysis* **2017**, 6352-6364. Copyright 2017, American Chemical Society.

The kinetic mechanism of D143H-*El*DyP was also briefly studied. The results obtained will pave the way for future protein engineering to improve DyPs' lignolytic activity.

4.2 Introduction

Dye-decolorizing peroxidases (DyPs) are a new family of heme peroxidases, which use H_2O_2 to catalyze oxidation of various dye substrates, specifically anthraquinone-derived dyes that have high redox potentials.[1-3] DyPs have recently received significant attention due to their potential applications in lignin degradation and valorization.[4-7] Lignin is a complex aromatic polymer that represents the second most abundant renewable carbon source on Earth after cellulose, constituting around 30% non-fossil organic carbon.[8] However, lignin valorization is challenging because it is recalcitrant to degradation.[9-11] More than 60% of lignin is wasted by combustion due to lack of methods to convert it into valuable end products.[12-14] Additionally, lignin degradation represents major hindrance for the competitiveness of biofuels *vs.* fossil-based gasoline.[15]

While class II plant peroxidases such as lignin peroxidase (LiP), manganese peroxidase (MnP), and versatile peroxidase (VP) can break down lignin efficiently,[16-17] they have not been used for industrial applications due to their fungal origins, which create challenges in genetic manipulation and large-scale protein production. Thus, the field is currently undergoing a paradigm shift to pursue lignin biodegradation using bacterial enzymes,[4, 18] among which DyPs are promising candidates. Several DyPs have been reported to show activities toward lignin model compounds and wheat straw lignocellulose,[19-23] albeit with low efficiency. Therefore, DyPs are considered as a potential functional equivalent of fungal LiP in bacteria.

The characteristics of DyPs, including primary sequence, tertiary structure, catalytic residues, substrate specificity, and pH optimum, differ significantly from those well-known heme

peroxidases such as class II plant peroxidases and horseradish peroxidase (HRP).[3, 24] In particular, DyP employs a distal aspartate, in place of the distal histidine used by other heme peroxidases, as a catalytic residue. This aspartate is also proposed to be responsible for the acidic optimum of DyP activity.[25] While it has been suggested that DyPs follow a similar mechanism as the class II plant peroxidases and HRP,[19, 21] their mechanistic details remain underexplored. This has severely limited our ability to engineer them in order to improve their lignolytic activity.

In this work, we have selected B-class *El*DyP from *Enterobacter lignolyticus* as a model to study the DyP molecular mechanism. Selection of *El*DyP is based on the fact that the host microbe is capable of growing anaerobically using lignin as the sole carbon source.[26] Also, the B-class DyPs appear to have the highest activity towards lignin and its non-phenolic model compounds among bacterial DyPs.[19, 22] Consequently, the *El*DyP may be directly involved in lignin degradation by *E. lignolyticus*. Additionally, while it is still in dispute,[27] the *Escherichia coli* YfeX, which has 93% sequence identity with *El*DyP, was proposed to be the first heme deferrochelatase.[28] Detailed mechanistic insights may facilitate to unraveling the true biological functions of DyPs. Here, we used solvent kinetic isotope effects (sKIEs) and viscosity effects determined under steady-state and transient-state conditions, together with structural biology, to dissect the reactions catalyzed by DyPs and to examine the individual roles of catalytic residues. This study provides the insights into the DyP mechanism and paves the way for the efforts in protein engineering.

4.3 Materials and methods

4.3.1 Instruments, biochemicals, and chemicals

All activity assays and steady-state kinetics were performed on a Cary 100 Bio UV-Vis spectrometer equipped with a temperature controller and magnetic stirring. Transient-state

kinetics was carried out on an Applied Photophysics SX20 stopped-flow spectrometer equipped with sequential mixing, a PDA detector, and a monochromator. All chemical and biochemical reagents were purchased at the highest grade and used without further purification. Protein concentrations were determined by bicinchoninic acid assays (BCA).[29] Stocks of H_2O_2 and ascorbate were prepared fresh before experiments. Concentrations of H_2O_2 were determined at 240 nm using ε_{240} = 43.6 $M^{-1}cm^{-1}$. Buffers of pH 2.0−6.5, 7.0−8.0, 8.5−9.0, and 9.5−11.5 were prepared using sodium citrate, potassium phosphate, Tris-HCl, and 3-(cyclohexylamino)-1-propanesulfonic acid (CAPS), respectively. All kinetic measurements were performed in triplicate and data were processed by OriginPro 2015.

4.3.2 Cloning, expression, and purification of *El*DyP and its mutants

The gene corresponding to *El*DyP was synthesized by GenScript and inserted into pET28-MHL (Addgene plasmid #26096) using restriction sites Nde*I* and Hind*III* to generate *pEl*DyP, which contains a His_6 tag and tobacco etch virus (TEV) cleavage site at the N-terminus. Active-site mutants of *El*DyP were generated using QuickChange from Agilent Technologies according to manufacturer's instructions. DNA sequences of the synthesized wild-type (*wt*) *El*DyP and mutant primers are summarized in Table A.4 (Appendix A).

Proteins of *wt* and mutant *El*DyPs were overexpressed in *Escherichia coli* BL21(DE3) cells (Lucigen). A 90-ml starter culture was grown overnight from a single colony in LB media in the presence of 50 μg/ml of kanamycin at 37 °C with shaking at 225 rpm and then used to inoculate 4.5 liters of LB medium. When the A_{600} reached 0.6, isopropyl-1-thio-β-D-galactopyranoside (IPTG) and hemin chloride were added to a final concentration of 0.2 mM and 30 μg/ml respectively. The cells were grown at 30 °C for an additional 15 h and then harvested

by centrifugation at 5,000×g for 20 min at 4 °C. The cell pellets were collected and stored at −80 °C until further use.

All of the following steps were carried out at 4 °C. Purification buffers consisted of buffer A (400 mM NaCl and 50 mM potassium phosphate, pH 7.8) and increasing concentrations of imidazole. Buffers B (lysis), C (wash), and D (elution) contained 10, 30, and 250 mM imidazole, respectively. The cell pellets were re-suspended in buffer B and lysed by sonication (25×30-s pulsed cycle). The cell debris was removed by centrifugation at 15,000×g for 45 min and the supernatant was incubated with 10 mL Ni-NTA resin that had been pre-equilibrated with buffer B for 1h. The resin was washed with 10 column volumes of buffer C and then eluted with buffer D. Fractions containing the DyP were collected, concentrated to ~70 mg/mL, and exchanged into buffer E (100 mM NaCl and 50 mM potassium phosphate, pH 7.8) using Amicon Ultra-15 filters (10K, EMD Millipore). The purified protein was stored in aliquots at −80 °C until further use. Protein purity was assessed by 12% acrylamide SDS-PAGE and protein concentration was determined by BCA using a BSA calibration curve. The Reinheitszahl values (R_z) of purified proteins were measured at 2.0−2.3. Their heme stoichiometric ratios were determined to be 1.1−1.3 using pyridine hemochromogen assays and $\Delta\varepsilon_{557-541}$ = 20.7 $mM^{-1}cm^{-1}$.[30]

The protein for crystallization was purified in the following way. Ten mg *wt-El*DyP were treated with 40 μg subtilisin A at 37 °C for 1 h before diisopropyl fluorophosphate was added to a final concentration of 100 μM to stop proteolysis. The protein was then exchanged into buffer B using a 10K Amicon Ultra-15 centrifugal filter and subsequently incubated with Ni-NTA resin for an additional hour. The flow-through fractions, which contained *El*DyP lacking a His_6-tag, were collected, concentrated, and subjected to size-exclusion chromatography (SEC) using a

HiLoad 26/600 Superdex 200 pg column (GE Healthcare) equilibrated with 150 mM NaCl in 50 mM potassium phosphate, pH 7.5. Fractions corresponding to dimeric *El*DyP were pooled, and buffer exchanged into 60 mM NaCl, 20 mM Tris-HCl, pH 7.9, before crystallization.

4.3.3 Crystallization and structure determination

Crystals were grown by the sitting drop vapor diffusion method in a crystallization solution consisting of 100 mM HEPES (pH 7.3) and 26% (w/v) PEG3350. Crystals of *wt-El*DyP (5.5 mg/ml) were grown at 16 ˚C. They began to appear after 48 h and matured after 72 h. Individual crystals were transferred to a buffer containing the crystallization solution with 10% glycerol (v/v) as a cryoprotectant before flash-cooling in liquid nitrogen. Diffraction data were collected at 100 K using beamline 22-BM of the Advanced Photon Source, Argonne National Laboratory, at a wavelength of 1.0 Å and processed with the HKL2000 package. The structure was solved by molecular replacement using a PHENIX software suite with coordinates of PDB entry 5DE0 as a starting model.[31] The final structure was obtained by iterative automated model building and refinement using PHENIX and interactive model modification in Coot.[32] Figures were prepared using PyMol (Schrödinger, LLC). The final coordinates have been deposited in the RCSB under accession ID 5VJ0.

4.3.4 Spectroelectrochemical determination of redox potential

In a 3.5-ml cuvette, a 3.0-ml solution consisting of 50mM potassium phosphate (pH 7.0), 100mM NaCl, and a mixture of redox mediators (10 μM each for methyl viologen, anthraquinone-2-sulfonic acid, anthraquinone-2,6-disulfonic acid, 2-hydroxy-1,4-naphthoquinone, 2,5-dihydroxy-1,4-benzoquinone, duroquinone, 1,2-naphthoquinone, and ferricyanide; 3μM each for Safferin and Neutral Red) was purged with water-saturated argon for 1 h. The electrodes (Ag/AgCl, 012167; Pt gauze, 011498; ALS Co, Japan) were connected to a

potentiostat. The *wt-El*DyP was added to a final concentration of 10μM. The entire mixture was completely reduced to ferrous state with ~5 μl of 100 mM freshly prepared sodium dithionite stock solution. This was then oxidized by stepwise addition of 2–5μl aliquots of argon-purged 2.5 mM $K_3Fe(CN)_6$. The reaction mixture was kept under water-saturated argon protection during the whole experiment. After each addition, the reaction was allowed to equilibrate with stirring until the difference in potential readings was less than 1 mV/min. Once the equilibrium was established, the UV-visible spectrum was recorded. The fraction of reduced *El*DyP was calculated by the $\Delta A_{434\ nm}$ and the midpoint reduction potential ($E°'$) was determined by fitting the data into the following Nernst Eq. 1,

$$f = \frac{1}{1 + exp\frac{n \times (E^o - E^{o'})}{25.6}} \qquad (Eq. 1)$$

Where, *f* is the fraction reduced, *n* is the number of electrons, *E*° is the potential at each point in mV, and *E*°' is the midpoint reduction potential in mV. The determined potential is with respect to a SHE. The experiment was performed again in D_2O. All reagents were prepared in 99.9% D_2O (Cambridge Isotope Laboratories).

4.3.5 Enzyme assays

Enzyme activities against various substrates were determined using a continuous assay by monitoring the absorbance change at a certain wavelength at 25 °C. Briefly, in a 480 μL solution consisting of 50 mM sodium citrate (pH 3.5), 10 mM H_2O_2, reducing substrate, and 0.02 mg/mL bovine serum albumin (BSA), the purified *wt* or mutant *El*DyP was added to initiate the reaction. Controls were performed in the absence of enzyme, H_2O_2, or both. The tested reducing substrates and their concentrations, *wt* enzyme concentrations, wavelengths monitored, and the corresponding extinction coefficients were summarized in Table 4.1.

To determine optimal pH, the assays were carried out with 2,2'-azino-bis(3-ethylbenzothiazoline-6-sulphonic acid) (ABTS) and Reactive Blue 19 (RB19) as described above in the pH range of 2.0-8.0 at 25 °C. To determine optimal temperature, the assays were performed in a similar way with ABTS at pH 3.5 at temperatures ranging from 10-60 °C.

4.3.6 Steady-state kinetics

To determine steady-state kinetic parameters (k_{cat} and K_M) of the *wt* and mutant *El*DyPs, reactions were performed in the same way as described above except that the concentration of one substrate was varied in the presence of the other substrate at saturation. The data obtained were fitted into either Michaelis-Menten Eq. 2 or Hill Eq. 3.

$$v = \frac{v_{max}[S]}{K_M + [S]} \qquad (Eq. 2)$$

$$v = \frac{v_{max}[S]^h}{K_M + [S]^h} \qquad (Eq. 3)$$

4.3.7 Transient-state kinetics

Stopped-flow experiments were performed at 25 °C at pH 2.0−11.5 and investigated at both defined (monochromator) and multiple (PDA) wavelengths. The PDA data were analyzed using singular value decomposition with the Pro-KIV Global Analysis program provided by Applied PhotoPhysics to obtain the number of reaction intermediates and their corresponding spectra. Reactions were then monitored at selected single wavelengths to follow the formation and decay of intermediates. Data were fitted to single exponential expressions to obtain pseudo-first-order rate constants (k_{obs}). Second-order rate constants were calculated from plots of k_{obs} *vs.* substrate concentrations.

All concentrations mentioned here were concentrations after mixing. Formation of compound (cmpd) I was carried out in a conventional mixing mode with 2.5 μM enzyme in 5

mM phosphate buffer (pH 7.8) containing 10 mM NaCl and equal volume of H_2O_2 in 50 mM buffer (pH 2.0−11.5) at various concentrations. Formation of cmpd I was monitored at wavelengths corresponding to Soret and Q bands. Regeneration of *wt* enzyme resting state (ERS^*) from cmpd I was performed in a sequential mixing mode, in which 2.5 μM *wt* enzyme in 5 mM phosphate buffer (pH 7.8) containing 10 mM NaCl was premixed with equal volume of 2.5 μM H_2O_2 in 50 mM citrate buffer (pH 3.5). After a 2s-delay to reach maximal formation of compound I, ABTS in 50 mM buffer (pH 2.0−11.5) was mixed with cmpd I in the presence of ascorbate at concentrations of 10, 50, and 75 μM for 0.1−1.0, 1.5−5.0, and 7.5 μM ABTS, respectively. Regeneration of ERS^* was monitored at 406 nm corresponding to the Soret band of *wt-El*DyP.

4.3.8 Solvent kinetic isotope effect (sKIE)

Experiments of steady-state and transient-state kinetics described above were performed again in deuterated buffers, which were prepared in 99.9% D_2O (Cambridge Isotope Laboratories). The pD (pH in D_2O) was adjusted based on the following relationship: $pD = pH_{obs} + 0.38$. Reducing substrates and H_2O_2 were directly dissolved in D_2O buffers. Enzymes were highly concentrated (≥ 60 mg/mL) to ensure minimal protium contribution to deuterated buffers and were equilibrated in D_2O buffer before analysis.

4.3.9 Viscosity effect

Experiments of steady-state and transient-state kinetics described above were performed at pH 3.5 with *wt-El*DyP in sucrose at various concentrations. For stopped-flow experiments, all reagents, including the enzyme, were prepared in a matching sucrose solution.

4.4 Results

4.4.1 Protein purification and characterization

Proteins of *wt* and mutant *El*DyPs were purified with an *N*-His_6 tag and a tobacco etch virus (TEV) protease cleavage site. Mutant H215A is not included in this report because the *holo*-enzyme could not be obtained. This is not surprising, as mutation of the axial ligand in heme proteins (H215 in *El*DyP) has been known to result in the failure of heme incorporation.[33-34] SDS-PAGE (Fig. E.2-A in Appendix E) reveals that the molecular weight (MW) of *El*DyP is 35 kDa, which is consistent with the calculated value. Since the presence of the His_6 tag did not interfere with enzyme activity, it was not removed prior to further biochemical studies. Size-exclusion chromatography (SEC) of *wt*-*El*DyP (Fig. 4.1A) shows that the enzyme mainly exists as a dimer in its native state, which is consistent with the result from its crystal structure. Spectroelectrochemical titrations of *wt*-*El*DyP (Fig. 4.1B) at pH 7.0 gave a Fe^{3+}/Fe^{2+} midpoint reduction potential ($E°'$) of −290 ± 0.96 mV vs NHE with Nernstian behavior (n = 1.13 ± 0.05). When the measurement was carried out in D_2O at pD 7.0, the $E°'$ shifted more positively to −263 ± 0.70 mV (n = 0.95 ± 0.02). As shown in Fig. 4.1C and Table D.8 (Appendix D), the UV-Vis spectrum of *wt*-*El*DyP displays Soret (406 nm), Q- (507 and 539 nm), and charge-transfer (635 nm) bands, corresponding to the presence of a heme cofactor. The mutants have the same absorbance maxima as the *wt* except that D143H contains an extra Q-band at 567 nm, suggesting that the heme environment has changed significantly in D143H. The pH dependence of enzyme activity (Fig. 4.1D) demonstrates that the *wt* and mutant *El*DyPs display the highest activities toward ABTS at pH 3.5 and 4.0, respectively. The same pattern was also observed with RB19 (data not shown). It has to be noted that the mutations, especially replacement of D143 with H143, did not result in significant shifts of pH optimum. The temperature-rate profile (Fig. E.2-

B in Appendix E) shows that the highest activity of *wt*-*El*DyP toward ABTS was achieved at 30 °C, while 93% *wt* activity was observed at 25 °C. Thus, for the sake of simplicity, further studies were carried out at 25 °C (r.t.).

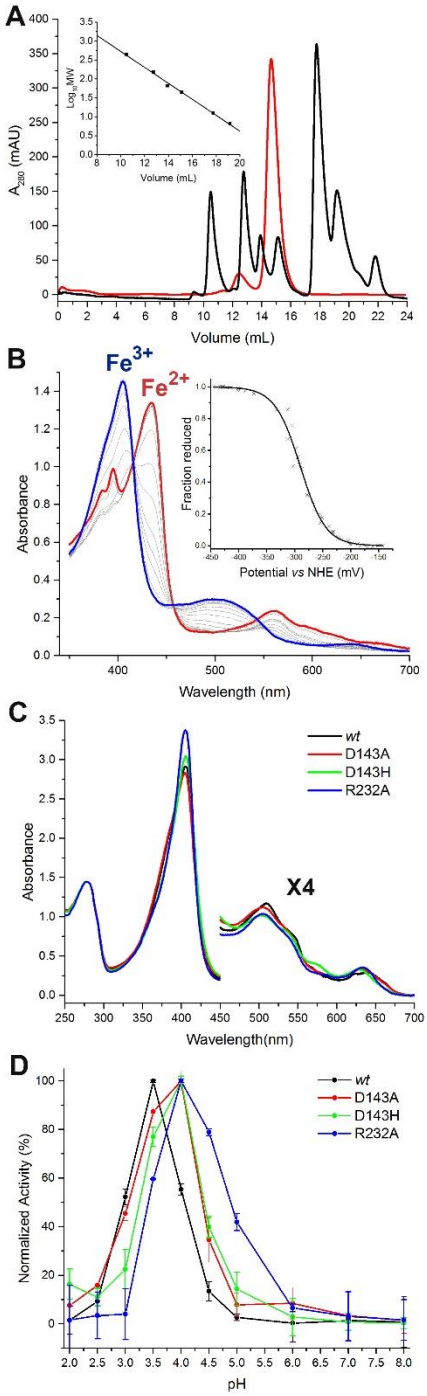

Figure 4.1 Biochemical characterization of *El*DyP.

(A) SEC chromatography of *wt-El*DyP (red) and molecular weight standards (black) loaded onto a GE Superdex 200 Increase 10/300 GL column eluted with 50 mM potassium phosphate buffer (pH 7.5) containing 150 mM NaCl. The inset represents a MW calibration curve. (B) Changes in the UV-Vis absorption spectrum showing stepwise oxidation of Fe^{2+}−*wt-El*DyP (red) to Fe^{3+}−*wt-El*DyP (blue). The inset represents three individual spectroelectrochemical titrations of *wt-El*DyP monitored by $\Delta A_{434\ nm}$. (C) Normalized UV-Vis absorption spectra of *wt* and mutant *El*DyPs with 450-700 nm region magnified by 4 times. (D) pH-activity profiles of *wt* and mutant *El*DyPs with ABTS.

4.4.2 Protein structure and access channels to heme active site

The crystal structure of *wt-El*DyP was solved by molecular replacement using the *Vc*DyP from *Vibrio cholerae* (PDB entry 5DE0) as a search model and refined to 1.93 Å limiting resolution. Data collection and refinement statistics are given in Table B.7 (Appendix B). The final model consists of four copies of the *El*DyP monomer, each with a heme bound in its active site. The monomers assemble into symmetric dimers composed of chains A and B, and chains C and D, as judged by buried surface area found at the dimerization interfaces. The *El*DyP monomer represented by chain B was used for all structural analyses described in this manuscript. As shown in Fig. 4.2A, the *El*DyP displays a ferredoxin-like fold consisting of four-strand, antiparallel β-sheet and peripheral α-helices. The overall structure is similar to B-class DyPB from *Rhodococcus jostii* RHA1, *Vc*DyP, and YfeX,[35-37] but is quite different from the structures of class II plant peroxidases, which contain mainly α-helices.[38-40] The heme active site shows that H215 acts as a proximal ligand. The distal site is occupied by D143, R232 and H_2O288. The H_2O288 acts as a sixth ligand to heme iron and forms hydrogen bonds with both D143 and R232. During enzyme oxidation, H_2O_2 is expected to displace this H_2O288 and initiates the oxidation reaction. R232 also forms a hydrogen bond with the heme 5-propionate group, which should contribute to the noteworthy pK_a shift of arginine as described below. Compared with the active site of LiP from *Phanerochaete chrysosporium* (PDB 1B82),[38] a

typical distal histidine in class II plant peroxidases (H47 in LiP) and HRP is replaced with a distal aspartate (D143 in *El*DyP) that is absolutely conserved across all four classes of DyPs.

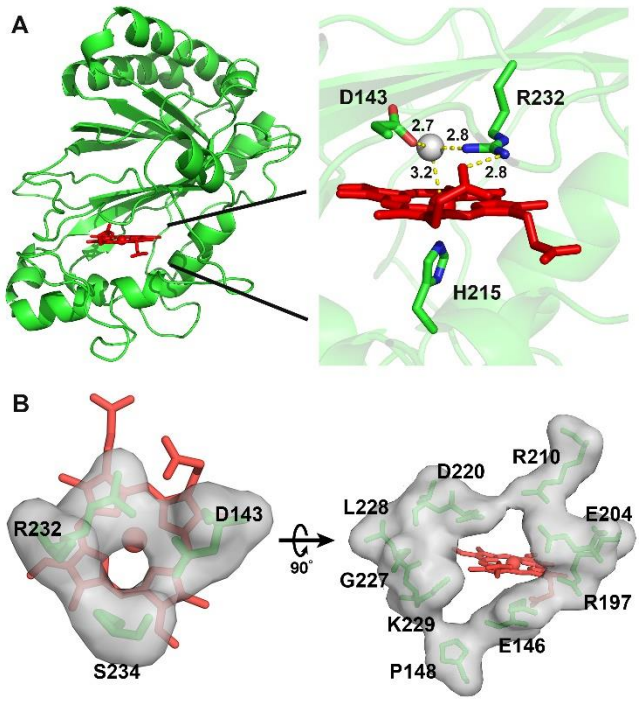

Figure 4.2 Crystal structure of *wt-El*DyP.

(A) Overall structure (left) and active site of the enzyme. Catalytic residues, heme, and water 288 are represented in green sticks, red sticks, and a grey ball, respectively. Distances in angstrom are labeled and shown in yellow dashed lines. (B) Surface representations of the small (left, diameter of ~3.0 Å) and large (right, diameter of ~8.0 Å) heme access channels.

Examination of the *El*DyP structure revealed two heme access channels. The first of these has a diameter of ~3.0 Å and points to the distal side of the heme (left panel in Fig. 4.2B). This channel is proposed to be the entrance of H_2O_2 and also exists in DyPB and *Vc*DyP.[35-36] The second heme access channel has a diameter of ~8.0 Å and leads to the heme 6-propionate group (right panel in Fig. 4.2B), which is larger than the corresponding channels in DyPB (~6.0 Å) and *Vc*DyP (~7.5 Å).[35-36] It has been reported that the propionate group can provide a direct electron transfer path from the porphyrin radical to a bound substrate.[41] Charged residues in *El*DyP are

mainly present in and around these two channels. Other areas are mostly occupied by hydrophobic and polar residues, which may facilitate surface interaction with dyes and lignin, both of which are rich in aromatic moieties.

Table 4.1 Activities of *wt-El*DyP toward various substrates

Substrate	λ (nm)	ε ($cm^{-1}mM^{-1}$)	[S] (mM)	[E] (nM)	SA* (U/mg)
ABTS	420	36.0	5	1	5560± 60
RB19	595	10.0	0.1	50	257 ± 7
RB4	610	4.20	0.1	50	218 ± 4
RB5	600	8.00	0.1	50	136 ± 3
RBlk5	598	30.0	0.1	50	22.9 ±0.5
Pyrogallol	430	2.47	400	1000	46.3 ± 0.6
HQ	247	21.0	5	200	38.0 ± 1.0
Guaiacol	465	26.6	10	1000	0.34 ± 0.01
VA	340	93.0	10	1000	ND*
Mn^{2+}	270	11.6	20	1000	2.08 ± 0.08

*SA: Specific Activity; ND: Not Detected.

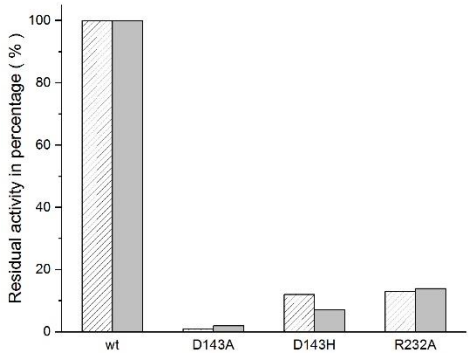

Figure 4.3 Activity percentages of *wt* and mutant *El*DyPs toward ABTS (sparse bar) and RB19 (solid bar).

4.4.3 Enzyme activities

The *wt-El*DyP is active toward a wide range of substrates summarized in Table 4.1. While ABTS and anthraquinone dyes such as reactive blue (RB) could be easily oxidized by

*El*DyP, low activities were observed with Reactive Black 5 (RBlk5) and small-size molecules like pyrogallol, hydroquinone (HQ), and guaiacol. No activity was detected with veratryl alcohol (VA). Similar to B-class DyPB and C-class DyP2,[20, 35] *El*DyP was also found to have low MnP activity. Such activity is thought to be important for microbial lignin degradation due to high Mn content of wood that facilitates formation of Mn^{3+} oxidant.[42]

To determine the catalytic importance of the distal aspartate and arginine, the corresponding mutants were studied with ABTS and RB19. As shown in Fig. 4.3, mutation of either residue is deleterious, resulting in significant loss of enzyme activity. D143A only retained <2% *wt* activity toward both tested substrates. D143H displayed 11% and 12% *wt* activities toward ABTS and RB19, respectively. The higher activity observed with D143H is attributed to the introduction of the distal histidine, which is present in class II plant peroxidases and HRP. R232A retained ~14% *wt* activity, which is much higher than the activity of D143A, suggesting that the distal aspartate may be catalytically more important than the distal arginine. That said, both residues are required for substrate oxidation.

Table 4.2 Steady-state kinetic parameters and sKIE[a]

Substrate	Solvent		wt	D143A	D143H	R232A
ABTS (H_2O_2)	H_2O	k_{cat} (s^{-1})	$(3.54 \pm 0.01)\times10^3$ [$(3.73 \pm 0.02)\times10^3$]	$(3.45 \pm 0.02)\times10$ [$(4.62 \pm 0.01)\times10$]	$(4.37 \pm 0.05)\times10^2$ [$(4.16 \pm 0.08\times10^2$]	$(4.87 \pm 0.06)\times10^2$ [$(5.25 \pm 0.02)\times10^2$]
		K_M (μM)	$(6.07 \pm 0.01)\times10^2$ [$(2.02 \pm 0.04)\times10^3$]	$(4.80 \pm 0.20)\times10^2$ [$(7.50 \pm 0.20)\times10^4$]	$(2.50 \pm 0.05)\times10^3$ [$(4.90 \pm 0.30)\times10^3$]	$(1.30 \pm 0.02)\times10^3$ [$(1.35 \pm 0.02)\times10^4$]
		k_{cat}/K_M ($s^{-1}.M^{-1}$)	$(5.80 \pm 0.10)\times10^6$ [$(1.85 \pm 0.03)\times10^6$]	$(7.20 \pm 0.30)\times10^4$ [$(6.10 \pm 0.10)\times10^2$]	$(1.75 \pm 0.02)\times10^5$ [$(8.40 \pm 0.40)\times10^4$]	$(3.76 \pm 0.03)\times10^5$ [$(3.90 \pm 0.10)\times10^4$]
	D_2O	k_{cat} (s^{-1})	$(5.10 \pm 0.20)\times10^3$		$(3.92 \pm 0.08)\times10^2$	
		K_M (μM)	$(1.00 \pm 0.10)\times10^2$		$(2.95 \pm 0.05)\times10^2$	
		k_{cat}/K_M ($s^{-1}.M^{-1}$)	$(5.10 \pm 0.20)\times10^7$		$(1.33 \pm 0.05)\times10^6$	
	sKIE	$^D(k_{cat})$	0.69 ± 0.02		1.11 ± 0.04	
		$^D(k_{cat}/K_M)$	0.11 ± 0.01		0.13 ± 0.01	
RB19 (H_2O_2)	H_2O	k_{cat} (s^{-1})	$(1.67 \pm 0.08)\times10^2$ [$(1.69 \pm 0.01)\times10^2$]	$(2.92 \pm 0.03)\times10^0$ [$(3.80 \pm 0.20)\times10^0$]	$(1.22 \pm 0.02)\times10$ [$(1.77 \pm 0.04)\times10$]	$(2.30 \pm 0.05)\times10$ [$(3.10 \pm 0.10)\times10$]
		K_M (μM)	$(3.90 \pm 0.30)\times10$ [$(3.70 \pm 0.10)\times10^2$]	$(3.93 \pm 0.05)\times10$ [$(1.60 \pm 0.20)\times10^4$]	$(7.70 \pm 0.20)\times10$ [$(5.70 \pm 0.40)\times10^2$]	$(4.60 \pm 0.20)\times10$ [$(2.20 \pm 0.20)\times10^3$]
		k_{cat}/K_M ($s^{-1}.M^{-1}$)	$(4.20 \pm 0.10)\times10^6$ [$(4.60 \pm 0.10)\times10^5$]	$(7.40 \pm 0.10)\times10^4$ [$(2.40 \pm 0.20)\times10^2$]	$(1.60 \pm 0.30)\times10^5$ [$(3.10 \pm 0.40)\times10^4$]	$(5.00 \pm 0.30)\times10^5$ [$(1.40 \pm 0.20)\times10^4$]

[a]Values shown in square brackets are parameters for H_2O_2.

4.4.4 sKIE on steady-state kinetics

To characterize *wt* and mutant *El*DyPs, their kinetic parameters were determined with ABTS, RB19, and H_2O_2. As summarized in Table 4.2, the turnover numbers (k_{cat}) of *wt*-*El*DyP with the two reducing substrates are among the fastest DyP-catalyzed reactions reported so far.[20-21, 35-36, 43] Moreover, the *wt* enzyme displayed 3- to 9-fold higher affinity (K_M) with the reducing substrate than with H_2O_2. While mutations of distal residues significantly decrease the turnover numbers, the values for D143H and R232A are still comparable with other *wt* DyPs,[35-36] suggesting that *El*DyP is a good target to study DyP mechanisms. The affinities of the mutants with reducing substrates and H_2O_2 are weakened except for D143A, in which the K_M values with ABTS and RB19 are similar to those of the *wt* enzyme.

The effect of D_2O on kinetics provides insights into the role of transfer of exchangeable protons during the reaction, thus revealing important mechanistic details. Since RB19 displayed a significant inhibitory effect in D_2O, determination of steady-state kinetic parameters in D_2O was carried out only with ABTS. As shown in Table 4.2, inverse sKIEs were observed with ABTS for both the turnover number [$^{D}(k_{cat}) = {}^{H2O}(k_{cat})/ {}^{D2O}(k_{cat})$] and catalytic efficiency [$^{D}(k_{cat}/K_M) = {}^{H2O}(k_{cat}/K_M)/{}^{D2O}(k_{cat}/K_M)$]. Their mechanistic implications will be discussed below in detail.

4.4.5 Transient-state kinetics of cmpd I formation

Formation of cmpd I between *El*DyPs and H_2O_2 was investigated using stopped-flow spectroscopy. Representative spectra at acidic and alkaline pH values are shown in Fig. 4.4A-D. The absorbance maxima are summarized in Table D.8 (Appendix D). While both *wt*- and R232A-*El*DyP displayed similar spectral transition characters under both acidic and alkaline pH values (Fig. 4.4A and 4.4D), the aspartate mutants gave vastly different transitional spectra under the same conditions (Fig. 4.4B and 4.4C). In particular, a red shift was observed in the aspartate mutants for the Soret band along with appearance of two peaks in Q-band region (526-556 nm) when buffer pH was increased from 4.0 to 10, suggesting the formation of cmpd II-like intermediates under alkaline and neutral pH in the presence of H_2O_2 (data not shown).

To determine second-order rate constants of cmpd I formation (k_I), reactions between enzymes and H_2O_2 were followed via the disappearance of a Soret band (406 nm) corresponding to ERS* (top panel in Fig. 4.4E). For the *wt-El*DyP, the reaction was also monitored at 615 nm (bottom panel in Fig. 4.4E), where cmpd I formation and decay were observed. The traces were fitted to single-exponential expressions to obtain k_{obs}, which was then plotted against H_2O_2 concentrations to derive a k_I (top panel in Fig. 4.4F). The results at optimal pH/pD are

summarized in Table 4.3. Both the distal aspartate and arginine are important for cmpd I formation, for which their replacement by alanine resulted in rate decrease by 10^4 and 10^2 magnitude, respectively. This is consistent with steady-state kinetic results, in which aspartate was found to be catalytically more important than arginine. Substitution of aspartate with histidine partially recovered enzyme activity in cmpd I formation and was only 22-fold less active than the *wt-El*DyP.

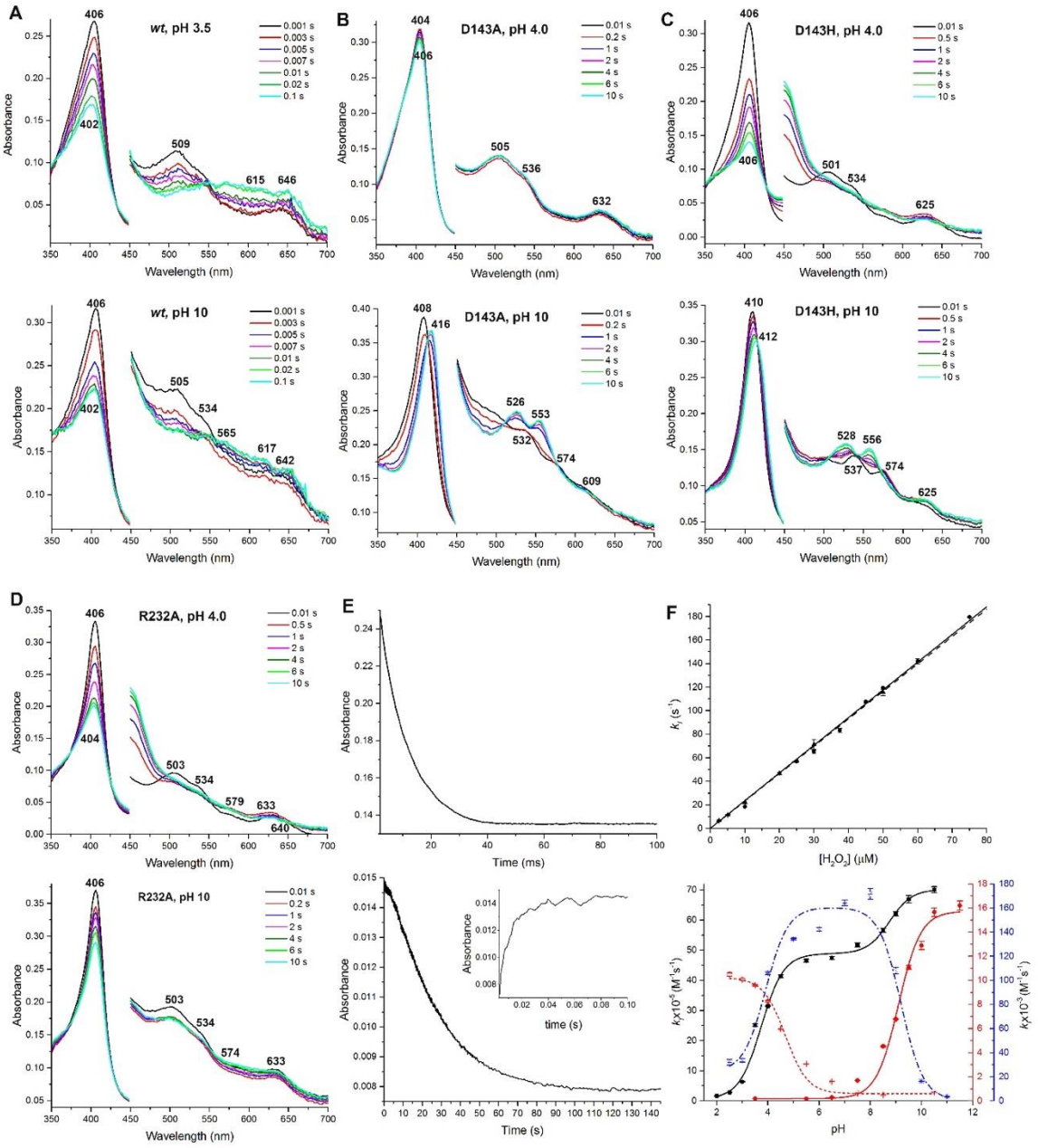

Figure 4.4 Single mixing of cmpd I formation.

Spectra in 450-700 nm are magnified by 4 times. All spectral transitions represent the reactions between 2.5 μM enzymes and 50 μM H_2O_2. (A) Spectral transition of *wt-El*DyP under acidic (top) and alkaline (bottom) conditions. (B) Spectral transition of D143A under acidic (top) and alkaline (bottom) conditions. (C) Spectral transition of D143H under acidic (top) and alkaline (bottom) conditions. (D) Spectral transition of R232A under acidic (top) and alkaline (bottom) conditions. (E) Formation and decay of *wt-El*DyP cmpd I monitored at 406 (top) and 615 nm (bottom), respectively. The bottom inset represents cmpd I formation monitored at 615 nm. (F) Second-order rate constants of cmpd I formation. The top panel represents the dependence of k_1 monitored at 406 (● and solid line) and 615 nm (▲ and dash line). The bottom panel represents pH-rate profiles of *wt* (□ and black solid line), D143A

(● and red solid line), D143H (✳ and blue dash line), and R232A (+ and red dot line). The color of Y-axes and curves correspond to each other.

4.4.6 pH dependence of cmpd I formation and decay

To study the pH-rate relationships of cmpd I formation, the k_I values of *wt* and mutant *El*DyPs were determined at various pH. Plots of k_I *vs* pH are shown in the bottom panel of Fig. 4.4F. Assuming that pH dependence is controlled by protonation/deprotonation of an ionizable group in or close to the active site, the data were fitted to equations 4, 5, 6, and 7 for *wt*, D143A, D143H, and R232A, respectively. The k_{1a}/k_{1b} and pK_1/pK_2 represent pH-independent second-order rate constant of cmpd I formation and the pK_a of ionizable groups, respectively. The latter is summarized in Table 4.3.

In contrast to LiP where cmpd I formation is pH independent,[44-45] *El*DyPs showed a clear dependence on pH. The rate of *wt* cmpd I formation increases as pH increases. Two ionizable residues with pK_a of 3.65 and 8.69 were identified, which were assigned to the distal aspartate and arginine in the heme center, respectively. While the observed pK_a of the distal aspartate is exactly the same as the intrinsic value, the arginine pK_a shifted drastically from the intrinsic value of 12.48 to 8.70 in the protein. Such a huge shift is not uncommon because the protein microenvironment can change a pK_a significantly via hydrogen bonds, electrostatic interactions, and hydrophobicity.[46] For example, the pK_a of the distal histidine in pristine peroxidase can vary from 5.1 for ERS to 7.8 for cmpd I during H_2O_2 oxidation.[47] The pK_a of K115, a catalytic residue in acetoacetate decarboxylase, shifts downward by 4.5 pH units to ~6.0.[48] In this regard, the crystal structure of *wt*-*El*DyP has revealed that R232 forms 6 hydrogen bonds (Fig. 4.2A) with neighboring residues (D143 and heme propionate) and solvent molecules (H_2O 42 and 288). In addition, there are several hydrophobic residues (I230, V231, and F248) within a distance of 4 Å

surrounding R232. These interactions may account for the large pK_a shift (3.78 pH units) associated with R232.

Table 4.3 Transient-state kinetic parameters, sKIEs, and pK_a of ionizable groups in cmpd I formation[a]

	k_I ($M^{-1}s^{-1}$)[b]	KIE	pK_a	
			Asp	Arg
wt	$(2.35 \pm 0.02)\times10^6$ [$(9.62 \pm 0.06)\times10^5$]	2.44 ± 0.06	3.65 ± 0.05 [4.15 ± 0.06]	8.70 ± 0.20 [8.20 ± 0.20]
D143A	$(1.97 \pm 0.01)\times10^2$			9.08 ± 0.08
D143H	$(1.06 \pm 0.01)\times10^5$ [$(6.90 \pm 0.20)\times10^4$]	1.54 ± 0.06	3.60 ± 0.20[c] [3.70 ± 0.20][c]	9.30 ± 0.20 [10.10 ± 0.20]
R232A	$(8.27 \pm 0.07)\times10^3$		4.80 ± 0.20	

[a]Values shown in square brackets were determined in D_2O. [b]Values were determined at optimal pH/pD of 3.5 and 4.0 for the *wt* and mutant enzymes, respectively. [c]For histidine.

$$k_1 = \frac{k_{1a}}{1 + 10^{[\mathrm{pK_1 - pH}]}} + \frac{k_{1b}}{1 + 10^{[\mathrm{pK_2 - pH}]}} \qquad (Eq.4)$$

$$k_1 = \frac{k_{1a}}{1 + 10^{[\mathrm{pK_1 - pH}]}} \qquad (Eq.5)$$

$$k_1 = \frac{k_{1a}}{1 + 10^{[\mathrm{pH - pK_1}]} + 10^{[\mathrm{pK_2 - pH}]}} \qquad (Eq.6)$$

$$k_1 = \frac{k_{1a}}{1 + 10^{[\mathrm{pH - pK_1}]}} \qquad (Eq.7)$$

To investigate if the distal aspartate and arginine are indeed responsible for these ionizable residues, the pH dependence of their mutants were also studied. It was predicted that mutation of a distal residue to alanine would result in removal of one of the pK_a identified in the *wt* enzyme. Indeed, both D143A and R232A displayed single pK_a at 9.08 and 4.81, respectively, confirming assignment of the residues for the observed pK_a in the *wt* enzyme. Moreover, while the rate of cmpd I formation becomes faster with increasing pH for D143A, the corresponding

rate in R232A decreases as the pH increases. Their implications will be discussed below. The pH dependence of cmpd I formation for D143H is bell-shaped, which is quite different from the *wt-El*DyP and other two mutants. Two pK_a values of 3.61 and 9.32 were determined, corresponding to the histidine and arginine in D143H, respectively. The pH dependence of D143H is similar to that of HRP cmpd I formation, in which a bell-shaped curve was obtained with pK_a of 4.11 and 10.90.[49]

The stability of cmpd I was also investigated at different pH values. By monitoring H_2O_2 oxidation of *wt-El*DyP (1:1 ratio) at 615 nm, cmpd I formation followed by decay to ERS* was observed sequentially (bottom panel in Fig. 4.4E). The half-life of cmpd I decayed to ERS* was 0.2, 4.4, and 2.0 min at pH 3.5, 7.5, and 10.0, respectively. Cmpd I would further decay into a new species, possibly cmpd III, in the presence of excess H_2O_2 over a long time (data not shown). Thus, *wt-El*DyP cmpd I has the shortest lifetime and is thus most reactive at acidic pH, suggesting that acidic conditions may facilitate its conversion to other reactive intermediates.

4.4.7 Transient-state kinetics of wt cmpd I reduction using ABTS and its pH dependence.

The reaction was performed in a sequential mode. Cmpd I was generated by mixing *wt-El*DyP with H_2O_2. After a 2 s delay to achieve maximal cmpd I formation, the mixture was then mixed with ABTS in the presence of ascorbate. Since the absorbance spectrum of the ABTS oxidation product overlaps with that of the *wt-El*DyP and interferes with the reaction monitored, ascorbate was used to instantaneously reduce the oxidation product back to ABTS.[50] Additionally, only low concentrations of ABTS (<10 μM) were required in order to maintain pseudo-first-order reaction conditions,[50] as too high concentrations would make the rate too fast to determine. A typical spectral transition at pH 3.5 is shown in Fig. 4.5A, where the

characteristics corresponding to cmpd II are absent.[21, 35] Analysis of the PDA data using the Pro-KIV Global Analysis program (Applied PhotoPhysics) did not show significant preference for a two-step reaction over a one-step reaction. Furthermore, when the data were fitted to a two-step reaction, the calculated spectra corresponding to cmpds I and II were almost identical. These results suggest that regeneration of ERS^* from cmpd I is likely to proceed via a 2-electron reduction. A one-electron reduction of cmpd I to ERS^* should produce cmpd II, which was not observed with our experiments. It has also to be noted that ABTS is a one-electron reductant. Thus, it is proposed that two molecules of ABTS donate their electrons to the protein simultaneously (one electron from each ABTS molecule). This requires the enzyme to have multiple sites for substrate binding, which has been found in several DyPs.[51-54]

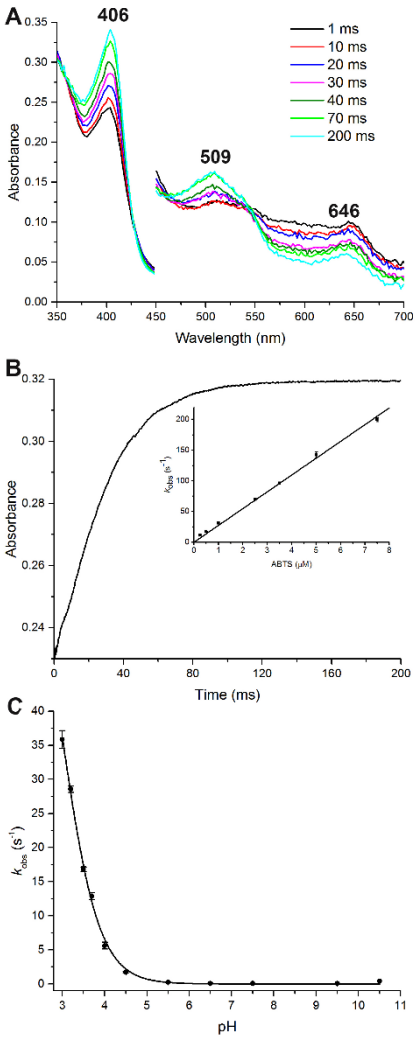

Figure 4.5 Transient-state kinetics of ERS regeneration from *wt-El*DyP cmpd I.

(A) Spectral transition of 2.5 μM *wt* cmpd I reduced by 2.5 μM ABTS at pH 3.5 in the presence of 10 μM ascorbate. The cmpd I was produced by reacting 2.5 μM *wt-El*DyP with 2.5 μM H_2O_2 followed by 2-s delay. (B) Regeneration of ERS from cmpd I monitored at 406 nm. The inset represents determination of second-order rate constant k_{ERS} in the presence of ABTS. (C) pH-dependence of 2.5 μM *wt* cmpd I reacted with 0.5 μM ABTS at various pH.

The reduction of cmpd I was monitored at 406 nm corresponding to ERS* regeneration and a typical absorbance change is shown in Fig. 4.5B. The k_{obs} was obtained by fitting the curve to a single exponential growth equation. The overall second-order rate constants (k_{ERS*}) were determined by plotting the k_{obs} *vs* ABTS concentrations (inset in Fig. 4.5B), giving a value of 2.74×10^7 M^{-1} s^{-1}. Thus, the rate of ERS* regeneration from *wt* cmpd I in the presence of ABTS is

more than 10-fold faster than that of cmpd I formation (2.35×10^6 $M^{-1}s^{-1}$). It has to be pointed out that the rate of ERS* regeneration is expected to be substrate-dependent. Consequently, it is possible that a slower rate than the cmpd I formation could be obtained if a less reactive reducing substrate were employed.

The rate of *wt* cmpd I reduction using ABTS was also determined at pH ranging from 3.0 to 10.5. Conditions lower than pH 3.0 were not studied due to protein instability. As shown in Fig. 4.5C, the overall k_{obs} increases significantly as the pH decreases, demonstrating that cmpd I reduction prefers acidic conditions. When the pH is higher than 5.0, the k_{obs} approaches zero. Additionally, fitting the data to Eq. 7 gave a pK_a of 3.00, indicating that an ionizable residue, possibly D143, is involved in this reduction process.

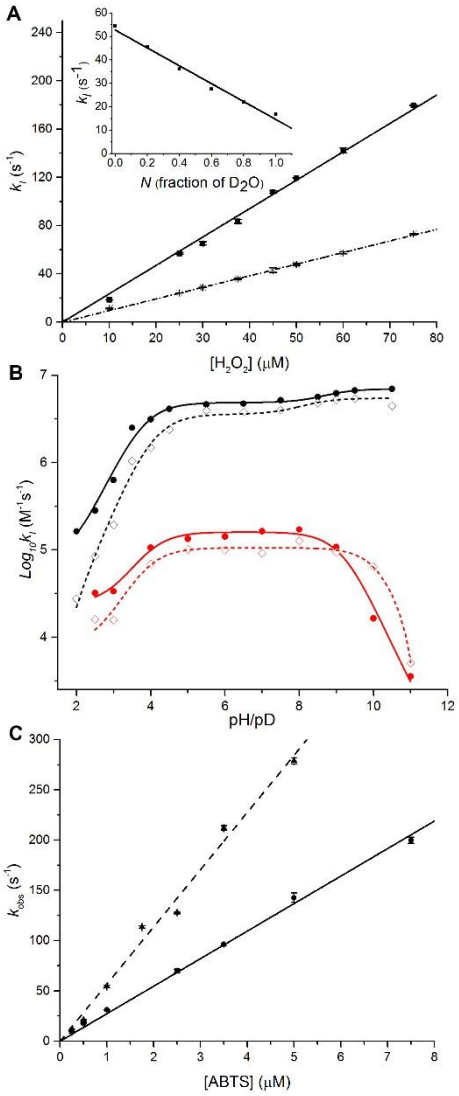

Figure 4.6 KIE and sKIE of transient-state kinetics.

Solid and dash lines represent reactions performed in H_2O and D_2O, respectively. (A) Rates of *wt*-*El*DyP cmpd I formation at pH/pD 3.5. The inset represents proton inventory plot of rates *vs* fraction of D_2O. (B) pH/pD dependence of *wt* (black lines) and D143H-*El*DyP (red lines) cmpd I formation on a logarithmic scale. (C) Rates of cmpd I reduction using ABTS as the reducing substrate at pH/pD 3.5.

4.4.8 sKIE on transient-state kinetics

D_2O_2 is a good mechanistic probe for studying compd I formation, which can be easily prepared from H-D exchange of concentrated H_2O_2 in D_2O. Thus, both the enzyme (*wt* or D143H-*El*DyP) and H_2O_2 at high concentrations were dissolved in D_2O before they were mixed

together using a stopped-flow spectrometer. Since the D_2O_2, rather than the H_2O_2, oxidizes the enzyme to produce cmpd I in D_2O, the KIE, instead of sKIE, should be used to describe cmpd I formation. As shown in Fig. 4.6A and summarized in Table 4.3, the rate of *wt* cmpd I formation at pD 3.5 was slowed in D_2O, resulting in a normal KIE of 2.44. A proton inventory experiment showed a linear relationship between the rates and fraction of D_2O, indicating that a single proton was involved in the rate-determining step (RDS) of cmpd I formation. The sKIE of D143H was determined to be 1.54 at pH/pD 4.0, which was much smaller than that of the *wt* enzyme. The KIE of *wt* cmpd I formation was also investigated as a function of pH/pD, which increased as the pH/pD decreased, to a maximum of 5.3 at pH/pD 2.0 (black lines in Fig. 4.6B). When the pH/pD was greater than 5.5, the KIE approached to unity. For D143H, a normal KIE was observed when pH/pD≤9.0 and the value slightly increased as the pH/pD dropped, to a maximum of 2.1 at pH/pD 3.0. Similarly to HRP,[49] an inverse KIE was observed at high alkaline pH/pD (> 9.0), reaching 0.26 at pH/pD 10.0. Additionally, most pK_as determined in D_2O shift upward (Table 4.3), consistent with the known effects of D_2O on pK_a.[55]

As shown in Fig. 4.6C, the second-order rate constants of cmpd I reduction (k_{ERS}) with ABTS in H_2O and D_2O were determined to be 2.74×10^7 and 5.68×10^7 $M^{-1}s^{-1}$, respectively, at pH/pD 3.5. This resulted in an inverse sKIE [$^D(k_{ERS})$] of 0.48, which suggests that cmpd I reduction to ERS^* is likely to involve water elimination from the heme iron. Their mechanistic implications will be discussed in the next section.

4.4.9 Viscosity effects on steady-state and transient-state kinetics

The effects of solvent viscosity upon k_{cat}/K_M and k_{cat} were determined to evaluate whether diffusion into and out of the active site plays a significant role in the steady-state kinetic parameters of *El*DyP. Additionally, viscosity could cause a small sKIE as D_2O is 25% more

viscous than H_2O at r.t. To probe this possibility, sucrose was used as a viscosogen to modulate the viscosity of reaction medium. The results are summarized in Fig. 4.7. For a completely diffusion-controlled reaction, the slope should equal to 1 as represented by the blue lines. When the slope approaches to zero, the reaction is independent of diffusion. Reactions with slopes between 0 and 1 are partially diffusion-controlled. It was found that k_{cat}/K_M of *wt-El*DyP with ABTS was 40% diffusion-controlled (black solid line in Fig. 4.7), suggesting that binding of a reducing substrate is partially diffusion-controlled and limits the rate of the overall reaction. The $k_{cat,}$ was observed to be viscosity independent (black dash line in Fig. 4.7), however, implying that product release is not rate-limiting. Similar observations were also made for reactions employing glucose as a viscosogen (data not shown), demonstrating that the viscosity effects are viscosogen independent for steady-state kinetics.

To characterize the origin of the viscosity effects found in steady-state kinetics, transient-state kinetics of cmpd I formation and reduction were performed in sucrose at various concentrations. It was found that the second- order rate constants of *wt* cmpd I formation (k_I) are insensitive to solvent viscosity (red solid line in Fig. 4.7). However, the reduction of cmpd I in the presence of ABTS and ascorbate was determined to be 34% diffusion-controlled (red dash line in Fig. 4.7), which accounts for the 85% viscosity effect on k_{cat}/K_M observed in steady-state kinetics.

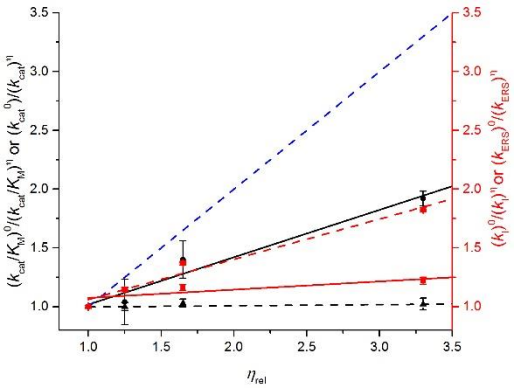

Figure 4.7 Effects of solvent viscosity on kinetic parameters at pH 3.5.

Blue dash lines reflect theoretical limit for a completely diffusion-controlled reaction. Effects on k_{cat}/K_M (black solid line, slope = 0.404) and k_{cat} (black dash line, slope = 0.007) with ABTS are scaled by left black Y-axis. Effects on second-order rate constants of cmpd I formation (k_I, red solid line, slope = 0.069) and reduction using ABTS (k_{ERS}, red dash line, slope = 0.342) are scaled by right red Y-axis.

4.5 Discussion

Based on the results described above, a bisubstrate Ping-Pong mechanism involving a final step of conformational change is proposed in Scheme 1. Several unique features associated with DyPs have been identified and are described below.

4.5.1 Cmpd 0 deprotonation is rate-limiting in DyP cmpd I formation

*El*DyP activation by H_2O_2 to form cmpd I was proposed in Scheme 1 based on the Poulos-Kraut mechanism.[56] After H_2O_2 displaces H_2O and binds with ERS as the sixth ligand, the conserved distal aspartate acts first as a general base to deprotonate H_2O_2 to form the iron-peroxide complex named cmpd 0, then as a general acid to protonate the outer oxygen of cmpd 0. Electrostatic interactions between the distal arginine and the outer oxygen atom are proposed to promote heterolysis of the O−O bond to form cmpd I.[57] Since the former two steps (k_3 and k_4) involve formation and breakage of an O−H bond, a primary KIE is expected with D_2O_2 if any of these steps is rate-limiting. However, no primary KIE should be observed if the O−O bond scission (k_5) is rate-limiting. We found that the *wt-El*DyP displayed an observed isotope effect of

2.44 in D_2O. Because H_2O_2 can exchange with D_2O to produce D_2O_2 quickly, the observed isotope effect should be a combination of the primary KIE (if it exists) and sKIE. Since two water molecules are released during cmpd I formation (k_1 and k_6), an inverse sKIE will be expected as described in the next sub-section. Thus, the observed normal isotope effect suggests that a primary KIE larger than 2.44 should be present, as the inverse sKIE will cancel the isotope effect resulting from a normal primary KIE. Proton inventory showed that only one proton is involved in cmpd I formation. Because the viscosity did not contribute to the observed isotope effect, the results suggest that either H_2O_2 deprotonation or subsequent outer oxygen protonation should be rate-limiting, which could be determined by studying pH-dependence of cmpd I formation.

Scheme 4.1 Proposed bisubstrate Ping-Pong mechanism for DyPs involving a final step of conformational change

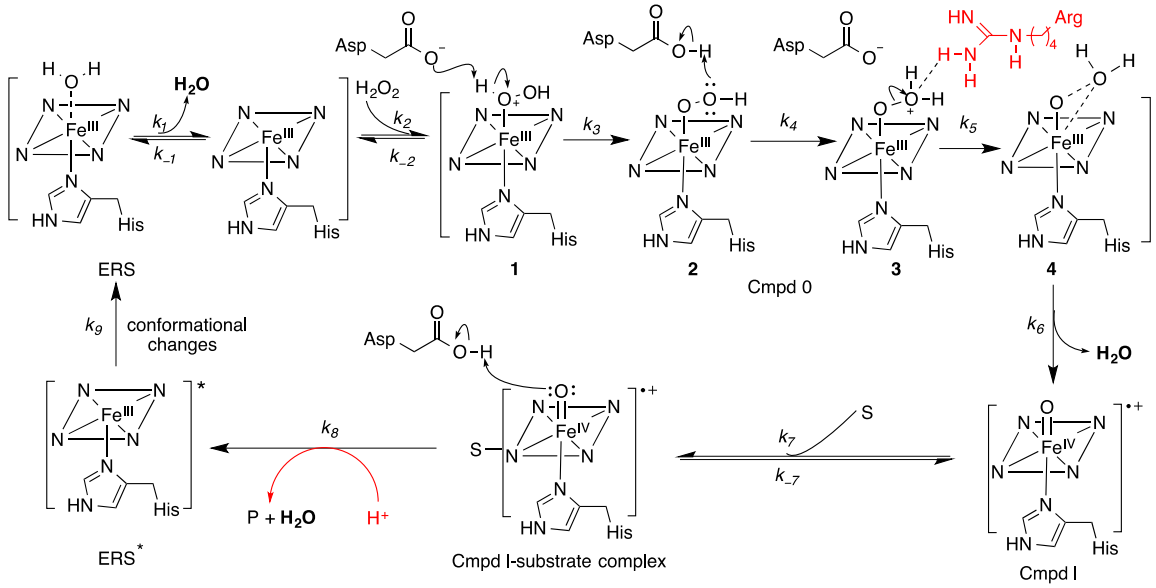

In sharp contrast with LiP, where the rates of cmpd I formation are pH-independent,[44-45] the rates of *El*DyP cmpd I formation displayed pH-dependence (Fig. 4.4F, bottom panel). The rate increases as pH increases for both the *wt* enzyme and D143A-*El*DyP. Moreover, cmpd I was formed only at alkaline pH for D143A. These observations indicate that the step of cmpd 0 deprotonation (k_3) is likely to be a RDS for *El*DyP cmpd I formation. While the distal aspartate is responsible for cmpd 0 deprotonation, alkaline conditions are expected to facilitate this process, resulting in an increased rate. When the aspartate was replaced with an alanine, deprotonation could only occur at alkaline pH due to the assistance of OH^-, which resulted in the rate decreased by four orders of magnitude. Furthermore, pH-dependence of *wt* cmpd I formation in H_2O and D_2O (black lines in Fig. 4.6B) revealed that the isotope effect becomes less pronounced as the acidity decreases, reaching 1.18 at pH 9.0. Under alkaline conditions, OH^- and OD^- are expected to participate in cmpd I formation as a specific base and thus, to have a small KIE. This provides additional evidence to support our hypothesis that cmpd 0 deprotonation is a RDS in *wt* cmpd I formation. The trend of pH-dependence was reversed in R232A, in which cmpd I was formed only at acidic pH and the rate increased as pH decreased. This suggests that O−O bond scission in *El*DyP does not necessarily require the assistance of the distal arginine, though loss of it will result in a rate-drop by more than two orders of magnitude. Moreover, unlike the *wt* and D143A-*El*DyPs, the step to protonate the outer oxygen atom (k_4) may become rate-limiting in R232A, in which the aspartate acts as a general acid. Acidic pH should facilitate the formation of a protonated aspartate. Together, these results demonstrate that cmpd 0 deprotonation is rate-limiting for *wt*-*El*DyP and that the aspartate is catalytically more important than the arginine.

4.5.2 Conformational change is the final step in the DyP mechanism

Transient-state kinetics of ERS^* regeneration revealed that cmpd I reduction (2.74×10^7 M^{-1} s^{-1}) was more than 10 times faster than that of cmpd I formation (2.35×10^6 $M^{-1}s^{-1}$) when ABTS was used as a reducing substrate. Thus, either cmpd I formation or a step after ERS^* regeneration would be rate-limiting in the overall ABTS oxidation catalyzed by *wt-El*DyP. This RDS should be described by k_{cat} in steady-state kinetics.

The inverse sKIE is not very common. Its chemical origins have been attributed to catalysis involving cysteine, water dissociation from metal centers, and medium effects.[58] Because the closest C249 in *El*DyP is 12.6 Å away from the heme iron, it is unlikely that cysteines participate in catalysis. Thus, the observed inverse sKIE should arise from either water release from the heme iron or medium effects during turnover. The fractionation factor (Φ, equilibrium distribution of the two isotopes) for L_2O (where L = H or D) is inverse when water is bonded to a metal, resulting in a tendency for D_2O to accumulate in bulk solvent.[59] It is commonly accepted that the water released from $M{-}OH_2 \leftrightarrow M + H_2O$ equilibrium has $\Phi \approx 0.70$.[60] Additionally, Φ is reported on a per-bond basis and multiplicative. Thus, the observed sKIE is diagnostic of the number of H_2O released from the metal center. For example, 0.49 (Φ^2), 0.24 (Φ^4), and 0.12 (Φ^6) are expected for the dissociation of one, two, and three H_2O molecules, respectively. Such a method has recently been employed to reveal kinetic mechanisms of two iron-containing enzymes, FIH and ToMO.[59, 61-62] While most inverse sKIE resulting from medium effects are due to viscosity-sensitive conformational changes,[58, 63-64] solvation can also cause inverse sKIE as demonstrated by the blue single-copper protein azurin from *Pseudomonas aeruginosa*.[65] The effect of solvation on azurin is reflected as a positive shift of $E°´$ by 10 mV from H_2O to D_2O.[65]

The $^{D}(k_{cat})$ values for *wt-El*DyP were determined to be 0.70 with ABTS. Although the value equals Φ of one hydroxyl group dissociated from a metal center, which is included in the step of cmpd I reduction to ERS* (k_8), our experimental results with ABTS eliminates this possibility as cmpd I reduction is much faster than cmpd I formation. Thus, a conformational change of ERS* to ERS was proposed as the final rate-limiting step in the presence of ABTS. Since the k_{cat} was found to be viscosity-independent, our results indicate that enzyme motion does not involve movement of large loops on protein surface. The observed inverse sKIE is likely due to protein solvation, which is further supported by a positive shift of $E°´$ from −290 mV in H_2O to −263 mV in D_2O for *wt-El*DyP.

It has to be pointed out that the two conformers, ERS* and ERS, are spectroscopically identical for *El*DyP. Moreover, whether this final step of conformational change is rate-limiting or not will depend on the reducing substrate. With fast substrates such as ABTS and RB19, conformational change (k_9) is a RDS. However, with slow substrates such as pyrogallol, guaiacol and HQ, cmpd I reduction (k_8) is more likely to be rate-limiting, which has been shown in *Tc*DyP and DyPB.[19, 21]

4.5.3 Aquo release is mechanistically important

While both the $^{D}(k_{cat})$ and $^{D}(k_{cat}/K_M)$ of *wt-El*DyP are inverse with ABTS, the inverse effect is much more pronounced with the latter than with the former. The sKIE of k_{cat}/K_M was determined to be 0.11, which is in excellent agreement with the theoretical value of 0.12, corresponding to the release of three water molecules ($\Phi^2\times\Phi^2\times\Phi^2 = 0.12$). Since the k_{cat}/K_M describes the steps preceding the RDS, examination of the mechanism proposed in Scheme 1 reveals that three waters are released before the RDS in the catalytic cycle, which include (1) one released from Fe (III) in ERS during H_2O_2 displacement. A water molecule was seen to act as the

sixth ligand in *wt-El*DyP crystal structure (Fig. 4.2A); (2) one dissociated from cmpd 0 prior to the formation of cmpd I. It was proposed that a water molecule is eliminated from cmpd 0-water complex **4**, though additional experimental evidence in support of this concept has yet to be obtained; and (3) one released in the reduction of cmpd I to generate ERS* via a two-electron process. To further demonstrate the importance of aquo release, the sKIE of cmpd I reduction (k_{ERS}) was investigated. An inverse sKIE of 0.48 was determined, which is again in excellent agreement with the theoretical prediction of 0.49 (Φ^2 = 0.49) as only one water is dissociated from the heme iron during cmpd I reduction. The excellent agreement between theoretical and experimental results suggests that aquo release in DyP is mechanistically important.

It has been postulated that cmpd I undergoes different redox pathways depending on whether the coproduced water is bound with the intermediate or not.[66] If the water is absent (dry form), the cmpd I will proceed through a two-electron equivalent reduction. However, only one-electron equivalent processes are accessible in the presence of water (wet form). Thus, the coproduced water may act as a gate to control enzyme function and activity.[66] In *El*DyP cmpd I reduction, only one water was found released based on the sKIE of 0.48. If the coproduced water is bound with cmpd I before its reduction, two water molecules should be expected, resulting in a sKIE of 0.49×0.49=0.24. Therefore, it was deduced that the *wt-El*DyP cmpd I is in a dry form and may undergo a two-electron reduction, which agrees with our experimental results: absence of cmpd II species in stopped-flow spectroscopy during cmpd I reduction.

4.5.4 Reducing substrates bind with cmpd I only

Viscosity experiments performed under steady-state kinetic conditions showed that, while k_{cat} was unchanged, the k_{cat}/K_M with reducing substrates decreased as the viscosity increased. The overall reaction of ABTS oxidation (k_{cat}/K_M) is 40% diffusion-controlled, suggesting that binding

of reducing substrate is important. Additionally, reduction of cmpd I (k_{ERS}) using ABTS accounts for most of the overall viscosity observed in steady-state kinetics. Thus, it is proposed that the reducing substrate only binds with cmpd I. This is further supported by isothermal titration calorimetry (ITC) and surface plasmon resonance (SPR) experiments (data not shown), where ABTS did not show bindings to free enzyme except for non-specific bindings under very high substrate concentrations. Similar results were also obtained in our study of *Tc*DyP with lignin model compounds.[23] Therefore, unlike some heme peroxidases, in which the reducing substrate binds randomly with free enzyme and cmpd I,[67-69] sequential binding of H_2O_2 with free enzyme followed by reducing substrate with cmpd I is proposed for DyPs.

4.5.5 DyPs' acidic optimum results from distal aspartate and other acidic residues

It has been claimed that the acidic optimum of DyP activity is due to the presence of the distal aspartate.[1-3, 25] While our results provided the first experimental evidence to support this claim, they also demonstrated that the distal aspartate is not the only determinant. Other acidic residues must have contributed to the enzyme's acidic optimum, as mutations of D143 shifted the pH optimum only by 0.5 pH unit to 4.0 (Fig. 4.1E). Should the distal aspartate be the sole origin of the acidic optimum, the mutant D143H would be expected to have the highest activity under neutral conditions due to the pK_a of histidine. This was clearly not the case. Consequently, in addition to the distal aspartate, other acidic residues around the heme center must also be responsible for the DyPs' acidic optimum, which are yet to be identified. Moreover, the pH dependence of ERS^* regeneration showed that the acidic optimum is essential for cmpd I reduction (Fig. 4.5C), which explains why the *El*DyP is inactivated above pH 5.0 (Fig. 4.1D) though cmpd I formation is actually enhanced at higher pH values (bottom panel in Fig. 4.4F). The distal aspartate is likely to be the ionizable group and act as a general acid to protonate cmpd

I in order to eliminate the oxygen atom attached to Fe(IV) as a water. These results provide convincing evidence that the distal aspartate plays key roles in catalysis and leads to acidic optimum of DyPs.

4.5.6 D143H-*El*DyP shows mechanistic difference from the wt enzyme

D143H-*El*DyP was selected for study because class II plant peroxidases and HRP contain a distal histidine. Elucidation of its properties will provide the basis to understand mechanistic difference between the DyPs and fungal lignolytic enzymes. The sKIE of cmpd I formation was determined to be much smaller for D143H than for the *wt* at the same pH/pD (Table 4.3 and Fig. 4.6B). Its pH-independent, second-order rate constants of cmpd I formation were determined to be 1.56×10^5 and $1.06 \times 10^5\ M^{-1}s^{-1}$ in H_2O and D_2O, respectively (red lines in Fig. 4.6B), yielding a pH-independent sKIE of 1.47. This is close to the pH-independent sKIE of 1.60 for HRP.[49] The decreased sKIE relative to the *wt* enzyme at the same pH suggests that deprotonation and protonation of cmpd 0 are less important for cmpd I formation in D143H than in the *wt* enzyme. When the pH was higher than 9.0, an inverse sKIE was observed, which could be ascribed to restrictions on torsional motions of exchangeable protons as reported for β–lactam synthetase.[64]

The $^{D}(k_{cat})$ of D143H with ABTS was close to unity, implying that the rate-limiting conformational changes are insensitive to the solvent. This is in contrast to *wt*-*El*DyP and indicates that the distal aspartate is important in determining the heme microenvironment, which is also reflected in their UV-absorbance spectra (Fig. 4.1D). An extra Q-band was observed at 567 nm when the distal aspartate was replaced with a histidine. The $^{D}(k_{cat}/K_M)$ of D143H was nearly identical to that of the *wt* (Table 4.2), displaying a large inverse sKIE. Similar to *wt*-*El*DyP, the large inverse sKIE was attributed to water dissociation from the heme iron, which

should result in an expected $^{D}(k_{cat}/K_M)$ of 0.12. Thus, the predicted value is in excellent agreement with the observed one at 0.13.

4.6 Conclusion

A bisubstrate Ping-Pong mechanism involving a final step of conformational change was proposed as a possible DyP mechanism based on the sKIEs and viscosity effects on steady-state and transient-state kinetics. The conformational change is also rate-limiting in ABTS oxidation. Spectra of ERS* and ERS present in the conformational change were indistinguishable. The normal KIE and pH-dependence of cmpd I formation demonstrated that cmpd 0 deprotonation is rate-limiting for *wt-El*DyP, which is less important for D143H. Cmpd I reduction to ERS* is likely a two-electron process in the presence of ABTS, in which the viscosity effects observed accounted for almost all of the viscosity effects found in k_{cat}/K_M. Together with the results of ITC and SPR (data not shown), this suggested that H_2O_2 and reducing substrates bind with free enzyme and cmpd I, respectively. The significant inverse sKIEs of k_{cat}/K_M and k_{ERS*} were ascribed to water dissociation from the heme iron, which are in excellent agreement with the predicted values. This demonstrates the unique mechanistic importance of aquo release in DyP-catalyzed reactions. Steady-state and transient-state kinetics showed that the distal aspartate is catalytically more important than the distal arginine. The drastic pK_a shift of 3.79 pH units for the distal arginine is likely caused by its extensive networks of hydrogen bonds. While the distal aspartate plays key roles in determining DyPs' acidic optimum, other acidic residues in the heme center also contribute to this unique property. Thus, the results reported here provide a detailed picture of DyP mechanism at the molecular level, which will pave the way for future protein engineering to improve DyPs' lignolytic activity.

4.7 References

1. Singh, R.; Eltis, L. D., The multihued palette of dye-decolorizing peroxidases. *Arch Biochem Biophys* **2015,** *574*, 56-65.

2. Strittmatter, E., Plattner, D. A., and Piontek, K., Dye-Decolorizing Peroxidase (DyP). In *Encyclopedia of Inorganic and Bioinorganic Chemistry*, John Wiley and Sons, Ltd.: New York, 2011.

3. Sugano, Y., DyP-type peroxidases comprise a novel heme peroxidase family. *Cell Mol Life Sci* **2009,** *66* (8), 1387-1403.

4. Brown, M. E.; Chang, M. C. Y., Exploring bacterial lignin degradation. *Curr Opin Chem Biol* **2014,** *19*, 1-7.

5. de Gonzalo, G.; Colpa, D. I.; Habib, M. H. M.; Fraaije, M. W., Bacterial enzymes involved in lignin degradation. *J Biotechnol* **2016,** *236*, 110-119.

6. Bugg, T. D.; Ahmad, M.; Hardiman, E. M.; Singh, R., The emerging role for bacteria in lignin degradation and bio-product formation. *Current opinion in biotechnology* **2011,** *22* (3), 394-400.

7. Linger, J. G.; Vardon, D. R.; Guarnieri, M. T.; Karp, E. M.; Hunsinger, G. B.; Franden, M. A.; Johnson, C. W.; Chupka, G.; Strathmann, T. J.; Pienkos, P. T.; Beckham, G. T., Lignin valorization through integrated biological funneling and chemical catalysis. *Proceedings of the National Academy of Sciences of the United States of America* **2014,** *111* (33), 12013-12018.

8. Ralph, J.; Brunow, G.; Boerjan, W., Lignins. *eLS* **2007,** *http://onlinelibrary.wiley.com/doi/10.1002/9780470015902.a0020104*.

9. Sanderson, K., A chewy problem. *Nature* **2011,** *474* (7352), S12-S14.

10. Zakzeski, J.; Bruijnincx, P. C. A.; Jongerius, A. L.; Weckhuysen, B. M., The Catalytic Valorization of Lignin for the Production of Renewable Chemicals. *Chemical reviews* **2010,** *110* (6), 3552-3599.

11. Ragauskas, A. J.; Beckham, G. T.; Biddy, M. J.; Chandra, R.; Chen, F.; Davis, M. F.; Davison, B. H.; Dixon, R. A.; Gilna, P.; Keller, M.; Langan, P.; Naskar, A. K.; Saddler, J. N.; Tschaplinski, T. J.; Tuskan, G. A.; Wyman, C. E., Lignin Valorization: Improving Lignin Processing in the Biorefinery. *Science* **2014,** *344* (6185), 709-+.

12. Rahimi, A.; Ulbrich, A.; Coon, J. J.; Stahl, S. S., Formic-acid-induced depolymerization of oxidized lignin to aromatics. *Nature* **2014,** *515* (7526), 249-252.

13. Boerjan, W.; Ralph, J.; Baucher, M., Lignin biosynthesis. *Annu Rev Plant Biol* **2003,** *54*, 519-546.

14. Sannigrahi, P.; Ragauskas, A. J., Characterization of Fermentation Residues from the Production of Bio-Ethanol from Lignocellulosic Feedstocks. *J Biobased Mater Bio* **2011,** *5* (4), 514-519.

15. Vishtal, A.; Kraslawski, A., Challenges in Industrial Applications of Technical Lignins. *Bioresources* **2011,** *6* (3), 3547-3568.

16. Wong, D. W. S., Structure and Action Mechanism of Ligninolytic Enzymes. *Appl Biochem Biotech* **2009,** *157* (2), 174-209.

17. Pollegioni, L.; Tonin, F.; Rosini, E., Lignin-degrading enzymes. *Febs Journal* **2015,** *282* (7), 1190-1213.

18. Bugg, T. D. H.; Ahmad, M.; Hardiman, E. M.; Rahmanpour, R., Pathways for degradation of lignin in bacteria and fungi. *Nat Prod Rep* **2011,** *28* (12), 1883-1896.

19. Ahmad, M.; Roberts, J. N.; Hardiman, E. M.; Singh, R.; Eltis, L. D.; Bugg, T. D. H., Identification of DypB from Rhodococcus jostii RHA1 as a Lignin Peroxidase. *Biochemistry* **2011,** *50* (23), 5096-5107.

20. Brown, M. E.; Barros, T.; Chang, M. C. Y., Identification and Characterization of a Multifunctional Dye Peroxidase from a Lignin-Reactive Bacterium. *Acs Chem Biol* **2012,** *7* (12), 2074-2081.

21. Chen, C.; Shrestha, R.; Jia, K.; Gao, P. F.; Geisbrecht, B. V.; Bossmann, S. H.; Shi, J. S.; Li, P., Characterization of Dye-decolorizing Peroxidase (DyP) from Thermomonospora curvata Reveals Unique Catalytic Properties of A-type DyPs. *J Biol Chem* **2015,** *290* (38), 23447-23463.

22. Min, K.; Gong, G.; Woo, H. M.; Kim, Y.; Um, Y., A dye-decolorizing peroxidase from Bacillus subtilis exhibiting substrate-dependent optimum temperature for dyes and beta-ether lignin dimer. *Sci Rep-Uk* **2015,** *5*.

23. Huang, G. C.; Shrestha, R.; Jia, K. M.; Geisbrecht, B. V.; Li, P., Enantioselective Synthesis of Dilignol Model Compounds and Their Stereodiscrimination Study with a Dye-Decolorizing Peroxidase. *Org Lett* **2017,** *19* (7), 1820-1823.

24. Yoshida, T.; Sugano, Y., A structural and functional perspective of DyP-type peroxidase family. *Arch Biochem Biophys* **2015,** *574*, 49-55.

25. Colpa, D. I.; Fraaije, M. W.; van Bloois, E., DyP-type peroxidases: a promising and versatile class of enzymes. *Journal of industrial microbiology & biotechnology* **2014,** *41* (1), 1-7.

26. DeAngelis, K. M.; D'Haeseleer, P.; Chivian, D.; Fortney, J. L.; Khudyakov, J.; Simmons, B.; Woo, H.; Arkin, A. P.; Davenport, K. W.; Goodwin, L.; Chen, A.; Ivanova, N.; Kyrpides, N. C.; Mavromatis, K.; Woyke, T.; Hazen, T. C., Complete genome sequence of "Enterobacter lignolyticus" SCF1. *Stand Genomic Sci* **2011,** *5* (1), 69-85.

27. Dailey, H. A.; Septer, A. N.; Daugherty, L.; Thames, D.; Gerdes, S.; Stabb, E. V.; Dunn, A. K.; Dailey, T. A.; Phillips, J. D., The Escherichia coli Protein YfeX Functions as a Porphyrinogen Oxidase, Not a Heme Dechelatase. *Mbio* **2011,** *2* (6).

28. Letoffe, S.; Heuck, G.; Delepelaire, P.; Lange, N.; Wandersman, C., Bacteria capture iron from heme by keeping tetrapyrrol skeleton intact. *Proceedings of the National Academy of Sciences of the United States of America* **2009,** *106* (28), 11719-11724.

29. Smith, P. K.; Krohn, R. I.; Hermanson, G. T.; Mallia, A. K.; Gartner, F. H.; Provenzano, M. D.; Fujimoto, E. K.; Goeke, N. M.; Olson, B. J.; Klenk, D. C., Measurement of Protein Using Bicinchoninic Acid. *Anal Biochem* **1985,** *150* (1), 76-85.

30. Berry, E. A.; Trumpower, B. L., Simultaneous Determination of Hemes-a, Hemes-B, and Hemes-C from Pyridine Hemochrome Spectra. *Analytical Biochemistry* **1987,** *161* (1), 1-15.

31. Adams, P. D.; Afonine, P. V.; Bunkoczi, G.; Chen, V. B.; Davis, I. W.; Echols, N.; Headd, J. J.; Hung, L. W.; Kapral, G. J.; Grosse-Kunstleve, R. W.; McCoy, A. J.; Moriarty, N. W.; Oeffner, R.; Read, R. J.; Richardson, D. C.; Richardson, J. S.; Terwilliger, T. C.; Zwart, P. H., PHENIX: a comprehensive Python-based system for macromolecular structure solution. *Acta Crystallogr D* **2010,** *66*, 213-221.

32. Emsley, P.; Lohkamp, B.; Scott, W. G.; Cowtan, K., Features and development of Coot. *Acta Crystallogr D* **2010,** *66*, 486-501.

33. Reyes, C.; Qian, F.; Zhang, A.; Bondarev, S.; Welch, A.; Thelen, M. P.; Saltikov, C. W., Characterization of Axial and Proximal Histidine Mutations of the Decaheme Cytochrome MtrA from Shewanella sp Strain ANA-3 and Implications for the Electron Transport System. *J Bacteriol* **2012,** *194* (21), 5840-5847.

34. Wilks, A.; Sun, J.; Loehr, T. M.; Demontellano, P. R. O., Heme Oxygenase His25ala Mutant - Replacement of the Proximal Histidine Iron Ligand by Exogenous Bases Restores Catalytic Activity. *Journal of the American Chemical Society* **1995,** *117* (10), 2925-2926.

35. Roberts, J. N.; Singh, R.; Grigg, J. C.; Murphy, M. E. P.; Bugg, T. D. H.; Eltis, L. D., Characterization of Dye-Decolorizing Peroxidases from Rhodococcus jostii RHA1. *Biochemistry* **2011,** *50* (23), 5108-5119.

36. Uchida, T.; Sasaki, M.; Tanaka, Y.; Ishimorit, K., A Dye-Decolorizing Peroxidase from Vibrio cholerae. *Biochemistry* **2015,** *54* (43), 6610-6621.

37. Liu, X. H.; Yuan, Z. L.; Wang, J. X.; Cui, Y. Q.; Liu, S.; Ma, Y. L.; Gu, L. C.; Xu, S. J., Crystal structure and biochemical features of dye-decolorizing peroxidase YfeX from Escherichia coli O157 Asp(143) and Arg(232) play divergent roles toward different substrates. *Biochemical and biophysical research communications* **2017,** *484* (1), 40-44.

38. Blodig, W.; Smith, A. T.; Doyle, W. A.; Piontek, K., Crystal structures of pristine and oxidatively processed lignin peroxidase expressed in Escherichia coli and of the W171F variant that eliminates the redox active tryptophan 171. Implications for the reaction mechanism. *Journal of Molecular Biology* **2001,** *305* (4), 851-861.

39. Sundaramoorthy, M.; Gold, M. H.; Poulos, T. L., Ultrahigh (0.93 angstrom) resolution structure of manganese peroxidase from Phanerochaete chrysosporium: Implications for the catalytic mechanism. *J Inorg Biochem* **2010,** *104* (6), 683-690.

40. Saez-Jimenez, V.; Acebes, S.; Garcia-Ruiz, E.; Romero, A.; Guallar, V.; Alcalde, M.; Medrano, F. J.; Martinez, A. T.; Ruiz-Duenas, F. J., Unveiling the basis of alkaline stability of an evolved versatile peroxidase. *Biochem J* **2016,** *473*, 1917-1928.

41. Poulos, T. L., Heme Enzyme Structure and Function. *Chemical reviews* **2014,** *114* (7), 3919-3962.

42. ten Have, R.; Teunissen, P. J. M., Oxidative mechanisms involved in lignin degradation by white-rot fungi. *Chemical reviews* **2001,** *101* (11), 3397-3413.

43. van Bloois, E.; Pazmino, D. E. T.; Winter, R. T.; Fraaije, M. W., A robust and extracellular heme-containing peroxidase from Thermobifida fusca as prototype of a bacterial peroxidase superfamily. *Appl Microbiol Biot* **2010,** *86* (5), 1419-1430.

44. Marquez, L.; Wariishi, H.; Dunford, H. B.; Gold, M. H., Spectroscopic and Kinetic-Properties of the Oxidized Intermediates of Lignin Peroxidase from Phanerochaete-Chrysosporium. *J Biol Chem* **1988,** *263* (22), 10549-10552.

45. Andrawis, A.; Johnson, K. A.; Tien, M., Studies on Compound-I Formation of the Lignin Peroxidase from Phanerochaete-Chrysosporium. *J Biol Chem* **1988,** *263* (3), 1195-1198.

46. Pace, C. N.; Grimsley, G. R.; Scholtz, J. M., Protein Ionizable Groups: pK Values and Their Contribution to Protein Stability and Solubility. *J Biol Chem* **2009,** *284* (20), 13285-13289.

47. Chreifi, G.; Baxter, E. L.; Doukov, T.; Cohen, A. E.; McPhillips, S. E.; Song, J. H.; Meharenna, Y. T.; Soltis, S. M.; Poulos, T. L., Crystal structure of the pristine peroxidase ferryl center and its relevance to proton-coupled electron transfer. *Proceedings of the National Academy of Sciences of the United States of America* **2016,** *113* (5), 1226-1231.

48. Highbarger, L. A.; Gerlt, J. A.; Kenyon, G. L., Mechanism of the reaction catalyzed by acetoacetate decarboxylase. Importance of lysine 116 in determining the pK(a) of active-site lysine 115. *Biochemistry* **1996,** *35* (1), 41-46.

49. Dunford, H. B.; Hewson, W. D.; Steiner, H., Horseradish-Peroxidase .29. Reactions in Water and Deuterium-Oxide - Cyanide Binding, Compound-I Formation, and Reactions of Compound-I and Compound-Ii with Ferrocyanide. *Can J Chem* **1978,** *56* (22), 2844-2852.

50. Goodwin, D. C.; Yamazaki, I.; Aust, S. D.; Grover, T. A., Determination of Rate Constants for Rapid Peroxidase Reactions. *Analytical Biochemistry* **1995,** *231* (2), 333-338.

51. Linde, D.; Pogni, R.; Canellas, M.; Lucas, F.; Guallar, V.; Baratto, M. C.; Sinicropi, A.; Saez-Jimenez, V.; Coscolin, C.; Romero, A.; Medrano, F. J.; Ruiz-Duenas, F. J.; Martinez, A. T., Catalytic surface radical in dye-decolorizing peroxidase: a computational, spectroscopic and site-directed mutagenesis study. *Biochem J* **2015,** *466*, 253-262.

52. Shrestha, R.; Chen, X. J.; Ramyar, K. X.; Hayati, Z.; Carlson, E. A.; Bossmann, S. H.; Song, L. K.; Geisbrecht, B. V.; Li, P., Identification of Surface-Exposed Protein Radicals and A Substrate Oxidation Site in A-Class Dye-Decolorizing Peroxidase from Thermomonospora curvata. *Acs Catalysis* **2016,** *6* (12), 8036-8047.

53. Strittmatter, E.; Serrer, K.; Liers, C.; Ullrich, R.; Hofrichter, M.; Piontek, K.; Schleicher, E.; Plattner, D. A., The toolbox of Auricularia auricula-judae dye-decolorizing peroxidase - Identification of three new potential substrate-interaction sites. *Arch Biochem Biophys* **2015,** *574*, 75-85.

54. Yoshida, T.; Tsuge, H.; Hisabori, T.; Sugano, Y., Crystal structures of dye-decolorizing peroxidase with ascorbic acid and 2,6-dimethoxyphenol. *Febs Letters* **2012,** *586* (24), 4351-4356.

55. Krezel, A.; Bal, W., A formula for correlating pK(a) values determined in D2O and H2O. *J Inorg Biochem* **2004,** *98* (1), 161-166.

56. Poulos, T. L.; Kraut, J., The Stereochemistry of Peroxidase Catalysis. *Journal of Biological Chemistry* **1980,** *255* (17), 8199-8205.

57. Derat, E.; Shaik, S., The Poulos-Kraut mechanism of Compound I formation in horseradish peroxidase: A QM/MM study. *J Phys Chem B* **2006,** *110* (21), 10526-10533.

58. Karsten, W. E.; Lai, C. J.; Cook, P. F., Inverse Solvent Isotope Effects in the Nad-Malic Enzyme Reaction Are the Result of the Viscosity Difference between D2o and H2o - Implications for Solvent Isotope Effect Studies. *Journal of the American Chemical Society* **1995,** *117* (22), 5914-5918.

59. Hangasky, J. A.; Saban, E.; Knapp, M. J., Inverse Solvent Isotope Effects Arising from Substrate Triggering in the Factor Inhibiting Hypoxia Inducible Factor. *Biochemistry* **2013,** *52* (9), 1594-1602.

60. Cook, P. F., *Enzyme mechanism from isotope effects*. CRC Press: Boca Raton, 1991; p 500 p.

61. Liang, A. D.; Wrobel, A. T.; Lippard, S. J., A Flexible Glutamine Regulates the Catalytic Activity of Toluene o-Xylene Monooxygenase. *Biochemistry* **2014,** *53* (22), 3585-3592.

62. Flagg, S. C.; Giri, N.; Pektas, S.; Maroney, M. J.; Knapp, M. J., Inverse Solvent Isotope Effects Demonstrate Slow Aquo Release from Hypoxia Inducible Factor-Prolyl Hydroxylase (PHD2). *Biochemistry* **2012,** *51* (33), 6654-6666.

63. Grissom, C. B.; Cleland, W. W., Isotope Effect Studies of Chicken Liver Nadp Malic Enzyme - Role of the Metal-Ion and Viscosity Dependence. *Biochemistry* **1988,** *27* (8), 2927-2934.

64. Raber, M. L.; Freeman, M. F.; Townsend, C. A., Dissection of the Stepwise Mechanism to beta-Lactam Formation and Elucidation of a Rate-determining Conformational Change in beta-Lactam Synthetase. *J Biol Chem* **2009,** *284* (1), 207-217.

65. Farver, O.; Zhang, J. D.; Chi, Q. J.; Pecht, I.; Ulstrup, J., Deuterium isotope effect on the intramolecular electron transfer in Pseudomonas aeruginosa azurin. *Proceedings of the National Academy of Sciences of the United States of America* **2001,** *98* (8), 4426-4430.

66. Jones, P., Roles of water in heme peroxidase and catalase mechanisms. *J Biol Chem* **2001,** *276* (17), 13791-13796.

67. Childs, R. E.; Bardsley, W. G., Steady-State Kinetics of Peroxidase with 2,2'-Azino-Di-(3-Ethylbenzthiazoline-6-Sulphonic Acid) as Chromogen. *Biochemical Journal* **1975,** *145* (1), 93-103.

68. Wang, W. C.; Noel, S.; Desmadril, M.; Gueguen, J.; Michon, T., Kinetic evidence for the formation of a Michaelis-Menten-like complex between horseradish peroxidase compound II and di-(N-acetyl-L-tyrosine). *Biochem J* **1999,** *340*, 329-336.

69. Koop, D. R.; Hollenberg, P. F., Kinetics of the Hydroperoxide-Dependent Dealkylation Reactions Catalyzed by Rabbit Liver Microsomal Cytochrome-P-450. *J Biol Chem* **1980,** *255* (20), 9685-9692.

Chapter 5 - Concluding remarks and future prospects

Here, we carried out the study of two types of DyPs from classes-A and B. *Tc*DyP is a class-A DyP from a thermophile actinobacter *Thermomonospora curvata* and *El*DyP is a class-B DyP from a proteobacter *Enterobacter lignolyticus*. Characterization of *Tc*DyP was carried out first where its fundamental biochemical properties were determined with the identification of Asp220, Arg327 and His312 as the most important catalytic residues. The major role played by Asp220 was as a general acid base catalyst in formation of Compound I. Its substitution by Ala220 diminished Compound I formation rate by ~10,000-folds and the ABTS oxidation rates to negligible levels. While the rate of guaiacol or hydroquinone oxidation remained unaffected by the mutation suggesting that the rate limiting step had changed. Similarly, Arg327 was also established as an essential catalytic residue in stabilization of transient negative charge during Compound I formation as no detectable Compound I was observed in the variant Arg327Ala. Similarly, His215 was found to be essential for heme binding at the catalytic center as its substitution by Ala215 caused negligible amount of heme incorporation. *Tc*DyP showed moderate thermostability and some activity toward phenolic lignin model compound, thereby suggesting its potential application in lignin degradation. Redox potentials of the wt-*Tc*DyP and the mutants were also determined that revealed the roles of the catalytic residues and pH in fine-tuning the heme microenvironment for efficient electron transfer.

The understanding of *Tc*DyP catalysis in oxidation of large substrate molecules like RB19 was furthered by another study targeting the identification of protein residues involved in substrate oxidation. The bulkier substrates like RB19 can barely fit at the heme access channel and its oxidation is not possible by direct electron transfer at the vicinity of heme center. Hence, it is proposed that oxidation of such substrate molecules take place at the enzyme surface via

long range electron transfer. Cross-linking of monomer units to higher oligomeric states in the presence of H_2O_2 only also suggested involvement of surface radicals. Since tyrosines and tryptophans are easily oxidizable and are known to host radical cations, these residues were projected as the most likely substrate oxidation site. So, all the 7 tryptophans and 3 tyrosines of *Tc*DyP were analyzed first with the help of its crystal structure then followed by the mutagenesis. Out of these 10 residues, 3 residues Trp263, Trp376 and Tyr332 were identified to be surface exposed radical sites. More importantly, the Trp263 was identified as one of the substrate oxidation site, as its substitution by Phe263, Ala263 and Cys263 caused about 50% reduction in RB19 decolorization activity. EPR signals of the mutants also had diminished protein radical intensity which further supported the involvement of Trp263. Similarly, based on SDS gels and SEC together with steady and transient state kinetics, Trp376 was found to be important in crosslinking of enzyme units and identified as off pathway radical sink. Trp376Phe variant showed higher RB19 oxidation rate compared to the wt and exhibited improved Compound I stability accompanied by noteworthy decline in crosslinking capability. Tyr332 residue, on the other hand, was not surface exposed enough to have influential effect on the rate of substrate oxidation. The importance of Trp376 in engineering of DyP activity was thus hinted.

The study with *El*DyP involved deciphering the molecular mechanism of peroxidation in class-B DyP. Unlike some other DyPs, essential roles of both Asp143 and Arg232 in Compound I formation and in overall catalytic cycle were realized. The steady state- and transient state-kinetics performed in D_2O and solvents of higher viscosity than water revealed that the rate limiting step in *El*DyP is the final step where the the pre-enzyme resting state (ERS*) undergoes conformational change to enzyme resting state (ERS). Similarly, the significant KIE observed during Compound I formation and its increased rate at neutral and alkaline pH suggested that the

proton shuffling between the oxygens of H_2O_2 as catalyzed by Asp143 must be the rate limiting step as opposed to the heterolytic O-O bond cleavage. Furthermore, the release of iron bound water molecule was deemed mechanistically important and showed that the absence of co-formed H_2O molecule during compound I formation most likely dictates two electron reduction pathway of Compound I to enzyme resting state. And thus, provides the rationale for the absence of Compound II in the catalytic cycle of DyPs of classes-B and -D. Asp143His mutant of *El*DyP was also studied briefly where as well the aquo release was found important. The role of Asp143, besides in Compound I formation, was also suggested in the reduction of Compound I to enzyme resting. Since the Asp is the most likely proton donor, acidic pH should increase the rate of reduction and hence partially explains why the DyPs are the most active enzymes at acidic pH.

Dye decolorizing peroxidases which have evolved along a different evolutionary branch to become a distant lineage to other classical peroxidases exhibit unparalleled structural and functional features of peroxidases. Reported for the first time during the turn of the twenty-first century and now classified as a separate (super) family of peroxidase, DyPs have garnered a significant prominence as a promising industrial oxidoreductase bio-catalyst, with potential applications in depolymerization of lignin biomass and its valorization, and bioremediation of environmentally hazardous chemicals like xenobiotic dye compounds and nitrophenols. As the β-carotene bleaching properties of some DyPs have already been commercialized in food industries, it would not be long before its other catalytic abilities will be put into further practical use. Along with the interest in digestion of lignin for making value added products, the pharmacological activities of lignin degraded products has made their value soar high. This has warranted for more efficient lignin treatment processes that can yield more of intact lignin end-products in an eco-friendly way. The enzyme based catalyst like DyP can provide a wholesome

solution to this and hence could play an imperative role in maintaining the health of humans and the environment alike. Moreover, the presence of some DyPs in pathogenic bacteria like *M. tuberculosis* and *V. cholera* but not in the host body, where they might be essential for surviving oxidative assaults of the host, can make DyPs a novel drug target in curing the serious illnesses caused by these pathogens. As the genome sequencing has become increasingly accessible, large number of putative DyP encoding genes have been reported and annotated in thousands of bacterial genomes and the account of such *dyp* genes is mounting precipitously on a daily basis. Studies carried out with a couple dozen DyPs from different sources has already revealed that there is no unifying working mechanism that binds all types of DyPs, not even among the members of the same DyP class. This suggests that in order to get a more complete picture on working principle of these enzymes, a lot more enzymological studies aimed at their characterization at the molecular level is essential. While this could be a daunting task, it is equally intriguing to notice that the annotated putative *dyp* genes are co-present within the operon of other genes known to carryout different functions. This suggests that the DyPs might be involved in more than one type of physiological functions and its potential application could be innumerable. Systematic enzymological data collection, analysis and comparison of DyPs will certainly pave the path for their exploitation to the fullest potential. The development of more advanced tools and technology in future can undeniably expedite their study and achieve growth in their applications.

Compared to classical lignolytic fungal peroxidases, DyPs exhibit lower activities toward lignin, non-phenolic compounds and Mn^{2+}. Such activities are especially low among the DyPs of prokaryotic origin. Hence, it has been proposed that the contribution of DyPs toward lignin degradation might be limited to degradation of phenolic units and lignin derived soil organic

matter[1]. However, with the advances in molecular biology it is now possible to manipulate enzymes for enhanced catalytic efficiencies and incorporation of novel attributes. The engineering of a 'better' enzyme uses two major tools of molecular biology, namely the site directed mutagenesis (or rational design) and random mutagenesis (or directed molecular evolution)[2]. The former technique has been practiced with VP where its resistance against the suicide inactivation due to H_2O_2 was increased by ~12 folds[3]. Even more aggressive results have been achieved in the realm of DyP where *Aau*DyP, bearing no prior sulfoxidation capability, was tailored by point mutations in carrying out highly stereospecific sulfoxidation reactions[4]. Similarly, Asn246Ala mutant of DyPB was 80 folds more efficient at Mn^{2+} turnover than the wt[5]. These observations show that DyPs can be tailored to possess non-native features and overcome the limits set by nature in becoming a more versatile enzyme. One area that DyP needs to be improved upon is its stability at acidic pH. Although the pH optimum for DyP activity lies at the acidic region it is not very stable at such pH. Hence, the engineering of DyPs aimed at gaining acidic pH stability can greatly increase its chances of being realized as the industrial biocatalyst. Such manipulations have been successfully achieved in VP where it had remarkable stability at pH < 3 with greater lignolytic capabilities[6].

Another interesting approach of creating more robust variants is via directed evolution, which basically is a lab version of Darwinian evolution that compresses the mutagenic processes spanning thousands of years to the matter of just few days[7]. Mimicking the natural selection process, it is a quicker, powerful and exciting way of achieving enzymes of improved catalytic features. More potent form of *Pp*DyP from *Pseudomonas putida* MET94 was generated by three rounds of random mutation. The evolved variant showed its versatility in increased substrate oxidation efficiency including lignin, higher enzyme yields, greater resistance against H_2O_2

inactivation and most interestingly the shift of pH optimum to basic region by as much as 4 pH units[8]. These results have opened the door for other enhancements in DyPs. As mentioned above, suicide inactivation due to H_2O_2 is one of the biggest problems of peroxidases in realizing these enzymes as the biocatalysts. Hence, DyPs could also use some modifications that can increase its resistance towards H_2O_2. The directed evolution of *Pp*DyP has shown such engineering is highly possible. On the other hand some DyPs are already reported that can tolerate higher concentrations of H_2O_2 and could be a step further as a potential candidate for industrial biocatalyst. For instance, the K_M values for H_2O_2 in the presence of ABTS lie in the micromolar range for many DyPs and other peroxidases, but *El*DyP and DyPA has such values at 2.0 and 4.1 mM respectively[9-10]. Hence, these DyPs could be considered as very stable peroxidases against damaging effects of H_2O_2. And indeed, *El*DyP shows exceptionally very high ABTS turnover rate which most probably could be the result of its high H_2O_2 tolerance. However, DyPA did not show such high ABTS turn over rate which could be the result of very narrow heme access channel as evidenced in some A-type DyPs[11].

Computer simulations can be of great assistance in designing of more potent variants. In silico studies involving biochemical and biophysical modeling can significantly reduce the need for several trials and length of time required for engineering[2]. Protein Energy Landscape Exploration (PELE) is a very powerful and state-of-the-art computational tool capable of more accurately simulating substrate diffusion to the active site, its interaction and binding at the active site and release of products from the active site to the solvent. In one of such computer aided design of novel polar binding sites in laccase significantly improved the binding and oxidation of negatively charged substrates[12]. Other attributes, like oxidation of aniline[13], have also been introduced in laccases with the help of computation inspired design of variants.

Similarly, MnP6, a MnP homolog from a basidiomycete *Ceriporiopsis subermispora*, lacking ABTS activity but having remarkable stability at low pH was engineered by computer assisted manipulations into the ABTS active variant[14]. Besides, the computational studies can also help explain the origin of variations in catalytic efficiencies. For instance, enhanced oxidation with shift in pH optimum of sinapic acid (a lignin related phenol) by laccases[15], identification of long range electron transfer in non-phenolic aromatic substrate oxidation by VP and LiP, and validated by directed mutagenesis[14]were rationalized using the computer based simulations. In *Aau*DyP as well, origin of the novel asymmetric sulfoxidation function in one of its variant was explained based on the computational methods[4]. From these discussions, it is apparent that DyPs have significant likelihoods for enhancements in realizing these enzymes as industrial biocatalysts, and the enzyme engineering approaches coupled with computer based simulations can greatly hasten the progress of more roboust and evolved variants.

5.1 References

1. Fernandez-Fueyo, E.; Linde, D.; Almendral, D.; Lopez-Lucendo, M. F.; Ruiz-Duenas, F. J.; Martinez, A. T., Description of the first fungal dye-decolorizing peroxidase oxidizing manganese(II). *Appl Microbiol Biotechnol* **2015,** *99* (21), 8927-42.

2. Martinez, A. T.; Ruiz-Duenas, F. J.; Camarero, S.; Serrano, A.; Linde, D.; Lund, H.; Vind, J.; Tovborg, M.; Herold-Majumdar, O. M.; Hofrichter, M.; Liers, C.; Ullrich, R.; Scheibner, K.; Sannia, G.; Piscitelli, A.; Pezzella, C.; Sener, M. E.; Kilic, S.; van Berkel, W. J. H.; Guallar, V.; Lucas, M. F.; Zuhse, R.; Ludwig, R.; Hollmann, F.; Fernandez-Fueyo, E.; Record, E.; Faulds, C. B.; Tortajada, M.; Winckelmann, I.; Rasmussen, J. A.; Gelo-Pujic, M.; Gutierrez, A.; Del Rio, J. C.; Rencoret, J.; Alcalde, M., Oxidoreductases on their way to industrial biotransformations. *Biotechnol Adv* **2017**.

3. Saez-Jimenez, V.; Fernandez-Fueyo, E.; Medrano, F. J.; Romero, A.; Martinez, A. T.; Ruiz-Duenas, F. J., Improving the pH-stability of Versatile Peroxidase by Comparative Structural Analysis with a Naturally-Stable Manganese Peroxidase. *PLoS One* **2015,** *10* (10), e0140984.

4. Linde, D.; Canellas, M.; Coscolin, C.; Davo-Siguero, I.; Romero, A.; Lucas, F.; Ruiz-Duenas, F. J.; Guallar, V.; Martinez, A. T., Asymmetric sulfoxidation by engineering the heme pocket of a dye-decolorizing peroxidase. *Catalysis Science & Technology* **2016,** *6* (16), 6277-6285.

5. Singh, R.; Grigg, J. C.; Qin, W.; Kadla, J. F.; Murphy, M. E.; Eltis, L. D., Improved manganese-oxidizing activity of DypB, a peroxidase from a lignolytic bacterium. *ACS Chem Biol* **2013,** *8* (4), 700-6.

6. Fernández-Fueyo, E.; Ruiz-Dueñas, F. J.; Martínez, A. T., Engineering a fungal peroxidase that degrades lignin at very acidic pH. *Biotechnology for Biofuels* **2014,** *7* (1), 114.

7. Mate, D.; Gonzalez-Perez, D.; Mateljak, I.; Gomez de Santos, P.; Vicente Martín, A. I.; Alcalde, M., *The Pocket Manual of Directed Evolution: Tips and Tricks*. 2016; p 185-214.

8. Brissos, V.; Tavares, D.; Sousa, A. C.; Robalo, M. P.; Martins, L. O., Engineering a Bacterial DyP-Type Peroxidase for Enhanced Oxidation of Lignin-Related Phenolics at Alkaline pH. *Acs Catalysis* **2017,** *7* (5), 3454-3465.

9. Shrestha, R.; Huang, G.; Meekins, D. A.; Geisbrecht, B. V.; Li, P., Mechanistic Insights into Dye-Decolorizing Peroxidase Revealed by Solvent Isotope and Viscosity Effects. *ACS Catalysis* **2017**, 6352-6364.

10. Roberts, J. N.; Singh, R.; Grigg, J. C.; Murphy, M. E.; Bugg, T. D.; Eltis, L. D., Characterization of dye-decolorizing peroxidases from Rhodococcus jostii RHA1. *Biochemistry* **2011,** *50* (23), 5108-19.

11. Liu, X.; Du, Q.; Wang, Z.; Zhu, D.; Huang, Y.; Li, N.; Wei, T.; Xu, S.; Gu, L., Crystal structure and biochemical features of EfeB/YcdB from Escherichia coli O157: ASP235 plays divergent roles in different enzyme-catalyzed processes. *J Biol Chem* **2011,** *286* (17), 14922-31.

12. Giacobelli, V. G.; Monza, E.; Fatima Lucas, M.; Pezzella, C.; Piscitelli, A.; Guallar, V.; Sannia, G., Repurposing designed mutants: a valuable strategy for computer-aided laccase engineering - the case of POXA1b. *Catalysis Science & Technology* **2017,** *7* (2), 515-523.

13. Monza, E.; Lucas, M. F.; Camarero, S.; Alejaldre, L. C.; Martínez, A. T.; Guallar, V., Insights into Laccase Engineering from Molecular Simulations: Toward a Binding-Focused Strategy. *The Journal of Physical Chemistry Letters* **2015,** *6* (8), 1447-1453.

14. Acebes, S.; Ruiz-Duenas, F. J.; Toubes, M.; Saez-Jimenez, V.; Perez-Boada, M.; Lucas, M. F.; Martinez, A. T.; Guallar, V., Mapping the Long-Range Electron Transfer Route in Ligninolytic Peroxidases. *J Phys Chem B* **2017,** *121* (16), 3946-3954.

15. Pardo, I.; Santiago, G.; Gentili, P.; Lucas, F.; Monza, E.; Medrano, F. J.; Galli, C.; Martinez, A. T.; Guallar, V.; Camarero, S., Re-designing the substrate binding pocket of laccase for enhanced oxidation of sinapic acid. *Catalysis Science & Technology* **2016,** *6* (11), 3900-3910.

Appendix A - Genes and primers

Table A.1 Synthesized gBlocks (Chapter 2)

1	TACTTCCAATCCAATGCAatggctccgtctcagcgccctctcagtcgccgcgggttgcttgcaggAggTgcaattgcagcTgccgcc ggagcgttggcTgcCtgttctgaagagcgtgctgctggagcccgccccagtgcgacgcaaacaactggtacggccaccgaaccgtttcatgggccg catcaggccggcattgctaccccgccccaggcacacgctgtgtttctgggtctggatctgcgtaagggcaccggccgcaaggaactgggtcgcctcatg cgcctgctgaccgatgacgcgcgccgcctcacgcagggccgcccggctctggcagacccagagccggatttggcgcctctgccttcgcgtctgacttttt acgttcggctttgggccggggctgtttaaagcggcggggctcgaaaaacagcgtccggaggggctgcgcccccttccgccattcaaagttgatcgctta gaagaccgctggtctggcgg
2	Tgacttttacgttcggctttgggccggggctgtttaaagcggcggggctcgaaaaacagcgtccggaggggctgcgcccccttccgccattcaaagttg atcgcttagaagaccgctggtctggcggcgatctgctggtccagatctgttgcgacgacccgatcaccctggctcatgcgttacgtatgacggtgaaagat gcccgcgcgtttacccgcgtgcgttgggtgcagcgtggttttcgccgtagcccgggtgttcagagcagtggcgccacccaacgtaacctgatgggtcag ctggacggcaccgttaatccAgtCccaggcacggccgacttcgatcaagctgtttgggttcaggatggcccagaatggctgcgtggcggtactaccttg gttctgcgtcgtattcgtatggagctggaaaaatgggacgaagcggatcccgccggcaaagaatttgctgttggtcgccgcttaaccagcggtgcgccgt tg
3	Atggctgcgtggcggtactaccttggttctgcgtcgtattcgtatggagctggaaaaatgggacgaagcggatcccgccggcaaagaatttgctgttggt cgccgcttaaccagcggtgcgccgttgacgggccgccatgaacacgatgaaccagattttgatgcagtggatagtgcgggttttccggtaatcgcggaa aatgcgcatatccgcctggctcacgtcgactctcctcgcctgcgcatgctgcgtcgcccgtataattacgacgagggtcttacggcggatgggcgtagcg acgcggggctgctgtttgcggcatatcaagcggacattgaccgccaattcatcccggtgcagcgccgtctggatgaaggtggcgacttgctgaacctgt ggactaccccgattggctctgccgtcttcgcgatcccacccggttgtgatgaaaacggttggatcggtcagggtctcctgggctgaCATTGGAAG TGGATAA

Table A.2 List of *Tc*DyP primer sequence (Chapter 2)

WT	Forward	5’−TACTTCCAATCCAATGCAgaagagcgtgctgctggag−3’
	Reverse	5’−TTATCCACTTCCAATGtcagcccaggagaccct−3’
D189A	Forward	5’−ctgatgggtcagctggcgggcaccgttaatccag−3’
	Reverse	5’−ctggattaacggtgcccgccagctgacccatcag−3’
D189H	Forward	5’−cctgatgggtcagctgcatggcaccgttaatccag−3’
	Reverse	5’−ctggattaacggtgccatgcagctgacccatcagg−3’
D189K	Forward	5’−cctgatgggtcagctgaaaggcaccgttaatccag−3’
	Reverse	5’−ctggattaacggtgcctttcagctgacccatcagg−3’
D189N	Forward	5’−tgatgggtcagctgaacggcaccgttaatcc−3’
	Reverse	5’−ggattaacggtgccgttcagctgacccatca−3’
D189F	Forward	5’−cctgatgggtcagctgttcggcaccgttaatcca−3’
	Reverse	5’−tggattaacggtgccgaacagctgacccatcagg−3’
D189G	Forward	5’−tgatgggtcagctgggcggcaccgttaatc−3’
	Reverse	5’−gattaacggtgccgcccagctgacccatca−3’
H281A	Forward	5’−gtaatcgcggaaaatgcggcgatccgcctggctcacgtc−3’
	Reverse	5’−gacgtgagccaggcggatcgccgcattttccgcgattac−3’
H281C	Forward	5’−gtaatcgcggaaaatgcgtgcatccgcctggctcacgtc−3’

	Reverse	5’−gacgtgagccaggcggatgcacgcattttccgcgattac−3’
R296A	Forward	5’−tcgcctgcgcatgctggcgcgcccgtataattacg−3’
	Reverse	5’−cgtaattatacgggcgcgccagcatgcgcaggcga−3’

Table A.3 Primers used in the construction of *Tc*DyP mutants[a] (Chapter 3)

W158F	Fwd	GATCGCTTAGAAGACCGC**TTC**TCTGGCG
	Rev	ATCGCCGCCAGA**GAA**GCGGTCTTCTAAG
W194F	Fwd	GCGTTTACCCGCGTGCG**TTT**CGTGCAGC
	Rev	CCACGCTGCACG**AAA**CGCACGCGGGTAA
W237F	Fwd	GGCCGACTTCGATCAAGCTGTT**TTC**GTTCAGGATGGCC
	Rev	GGCCATCCTGAAC**GAA**AACAGCTTGATCGAAGTCGGCC
W244F	Fwd	GTTCAGGATGGCCCAGAA**TTT**CTGCGTGGCGGT
	Rev	ACCGCCACGCAG**AAA**TTCTGGGCCATCCTGAAC
W263F	Fwd	TCGTATTCGTATGGAGCTGGAAAAA**TTC**G
	Rev	GGATCCGCTTCGTC**GAA**TTTTTCCAGCTC
W263S	Fwd	CGTATTCGTATGGAGCTGGAAAAA**TCT**GACGAAGCGGATC
	Rev	GATCCGCTTCGTC**AGA**TTTTTCCAGCTCCATACGAATACG
W263A	Fwd	TCGTATTCGTATGGAGCTGGAAAAA**GCG**GACGAAGCGGAT
	Rev	ATCCGCTTCGTC**CGC**TTTTTCCAGCTCCATACGAATACG
W376F	Fwd	GTGGCGACTTGCTGAACCTG**TTC**ACTACC
	Rev	ATCGGGGTAGT**GAA**CAGGTTCAGCAAGT
W396F	Fwd	CCCGGTTGTGATGAAAACGGT**TTC**ATCGGTCAGGGT
	Rev	ACCCTGACCGAT**GAA**ACCGTTTTCATCACAACCGGG
Y330F	Fwd	GCTGCGTCGCCCG**TTT**AATTACGACGAGG
	Rev	CCTCGTCGTAATT**AAA**CGGGCGACGCAGC
Y332F	Fwd	CTGCGTCGCCCGTATAAT**TTC**GACGAGG
	Rev	ACCCTCGTC**GAA**ATTATACGGGCGACGC
Y332L	Fwd	CGCCCGTATAA**TCT**CGACGAGGGTCTTACGGCG
	Rev	AAGACCCTCGTC**GAG**ATTATACGGGCGACGCAG
Y351F	Fwd	GCTGCTGTTTGCGGCA**TTT**CAAGCGGACAT TG
	Rev	CAATGTCCGCTTG**AAA**TGCCGCAAACAGCAGC

[a]Mutation sites are in bold and underlined.

Table A.4 Synthesized DNA sequence of *wt-El*DyP and primers for site-directed mutagenesis [a] (Chapter 4)

*wt-El*DyP		ATGTCCCAAGTCCAAAGCGGTATTCTGCCGGAACACTGTCGTGCAGCCATCT GGATTGAAGCAAATGTGAAAGGCGATGTGAACGCACTGCGTGAATGCAGTA AAGTGTTTGCAGATAAACTGGCTGGCTTTGAAGCACAGTTCCCGGACGCACA TCTGGGTGCAGTGGTTGCTTTTGGTCACGATACCTGGCGTGCACTGTCAGGT GGTGTTGGTGCAGAAGAACTGAAAGACTTCACCCCGTATGGCAAAGGTCTG GCGCCGGCCACGCAGTACGATGTCCTGATTCATATCCTGAGTCTGCGTCACG ACGTCAACTTTTCCGTGGCTCAAGCGGCGATGGCAGCTTTCGGCGATGCAGT CGAAGTGAAAGAAGAAATTCACGGTTTTCGTTGGGTTGAAGAACGCGATCT GAGCGGCTTCGTCGACGGTACCGAAAATCCGGCCGGCGAAGAAACGCGTCG CGAAGTTGCTGTCATCAAAGATGGTGTGGACGCGGGCGGTAGCTATGTGTTT GTTCAGCGTTGGGAACATAACCTGAAACAACTGAATCGCATGTCGGTGCACG ATCAGGAAATGATGATTGGCCGCACCAAAGTTGCGAACGAAGAAATCGATG GTGACGAACGTCCGGAAACCTCCCATCTGACGCGCGTCGATCTGAAAGAAA ATGGCAAAGGTCTGAAAATTGTGCGTCAAAGCCTGCCGTATGGCACCGCATC TGGTACGCACGGTCTGTATTTTTGCGCGTACTGTGCCCGCCTGTACAACATCG AACAGCAACTGCTGAGCATGTTCGGCGATACCGACGGTAAACGTGATGCGAT GCTGCGCTTTACCAAACCGGTTACGGGCGGTTATTACTTCGCCCCGTCTCTGG ACAAACTGCTGG
D143A	Fwd	5'-GAGCGGCTTCGTC**GCC**GGTACCGAAAATC-3'
	Rev	5’-GATTTTCGGTACC**GGC**GACGAAGCCGCTC-3'
D143H	Fwd	5'-CTGAGCGGCTTCGTC**CAC**GGTACCGAAAATC-3'
	Rev	5’-GATTTTCGGTACC**GTG**GACGAAGCCGCTCAG-3'
H215A	Fwd	5’-GTCCGGAAACCTCC**GCT**CTGACGCGCGTCG-3'
	Rev	5’-CGACGCGCGTCAG**AGC**GGAGGTTTCCGGAC-3’
R232A	Fwd	5’-GGCAAAGGTCTGAAAATTGTG**GCT**CAAAGCCTGCCGTAT-3’
	Rev	5’-ATACGGCAGGCTTTG**AGC**CACAATTTTCAGACCTTTGCC-3’

[a]Mutation sites are in bold and underlined.

Appendix B - Crystallization data

Table B.5 X-ray diffraction data collection and refinement statistics of *Tc*DyP (Chapter 3)

Data Collection	
beamline	APS SER-CAT BM-22
wavelength (Å)	1.0000
temperature (K)	100
space group	P21 21 21
cell dimensions	
a, b, c (Å)	77.296, 92.319, 97.187
α, β, γ (deg)	90, 90, 90
resolution range (Å)	35.91−1.75 (1.81−1.75)[a]
total no. of reflections	959093
no. of unique reflections	70532 (6904)[a]
completeness (%)	99.9 (99.5)[a]
I/σ (I)	22.7 (1.0)[a]
R_{pim}	3.9 (70.4)[a]
redundancy	13.6 (8.0)[a]
Refinement	
R_{work}	16.5
R_{free}	22.5
root-mean-square deviation	
bond lengths (Å)	0.004
bond angles (deg)	0.94
no. of atoms	6257
protein	5578
water	593
ligand	86
Ramachandran plot (%)	
most favored	97.6
additionally allowed	2.4

[a]Numbers in parentheses correspond to values in the highest resolution shell.

Table B.6 Calculated solvent accessible areas of aromatic redox active residues in *Tc*DyP (Chapter 3)

Amino acid residue	Solvent accessible area (Å^2)[a]
W158	34.082
W194	6.574
W237	22.525
W244	22.223
W263	10.400
W376	30.164
W396	31.063
Y330	0
Y332	2.751
Y351	0.674

[a]Calculated using PyMol with default parameters.

Table B.7 X-ray diffraction data collection and refinement statistics of *El*DyP (Chapter 4)

Data Collection		
Beamline		APS SER-CAT BM-22
Resolution range (Å)		43.45-1.93 (1.99-1.93)
Space group		*P* 1 21 1
Unit cell	*a*, *b*, *c* (Å)	75.87, 74.16, 118.64
	α, *β*, *γ* (˚)	90, 108.17, 90
Total reflections		716,348
Unique reflections		92,368 (6,739)
Multiplicity		7.76 (7.83)
Completeness (%)		98.00 (96.90)
Mean I/sigma(I)		19.45 (3.83)
Wilson B-factor		23.97
R-merge		7.1 (60.8)
CC1/2		99.9 (91.8)

Refinment	
R_{work}	0.1726
R_{free}	0.2010
Number of non-hydrogen atoms	10,604
macromolecules	9,290
ligands	172
solvent	1,142
Protein residues	1,198
RMS (bonds)	0.006
RMS (angles)	0.85
Ramachandran favored (%)	98.23
Ramachandran allowed (%)	1.77
Ramachandran outliers (%)	0.00
Rotamer outliers (%)	0.42
Average B-factor	30.40
macromolecules	30.07
ligands	24.39
solvent	34.01

Appendix C - Protein sequence alignment

Figure C.1 Sequence alignment of DyPs (Chapter 3)

```
A_TcDyP_D1A807          ----------------------------MAPSQRPLSRRGLLAG-G---AIA----AAAG      24
A_EfeB/YcdB_H9UQT0      ------------------------MQYKDENGVNEPSRRRLLKVIGALALAG----SCPV      32
A_ScDyP_Q9ZBW9          MPDQSIPQTRSPEATRGTPGPLDSDNPGAATAPQGVSRRRLLGTAGATGLVL----GAAG      56
A_TfDyP_Q47KB1          -------------------------MTEPDTERKGSSRRGFLAGLGAAALTG----AGIG      31
B_VcDyP_Q9KQ59          ------------------------------------------------------------      0
B_TyrA_Q8EIU4           ------------------------------------------------------------      0
B_DyPB_RHA1_Q0SE24      ------------------------------------------------------------      0
B_ElDyP_E3G9I4          ------------------------------------------------------------      0
C_DyP2_K7N5M8           ------------------------------------------------------------      0
C_AsDyP_Q8YWM0          ------------------------------------------------------------      0
C_MpDyP_Q744F3          ------------------------------------------------------------      0
C_NpDyP_B2JAD2          ------------------------------------------------------------      0
D_DyP_Q8WZK8            ------------------------MRL-------SLFVVSV-A----VLVGS----SSHV      20
D_AauDyP_I2DBY1         ------------------------MRL-------SPVFVALLSGLLAADLGLARSVAPRV      29
D_MscDyP2_B0BK72        ------------------------MRL-------TYL--PLFAGIAIQ---SAS--ALPD      22
D_TalDyP_Q8NKF3         ------------------------MQL-------KNFLAAT-A----AFVAL----SQPI      20

A_TcDyP_D1A807          ALAACSEE---------RAAGARPSAT-------QTTGTATEPFHGPHQAG-----IATP      63
A_EfeB/YcdB_H9UQT0      AHAQK--------------TQSAPG-TL-----SPDARNEKQPFYGEHQAG-----ILTP      67
A_ScDyP_Q9ZBW9          AAAGYAAA-----------PSSAATPL-------TSLGSERAMFHGKHQPG-----ITTP      93
A_TfDyP_Q47KB1          MAAGEVLRPLLPD----SDPAASPEAEQ-----RLRMAAQRADATAAPQPG-----ISGP      77
B_VcDyP_Q9KQ59          ---------------------------------------------MFKSQTA-----ILPE      11
B_TyrA_Q8EIU4           ----------------------------------MDIQ-----NMPREQLG-----VCAE      16
B_DyPB_RHA1_Q0SE24      ------------------------------------------MPGPVARLAPQAVLTP      16
B_ElDyP_E3G9I4          ---------------------------------------MSQVQSG-----ILPE      11
C_DyP2_K7N5M8           --------MPV---------------DLSTTLSWKSATGEAATMLDELQPN-----ILKA      32
C_AsDyP_Q8YWM0          ---------MALTE---------KDLKNLPEDGIDSENPGKYRNLLNDLQGN-----ILKG      38
C_MpDyP_Q744F3          ------------------------------------------------------------      0
C_NpDyP_B2JAD2          ----------MTEQIIREVPAPNPLAGPEESVLYIPALGEPILRVNNIQGN-----ILGG      45
D_DyP_Q8WZK8            NAAKLGARQTRTTPLLTNFPGQAPLPTL-TQHTTESGANDTILPLNNIQGD-----ILVG      74
D_AauDyP_I2DBY1         ADSPAAVTGTRKTSLLKNVAGLPPVPSA-AQVAAT------SLNTDDIQGD-----ILVG      77
D_MscDyP2_B0BK72        FFKSSVLKPRRTNSLLINPDAQPDLPTA-QQASTA--AASVGLNLTDIQGD-----ILIG      74
D_TalDyP_Q8NKF3         --AAYHVKRARSSPLIVPFPGQGALPTA-AQVQSTS-AGDDSIPFENIQAD-----ILVG      71

A_TcDyP_D1A807          PQA-HAVFLGLDLRKGT------GRKELGRLMRLLTDDARRLTQGRPALA---------D     107
A_EfeB/YcdB_H9UQT0      QQA-AMMLVAFDVLASD-------KADLERLFRLLTQRFAFLTQGGAAPETPNPRLPPLD     119
A_ScDyP_Q9ZBW9          MQA-RGHLVAFDLAAGA------GRKEAAALLRRWSDTARRLMAGEPAGS---------R     137
A_TfDyP_Q47KB1          APA-FVHVIALDLAEEARKNPDTARDSAAAALRSWTELAARLHEESPHDI---------A     127
B_VcDyP_Q9KQ59          AGP-FALYTLLKVRQNH--------AHVLQALKALPALV----------------------      41
B_TyrA_Q8EIU4           GNL-HSVYLMFNANDNVE-------SQLRPCIANVAQYI----------------------      47
B_DyPB_RHA1_Q0SE24      PSA-ASLFLVLVAGDSDDD-----RATVCDVISGIDGPL----------------------      49
B_ElDyP_E3G9I4          HCR-AAIWIEANVKGDV--------NALRECSKVFADKL----------------------      41
C_DyP2_K7N5M8           HVRDRLTVLFLGFGDAA-----------EA--RTFLNGLSG-LMKSARTHLQE-------      71
C_AsDyP_Q8YWM0          HGRDHSVHLFLQFKPEQ-----------VEVVKQWIQSFAQTYITSAKKQADE-------      80
C_MpDyP_Q744F3          ---------------------------------------MQSA--------------      4
C_NpDyP_B2JAD2          FNKDYQTLLFLEIENSN-----------A--FKEWLKTQIKFIATASEVIAFNRIF---K      89
D_DyP_Q8WZK8            MKKQKERFVFFQVNDAT-----------S--FKTALKTYVPERITSA-------------     108
D_AauDyP_I2DBY1         MHKQKQLFYFFAINDPA-----------T--FKTHLASDIAPVVASV-------------     111
D_MscDyP2_B0BK72        MKKNKEMFFFFSIADAT-----------A--FKSHLDSAILPLITST-------------     108
D_TalDyP_Q8NKF3         MKKQNEKFVFFHINNAA-----------T--FKSVLKTYAPANITSV-------------     105

A_TcDyP_D1A807          -PEPDLAPLPSRLTFTFGFGPGL--FK-AAGLEKQRPEGL-RPLP-PFKVD---------     152
A_EfeB/YcdB_H9UQT0      SGILGGYIAPDNLTITLSVGHSL--FDERFGLAPQMPKKL-QKMT-RFPND---------     166
A_ScDyP_Q9ZBW9          DTDVARDAGPSSLTVTFGFGHSF--FG-RTGLEEQRPVAL-DPLP-DFSSD---------     183
A_TfDyP_Q47KB1          EGAASAGLLPASLMVTVGIGGSL--LS-AIDAEDRRPDAL-ADLP-EFSTD---------     173
B_VcDyP_Q9KQ59          -EEINQNQPGAELTVSVAFSKGF--WS-HFE-MA-SPPEL-IDFP-ELGEG---------      84
B_TyrA_Q8EIU4           -YELTDQYSDSAFNGFVAIGANY--WD-SLY-PESRPEML-KPFP-AMQEG---------      91
B_DyPB_RHA1_Q0SE24      -KAVGFRELAGSLSCVVGVGAQF--WD-RVS-ASSKPAHL-HPFV-PLSGP---------      93
```

```
B_ElDyP_E3G9I4          -AGFEAQFPDAHLGAVVAFGHDT--WR-ALS-GGVGAEEL-KDFT-PYGKG---------      85
C_DyP2_K7N5M8           --VEAHKLTKAVGTPYLGVGLTAHGYA-TLG---VT---APADP--SFTAGAK--AA-VE     117
C_AsDyP_Q8YWM0          --AFKYRQKGVSGDVFANFFLSRHGYE-YLE---IEPFQIPGDK--PFRMGMKNEEI-RS     131
C_MpDyP_Q744F3          ---ASVRDTMDSAKRWVTLGFTWNGLR-ALG---VPGDAL-ASFPEEFRQGMAARADILG      56
C_NpDyP_B2JAD2          SARERRGREGTVKATWVNIAFSFQGLK-KLT---QDANNF-TDE--AFKAGLAARAAELN     142
D_DyP_Q8WZK8            --AILISDPSQQPLAFVNLGFSNTGLQ-ALG---IT-DDL-GDA--QFPDGQFADAA---     155
D_AauDyP_I2DBY1         ---TQLSNVATQPLVALNIAFSNTGLL-ALG---VT-DNL-GDS--LFANGQAKDAT---     157
D_MscDyP2_B0BK72        --Q-QLLTVATQPTTAVNLAFSQTGLN-ALG---LASQGL-GDS--LFASGQFSGAE---     155
D_TalDyP_Q8NKF3         --ATLIGPISAQPQAVVNVAFSQAGLG-ALG---VT-DNL-GDT--AFTGGQFADAS---     152
                                                  .
A_TcDyP_D1A807          ------RLEDRWS-------GGDLLVQICCDDPITLAHALRMTVKDA-----------RA     188
A_EfeB/YcdB_H9UQT0      ------SLDAALC-------HGDVLLQICANTQDTVIHALRDIIKHT-----------PD     202
A_ScDyP_Q9ZBW9          ------HLDKNRS-------NGDLWVQIGADDALVAFHALRAIQRDA-----------GA     219
A_TfDyP_Q47KB1          ------DLHPRWC-------GGDFMLQVGAEDPMVLTAAVEELVAAA-----------AD     209
B_VcDyP_Q9KQ59          ------ETHAPST-------DVDVLIHCHATRHDLLFYTLRKGISDI-----------AQ     120
B_TyrA_Q8EIU4           ------NREAPAI-------EYDLFVHLRCDRYDILHLVANEISQMF-----------ED     127
B_DyPB_RHA1_Q0SE24      ------VHSAPST-------PGDLLFHIKAARKDLCFELGRQIVSAL-----------GS     129
B_ElDyP_E3G9I4          --------LAPAT-------QYDVLIHILSLRHDVNFSVAQAAMAAF-----------GD     119
C_DyP2_K7N5M8           KLAD--PAVTEWEGHYQQ-TIDA-VLLLGDATAGPVRTLRRQVEALR-----------PA     162
C_AsDyP_Q8YWM0          SLGD--PKIATWELGFQS-EIHA-LVLIADDDIVDLLQIVNQITQKL-----------RQ     176
C_MpDyP_Q744F3          DTGR--NHPDNWVGGLAGADLHA-IAILFARDDAEHARATNA-HDDLLKR--------CQ     104
C_NpDyP_B2JAD2          DPVDSEGKPTGWVVGGPDNGKVDVVLIVASDEHTDLLEEVSRILKSIVIFTDEKGHAKSS     202
D_DyP_Q8WZK8            -NLG--DDLSQWVAPFTGTTIHG-VFLIGSDQDDFLDQFTDD-ISS--TF--------GS     200
D_AauDyP_I2DBY1         -SFK--ESTSSWVPQFAGTGIHG-VIILASDTTDLIDQQVAS-IES--TF--------GS     202
D_MscDyP2_B0BK72        SLGD--PGTSNWVQAFAGTGIHG-VFLLASDTIDNVNAELSQ-IQS--IL--------GT     201
D_TalDyP_Q8NKF3         DGLG--DDTNTWEPAFKGTNIDG-VFLIISDQDSIITQYQDD-LQA--KL--------GD     198


A_TcDyP_D1A807          FTRVRWVQRGFRRSPGVQS-SGATQRNLMGQLDGTVNPVPGTAD-FD-------------     233
A_EfeB/YcdB_H9UQT0      LLSVRWKREGFISDHAARSKGKETPINLLGFKDGTANPDSQNDKLMQ-------------     249
A_ScDyP_Q9ZBW9          AARVRWQMNGFNRSPGATA-HPMTARNLMGQVDGTRNPKPGEAD-FD-------------     264
A_TfDyP_Q47KB1          ATAVRWSLRGFRRTAAAARDPDATPRNLMGQIDGTANPAQDHPL-FD-------------     255
B_VcDyP_Q9KQ59          DIEIVDETYGFRY---------LDARDMTGFIDGTENPKAE-KR-AE-------------     156
B_TyrA_Q8EIU4           LVELVEEERGFRF---------MDSRDLTGFVDGTENPKGR-HR-QE-------------     163
B_DyPB_RHA1_Q0SE24      AATVVDEVHGFRY---------FDSRDLLGFVDGTENPTDD-DA-AD-------------     165
B_ElDyP_E3G9I4          AVEVKEEIHGFRW---------VEERDLSGFVDGTENPAGEETR-RE-------------     156
C_DyP2_K7N5M8           SVTVVGEESGLGLAN-----ANGDGIEHFGYVDGRSQPLFLTED-VDAERDTTDGVNDWD     216
C_AsDyP_Q8YWM0          IAEIVHREDGFILRN-----QAGQIIEHFGFVDGVSQPLFMKRD-VVRERVNNCDFDKWD     230
C_MpDyP_Q744F3          GVRRLSHLDLNA-TP-----PFNYAHDHFGFRDGLSQPVIEGSG-EE-------------     144
C_NpDyP_B2JAD2          GAKITFIEEGAN-LP-----PPLTGHEHFGNLDGISQPGIRGRV-SDNPKDLLT--PRQD     253
D_DyP_Q8WZK8            SITQVQALSGSA-RP-----GDQAGHEHFGFLDGISQPSVTGWE-TT-------------     240
D_AauDyP_I2DBY1         SISKLYSLSASI-RP-----GNEAGHEMFGFLDGIAQPAINGFN-T--------------     241
D_MscDyP2_B0BK72        SITEAYRLQGEA-RP-----DDQQGHEHFGFMDGISNPAIDGFS-T--------------     240
D_TalDyP_Q8NKF3         AWTVVYDLSGAA-RP-----GDQFGHEHFGYLDGISNPLIKGFG-E--------------     237
                                              :  *  *   :*

A_TcDyP_D1A807          ------------------QAVWVQD-------------------GPEWLRGGTTLVLRRI     256
A_EfeB/YcdB_H9UQT0      ------------------KVVWVT----ADQ------------QEPAWTIGGSYQAVRLI     275
A_ScDyP_Q9ZBW9          ------------------RRIFVPEEPEAGK------------GGPAWMANGSYVVVRRI     294
A_TfDyP_Q47KB1          ------------------RTITARP---ADN------------PAHAWMDGGSYLVVRRI     282
B_VcDyP_Q9KQ59          ------------------VALV----------------------ADGDFAGGSYVMVQRF     176
B_TyrA_Q8EIU4           ------------------VALVGS--------------------EDPEFKGGSYIHVQKY     185
B_DyPB_RHA1_Q0SE24      ------------------SALIGD--------------------EDPDFRGGSYVIVQKY     187
B_ElDyP_E3G9I4          ------------------VAVI----------------------KDGVDAGGSYVFVQRW     176
C_DyP2_K7N5M8           PSAPLE------------QVLVPDPA-----------------APDPTVHFGSYFVFRKL     247
C_AsDyP_Q8YWM0          PKAPLD------------SILVEDPN-----------------GN-TKDSYGSYLVYRKL     260
C_MpDyP_Q744F3          ------PTPGSGAPLKAGEFILGYPDEVGPV--------ANQPEPEVLSRNGTYAAYRRL     190
C_NpDyP_B2JAD2          PKNPNQGKPGQD-VLWPGEFVFGYEGQNADAQQLENSRGAITSAGPKWADDGSYLVFRRL     312
D_DyP_Q8WZK8            ------VFPGQA-VVPPGIILTGRDGDT-----------G---TRPSWALDGSFMAFRHF     279
D_AauDyP_I2DBY1         ------PLPGQN-IVDAGVIITGATNDP-----------I---TRPSWAVGGSFLAFRQL     280
D_MscDyP2_B0BK72        ------ALPGQA-VLSPGLFLLAEDGDGS-S--------S---SRPSWAKDGSLLAFRQL     281
D_TalDyP_Q8NKF3         ------PLPGQA-FIDPGIILVGRANDT--V--------T---TRPAWALDGSFLAFRKL     277
                                     :                                  *:    :

A_TcDyP_D1A807          RMELEKWDEADPAG------------------KEFAVGRRLTSGAPLTGRHE---HDEP     294
A_EfeB/YcdB_H9UQT0      QFRVEFWDRTPLKE------------------QQTIFGRDKQTGAPLGMQHE---HDVP     313
A_ScDyP_Q9ZBW9          RMLLDDWEELSLKA------------------QEDVIGRRKSDGAPLSGGSGATESTEM     335
```

```
A_TfDyP_Q47KB1          RMLLTEWRKLDVAA-------------------RERVIGRRLDTGAPLGSRNE---TDPV      320
B_VcDyP_Q9KQ59          VHNLPAWNRLNLAA-------------------QEKVIGRTKPDSVE--LEN--------      207
B_TyrA_Q8EIU4           AHNLSKWHRLPLKK-------------------QEDIIGRTKQDNIEYESED--------      218
B_DyPB_RHA1_Q0SE24      LHDMSAWNTLSTEE-------------------QERVIGRTKLENVELDDDA--------      220
B_ElDyP_E3G9I4          EHNLKQLNRMSVHD-------------------QEMMIGRTKVANEEIDGDE--------      209
C_DyP2_K7N5M8           EQNVRLFKEAERDLAHDLGL-----RGEDRERAGAMLVGRFE-DGTPLTAQSA-------      294
C_AsDyP_Q8YWM0          EQNVKAFREDQRKLAQKLNI-----Q---ENLAGALIVGRFA-DGTPVTLSDI-------      304
C_MpDyP_Q744F3          REHVAVFRDYLRSVAGA---------DRQEELLAAKLMGRWR-SGAPLVLAPD---EDDP      237
C_NpDyP_B2JAD2          RQDVFKFHKFLNDTAAN--------LNADPRKVSAKLIGRWP-SGAPTVRTPE---ADSP      360
D_DyP_Q8WZK8            QQKVPEFNAYTLANAIPANSAGNLTQQEGAEFLGARMFGRWK-SGAPIDLAPT---ADDP      335
D_AauDyP_I2DBY1         EQLVPEFNKYLLDNAPA----GSGSLQARADLLGARMVGRWK-SGAPIDLTP T---ADDP     332
D_MscDyP2_B0BK72        QQRVPEFNKFLADNAAL--------TQGNADLLGARMMGRWK-SGAPVDLAPT---ADDV      329
D_TalDyP_Q8NKF3         KQLVPEFHKYTLDNALQ-NQSGNLSTEEGALLLGSRMFGRWN-SGAPIDLTPD---VDDP      332
                           :                                  .**

A_TcDyP_D1A807          DFDAV----------------------------DSAGFPVIAENAHIRLAHVDS---PR-      322
A_EfeB/YcdB_H9UQT0      DYASD----------------------------PEGKVIALDSHIRLANPRTAESES-      342
A_ScDyP_Q9ZBW9          DLEKT----------------------------DGSGELVVPINAHARITRPDQN--GG-      364
A_TfDyP_Q47KB1          VLSAR----------------------------DEEGEPLIPENAHVRLASPENN--LG-      349
B_VcDyP_Q9KQ59          ---------------------------------------VPAASHVGRVDIK-EEGKG-      225
B_TyrA_Q8EIU4           ---------------------------------------KPLTSHIKRVNLKDENGKS-      237
B_DyPB_RHA1_Q0SE24      ---------------------------------------QPSNSHVTLNTIVDDDGVE-      239
B_ElDyP_E3G9I4          ---------------------------------------RPETSHLTRVDLK-ENGKG-      227
C_DyP2_K7N5M8           -PGSHHPVGNDFSYDS-----------------DKLGQKCPFHAHIRKTNPRGSGGAE-      334
C_AsDyP_Q8YWM0          -PTYAVTPTNNFNYDG-----------------DLAATKCPFHSHTRKTNPRGDTARLL      345
C_MpDyP_Q744F3          ELGADPLRNNDFNYKEM----------------DPFGYACPLGAHARRLNPRDTAHN--      278
C_NpDyP_B2JAD2          NLGNDDNANNDFEFNGDDPAVNGFFKNDVVPPSKDATGLRCPFIAHTRKTYPRNDKTPGG     420
D_DyP_Q8WZK8            ALGADPQRNNNFDYSD-----------------TLTDETRCPFGAHVRKTNPRQDLGG--      376
D_AauDyP_I2DBY1         ALGADAQRNNNFTYSHAGF-------------DLGSDQSHCPFSAHIRKTRPRADLGGSL     379
D_MscDyP2_B0BK72        DLANDPQRNNNFNFTHPDF-------------TETTDQTHCPFSAHIRKTNPRSDFNP--      374
D_TalDyP_Q8NKF3         ALGNDPNRNNNFNYIHPGE-------------DPATDQSRCPFTAHIRKTNPRDLESQNL     379
                                                                    :*

A_TcDyP_D1A807          -----------------LRMLRRPYNYDEGLTA----------DGRSDAGLLFAAYQADI      355
A_EfeB/YcdB_H9UQT0      -----------------SLMLRRGYSYSLGVTN----------SGQLDMGLLFVCYQHDL      375
A_ScDyP_Q9ZBW9          -----------------AAMVRRPFSYHDGFDA----------DGVPDAGLLFVCWQADP      397
A_TfDyP_Q47KB1          -----------------ARMFRRGYSYDQGWRD----------DGVRDAGLLFMAWQGDP      382
B_VcDyP_Q9KQ59          -----------------LKIVRHSLPYGS--------------VS-GDHGLLFIAYCHTL      253
B_TyrA_Q8EIU4           -----------------IEILRQSMPYGS--------------LK--EQGLMFISTCRTP      264
B_DyPB_RHA1_Q0SE24      -----------------HDILRDNMAFGS--------------LGEAEYGTYFIGYAKDP      268
B_ElDyP_E3G9I4          -----------------LKIVRQSLPYGT--------------AS-GTHGLYFCAYCARL      255
C_DyP2_K7N5M8           ----------APEEERKHLMARRGQTYGRRHDDPNADLPPRLR-PAKDVGLLFMAFNSNL     383
C_AsDyP_Q8YWM0          TTDGHFD--EAFKEERGHRITRRAVSYGEN--------NPSKE-PVSGSGLLFLCFQSNI      394
C_MpDyP_Q744F3          --------------MNRRRMIRRGATYGPALPEGAP-------DDGEDRGIAAFIICASL     317
C_NpDyP_B2JAD2          EGPGPKEIDRSEVTTQTHRLLRRGIPYGPVSASTPDE--PLQDPNFVDRGLHFLAYQTSI     478
D_DyP_Q8WZK8            P--------VDTF-----HAMRSSIPYGPETSDAELASGVT----AQDRGLLFVEYQSII     419
D_AauDyP_I2DBY1         T--------PPNLSAGANSIMRSGIPYGPEVTSAESASNTT----TQERGLAFVAYQAQL     427
D_MscDyP2_B0BK72        -------------LNTANHIIRAGIPYGPEVTDAEASSNTSSTDASLERGLAFVAYQSNI     421
D_TalDyP_Q8NKF3         I--------PEFF-----HAIRAGTPYGPEVSYAESSSNTT----QIDRGLAFVEYQSNI     422
                                      *    :                    *

A_TcDyP_D1A807          DRQFIPVQRR----L---------------------------------------------      366
A_EfeB/YcdB_H9UQT0      EKGFLTVQKR----L---------------------------------------------      386
A_ScDyP_Q9ZBW9          LRGFVPVQRK----L---------------------------------------------      408
A_TfDyP_Q47KB1          ATGFIPVQRS----L---------------------------------------------      393
B_VcDyP_Q9KQ59          HNFKTMLESM-YGVT---------------------------------------------      267
B_TyrA_Q8EIU4           DHFEKMLHSMVFGDG---------------------------------------------      279
B_DyPB_RHA1_Q0SE24      AVTELMLRRMFLGEP---------------------------------------------      283
B_ElDyP_E3G9I4          YNIEQQLLSM-FGDT---------------------------------------------      269
C_DyP2_K7N5M8           GNQFEFTQQIWANNPAFPFPP-------DGSQPGLDPVIGQGARAPQK----YAPEWGH-      431
C_AsDyP_Q8YWM0          ENQFNFMQSRWANPQNFVQVN-------T----GPDPLIGQPS-GTQK----WPKKWGE-      437
C_MpDyP_Q744F3          IRQFEFAQNVWINDRTFHELG------------NEHDPICGTQDGTLDFTIPKRP------     360
C_NpDyP_B2JAD2          VDQFEFVTKFWSNNPDFSTEAATDHEFEGQLTLGHDPIIGQNKGQNGDRTRKFFIHLEDN     538
D_DyP_Q8WZK8            GNGFRFQQINWANNANFPFSK-------PI-TPGIEPIIGQTT---------PRT-VGGL     461
D_AauDyP_I2DBY1         SQGFHFLQQTWADNANFPPGK-------TPATVGLDPIIGQNNG-------QPRV-VNGL     472
```

```
D_MscDyP2_B0BK72        GNGFAFIQQNWVDNANFFFGK-------TT-PPGIDPIIGSNAAQNNFAPNSPRP-VSGL      472
D_TalDyP_Q8NKF3         SNGFRFQQVNWANNNKFPFNK-------SISEPGLDPVIGQDKG-------ANRI-TTGL      467


A_TcDyP_D1A807          -----DEGGDLLNLWTTPIGSAV-FAIPPGCDE----------------------NGWIG      398
A_EfeB/YcdB_H9UQT0      -----N--GEALEEYVKPIGGGYFFALPGVKDA----------------------NDYFG      417
A_ScDyP_Q9ZBW9          -----DRGDALS-QFIRHEASGL-FAVPGGAAE----------------------GEYVG      439
A_TfDyP_Q47KB1          -----ADQGDALNRYIRHEGSAL-FAVPA-ARE----------------------GRYLG      424
B_VcDyP_Q9KQ59          -----DGKTDQLLRFTKAVTGAYFFAPSQVMLQELTLKNQ--------------------      302
B_TyrA_Q8EIU4           -----AGNHDHLMHFTSALTGSSFFAPSLDFLMQFDN------------------------      311
B_DyPB_RHA1_Q0SE24      -----PGNYDRVLDFSTAATGTLFFVPSRDVLESLGDEPAGAESAPEDPVEPAAAGPYDL      338
B_ElDyP_E3G9I4          -----DGKRDAMLRFTKPVTGGYYFAPSLDKLLAL--------------------------      299
C_DyP2_K7N5M8           --NNVAEATDPIPQAVTMKGGEYFFMPSLAFLRSL--------------------------      464
C_AsDyP_Q8YWM0          --PETEEY--NFQLWINMKGGEYFFAPSISFLKTLA-------------------------      469
C_MpDyP_Q744F3          ----IRRVLKGLPAFTTLTGGAYFFLPGINAMRYLAALGERS------------------      398
C_NpDyP_B2JAD2          NSQPLTKELTAPEDWVIPTGGGYFFAPSISALKNVLT-----------------------      575
D_DyP_Q8WZK8            DPLNQNETFTV-PLFVIPKGGEYFFLPSISALTATIAA-----------------------      498
D_AauDyP_I2DBY1         LPSNSSASLSI-PQFVVSHGGEYFFSPPISAIGGRLSA-----------------------      509
D_MscDyP2_B0BK72        DPTDSTTIVTLNTDFVVSRGGEYFFSPSLSAIQNTLSV-----------------------      510
D_TalDyP_Q8NKF3         NPLNVSESLSI-PDFIVSNGGEYFFAPSITSIVETLAA-----------------------      504
                                              .   *


A_TcDyP_D1A807          QGLLG-------  403
A_EfeB/YcdB_H9UQT0      SALLRV------  423
A_ScDyP_Q9ZBW9          QRLLEG------  445
A_TfDyP_Q47KB1          QDLIEG------  430
B_VcDyP_Q9KQ59          ------------  302
B_TyrA_Q8EIU4           ------------  311
B_DyPB_RHA1_Q0SE24      SLKIGGLKGVSQ  350
B_ElDyP_E3G9I4          ------------  299
C_DyP2_K7N5M8           ------------  464
C_AsDyP_Q8YWM0          ------------  469
C_MpDyP_Q744F3          ------------  398
C_NpDyP_B2JAD2          ------------  575
D_DyP_Q8WZK8            ------------  498
D_AauDyP_I2DBY1         ------------  509
D_MscDyP2_B0BK72        ------------  510
D_TalDyP_Q8NKF3         ------------  504
```

Catalytic residues, W263, and Y332 are highlighted in yellow, pink, and blue, respectively. Motif GXXDG is underlined. Protein Unitprot identification numbers are listed after protein abbreviation.

Appendix D - Absorbance maxima

Table D.8 Absorbance maxima of enzyme resting state and catalytic intermediates of *wt-El*DyP and its mutants (Chapter 4)

Enzyme	pH	Resting state	Compound I	Compound II-like int.
wt	3.5	406, 509, 536(sh), 640	402, 517, 549, 570, 615, 646	
	7.5	406, 509, 538, 642	402, 517, 549, 570, 617, 646	
	10.0	406, 505, 534(sh), 642(sh)	402, 509, 544, 565(sh), 617, 644	
D143A	4.0	404, 505, 536(sh), 632	406, 503, 539(sh), 630	
	7.5	404, 507, 532(sh), 632	406, 512, 536(sh), 631	416, 526, 553
	10.0	408, 532(sh), 574(sh), 609(sh)	416, 526, 553	418, 526, 553
D143H	4.0	406, 455(sh), 501, 534(sh), 567(sh)	406, 446(sh), 625	
	7.5	408, 457(sh), 507, 530(sh), 555(sh)	416, 454, 515, 530(sh), 555, 630	418, 530, 557, 625(sh)
	10.0	410, 537, 574, 615(sh)	412, 528, 556, 625	418, 530, 557, 625(sh)
R232A	4.0	406, 503, 534(sh), 633	404, 503, 579, 640	
	7.5	406, 507, 534(sh), 634	408, 542, 590(sh)	
	10.0	406, 499, 534(sh), 633	404, 498, 527(sh), 638	

Appendix E - SDS-PAGE and temperature rate profile

Figure E.2 (A). SDS-PAGE of *El*DyP-wt and mutants (B). Temperature rate profile of wt-*El*DyP

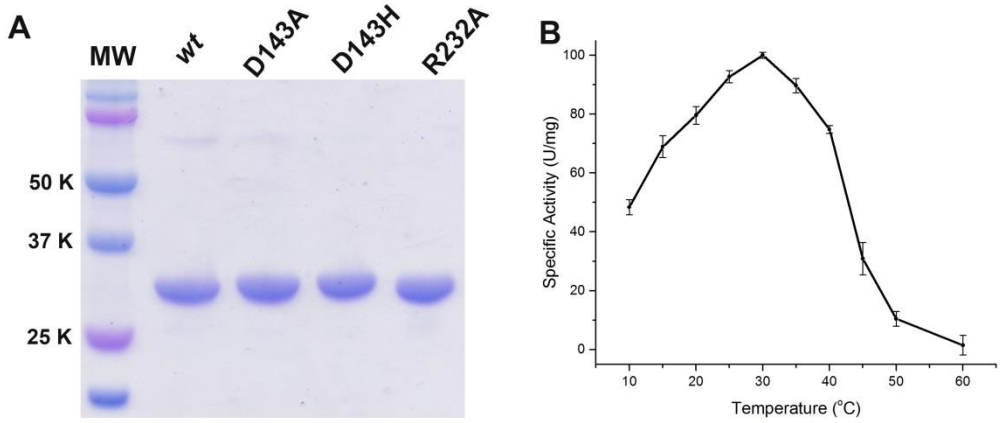

Appendix F - Permission to reprint

11200 Rockville Pike
Suite 302
Rockville, Maryland 20852

August 19, 2011

American Society for Biochemistry and Molecular Biology

To whom it may concern,

It is the policy of the American Society for Biochemistry and Molecular Biology to allow reuse of any material published in its journals (the Journal of Biological Chemistry, Molecular & Cellular Proteomics and the Journal of Lipid Research) in a thesis or dissertation at no cost and with no explicit permission needed. Please see our copyright permissions page on the journal site for more information.

Best wishes,

Sarah Crespi

American Society for Biochemistry and Molecular Biology
11200 Rockville Pike, Rockville, MD
Suite 302
240-283-6616
JBC | MCP | JLR